U. S. GOVERNMENT AGENCIES AND THEIR
CONTRACTORS ONLY

NASA CR-132374
COPY NO. 41

204017

ADVANCED SUPERSONIC TECHNOLOGY CONCEPT STUDY

REFERENCE CHARACTERISTICS

AST

(NASA-CR-132374) ADVANCED SUPERSONIC TECHNOLOGY CONCEPT STUDY REFERENCE CHARACTERISTICS (LTV Aerospace Corp.) 307 p

N76-71826

Unclas
00/98 14809

HAMPTON TECHNICAL CENTER
LTV AEROSPACE CORPORATION
HAMPTON, VA
DECEMBER 21, 1973

FOR

ADVANCED SUPERSONIC TECHNOLOGY OFFICE
LANGLEY RESEARCH CENTER
NATIONAL AERONAUTICS AND SPACE ADMINISTRATION
CONTRACT NAS1-10900

U.S. DEPARTMENT OF COMMERCE
National Technical Information Service

N76-71826

ADVANCED SUPERSONIC TECHNOLOGY CONCEPT STUDY REFERENCE CHARACTERISTICS

LTV Aerospace Corporation

21 December 1973

74-10055

I

FOREWORD

The work described herein was conducted by the Technical Staff of the LTV Aerospace Corporation/Hampton Technical Center for the Advanced Supersonic Technology Office, NASA Langley Research Center. The effort was performed under Contract NAS1-10900. The LTV/Hampton Technical Center team provides technical integration assistance to the Advanced Supersonic Technology Office for promising conceptual configurations. The purpose of this study was to develop and define a Reference Configuration Concept and its Characteristics to serve as a baseline reference for further trade studies, future configuration development, and for comparison with other industry developed configurations. The work was performed under NASA Project Manager, Mr. Cornelius Driver, Aeronautical Systems Office - Advanced Supersonic Technology Office, and Technical Coordinator, Mr. J. D. Pride, Jr., Systems Engineering Division - Aeronautical Systems Engineering Branch, NASA - Langley Research Center. This report was prepared by the Technical Staff members shown below under the direction of C. W. Pearce, the Hampton Technical Center Advanced Aircraft Technology Project Manager. The contents of this document represent a level of effort of 4500 man hours.

°Technical Integration - B. Downie
°Configuration Concept - W. Berry, E. Swanson
°Aerodynamics - J. DeYoung, W. Holmquist, J. Russell
°Stability and Control - P. Smith
°Propulsion - W. Lovell
°Weights - J. Espil
°Noise - J. Russell
°Mission Analysis - B. Quartero

NASA Contract No. NAS1-10900

ADVANCED SUPERSONIC TECHNOLOGY CONCEPT STUDY

REFERENCE CHARACTERISTICS

APPROVAL

LTV Aerospace Corporation	NASA Langley Research Center
R. R. Lynch Advanced Aircraft Technology Manager	C. Driver Aeronautical Systems Office Advanced Supersonic Technology Office
C. W. Pearce Project Manager	J. D. Pride, Jr. Systems Engineering Division Aeronautical Systems Engineering Branch

TABLE OF CONTENTS

NOTE: List of symbols, figures, tables, and references appear at the end of each analysis section as appropriate.

III

SUMMARY

The study results to be summarized are a critical function of the design mission, ground-rules, criteria, and technology used. While every effort has been made to make these studies compatible with previous studies and national objectives the reader is cautioned that small changes in these parameters can have a large effect on study results.

The study results show a considerable increase in the payload and range capability of the Reference Configuration compared with the 1968 Boeing 336C Configuration in spite of more stringent takeoff noise requirements. In addition the Reference Configuration is much less complicated (no folding canard or demand leading edge devices, shorter more simple landing gear) and offers a more desirable 5 abreast seating arrangement. Many of these favorable changes are a result of improved low speed aerodynamic performance in conjunction with linear pitching moments to extreme angles of attack areas which were less well understood in the 1968 time period. These study results are believed to provide a solid base for trade studies on the effects of engine cycle and airplane size, takeoff and landing noise requirements, stability and control criteria, reserve fuel requirements, structural design approaches, and flutter criteria.

The Reference Configuration concept of this study exhibits the following performance characteristics:

For a design mission of 4000 nautical miles, with 292 passengers requires a TOGW of 762,000 pounds. This mission requires the

800#/sec dry turbojet engine to be suppressed by 11.7 DB to meet the FAR 36 T.O. noise requirements.

For a New York to Paris mission the TOGW would be 696,500 pounds and the suppression required to meet FAR 36 would be 7.3 DB.

For the design mission the bare airframe noise at the FAR 36 takeoff measuring point is 105.6 DB and for landing the bare airframe noise exceeds the engine jet noise by 11.1 DB.

IV

INTRODUCTION

The supersonic transport has become a reality in the Concorde and TU-144. Although marginally acceptable because of deficiencies in range, payload, D.O.C., and community noise these configurations can be expected to sell and earn a profit. It is clear, however, that future configurations for supersonic commercial application must have increased capability. If the foreseeable advanced technologies can be successfully implemented it is reasonable to expect substantial increases in payload fraction and range, at least FAR 36 noise levels, and D.O.C.'s competitive with the present generation of subsonic transports.

The NASA-Langley Research Center has been a leader in the development of advanced technology suitable for supersonic cruise applications. Some of these technologies have included the supersonic area rule, variable-sweep wings, supersonic wing camber and twist for drag due-to-lift reduction, favorable interference techniques, and sonic boom estimation techniques. Application of these and other advanced technologies has been high-lighted by the integration of several of these technologies into study airplane configurations. One of these concepts, with a subsonic leading edge wing, was evaluated in-depth by the Boeing Company in 1968. In the course of this study, a number of configuration, stability and control, and performance problems were identified. Continuing research has led to solutions to most problems of an aerodynamic nature, but these solutions have not been integrated into an updated configuration concept. There have also been advances in propulsion system concepts and materials that have not been previously considered.

The objective of this study is to identify a Reference Configuration concept and the associated characteristics obtainable through the application of the results of recent research. This concept is a 292 passenger M 2.7 design with a subsonic leading edge wing and utilizes four dry turbojet engines for propulsion. The engines use the variable geometry turbine feature to reduce the engine-size required to meet the FAR 36 noise requirements. The wing geometry has been refined to provide improvements in stability and control, and performance indicated by extensive wind tunnel tests. The Boeing 1968 study concept is used as a base from which the current study concept and characteristics are developed. It is anticipated that the present reference study configuration will provide a reasonable baseline for future trade studies and for application of further technology improvements. The Reference Configuration concept is defined in Section V. The characteristics of this concept are then analyzed and presented in Section VI. The major areas addressed are:

- °Aerodynamics
- °Stability and Control
- °Propulsion
- °Weights
- °Noise
- °Mission Payload/Range

Each of the areas addressed contain a further introduction which provides the objective and scope of the analyses and a summary which highlights the results. It is intended that each of these areas of study be self sustaining, therefore, each contains its own list of symbols and references.

The design requirements used for this study are as follows:

°Cruise Mach no. 2.7

°Subsonic wing leading edge

°4000 nautical mile range

°Sea level standard day take-off field length $\leq$ 10,500 feet

°1.2 thrust margin at M 2.7 at 60,000 feet

°FAR-121:648 fuel reserves (modified)

°FAR 36 noise rules

The mission profile is shown in Figure IV-1.

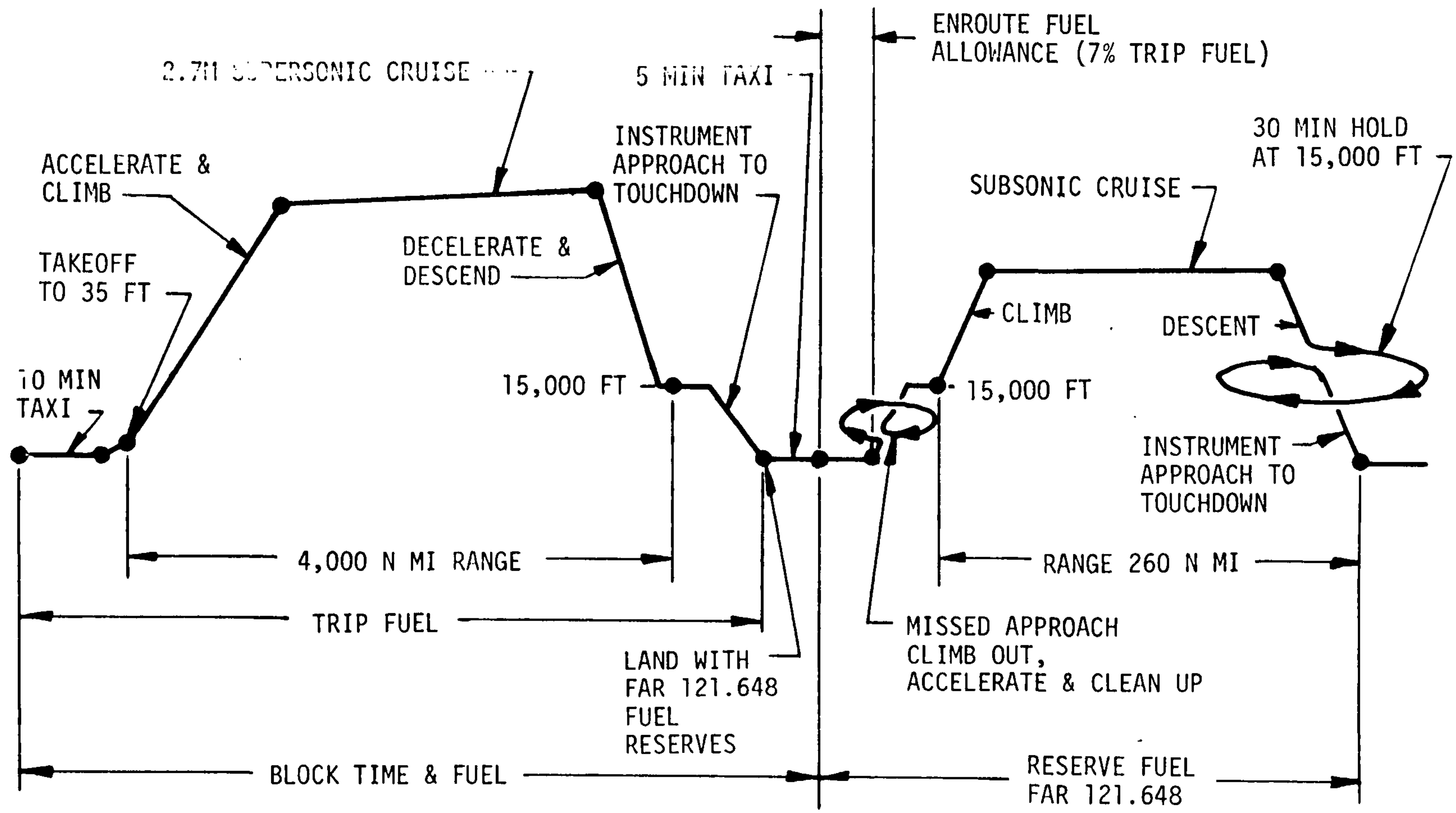

FIGURE IV-1 MISSION PROFILE

SECTION V

REFERENCE CONFIGURATION CONCEPT

INTRODUCTION

The development of configurations suitable for supersonic cruise involve in part subsystem integration to maximize the benefits obtainable through application of advanced supersonic technology. The initial JP-4 fueled baseline configuration, evaluated by NASA, was based on the Boeing 336C airplane, but did not incorporate a canard, and used only a horizontal tail for pitch control and trim. The airplane was configured for 4 abreast seating and Mach 2.7 cruise. The geometry of this configuration is defined by the NASA computerized design identified as the 733-336C Follow-on 2 dated March 1973.

A preliminary investigation of subsystem integration of the above configuration identified several areas of concern primarily in the areas of the main landing gear, wing structure and fuselage interface, and the passenger arrangement. The solutions to these areas of concern has resulted in significant changes in the airplane geometry. A new computerized geometry definition to reflect these changes has been generated and is identified as 336C Follow-on 3 dated October 1973 hereinafter referred to in this document as the Reference Configuration. It is to these areas of change that the following is addressed. A planform comparison of the Boeing 336C aircraft and the Reference Configuration is shown in Figure V-1. The general arrangement, inboard profile, geometric characteristics, and weights of the Reference Configuration is shown in Figures V-2 and V-3 and Tables V-I and II.

REFERENCE AIRCRAFT DIFFERENCES

CANARD REMOVED

WING PLANFORM CHANGED & INCREASED SPAN

HORIZONTAL TAIL VOLUME INCREASED

LEADING EDGE DEVICES SIMPLIFIED

TRAILING EDGE FLAP SIZES INCREASED

WING MOVED FWD.

HARD SAS WITH C.G. CONTROL

PASSENGER VOLUME INCREASE TO 292

BODY LENGTH INCREASED

BODY DIAMETER INCREASED

LARGER DRY TURBO JET ENGINES

LANDING GEAR SHORTENED

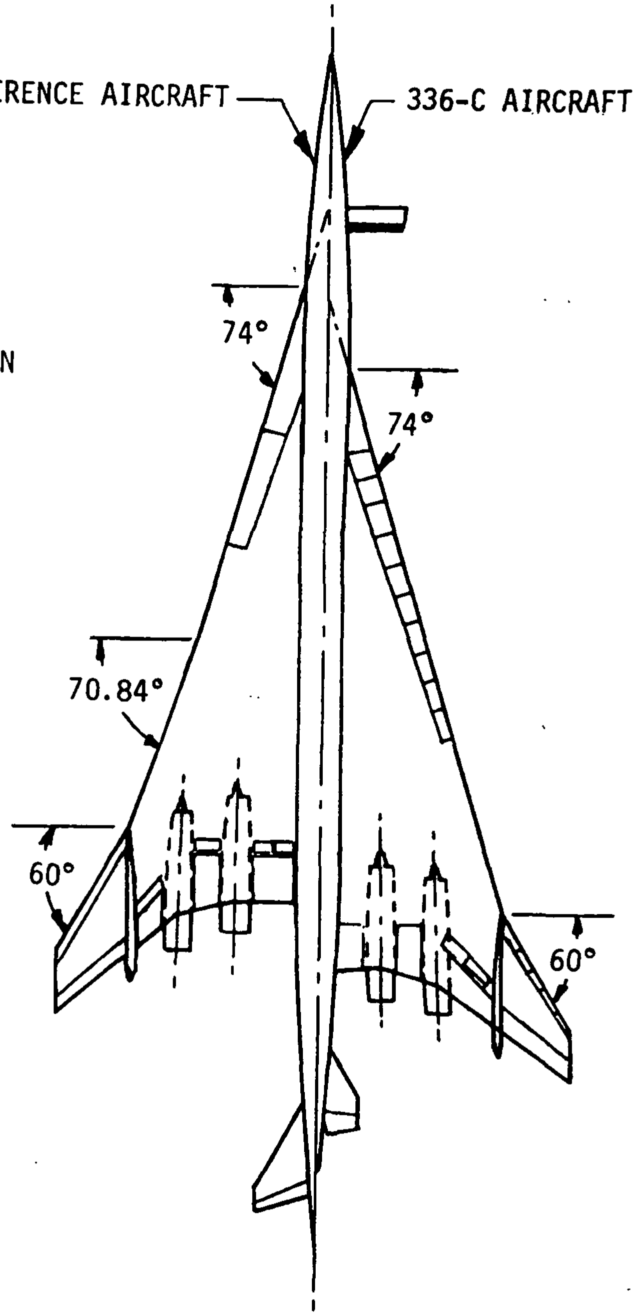

Figure V-1 — Reference Configuration Differences from 336-C Configuration

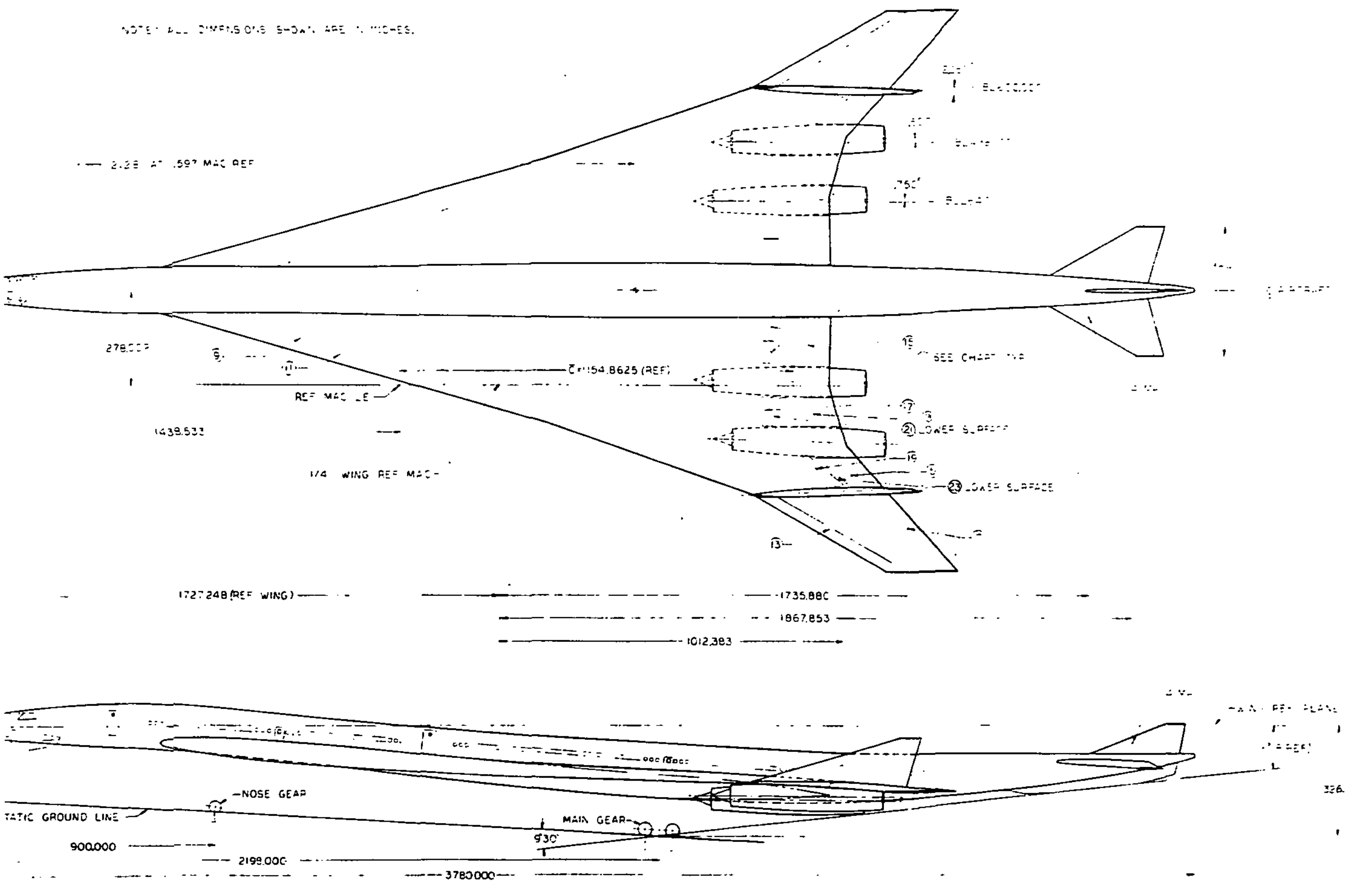

FIGURE V-2 - REFERENCE CONFIGURATION GENERAL ARRANGEMENT

WING CONTROL SURFACES

MOD. W.T. DATA	NUMBER *	AREA FT² EACH
1	1 AND 2	146
†2	3 AND 4	[illegible]
†3	5 AND 6	6
†4	7 AND 8	9
[illegible]	9 AND 10	198
[illegible]	11 AND 12	195
[illegible]	13 AND 14	92
	15 AND 16	40
	17 AND 18	26
	19 AND 20	18
	21 AND 22	6
	23 AND 24	8

* ODD NUMBERS — LEFT WING
EVEN NUMBERS — RIGHT WING

GEOMETRY	WING	HORIZ	VERT	VERT FIN ON WING
AREA GROSS S FT²	10996.365	600.000	109.000	233.275 EA.
MAC (GROSS) $\bar{c}$ IN	1343.0684	254.964	194.124	310.560
AREA (REF) S FT²	9969.000	——	——	——
MAC (REF) $\bar{c}$ IN	1154.8625	——	——	——
AREA (EXPOSED) S FT²	——	441.0	——	——
SPAN b FT	137.7778	32.0	7.6	10.75
ASPECT RATIO (GROSS)	1.72627	1.707	.527	.495
ASPECT RATIO (REF)	1.90417	——	——	——
SWEEP ANGLE DEG	[illegible] 70.84	60.64	68.20	73.42
ROOT CHORD IN	2196.935	367.200	278.400	458.400
TIP CHORD IN	211.6667	82.80	66.00	62.40
ROOT T/C %	SEE FIG V-7	3.0	2.996	2.996
TIP T/C %	SEE FIG V-7	3.0	2.996	2.996
TAPER RATIO	——	.257	.237	.136
INCIDENCE DEG	——	——	——	—
DIHEDRAL DEG	——	-15.0	—	—
VOL. COEFF (GROSS) $\bar{V}$	——	.070	.01	.026
VOL. COEFF (REF) $\bar{V}$	——	.090	.012	.029

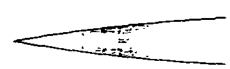

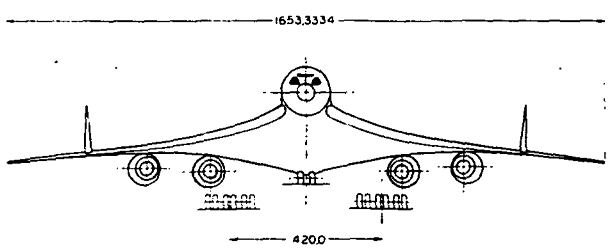

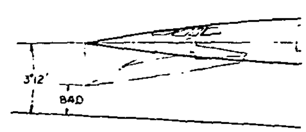

FOLDOUT FRAME

FOLD

TABLE V-I

REFERENCE CONFIGURATION GEOMETRIC CHARACTERISTICS

GEOMETRY	WING	HORIZ	VERT	VERT FIN ON WING
AREA (GROSS) S FT^2	10996.365	600.000	109.000	233.275 EA
MAC (GROSS) $\bar{C}$ IN	1343.0684	254.964	194.124	310.560
AREA (REF) S FT^2	9969.000	—	—	—
MAC (REF) $\bar{C}$ IN	1154.8625	—	—	—
AREA (EXPOSED) S FT^2	—	441.0	—	—
SPAN b FT	137.7778	32.0	7.6	10.75
ASPECT RATIO (GROSS)	1.72627	1.707	.527	.495
ASPECT RATIO (REF)	1.90417	—	—	—
SWEEP Λ_{LE} DEG	74.0; 70.84; 60.0	60.64	68.20	73.42
ROOT CHORD IN	2196.935	367.200	278.400	458.400
TIP CHORD IN	211.6667	82.80	66.00	62.40
ROOT T/C %	SEE FIG V-7	3.0	2.996	2.996
TIP T/C %	SEE FIG V-7	3.0	2.996	2.996
TAPER RATIO	—	.257	.237	.136
INCIDENCE DEG	—	—	—	—
DIHEDRAL DEG	—	-15.0	—	—
VOL COEFF (GROSS) $\bar{V}$	—	.070	.011	.026
VOL COEFF (REF) $\bar{V}$	—	.090	.012	.029

TOTAL AIRCRAFT TOGW MOMENT OF INERTIA	I_X, ROLL	I_Y, PITCH	I_Z, YAW
	105115×10^6	339028	471667
	LB. IN^2	LB. IN^2	LB. IN^2

TABLE V-II

REFERENCE CONFIGURATION WEIGHT SUMMARY

Item		Weight (lbs.)
Wing		83,347
Horizontal Tail		5,271
Vertical Tail		4,735
Canard		0
Fuselage		54,314
Landing Gear		28,965
Nacelle		19,015
Structure Total		(195,646)
Engines		59,832
Thrust Reversers		10,601
Miscellaneous Systems		1,780
Fuel System-Tanks and Plumbing		5,781
-Insulation		0
Propulsion Total		(77,994)
Surface Controls		9,981
Auxiliary Power		0
Instruments		3,400
Hydraulics		5,600
Electrical		5,050
Avionics		2,690
Furnishings and Equipment		25,111
Air Conditioning		8,200
Anti-icing		210
Systems and Equipment Total		(60,242)
Mfg and Certif Tolerance		0
Weight Empty		333,882
Crew and Baggage-Flight,		675
-Cabin,		1,640
Unusable Fuel		2,335
Engine Oil		795
Passenger Service		8,852
Cargo Containers		2,960
Adjustment for Computer Deviation		0
Operating Weight		351,139
Passengers,	(292)	48,180
Passenger Baggage		12,848
Cargo		0
Zero Fuel Weight		412,167
Mission Fuel		349,833
Design Gross Weight		762,000

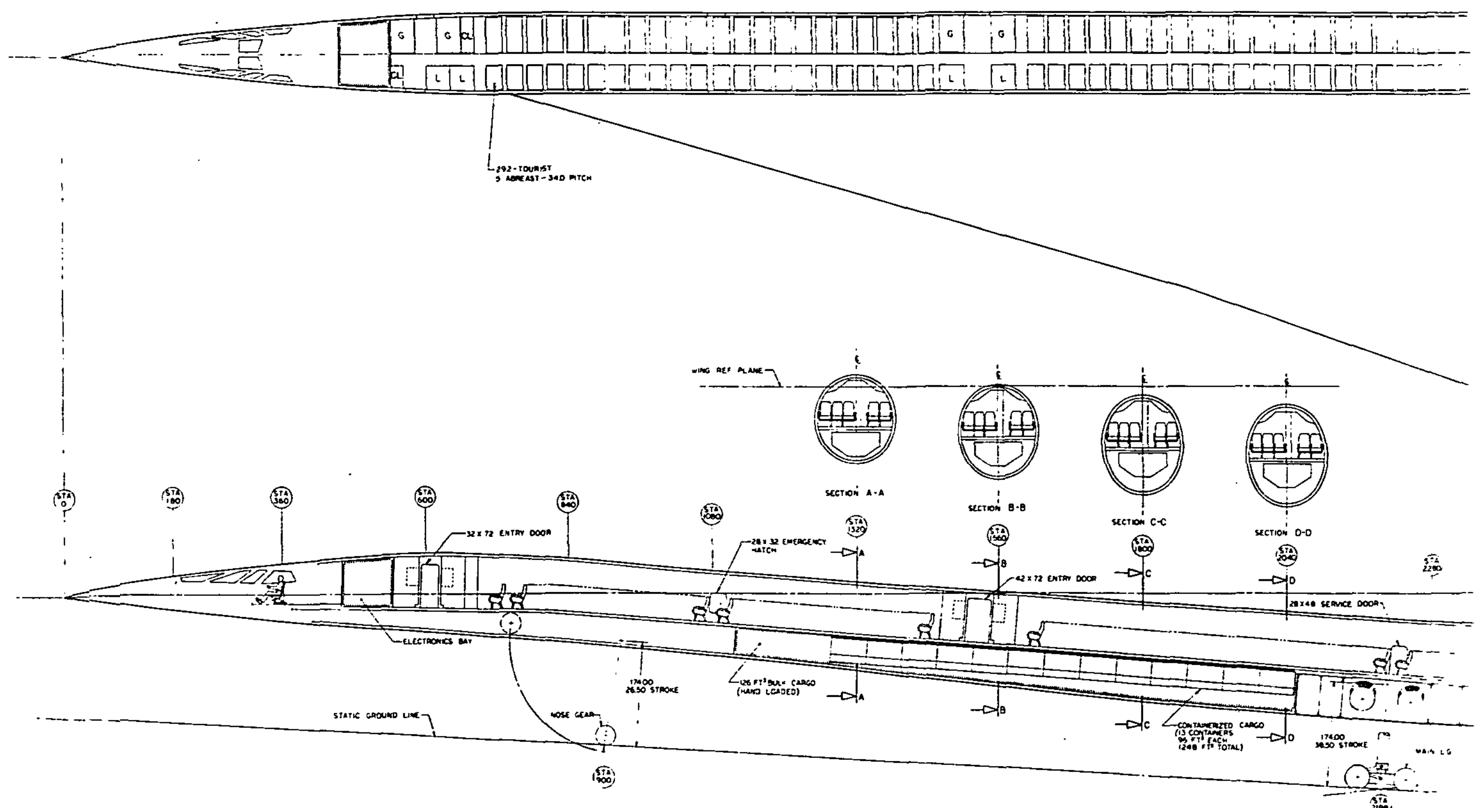

FOLDOUT FRAME 1

FOLDOUT FRAME 2

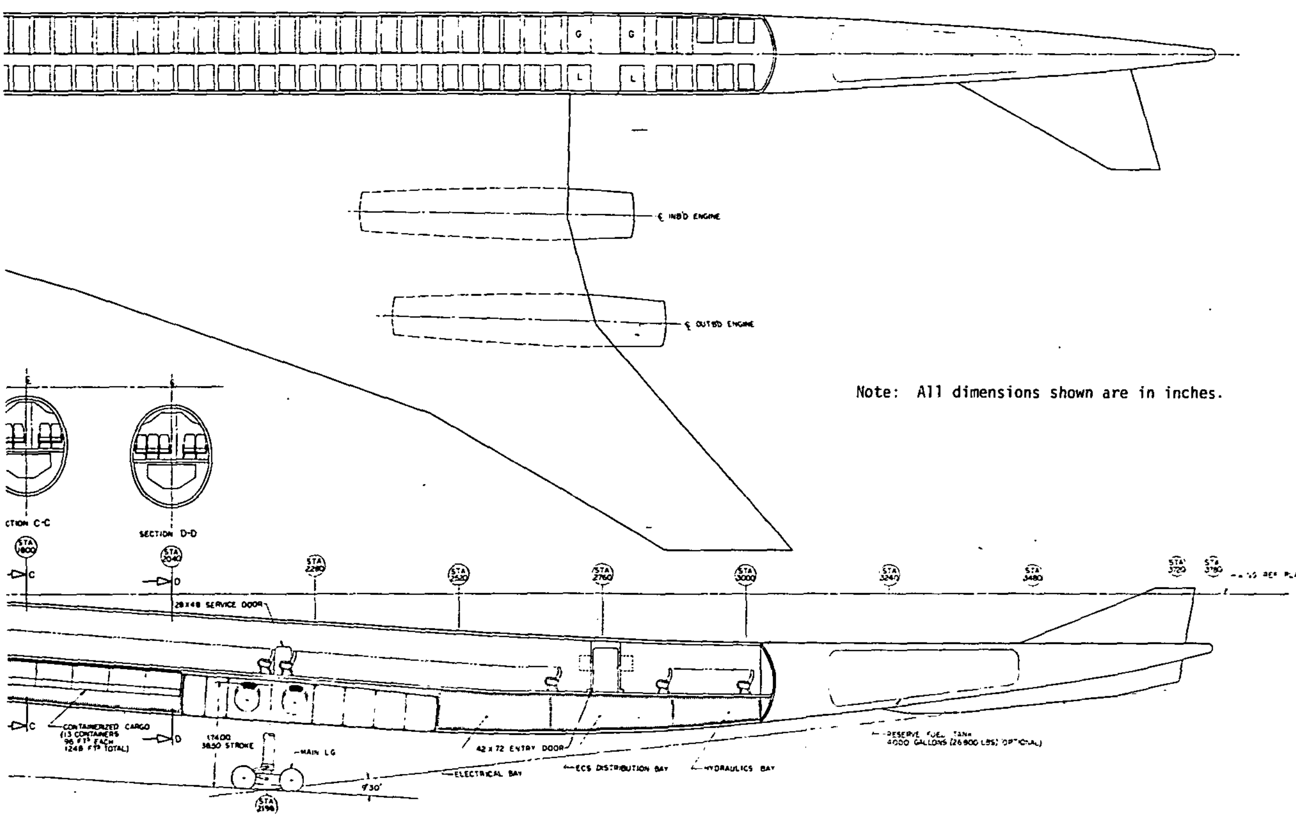

Note: All dimensions shown are in inches.

Figure V-3 - REFERENCE CONFIGURATION INBOARD PROFILE

SUMMARY

The Reference Configuration was derived from the Boeing 336C (reference V-1) and the application of results of further research conducted by the Langley Research Center. The Reference Configuration exhibits significant changes some of which are:

- °no canard
- °simplified leading edge devices
- °different wing planform & increased span
- °hard SAS with C.G. control through fuel management
- °longer fuselage
- °shorter landing gear
- °5 abreast seating
- °larger turbojet dry engines

A comparison of the planform of the two configurations is shown in Figure V-1.

The combination of longer fuselage and slightly larger diameter fuselage, while maintaining a smooth area distribution at Mach 2.7 cruise, provides an increase in payload from 234 passengers to 292 passengers. A comparison of the cross sectional area distribution at Mach 2.7 is shown in Figure V-10. The impact of the area distribution on the aerodynamic characteristics is discussed in more detail in Section VI-1B. In addition, the increased fuselage length provides sufficient room aft of the passenger compartment for an optional fuel tank of 4000 gallons capacity. This as well as the additional tanks in the forward wing section, shown in Figure V-6, could be used for more precise control of C.G. travel, or an increase in range under lower load factor conditions.

The locating of the wing forward in combination with a longer aft fuselage arm, to meet aft stability C.G. travel requirements, resulted in a further aft aircraft C.G. thereby permitting a shorter lighter main landing gear.

Wing geometry changes both in planform and thickness ratio has permitted stowing of the main landing gear in the wing and fuselage eliminating an external protuberance on the upper surface of the wing.

Configuration Development

Fuselage

The fuselage lines of the initial NASA derivative of the 336C configuration were based on a nominal 4 abreast seating with 58 rows of seats at 34 inch pitch all economy class (234 passengers). Because the rear spar of swept wing aircraft has considerably higher loads the floor height was based on maintaining the wing carry through structure at the depth of the rear beam. The rear beam has less depth than the front beam therefore resulting in a step in the forward box structure which could result in a significant weight penalty.

Examination of the initial fuselage constant section shows a fuselage outside moldline width of approximately 134 inches. This size of fuselage with its equivalent diameter is required to provide a smooth area distribution curve at Mach 2.7. Based on currently available commercial seats an additional four inches in fuselage width will provide a more desirable five abreast seating arrangement (292 passengers). A cross section of the constant section of the Reference Configuration aircraft is shown in Figure V-4.

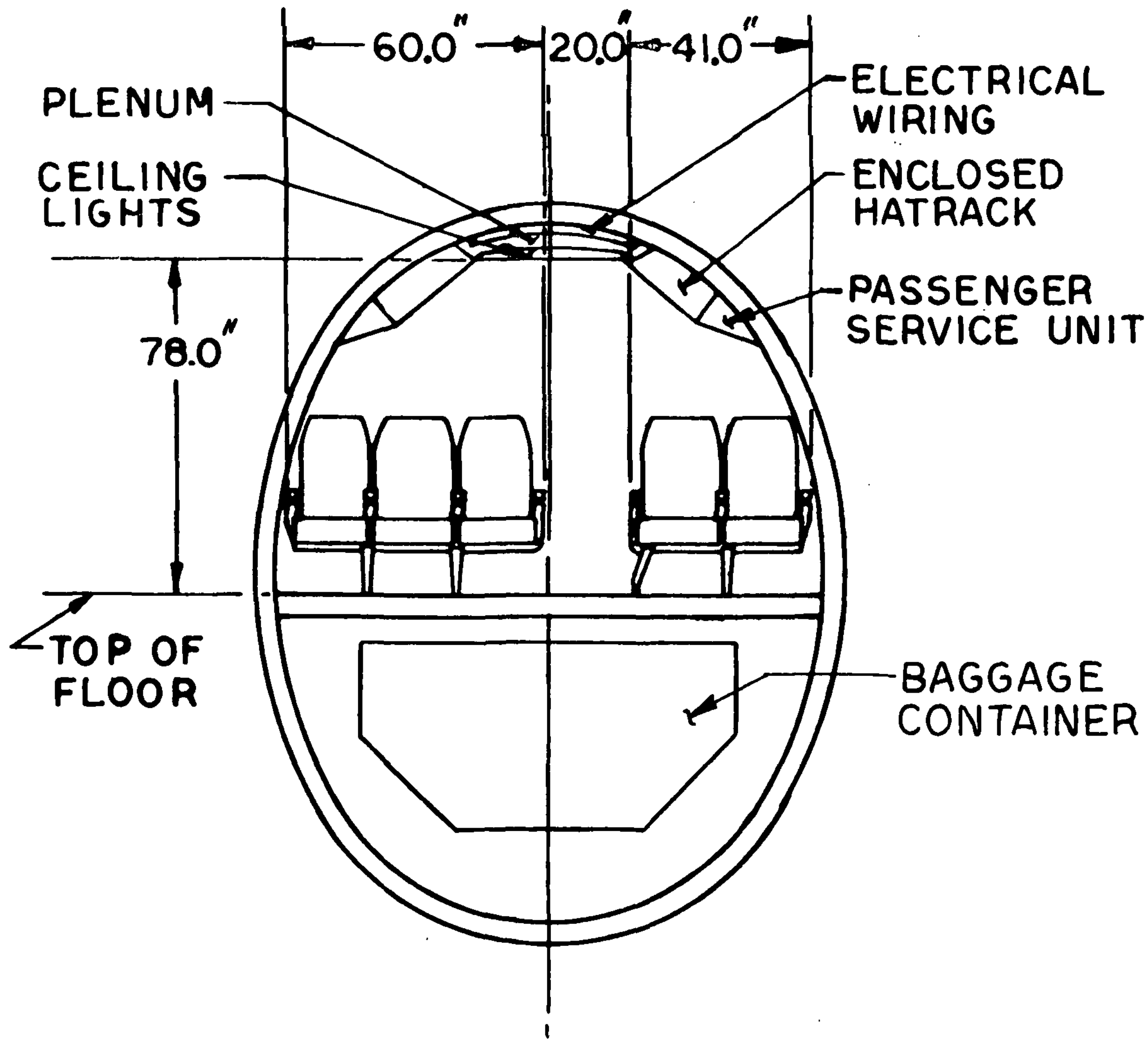

Figure V-4 TYP BODY SECTION REFERENCE CONFIGURATION

Floor location is based on a minimum 78 inch head height at the centerline of the aisle and maintaining a full depth front spar carry through structure for the wing box.

The increase in fuselage diameter and changes in wing thickness, to be discussed later, require an increase in aircraft length to maintain approximately the same overall aircraft fineness ratio. The fuselage was therefore increased from 297 feet for the initial baseline to 315 feet for the Reference Configuration. This additional length provides room aft of the passenger compartment for an optional fuel tank of 4000 gallons capacity. Providing a tank in this area will give a more precise control of aircraft center of gravity travel plus additional fuel for increased range.

Cargo volume below the floor is provided from the front spar forward to the nose landing gear. With the use of standard cargo containers, only 1650 cubic feet is utilized of the available 3370 cubic feet.

Landing Gear

It will be demonstrated that this aircraft could be flown under relaxed static stability requirements (Reference Section VI-2). Under these conditions, the Reference airplane geometry could be configured to move the C.G. to approximately 60% of the MAC as opposed to the Boeing 969-336C location of approximately 50% of the MAC. Since the main landing gear location is a function of C.G. position, this requires the landing gear to move aft. For the same flare angle, the length of the gear strut can be shortened and consequently results in a significant reduction in landing gear weight.

The initial NASA 336 derivative configuration main landing gear was a two strut gear with 12 wheels per strut and the tire size required for present airport runway and taxiway compatibility. This gear retracted forward into the wing; however, the wing was too thin to completely house the assembly. A protuberance was required on either the upper or lower wing surface to enclose the tires thereby adding additional drag to the cruise performance. Also, by moving the gear aft and retracting forward on this configuration a large portion of the wing structural box would be effected causing an additional weight penalty.

Studies indicate that the same type two post landing gear can be used and any upper or lower wing surface protuberance could be eliminated by retracting the gear inboard, partially into the fuselage and wing. This requires increasing the thickness slightly of the inboard portion of the wing and moving the maximum thickness point aft on the wing section. The housing of the landing gear in this manner would minimize performance and weight penalties.

In this landing gear system, each strut has a single boagie truck comprised of twelve (12) 40 x 13-20 tires. A schematic of the landing gear enclosure is shown in Figure V-5. A multi-spar concept surrounding the landing gear cutout provides a reduced weight structure for this configuration. A structural diagram of the aircraft is shown in Figure V-6.

Wing

The wing definition for the Reference Configuration is the result of aerodynamic considerations and a solution to the landing gear stowage

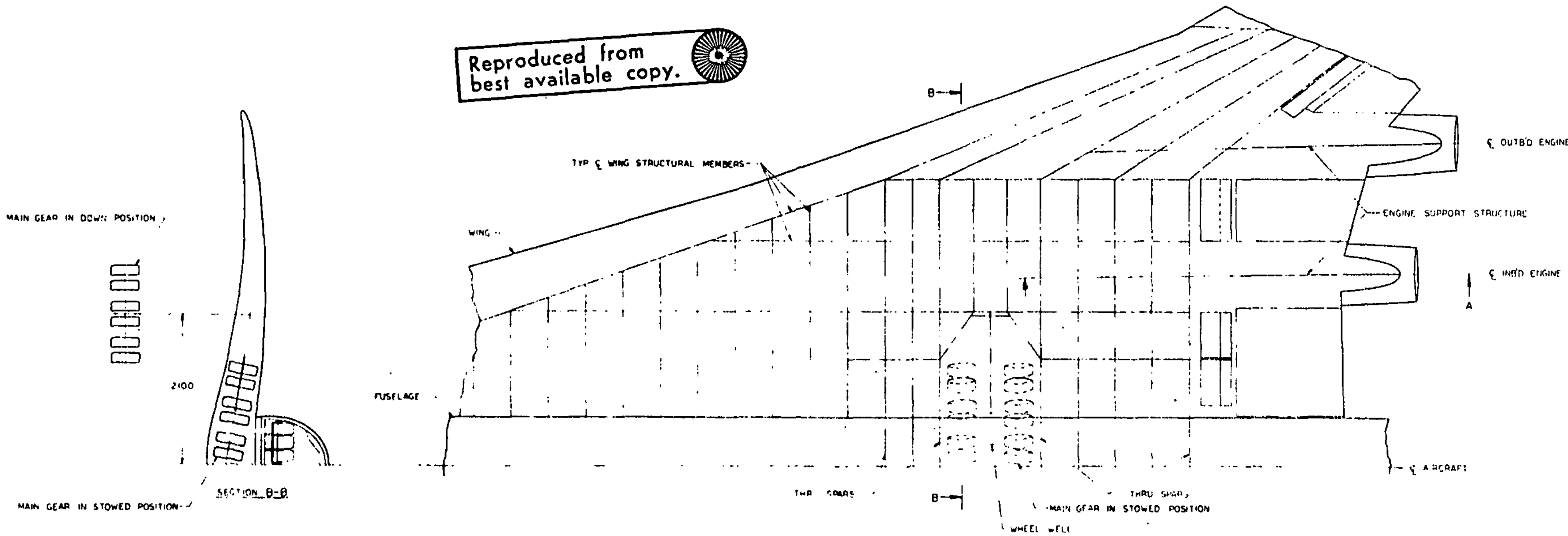

Note: All dimensions shown are in inches.

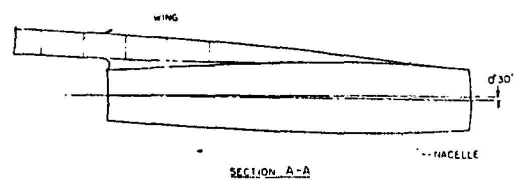

Figure V-5 - Wing Interface to M.L.G. and Engine Nacelles

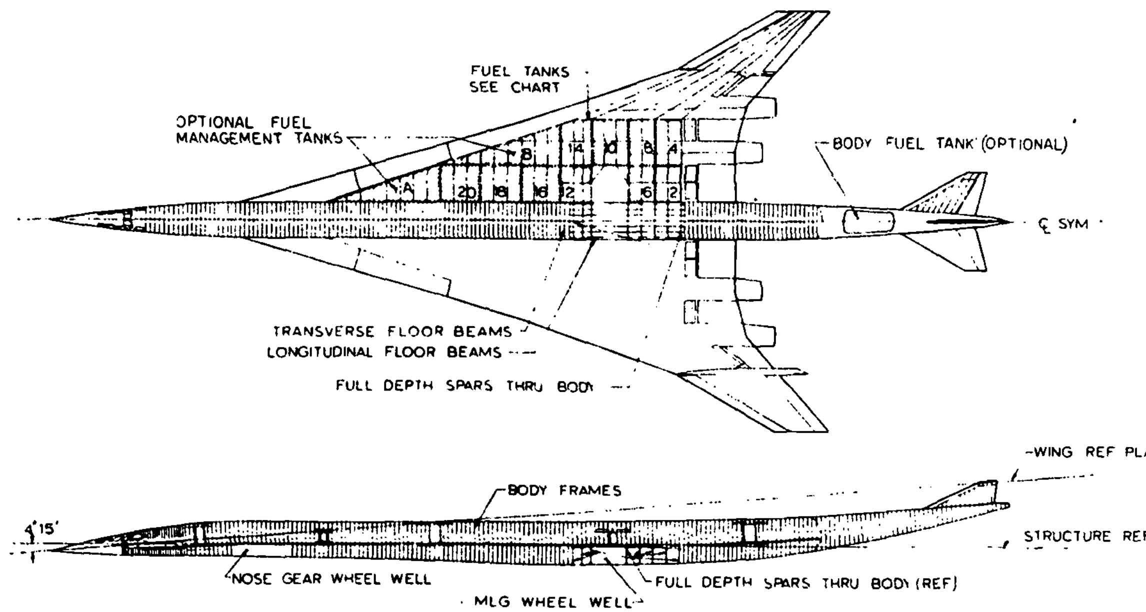

FUEL TANKS	
TANK NO	VOLUME FT³
1	306
2	306
3	241
4	241
5	383
6	383
7	273
8	273
9	371
10	371
11	456
12	456
13	311
14	311
15	562
16	562
17	536
18	536
19	510
20	510
BODY	539
A	700 EA WING
B	500 EA WING

ODD NUMBERS — LEFT WING
EVEN NUMBERS — RIGHT WING

Figure V-6 — REFERENCE CONFIGURATION STRUCTURAL DIAGRAM problem. As noted above the inboard portion of the wing was increased in depth and the maximum thickness was moved aft. A plot of the wing thickness and t/c ratio for the Reference Configuration is shown in Figure V-7. A comparison of the rear beam depth of the initial NASA derivative configuration and the Reference Configuration is shown in Figure V-8. It can be seen that an average increase of 45% in rear beam depth is achieved from the inboard nacelle into the side of the fuselage. This results in weight savings for the same loading condition. No change was made in the wing thickness from wing station 400 to the tip.

Ten separate fuel tanks plus two optional tanks are provided in each wing. The ten main tanks provide for a total of 349,830 pounds of fuel. The two optional tanks provide an additional volume for 109,220 pounds of fuel. The location and capacity of each tank is shown on the structural diagram Figure V-6. Although not shown on the inboard profile, Figure V-3, additional fuel volume is available in the center wing box below the fuselage floor. With the use of bladder type tanks in this area an additional volume is available for 45,665 pounds of fuel. However, the structural weight increase associated with this installation was not considered in this study.

Engine Nacelle

The boundary layer splitter at the forward end of each nacelle is faired out at a point slightly aft of the mid-point of the nacelle length. From this point the nacelle is faired into the wing lower surface aft to the trailing edge where the wing upper surface is blended into the nacelle upper moldline. Figure V-9 is an illustration of the wing to nacelle aft fairing.

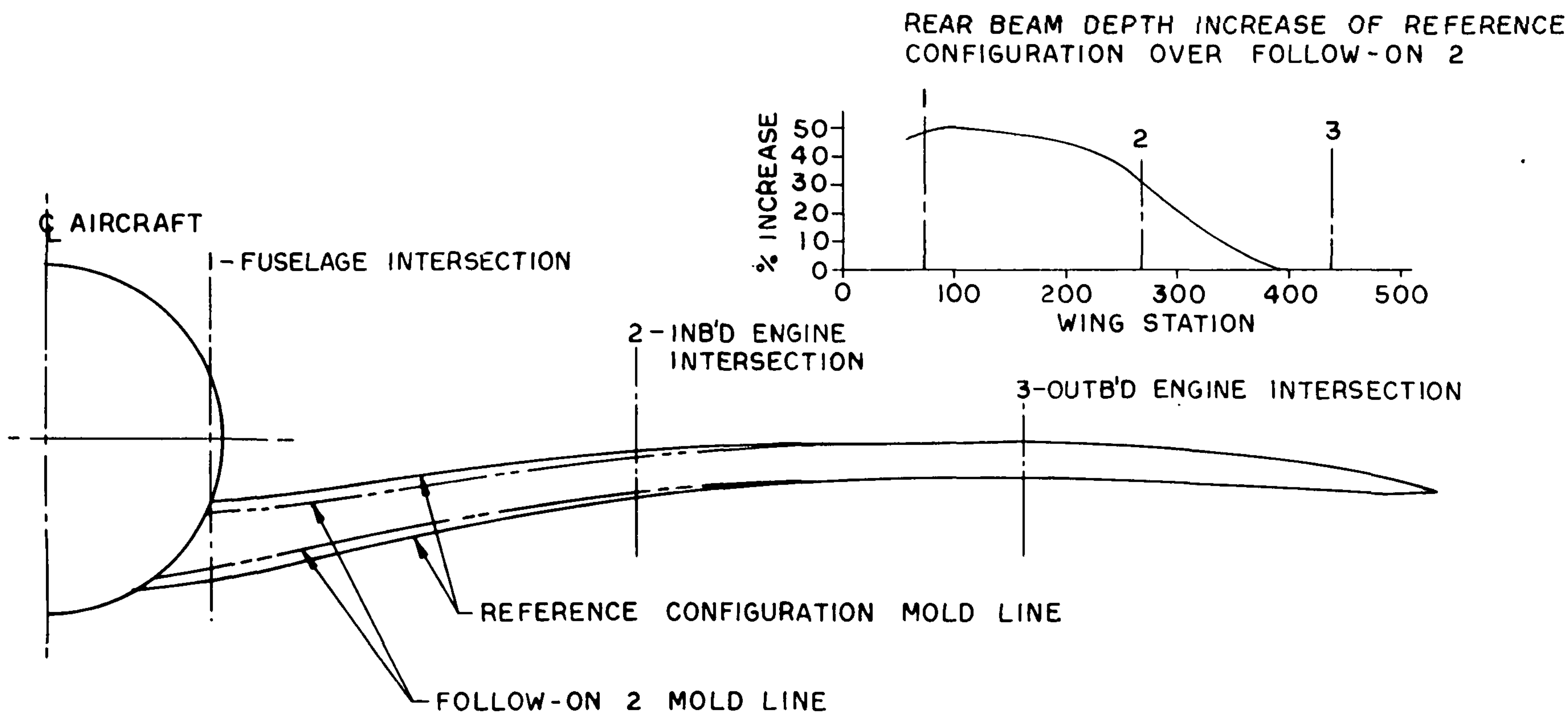

Figure V-8 WING REAR SPAR DEPTH COMPARISON

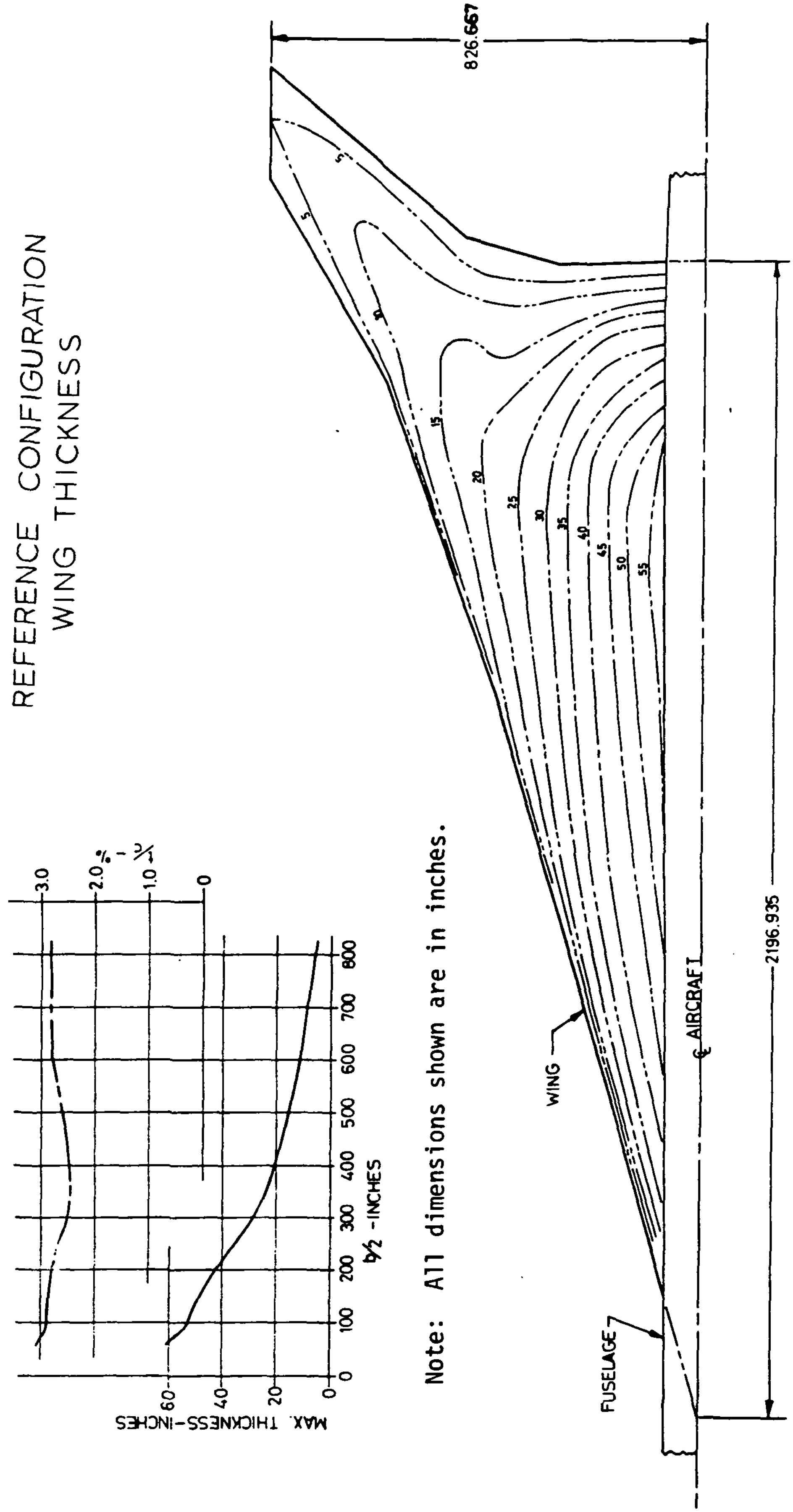
REFERENCE CONFIGURATION
WING THICKNESS
826.667
2196.935
WING
FUSELAGE
℄ AIRCRAFT
5
10
15
20
25
30
35
40
45
50
55
MAX. THICKNESS-INCHES
b/2 -INCHES
t/c - %
0
20
40
60
100
200
300
400
500
600
700
800
1.0
2.0
3.0
Note: All dimensions shown are in inches.

Figure V-7

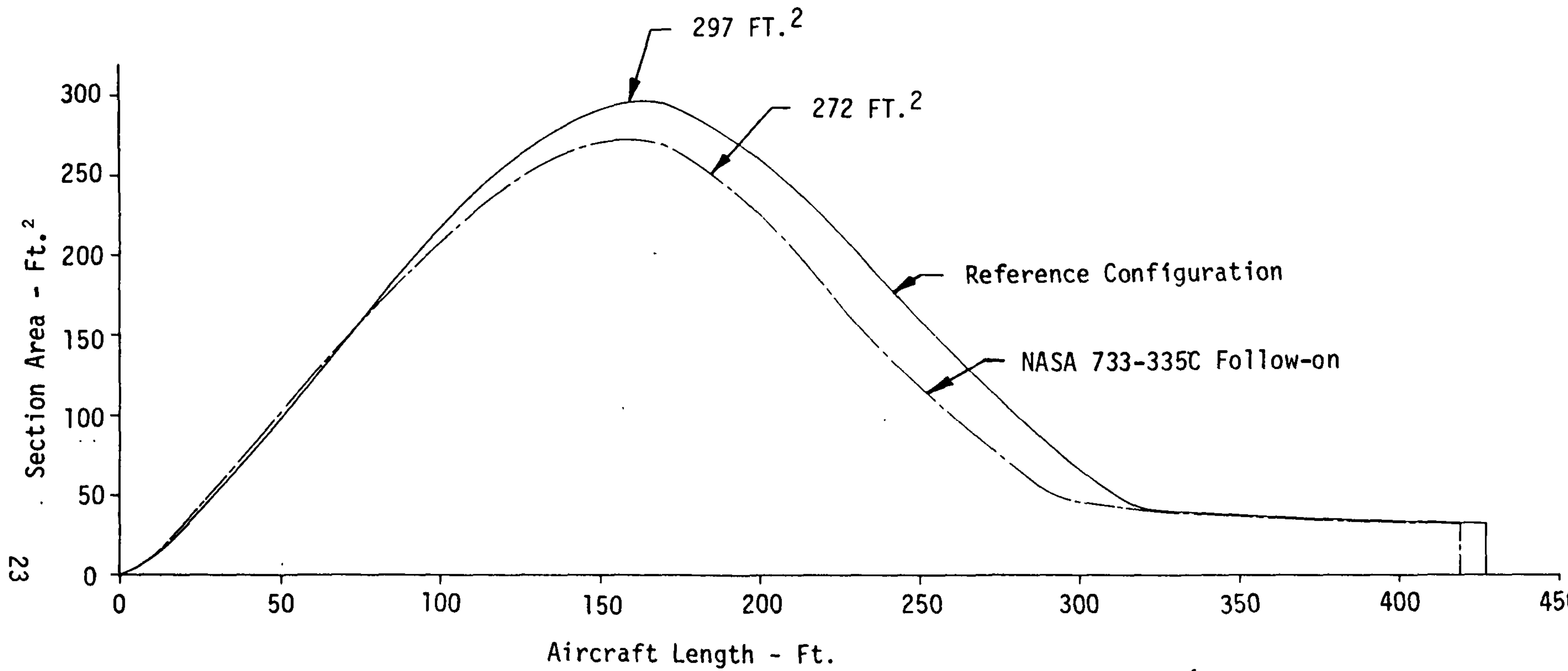

Figure V-10 - Equivalent Area Distribution Comparison at Cruise M 2.7

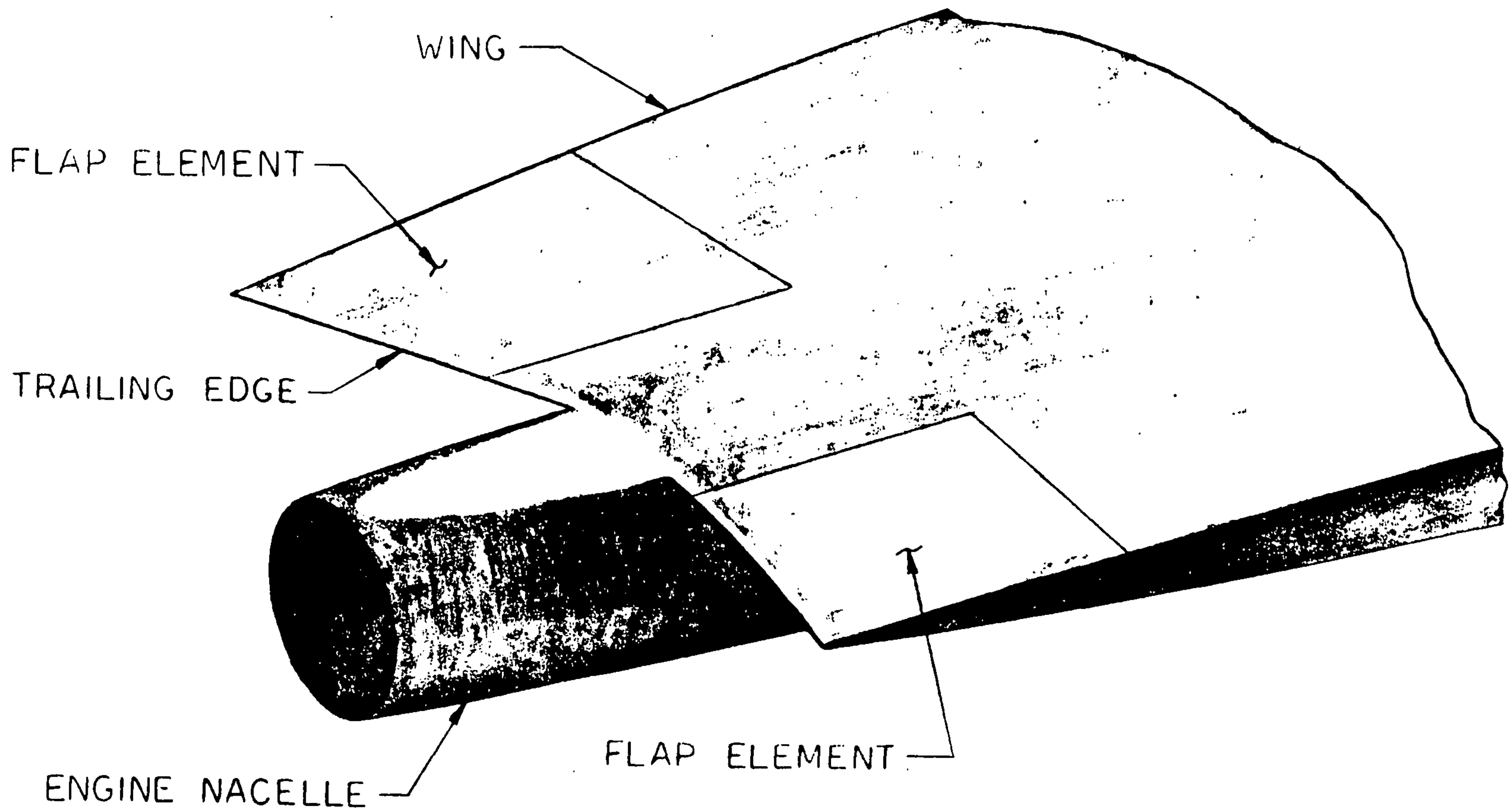

Figure V-9 WING TO NACELLE AFT FAIRING

LIST OF FIGURES

REFERENCES

Reference No.	Title
V-1	The Boeing Co.; "Mach 2.7 Fixed Wing SST Model 969-336C (SCAT-15F), Document No. D6A-11666-1, dated November 1969.

LIST OF TABLES

SECTION VI

REFERENCE CONFIGURATION CHARACTERISTICS

VI-1 AERODYNAMICS

A. LOW SPEED AERODYNAMICS

INTRODUCTION

This section presents the derivation of the low speed aerodynamic characteristics for the Reference Configuration during take-off and landing conditions. These aerodynamic characteristics were developed from unpublished data (References VI-1A-1, -2, -3, -5, -8) obtained in the LRC 7x10 high speed wind tunnel. A layout of the Reference Configuration is shown in Figure V-2. The wind tunnel models employed as a basis for estimating the aerodynamic characteristics had the same wing planform, but different wing trailing-edge-flap geometry and deflections, and a different horizontal tail size. The effects of these different control surfaces on the aerodynamic characteristics are analyzed and presented. The influence of the ground on the aerodynamic characteristics are also analyzed for this low aspect ratio wing configuration. The equations and procedures are developed to predict ground induced lift, drag, moment, and downwash, which include effects of changes in planform, flap, and/or tail configurations. Experimental test data of ground effect on aerodynamic characteristics are analyzed to determine the significant parameters. Combining this data with image method theory for the wing leads to accurate generalized expressions for lift, drag, moment, and downwash.

The full scale airplane lift and drag characteristics are then developed for use in the take-off and landing performance analysis.

SUMMARY

Take-off and Landing Characteristics

During take-off, the airplane center of gravity (C.G.) is located at its most forward position which is 0.575 MAC (see Section VI-4). For take-off the three inboard wing trailing-edge flaps (t_1, t_2, t_3 Figure V-2) were deflected down 20 degrees and the outboard trailing-edge flap t_4 was deflected down 5 degrees. The wing leading-edge flaps L_1, L_2, and L_6 were deflected down 30, 30, and 60 degrees respectively. The take-off aerodynamic characteristics are presented in Figures VI-1A-1 through VI-1A-8. The specific L/D and C_L's during take-off are presented in the Noise Section (Section VI-5).

During landing the airplane C.G. is located at its most aft position which is 0.597 MAC (Section VI-3). Thus the trimmed aerodynamic characteristics are different than those used for the take-off condition. The leading and trailing-edge flap deflections are the same as those used in the take-off condition. The aerodynamic characteristics during the landing condition are shown in Figures VI-1A-9 through VI-1A-13. The effect of the landing gear and spoilers during the ground roll are presented in paragraph 4(Analysis of Landing Gear and Spoilers)of this section.

The ground effect equation (Eq. 5 and 7) used for predicting the lift of the arrow wing, is derived by combining generalized ground image theory with experimental data results. This lift ground factor with ground height measured to 1/3 the distance aft of the aerodynamic center on the MAC is independent of angle of attack, planform shape, and how the lift is generated. The lift performance near ground is directly the product of the ground factor and the lift performance away from ground.

The arrow wing pitching moment change near ground is given in Figure VI-1A-32 which can be used with Eq. (13) to predict changes due to large tail configuration changes. The drag change is given in Figure VI-1A-33 which can be used with Eq. (20) to predict changes due to large flap configuration changes.

Included is a method for predicting lift due to flap configuration changes (Eq. 23). These changes include sizing, span location on wing, and chord extent.

1. <u>Aerodynamic Control Surface Characteristics</u>

The summary aerodynamic characteristics of the Reference Configuration have been presented. The individual aerodynamic characteristics of the various control surfaces are discussed in detail in this section. These include the wing trailing edge flaps, the wing leading edge flaps, the horizontal tail, and the outboard vertical fins.

Wing Trailing Edge Flaps

Because the summary lift and drag characteristics were derived from Reference VI-1A-2 model test data which had varied the deflection of the two inboard flaps (t_1, t_2) only, it was necessary to estimate the effect of the different wing trailing edge geometry and flap deflections on lift and drag. The Reference Configuration has three inboard trailing edge flaps (t_1, t_2, t_3) all deflected at 20°, 13.3°, or 5° and the outboard trailing edge flap (t_4) deflected at 5°. The change in drag coefficients associated with changing these flap angles from the Reference VI-1A-2 model test is shown on Figure VI-1A-14. The incremental change in lift due to change in flap deflection angle for the Reference Configuration is shown on Figure VI-1A-15.

The effect of trailing edge flaps on lift and drag was ascertained by adjusting unpublished test data (Reference VI-1A-2) using the procedures described below. The variation of C_L with flap deflection angle was determined at several angles of attack for the two inboard flaps of the test model (Reference VI-1A-2). It was found that the angle of attack had negligible effect on the lift increment associated with the flap deflection. Figure VI-1A-15 presents this variation of C_L with flap angle for the two inboard flaps of the Reference VI-1A-2 test model. Also shown on Figure VI-1A-15 is the variation of incremental change in lift with flap angle for the three inboard flaps of the Reference Configuration. This curve was obtained by correcting the Reference VI-1A-2 lift curve for flap chord to wing chord ratio, flap span to wing span ratio, flap span location, and the ratio of model wing area to wing reference area for the Reference Configuration.

The lift due to small configuration changes in the flap system can be predicted by ratioing unknown to known flap data.

If flap (a) differs in size and location from flap (b), its lift can be estimated from the ratio (with same δ):

$$\frac{C_{L_{fa}}}{C_{L_{fb}}} = \frac{\sum_{i=1}^{M_o} (1 - \eta_{av_{ai}})\, \Delta\eta_{a_i} \frac{\sigma_{a_i}}{1 + 3\sigma_{a_i}}}{\sum_{i=1}^{M_1} (1 - \eta_{av_{bi}})\, \Delta\eta_{b_i} \frac{\sigma_{b_i}}{1 + 3\sigma_{b_i}}} \qquad \text{Equation (1)}$$

Where: The summation is of individual flap segments along the span.

η = $2Y/b$

η_{av} = spanwise midpoint of flap segment

$\Delta\eta$ = spanwise span of flap segment

σ = flap chord ratio c_f/c of flap segment

For example, if flap (b) extends from $.2 \leq \eta \leq .3$ and σ_b is .10; while flap (a) extends from $.2 \leq \eta \leq .5$ and σ_a is .20; then the lift ratio is:

$$\frac{C_{L_{fa}}}{C_{L_{fb}}} \quad \frac{(.65)(.3)(.2/1.6)}{(.75)(.1)(.1/1.3)} = 4.22$$

It can be seen that the area of flap (a) is 6 times larger than that of flap (b) but the lift is 4.22 times larger.

It should be noted that for the two inboard flaps (t_1, t_2) of the Reference VI-1A-2 test model, the combined flap lift factor is 0.02346; whereas for the three trailing edge flaps of the Reference Configuration the combined flap lift factor is 0.02221. In addition to this flap lift factor the ratio of the wing gross area to the wing reference area for the two configurations must be included in the analysis. From these factors the lift curve presented in Figure VI-1A-15 for the three inboard flaps of the Reference Configuration was obtained.

Figure VI-1A-16 presents the variation of incremental change in drag coefficient with flap deflection angle and angle of attack for the two inboard flaps (t_1, t_2) of the Reference VI-1A-2 test model. In order to obtain the flap drag of the Reference Configuration from the flap drag of the reference test model, an analysis was made to determine the effectiveness of the induced drag associated with the induced lift. The drag of the wing with a flap was represented by the following equation:

$$C_{D_{wing+flap}} = C_{D_\circ} + K_\circ C_{L_{wing}}^2 + K_1 C_{L_{wing}} C_{L_{flap}} + K_2 C_{L_{flap}}^2 \qquad \text{Equation (2)}$$

If the flap deflection angle is altered, the total drag will change because of the change in lift.

$$C_{D_{wing+new\ flap}} = C_{D_\circ} + K_\circ C_{L_{wing}}^2 + K_1 C_{L_{wing}} C_{L_{newflap}} + K_2 C_{L_{newflap}}^2$$

The difference between the two drag values can be found as a function of flap lift as follows:

$$C_{D_{wing+new\ flap}} - C_{D_{wing+flap}} = K_1 C_{L_{wing}} (C_{L_{newflap}} - C_{L_{flap}}) + K_2 (C_{L^2_{newflap}} - C_{L^2_{flap}})$$

Let $K_1 C_{L_{wing}} = K_1$ (a new constant)

Let $C_{D_{wing+newflap}} - C_{D_{wing+flap}} = \Delta C_{D_{flap}}$

$$\Delta C_{D_{flap}} = K_1 (C_{L_{newflap}} - C_{L_{flap}}) + K_2 (C_{L^2_{newflap}} - C_{L^2_{flap}})$$

Equation (3)

Using this equation and the flap deflection drags and lifts from the Reference VI-1A-2 test model presented in Figures VI-1A-15 and -16 the value of K_1 and K_2 were determined for a particular change in flap angle and at a selected angle of attack. Using these same constants and the lift curve (Figure VI-1A-15) of the Reference Configuration, the incremental change in drag associated with change in flap lift and angle of attack was determined for three flap deflection angles.

It should be noted that the techniques described above were also employed to define the incremental change in the lift and drag associated with changing the outboard flap (t_4) deflection angle from 0 degrees for Reference VI-1A-1 test model to 5 degrees on the Reference Configuration. The variation of drag changes with angle of attack shown on Figure VI-1A-14 include both the three inboard flaps and the outboard flap. Similarly Figure VI-1A-15 show the change in lift associated with changing the deflection angles of the three inboard trailing edge flaps (t_1, t_2, t_3) of the Reference Configuration.

Wing Leading Edge Flaps

The leading edge flap settings of Reference VI-1A-1 model test data are the same as the Reference Configuration leading edge flap settings (L_1, L_2 = 30°, L_3, L_4, L_5 = 0°, L_6 = 60°). Therefore, no analysis was conducted on the effect of wing leading edge flap settings on the lift and drag characteristics of the Reference Configuration. The effect of wing leading edge flaps on lift and drag is presented in Reference VI-1A-3. The data of Reference VI-1A-4 would suggest that a correction should be applied to the low Reynolds number wind tunnel test data for leading edge suction effects when correcting to full scale conditions; however, no correction has been applied in this analysis.

Horizontal Tail and Elevator

The summary drag polars and L/D curves of the Reference Configuration are presented in Figures VI-1A-1 through VI-1A-13 and include the trim effects associated with tail incidence angle.

The variation of the incremental change in lift with tail incidence angle for the Reference Configuration is shown as the solid line on Figure VI-1A-17. This was obtained from analysis of Reference VI-1A-2 model test data (dashed line shown on Figure VI-1A-17) with corrections made to account for changes in the ratio of tail area to reference area. It should be noted that the angle of attack had very little effect on the tail lift characteristics. A change in wing trailing edge flap angle from 15 to 20 degrees was found to have little effect on the tail lift characteristics.

Figure VI-1A-18 shows the effect of tail incidence angle on the incremental changes in drag for the Reference VI-1A-2 test model. As the angle of attack increases the incremental change in drag associated with the tail incidence angle decreases. Although not shown on Figure VI-1A-19, as the wing inboard trailing edge flaps change from 20 degrees to 15 degrees, the incremental change in drag decreases slightly for tail incidence angles greater than 10 degrees. However, for this analysis, the effect of flap angle on tail drag was not included; therefore, the summary drag polars for the 5 degree flap case are slightly conservative. The drag associated with tail incidence is shown in Figure VI-1A-18.

In addition to the analysis of the lift and drag associated with tail incidence, the Reference VI-1A-2 data was evaluated to determine the effect of elevator deflection on lift and drag. This data is shown in Figures VI-1A-19 and VI-1A-20.

The variation of tail incidence angle with angle of attack was determined for three wing trailing edge flap settings for the C.G. located at 0.575 MAC, and is presented as Figure VI-1A-21. Figure VI-1A-22 shows the variation of tail incidence angle with angle of attack for the C.G. positioned at 0.597 MAC at trailing edge flap settings of 5 degrees and 20 degrees respectively. Figures VI-1A-23 and VI-1A-24 present the variation with angle of attack of incremental change in lift and the incremental change in drag respectively of the Reference Configuration with wing trailing edge flap deflections of 20 degrees at the C.G. position of 0.575 MAC.

Outboard Vertical Tail Fins

The outboard vertical tail fins were added to the Reference Configuration (Figure V-2) to increase the directional stability during cruise. At low speeds and high angle of attack while there is no effect on lift there is a drag penalty associated with the addition of the two outboard vertical tail fins. See model test data (Reference VI-1A-1) and Figure VI-1A-25.

Skin Friction Effects

The drag polars of the Reference Configuration were derived from the Reference VI-1A-1 data which includes the skin friction drag associated with the 0.03 scale model without outboard vertical fins. At Mach 0.2 the skin friction of the Reference VI-1A-1 model was 0.0113 whereas the skin friction of the full scale Reference Configuration with vertical tails was found to be 0.0068. The effect of the test model boundary layer transition strips on the skin friction were not accounted for in this analysis.

Aerodynamic Characteristics in Ground Effect

The Reference Configuration flying near ground is in a flow field which is displaced upwards since the flow cannot penetrate the ground. The condition of zero normal flow at the ground surface and the flow about the aircraft at h height from ground is duplicated by an inverted image of the aircraft at the same height below the ground. This image method representation simplifies the potential flow solution for the aircraft near the ground. Near the ground the wing floats on a layer of pressured air and high velocities over the wing are not necessary for high lift. This pressured air on the lower surface also contributes to drag which at some angle of attack can exceed the reduction in induced drag due to ground induced upwash.

The objective is to predict ground induced increments in lift, drag, moment, and downwash, which include effects of changes in planform, flap, and/or tail configuration. Experimental test data of ground effect on the aerodynamic characteristics can be analyzed to determine significant parameters. Combining this data with image method theory for the wing, leads to accurate generalized expressions for lift, drag, moment, and downwash. This combination of analytical development with experimental data takes into account the complicated flow field described above. The lift due to the aircraft near ground can be expressed as the product of a lift ground factor and the lift of the aircraft away from ground. For a constant aspect ratio this factor is relatively independent of how the lift is generated, by angle of attack, flaps, or planform change.

Near ground test data of an arrow winged aircraft is available in unpublished form in Reference VI-1A-5. Low aspect ratio wing ground effect analysis based on theory, experiment, and image method theory is derived in Reference VI-1A-6.

Development

The ratio of lift coefficient near ground to lift coefficient away from ground is defined as a lift ground factor. If height h from ground is measured to the wing leading edge, then as angle of attack α is increased the ground factor will increase since most of the wing is then nearer the ground. Similarly, if h is measured to the wing trailing edge, the ground factor will decrease with α. There is, thus, some rotation point on the wing chord for which the ground factor is relatively independent of α. The rotation point at mid-chord in effect results in an averaged height from ground. For a two-dimensional wing section, the mid-chord is the same as $X_{ac} + (1/3)(\bar{c} - X_{ac})$ where the aerodynamic center is at $X_{ac} = \bar{c}/4$. For a delta wing, $X_{ac} = \bar{c}/2$, then $h_\circ$ is taken at 2/3 mean aerodynamic chord aft of the leading edge of the mean aerodynamic chord.

Experimental lift ground factors evaluated from Reference VI-1A-5 data are presented in Figure VI-1A-26. These values were measured with h taken at .435 $\bar{c}$. These h values are changed to $h_\circ$ values by the relation, $h_\circ/b = (h/b)_{.435\bar{c}} - .0034\alpha°$.

With this transformation, the experimental data approach a curve as shown with high scale in Figure VI-1A-26. These data follow a reciprocal function of the form

$$\frac{C_{L_g}}{C_L} = 1 + \frac{a_o}{(a_1 + h_\circ/b)^2} \qquad \text{Equation (4)}$$

The constants are evaluated by simultaneous solution from two values of the experimental fairing. The resulting function is given by Equation (5) and is plotted in Figure VI-1A-26.

Empirical formula (A = 1.62):

$$\frac{C_{L_g}}{C_L} = 1 + \frac{.01}{(.045 + h_\circ/b)^2} \qquad \text{Equation (5)}$$

Theory of the aerodynamics of a blown (and unblown) wing near ground is developed in Reference VI-1A-6 for the wing of arbitrary planform and the jet of arbitrary cross-section. The theory is based on the ground image system as shown in Sketch a. It can be seen that the trailing vortex

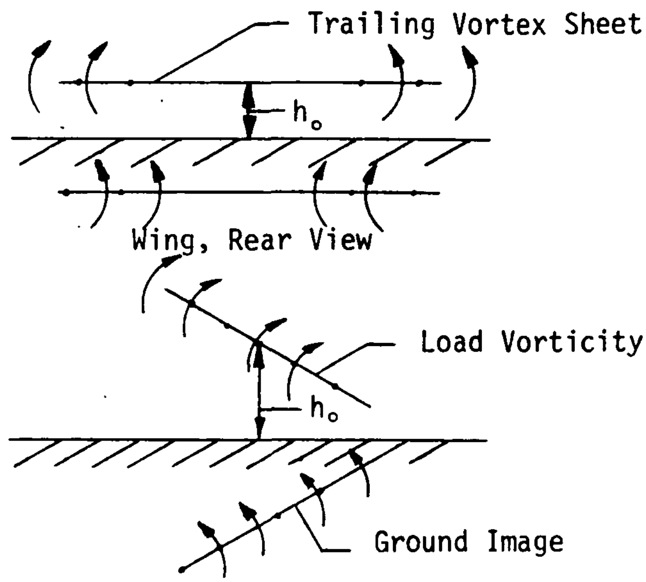

SKETCH a. - Ground Image System of Wing.

sheet induces an upwash at the wing while the load vorticity induces downwash ahead and forward on the wing and upwash aft on the wing. Applying vortex laws the induced upwash and lift can be determined. Following the procedure of Reference VI-1A-6, a simplified version for the wing near ground can be made:

For $A \to 0$

$$\frac{C_{L_g}}{C_L} = 1 + \frac{1}{(1/2) + 32(h_o/b)^2 + 4(h_o/b)[1 + 32(h_o/b)^2]^{1/2}}$$

Equation (6)

The same function is obtained for $A \to \infty$ except that the variable is height per unit chord, h/c. Therefore, the effect of aspect ratio is simply the changing of b to c as aspect ratio increases. This is obtained by factoring b by the assumed function $(k^2 + A)(k + A)^2$ where k is a constant. In Equation (7), k = 6, and Equation (7) correlates accurately with the data of the arrow wing aircraft given in Figure VI-1A-26.

$$\sigma_L = \frac{C_{L_g}}{C_L} = 1 + \frac{1}{\frac{1}{2} + 32\left(\frac{h_o}{b}\right)^2 \frac{(6 + A)^4}{(36 + A)^2} + 4\,\frac{h_o}{b}\,\frac{(6 + A)^2}{36 + A}\left[1 + 32\left(\frac{h_o}{b}\right)^2 \frac{(6 + A)^4}{(36 + A)^2}\right]^{1/2}}$$

Equation (7)

Equation (7) is independent of planform shape and twist or camber, or in effect, the ground factor is independent of how the lift was generated. For a finite aspect ratio, the shape of the surface pressure distribution has some effect on the ground factor. However, vortex theory shows that induced velocities depend on total lift and independent of loading distribution as distance increases. The distance to the ground image is twice times h_o. In general, with $(k^2 + A)/(k + A)^2$ factoring h_o/b, Equation (7) applies to arbitrary aircraft configurations where k is evaluated from data of an aircraft of similar wing planform. For an arrow wing airplane with small flap deflection, k = 6. For other wing planforms k is near 6.

Reference VI-1A-5 ground effect experimental data of pitching moment and drag was analyzed for significant parameters.

The longitudinal loading changes on a wing due to ground proximity can be estimated directly from flow logic. The ground induces a vertical velocity along the wing chord. This vertical velocity varies approximately linearly with x, being a downwash ahead of the wing and linearly progressing to an upwash behind the wing. For an airfoil section a linearly varying upwash induces a positive symmetric camber. The symmetric camber has a center of pressure at midchord which is the same as 1/3 of the distance from wing aerodynamic center to wing trailing edge, that is it is the same as x_o. The lift proportion induced by ground effect acts at this center of pressure, that is at x_o. This change in chordwise loading distribution results in a change in pitching moment due to ground effect. Then in equation form the pitching moment due to ground effect is approximated as

$$C_{m_g} = C_m - C_L(\sigma_L - 1)\left[\frac{x_o}{\bar{c}} + \frac{C_m}{C_L} - \frac{X_{cg}}{\bar{c}}\right] f(h_o) \qquad \text{Equation (8)}$$

where C_{m_g} is pitching moment coefficient about x_{cg} near ground; C_m is the value away from ground, σ_L is lift ground factor of Eq. (7); and $f(h_o)$ is a secondary function near unity. Statistically analyzing the arrow wing aircraft experimental data of Reference VI-1A-5 results in the function: $f(h_o) = \tanh[6.5\,(1 + \sin\alpha)\,h_o/b]$. A correlation plot of Eq. (8) with data of Reference VI-1A-5 is shown in Figure VI-1A-27.

Away from ground the drag can be expressed as

$$C_D = C_{D_m} + (C_L - C_{L_m})\alpha_i$$

Near ground

$$C_{D_g} = C_{D_m} + (C_{L_g} - C_{L_{m_g}})\,\alpha_{i_g} + \alpha C_{L_g}(h_1)$$

where the $\alpha C_{L_g}(h_1)$ term represents the static pressure drag near ground.

A ratio of these two drag equations gives

$$\frac{C_{D_g} - C_{D_m} - \alpha C_{L_g}(h_1)}{C_D - C_{D_m}} = \frac{C_{L_g}\left(1 - \frac{C_{L_{m_g}}}{C_{L_g}}\right)}{C_L\left(1 - \frac{C_{L_m}}{C_L}\right)} \frac{\alpha_{i_g}}{\alpha_i} = \sigma_L \sigma_i$$

Then the drag near ground is

$$C_{D_g} = C_{D_m} + \sigma_L \sigma_i \left(C_D - C_{D_m}\right) + \sigma_i C_{L_g}(h_1) \qquad \text{Equation (9)}$$

By a similar derivation to that in Reference VI-1A-6

$$\sigma_i = \frac{\alpha_{i_g}}{\alpha_i} = 1 - \frac{1}{1 + 32\left(\frac{h_o}{b}\right)^2 + 4\,\frac{h_o}{b}\left[1 + 32\left(\frac{h_o}{b}\right)^2\right]^{1/2}}$$

Equation (10)

When the wing trailing edge touches ground the wing and image form a cone as shown in Sketch b. In this static condition the drag and lift are

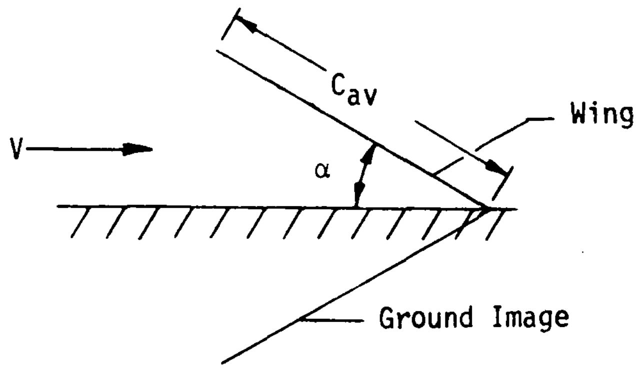

SKETCH b. - Wing with Trailing Edge on Ground.

approximately related directly by $C_{D_g} = C_{L_g} \tan\alpha \cong \alpha\, C_{L_g}$. For the wing near ground the static lift part is approximately $C_{L_g} - C_L$, then

$$\alpha C_{L_g}(h_1) \cong \alpha\left(C_{L_g} - C_L\right) = \alpha C_L\left[\sigma_L(h_1) - 1\right] \qquad \text{Equation (11)}$$

Statistically analyzing the arrow wing aircraft experimental data of Reference VI-1A-5 applied to Eq. (9) with Eqs. (10) and (11), results in

$$C_{D_g} = C_{D_m} + \frac{1.017}{1 + .017 \dfrac{4h_o^3}{1 + 4h_o^3}} \sigma_{L_{h_o}} \sigma_{\alpha_{h_o}} (C_D - C_{D_m}) +$$

$$1.017 (\sigma_{L_{h_1}} - 1) \alpha C_L$$

Equation (12)

where σ_L is given by Eq. (7), σ_α by Eq. (10). The height h_1 is given by

$$h_1 = 5/6 \; h_{TE} + 1/6 \; h_o$$

where for partial span flaps h_{TE} is the mean height to wing and flap trailing edge. A correlation plot of Eq. (12) with data of Reference VI-1A-5 is shown in Figure VI-1A-28.

Moment and drag predictions by use of Eqs. (8) and (12) are presented in Figures VI-1A-29 through VI-1A-33 for the arrow wing aircraft defined by: Λ = 74/70.5/60, $W_3(L_{1-2} = 30)$, $(L_6 = 60)$, $B_9N_2H_3E_2V_1$; $t_{1_f} = t_2 = t_3 = 15°$ which mean: L.E. sweep inboard of 74°, midsemispan of 70.5°, and outboard of 60°; inboard L.E. radius of 1%, W_3, with inboard L.E. flap deflected 30°, and outboard L.E. flap deflected 60°; long body; notched apex of wing; medium horizontal tail; engine nacelles; vertical tail; with trailing edge staggered flaps deflected 15°. This is referred to as the (Case 8) configuration for analysis purposes.

For configurations which differ a small amount from the above configuration, the change due to ground effect given in Figures VI-1A-32 and VI-1A-33 can be added to the away from ground values of the new configuration. These are design values to be added to the out of ground effect moment and drag of Follow-On configurations. The lift near ground is obtained directly by use of Eq. (7). For the same lift coefficient

Figure VI-1A-32 indicates that the pitching moment is relatively independent of ground effect (however, α must decrease as h_o becomes smaller).

Application to Other Configurations

The primary effect of configuration changes on drag is the flap size and deflection and on moment is the tail size and body length which governs the distance to ground with angle of attack. Moment and drag of configurations which have an appreciable different horizontal tail size or tail distance and flap size or deflection from that described as in (Case 8), can be predicted by adding a correction term to the values of Figures VI-1A-32 and VI-1A-33.

The horizontal tail on the aircraft near ground is in a reduced downwash field from the wing and in ground induced upwash; and gains lift from both effects. For pitching moment, the moment change of a different configured aircraft is written as (at same h_o and same α),

$$(C_{m_g} - C_m)_{DC} = (C_{m_g} - C_m)_{Case\ 8} - \left[\frac{l_t}{\bar{c}} C_{Lt}\left(\frac{C_{L_{tg}}}{C_{Lt}} - 1\right)\right]_{DC} + \left[\frac{l_t}{\bar{c}} C_{Lt}\left(\frac{C_{L_{tg}}}{C_{Lt}} - 1\right)\right]_{Case\ 8} \qquad \text{Equation (13)}$$

where DC indicates different configuration.

where $l_t = x_{tail} - x_{cg}$ is tail distance.

The tail lift coefficient is given by

$$C_{Lt} = C_{L_{\alpha_{tail}}} \alpha \left(1 - \frac{\varepsilon}{\alpha} - \frac{i_t}{\alpha}\right) \frac{q_t}{q} \frac{S_t}{S} \qquad \text{Equation (14)}$$

where

$$C_{L_{\alpha tail}} = \frac{2\pi A_t}{A_t + 2\left(\frac{A_t + 4}{A_t + 2}\right)} \qquad \text{Equation (15)}$$

The tail lift ground factor is

$$\frac{C_{Lt_g}}{C_{Lt}} = \alpha_{Lt} \left[1 + \frac{\varepsilon}{\alpha} (1 - \sigma_\varepsilon)\right] \qquad \text{Equation (16)}$$

Where σ_{Lt} is evaluated from Eq. (7) but with the tail aspect ratio, A_t, tail ground height, h_{ot}, and tail span, b_t. The tail height from ground is given by

$$h_{ot} = h_\circ + Z_t - (l_t - x_\circ + x_{cg}) \sin \alpha \qquad \text{Equation (17)}$$

where Z_t is tail height above wing extended chord plane.

The near ground wing induced downwash at tail is

$$\varepsilon_g = \sigma_\varepsilon \varepsilon$$

where

$$\sigma_\varepsilon = 1 - \frac{1}{1 + 32\left(\frac{h_s + .5Z}{b}\right)^2 + 4\left(\frac{h_s + .5Z}{b}\right)\left[1 + 32\left(\frac{h_s + .5Z}{b}\right)^2\right]^{1/2}}$$

Equation (18)

where h_s is height from ground to the wing trailing vortex sheet or wake; Z is distance from wake to tail positive up; b is wing span. Actually

$$h_s + .5Z = h_{ot} - .5Z \qquad \text{Equation (19)}$$

which equals h_{ot} for small z or as an approximation.

For the (Case 8) configuration, the tail geometry values are:

$$\frac{l_t}{\bar{c}} = .95; \; A_t = 1.74; \; \frac{S_t}{S} = .045; \; \frac{b_t}{b} = .22$$

For drag prediction the drag change of a different configured AST is written as (same h_o and same α),

$$(C_{D_g} - C_D)_{DC} = (C_{D_g} - C_D)_{Case\ 8} + [C_{L_g}(h_{TE})]^{\alpha}_{DC} - [C_{L_g}(h_{TE})]^{\alpha}_{Case\ 8}$$

Equation (20)

where C_{L_g}'s are determined from Eq. (7) with the height h_{TE} substituted for h_o. The trailing edge averaged height from ground is given by,

$$h_{TE} = h_o - (\bar{c} - c_f - x_o) \sin \alpha - c_f \frac{b_f}{b} \sin(\delta_f + \alpha)$$

$$\cong h_o - [\bar{c} - (1 - \frac{b_f}{b}) c_f - x_o] \frac{\alpha^\circ}{57.3} - c_f \frac{b_f}{b} \sin \delta_f$$ Equation (21)

where b_f is the summed flap spans and c_f is average flap chord.

For the Case 8 configuration,

$$\frac{\bar{c}}{b} = .839; \; \frac{c_f}{c} = .13; \; \frac{b_f}{b} = .4; \; \frac{x_o}{\bar{c}} = .667; \; \delta_f = 15^\circ; \text{ then}$$

$$\left.\frac{h_{TE}}{b}\right)_{Case\ 8} = \frac{h_o}{b} - .113 - .00374\ \alpha^\circ$$ Equation (22)

The lift due to configuration changes in the flap system can be predicted by ratioing unknown to known flap data.

If flap (a) differs in size and location from flap (b), its lift can be estimated from the ratio (with same δ):

$$\frac{C_{L_{fa}}}{C_{L_{fb}}} = \frac{\sum_{i=1}^{M_o} (1 - \eta_{av_{ai}}) \Delta\eta_{a_i} \frac{\sigma_{a_i}}{1 + 3\sigma_{a_i}}}{\sum_{i=1}^{M_1} (1 - \eta_{av_{bi}}) \Delta\eta_{b_i} \frac{\sigma_{b_i}}{1 + 3\sigma_{b_i}}}$$ Equation (23)

where: The summation is of individual flap segments along the span.

For example, if flap (b) extends from $.2 \leq \eta \leq .3$ and σ_b is .10; while flap (a) extends from $.2 \leq \eta \leq .5$ and σ_a is .20; then the lift ratio is:

$$\frac{C_{L_{fa}}}{C_{L_{fb}}} = \frac{(.65)(.3)(.2/1.6)}{(.75)(.1)(.1/1.3)} = 4.22$$

It can be seen that the area of flap (a) is 6 times larger than that of flap (b) but the lift is 4.22 times larger.

Evaluation of Reference Configuration with Ground Effects

Utilizing the prediction procedure outlined above the effect of ground on the aerodynamic characteristics was determined. For the Reference Configuration the wing aerodynamic center is located about 170 inches above the ground (h_o = 120.0) during ground run. Thus for the wingspan (b) of 1653.33 inches the h_o/b is 0.1028. Using this as an initial point, the ratio of the C_L in ground to the C_L out of ground as a function of the height of the wing aerodynamic center was computed using Equation (5) and the results are presented in Figure VI-1A-34. Based on the curves presented in Figure VI-1A-33, an equation was developed which approximates the effect of height above ground and angle of attack on the ratio of the in ground drag to the out of ground drag. The equation is as follows:

$$\frac{C_{D_{in\ ground}}}{C_{D_{out\ ground}}} \doteq 1 + \frac{0.00261058\ (\alpha - \alpha_o) - 0.00010815\ (\alpha - \alpha_o)^2}{\left[\frac{h}{b} - 0.0668 - 0.0017\ (\alpha - \alpha_o)\right]}$$

Equation (24)

where α_o defines the angle of attack corresponding to zero lift. For the Reference Configuration with the three inboard trailing edge flaps set at a deflection angle of 20 degrees and the outboard flap set at 5 degrees, the value of α_o is -4.67 degrees. Using this value in Equation (24), the effect of angle of attack and height above ground of wing aerodynamic center on the ratio of C_D in ground to C_D out of ground was computed and the results are presented in Figure VI-1A-35.

4. Analysis of Landing Gear and Spoilers

The landing gear of the Reference Configuration consists of two main landing gear struts with twelve wheels on each strut. The nose gear has one strut with two wheels. The major portion of the gear drag is due to the struts rather than the wheels. The drag of the main landing gear struts is based on a diameter of 18 inches and an exposed length equal to the compressed length of 162 inches as shown in Figure V-2 and the stroke length. Similarly, the drag of the nose landing gear strut is based on a diameter of 12 inches and an exposed length equal to the compressed length of 174 inches as shown in Figure V-2 and the stroke length. The stroke length is the difference between the strut length with the aircraft in the air. Based on the landing gear drag presented in Hoerner (Reference VI-1A-7) the gear drag for the Reference Configuration was estimated to be 0.0087.

To assist in the braking during ground run, spoilers were employed in front of the three inboard flaps. The spoilers spoil the flow over the flaps and thus decrease the flap lift. Based on Reference VI-1A-8 test data, the decrease in lift was found to be dependent on the spoiler angle. For the Reference Configuration which uses spoiler deflection angles of 60°, it was determined that the flaps lose 36.7 percent of the associated flap lift. The incremental drag of the spoiler was obtained from the Reference VI-1A-8 test data and then adjusted to the Reference Configuration geometry.

5. <u>Droop Nose Effects</u>

Based on Reference VI-1A-8 test data, the effect of drooping the nose 12.5 degrees on the incremental change in lift and drag was evaluated. The effect was determined to be negligible during take-off and landing (Figure VI-1A-36).

LIST OF SYMBOLS

A	aspect ratio (b^2/S)
A_t	aspect ratio of tail ($b_t{}^2/S_t$)
a.c.	Aerodynamic Center
a_o, a_1	constants
b	wing span - ft.
b_f	summed trailing edge flap spans, ft.
b_t	tail span - ft.
c	wing chord - ft.
$\bar{c}$	mean aerodynamic chord - ft.
C_D	drag coefficient (D/qS)
C_{D_g}	drag coefficient in ground effect
C_{D_m}	minimum drag coefficient
C.G., cg	Center of gravity
c_f	flap chord - ft.
C_L	lift coefficient (L/qS)
C_{L_f}	lift coefficient due to flap
C_{L_g}	lift coefficient in ground effect
C_{L_m}	lift coefficient at minimum drag
$C_{L_{mg}}$	minimum lift coefficient in ground effect
C_{Lt}	lift coefficient of tail (L_{tail}/qS)
C_{Lt_g}	lift coefficient of tail in-ground effect
$C_{L_{\alpha tail}}$	lift curve slope of tail
C_m	pitching moment coefficient ($M/qS\bar{c}$)

LIST OF SYMBOLS (continued)

C_{m_g}	pitching moment coefficient in ground effect
D	drag - lbs.
DC	different configuration
h_o	height from ground at x_o station, ft.
h_{ot}	tail ground height, ft.
h_s	height from ground to wing trailing vortex sheet, ft.
h_{TE}	mean height to wing and trailing flap edge, ft.
h_x, h	height from ground at other longitudinal station $[h_x = h_o + (x_o - x)\ \alpha°/57.3]$, ft.
h_1	reference wing height $(5/6\ h_{TE} + 1/6\ h_o)$, ft.
i_t	tail incidence angle, degrees
k, k_o, k_1, k_2	constants
L	lift, lbs.
L_1, L_2, L_6	wing leading edge flap designation
lt	tail distance $(x_{tail} - x_{1g})$, ft.
L/D	lift to drag ratio
MAC	mean aerodynamic chord, ft.
q	free stream dynamic pressure psf.
q_t	stream dynamic pressure near tail - psf.
S	wing area, ft.
S_t	tail area, ft.
t_1, t_2, t_3, t_4	wing trailing edge flap designation
x	longitudinal distance from leading edge of MAC ft.

LIST OF SYMBOLS (continued)

x_o	MAC position at which h_o is measured $[x_o = x_{ac} + \frac{1}{3}(\bar{c} - X_{ac})]$, ft.
x_{ac}	aircraft aerodynamic center on MAC
y	lateral coordinate, ft.
Z_t	tail height above wing extended chord plane, ft.
$\alpha, \alpha_o, \alpha_L$	angle of attack, degrees
α_{1g}	angle of attack near ground, degrees
$\Delta C_{D_{flap}}$	incremental change in drag due flap deflection
$\Delta\eta$	spanwise span of flap segment
δ_f	flap deflection angle, degrees
ε	downwash angle, degrees
ε_g	ground induced downwash
η	lateral station (Y/b/2)
η_{av}	spanwise midpoint of flap segment
σ	flap chord ratio (c_f/c)
σ_i	ground induced angle factor ($\alpha i_g/\alpha i$)
σ_L	lift ground factor (C_{L_g}/C_L)
σ_{Lt}	tail lift ground factor (C_{Lt_g}/C_{Lt})
σ_ε	downwash ground factor ($\varepsilon_g/\varepsilon$)

REFERENCES

Reference No.	Title
VI-1A-1	Unpublished Data.
VI-1A-2	Unpublished Data.
VI-1A-3	Unpublished Data.
VI-1A-4	Henderson, W. P.; Studies of Various Factors Affecting Drag Due to Lift at Subsonic Speeds, NASA TN D-3584, October 1966.
VI-1A-5	Unpublished Data.
VI-1A-6	DeYoung, J.; Symmetric Loading of a Wing in a Wide Slipstream, Grumman Report No. ADR 01-04-66.1, dated October 1966.
VI-1A-7	Hoerner, S. F.; "Fluid Dynamic Drag" dated 1958.
VI-1A-8	Unpublished Data.

VI-1A

LIST OF FIGURES

LIST OF FIGURES (continued)

LIST OF FIGURES (continued)

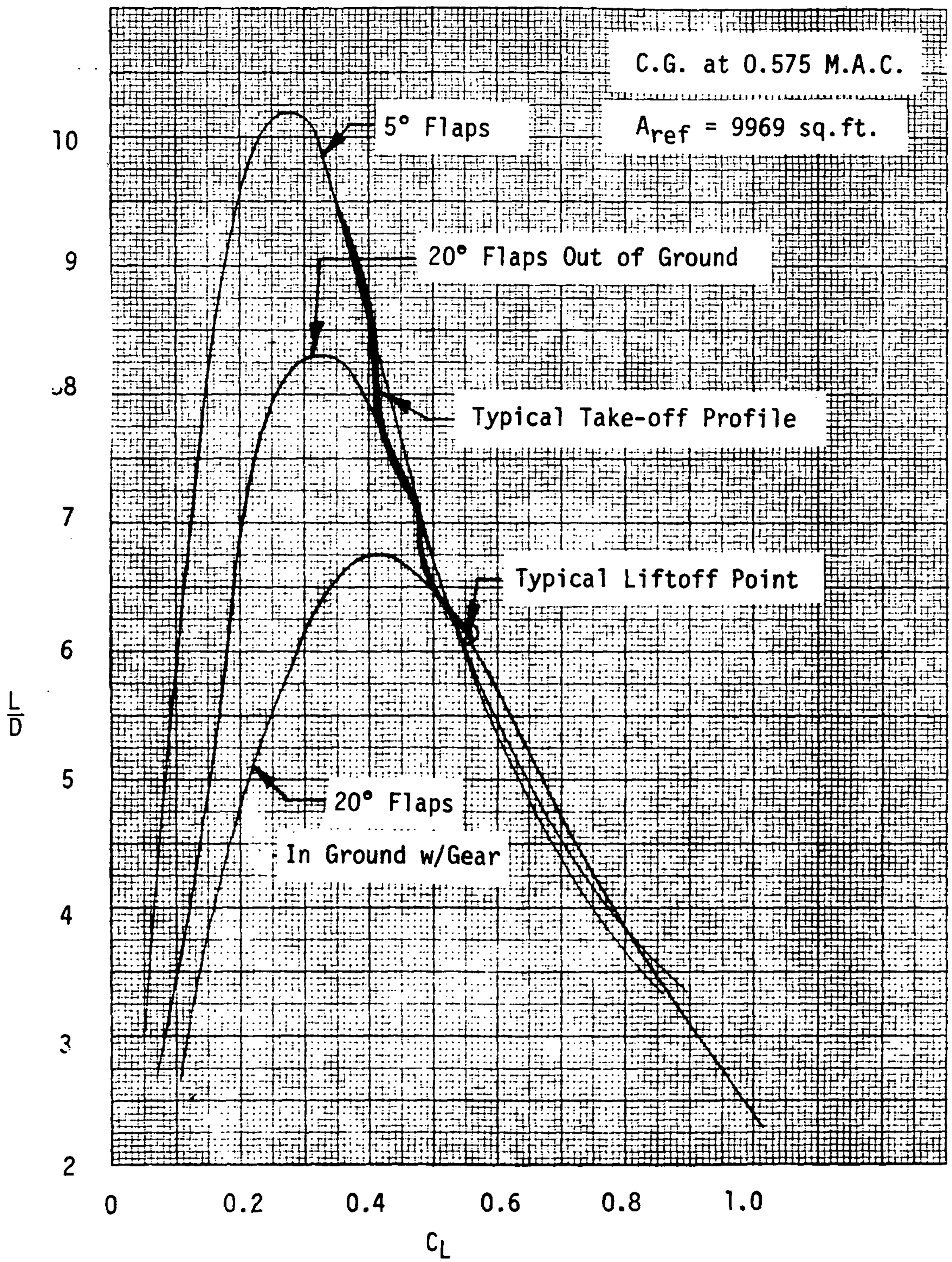

Figure VI-1A-1 — L/D vs C_L with 20° Flaps During Take-off of Reference Configuration

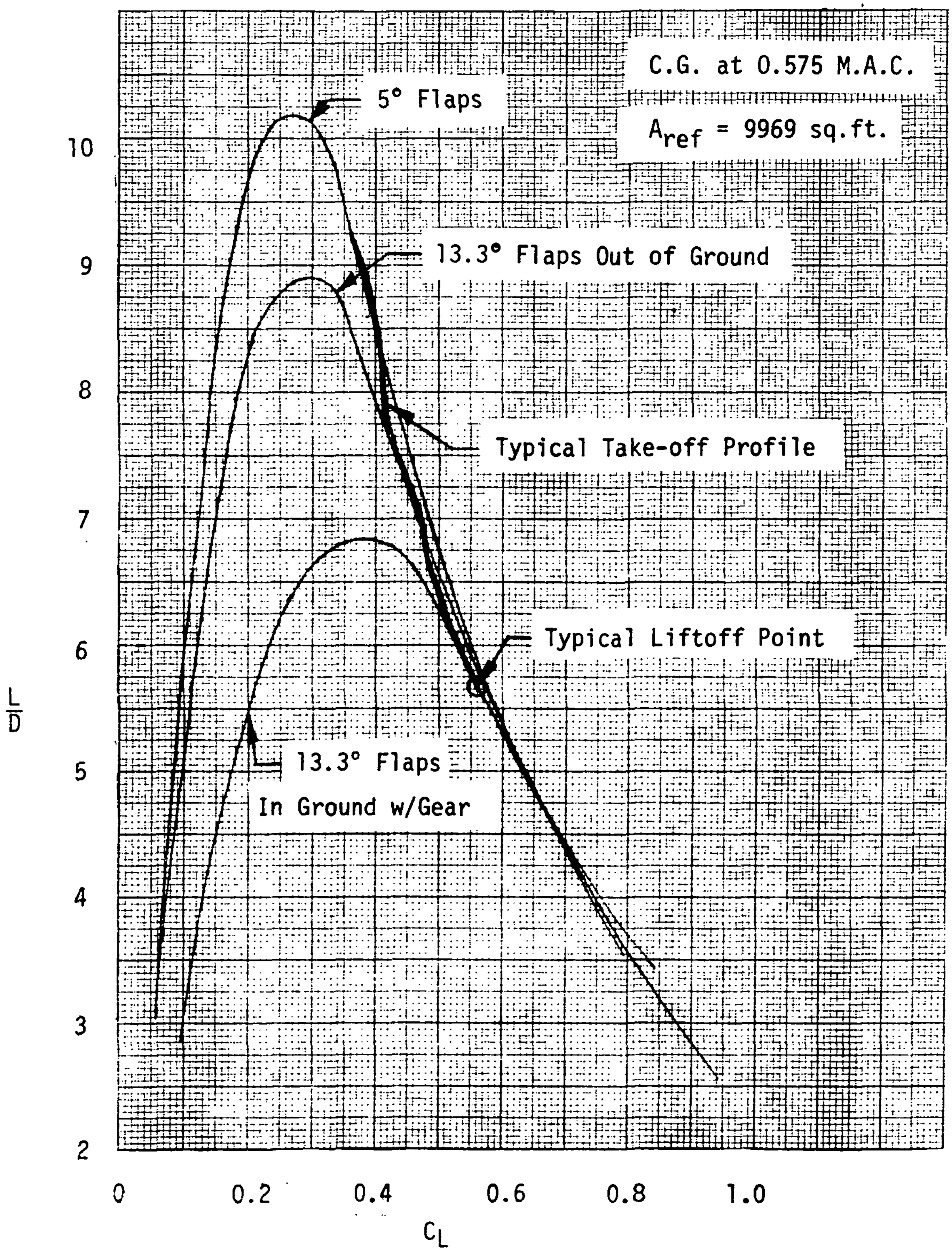

Figure VI-1A-2 — L/D vs C_L with 13.3° Flaps During Take-off of Reference Configuration

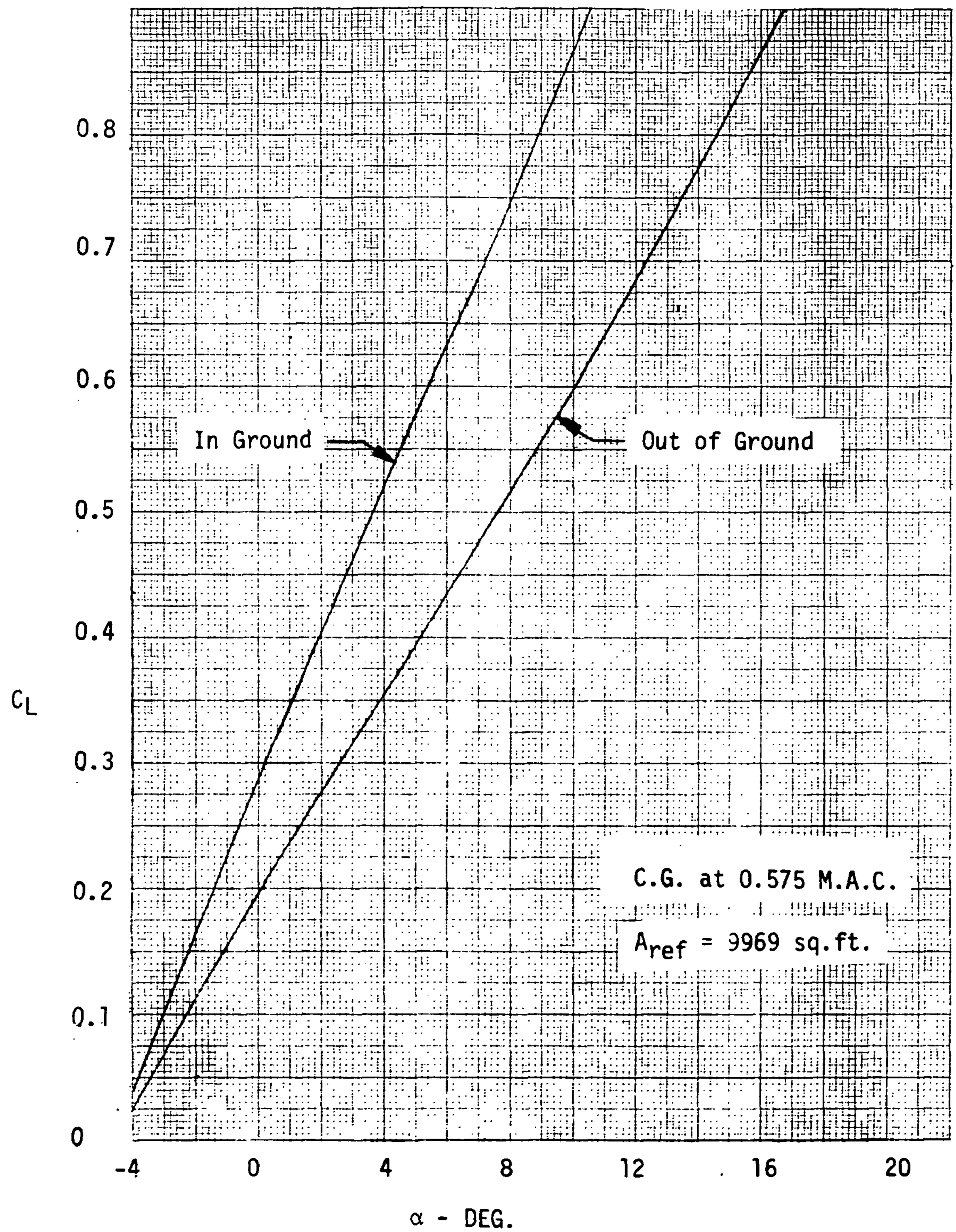

Figure VI-1A-3 — Variation of C_L vs α for Reference Configuration with 20° Flaps

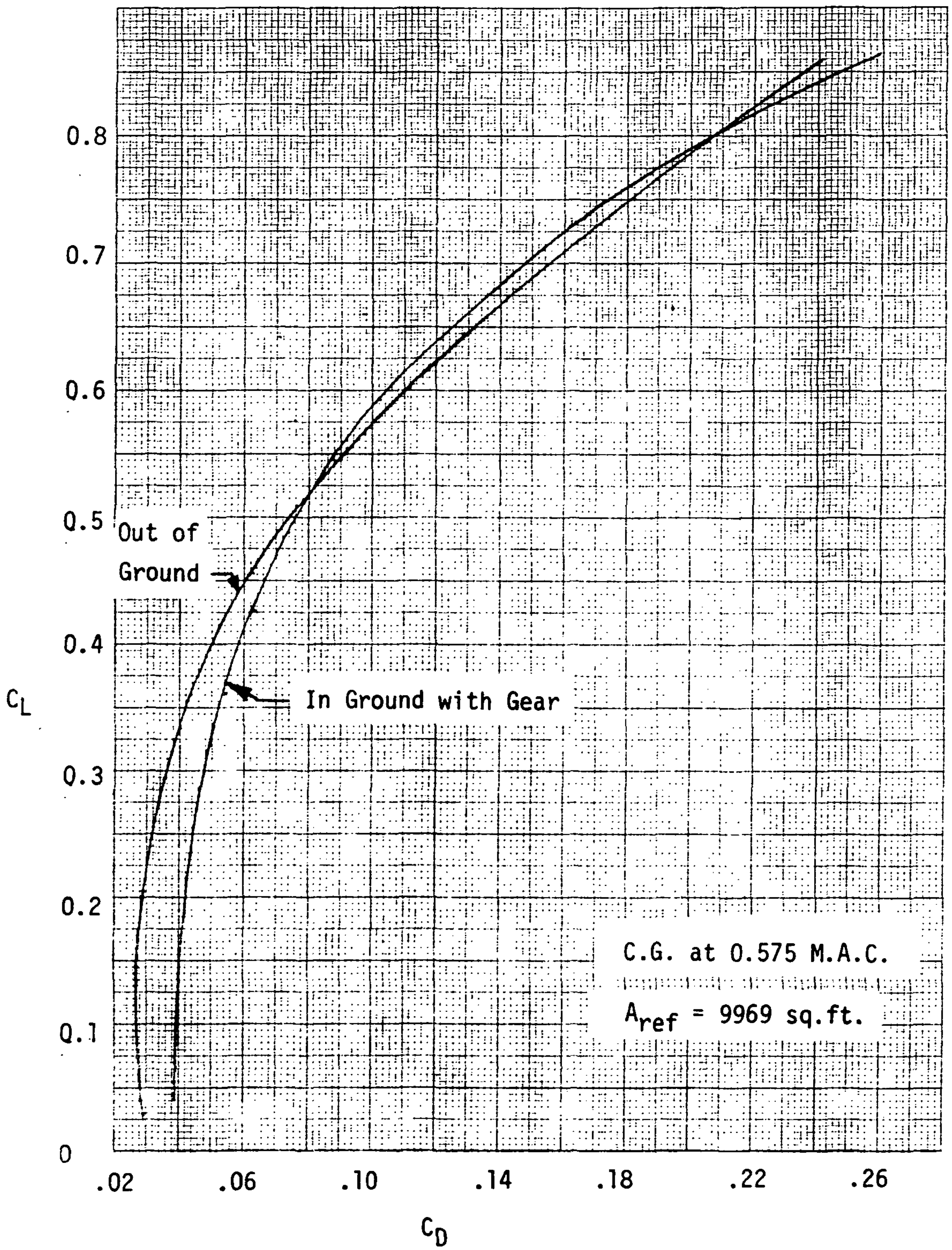

Figure VI-1A-4 — Drag Polar of Reference Configuration with 20° Flaps

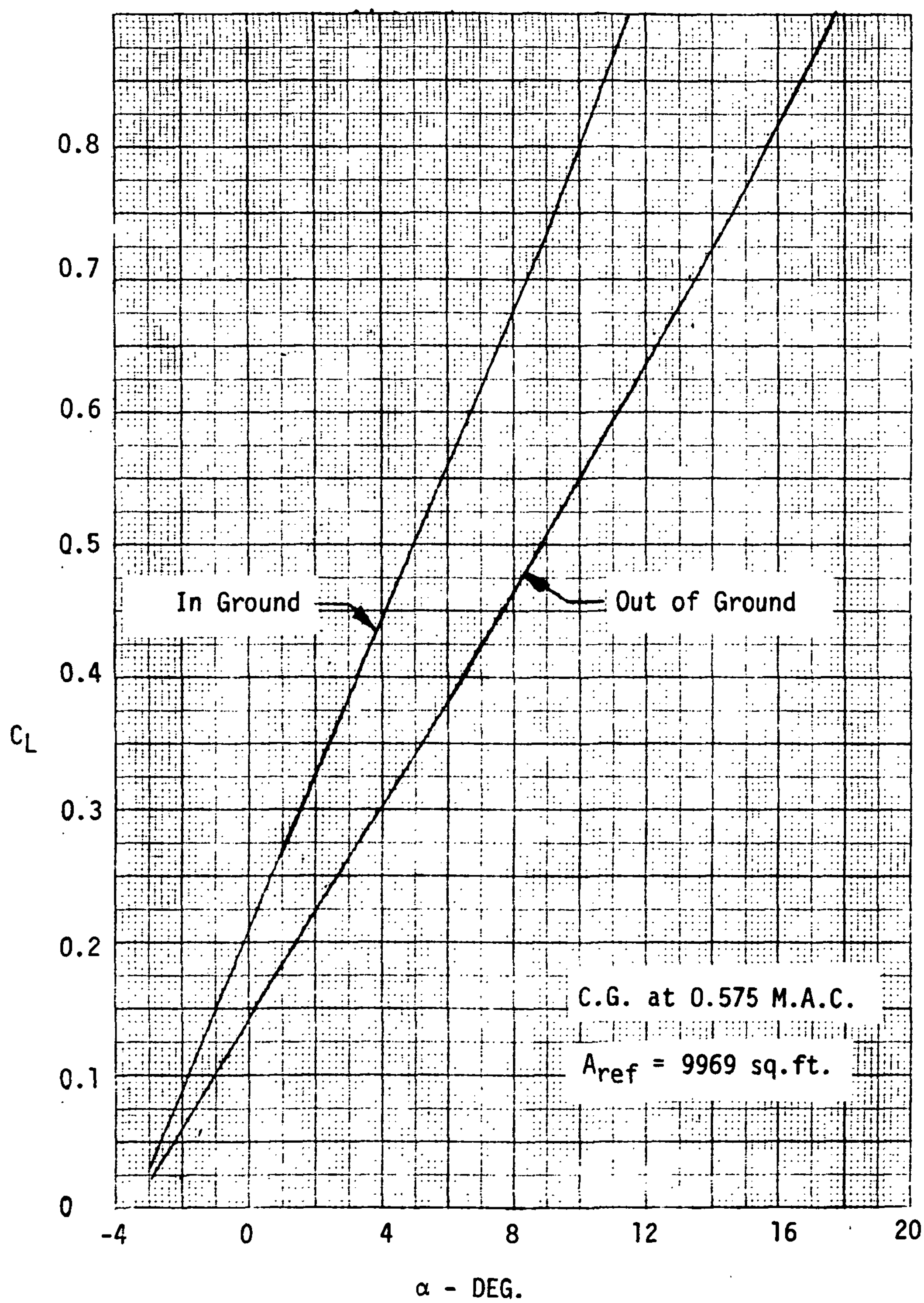

Figure VI-1A-5 — Variation of C_L with α for Reference Configuration with 13.3° Flaps

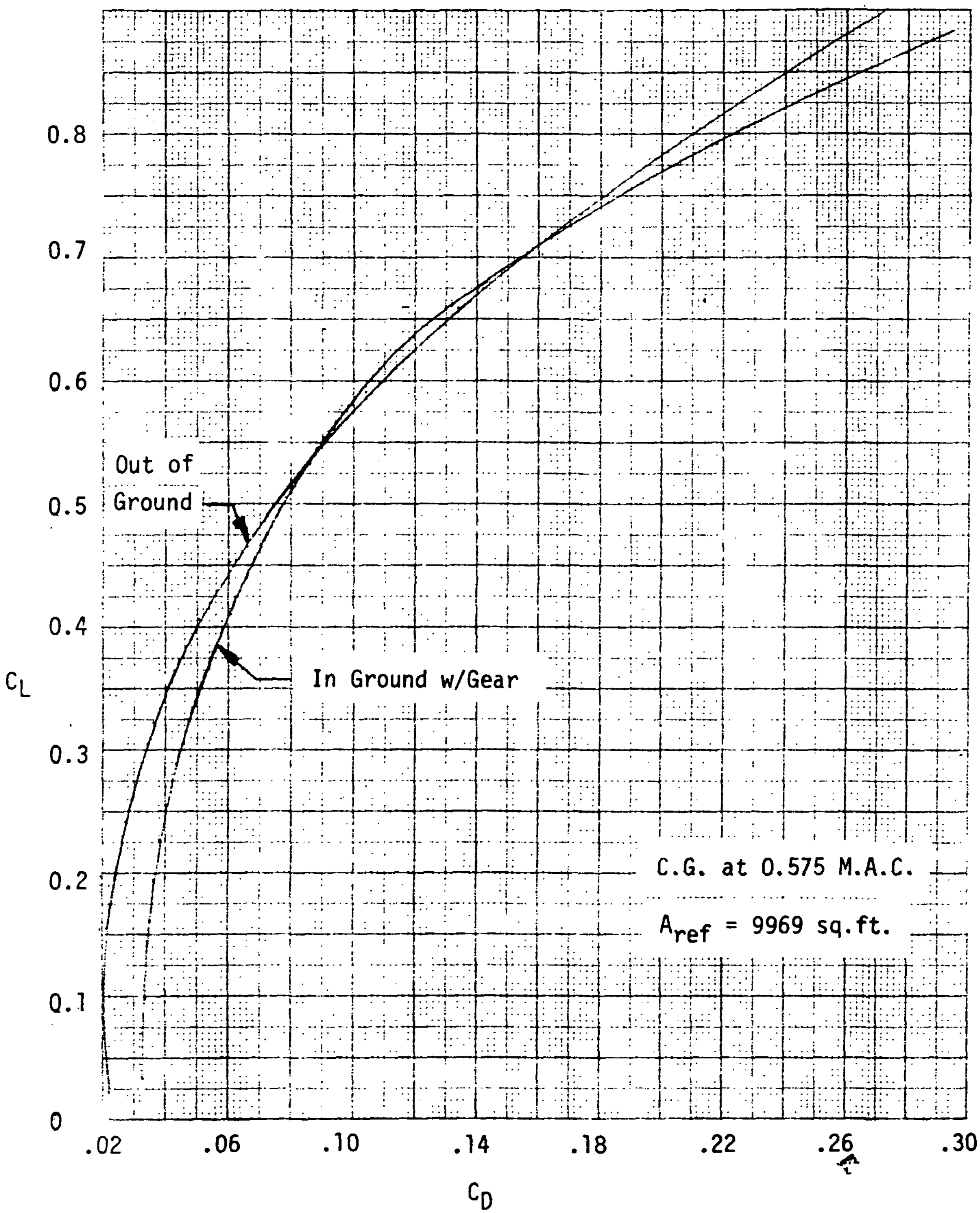

Figure VI-1A-6 — Drag Polar of Reference Configuration with 13.3° Flaps

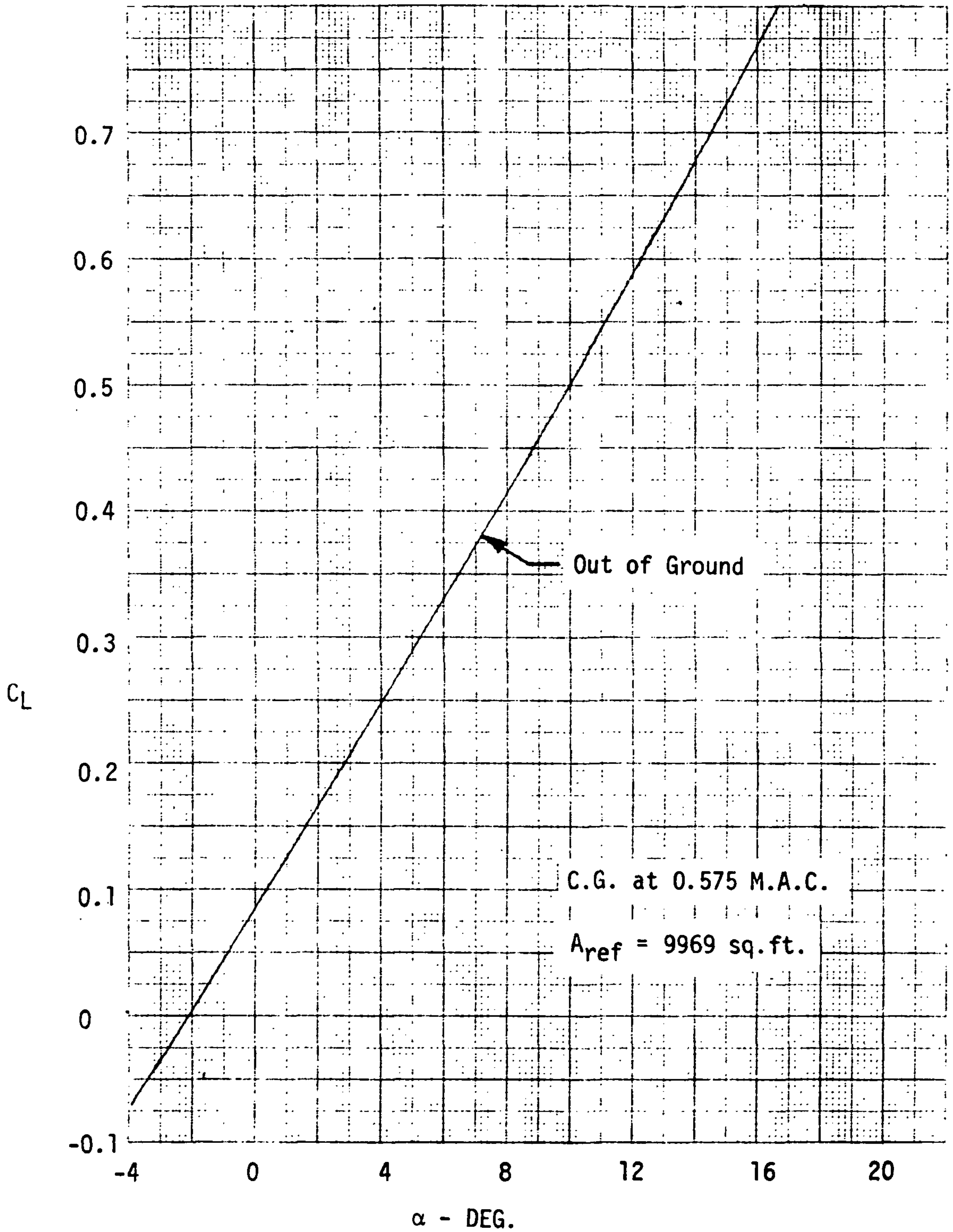

Figure VI-1A-7 — Variation of C_L with α for Reference Configuration with 5° Flaps

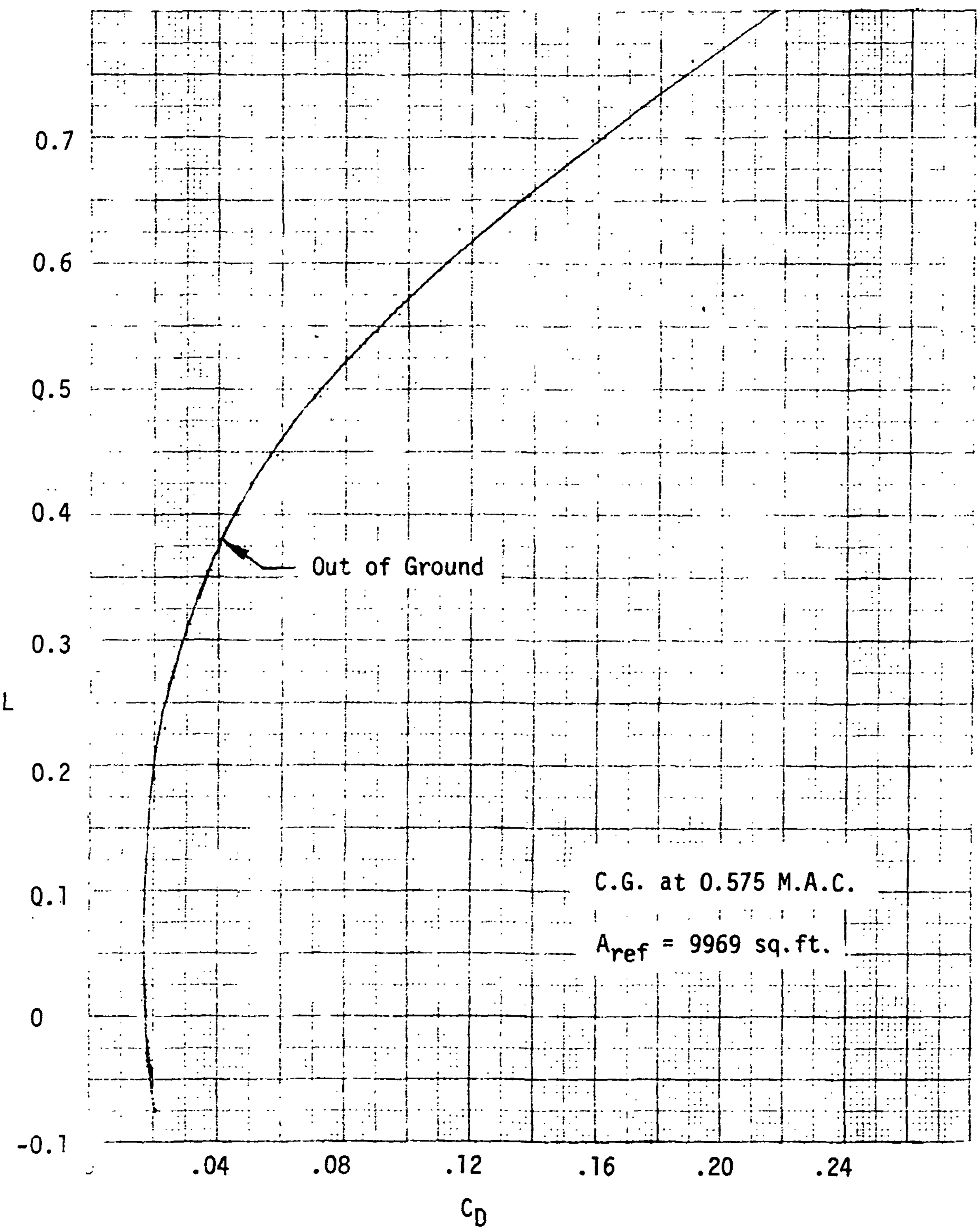

Figure VI-1A-8 — Drag Polar for Reference Configuration with 5° Flaps

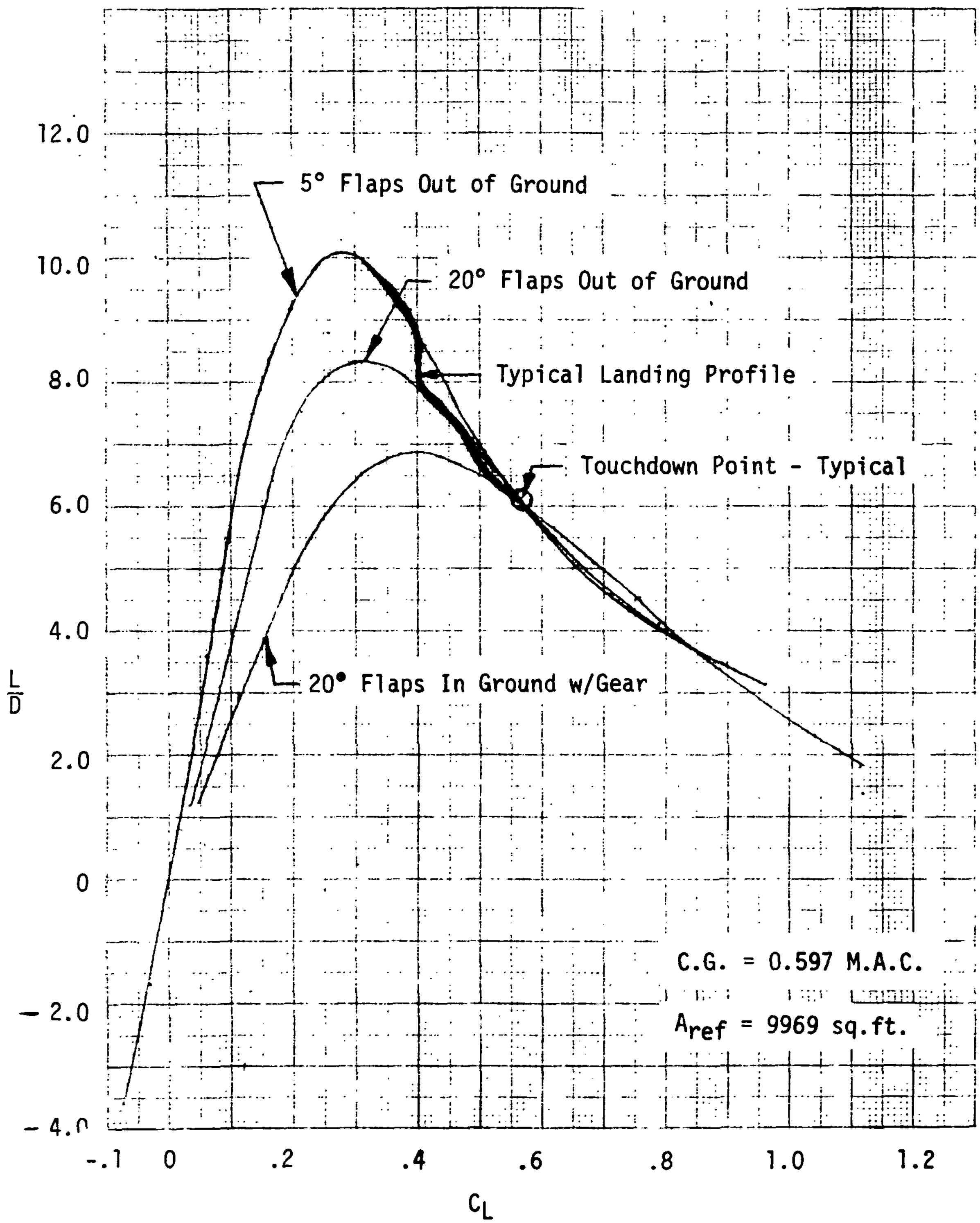

Figure VI-1A-9 — L/D vs C_L of Reference Configuration with 20° Flaps During Landing

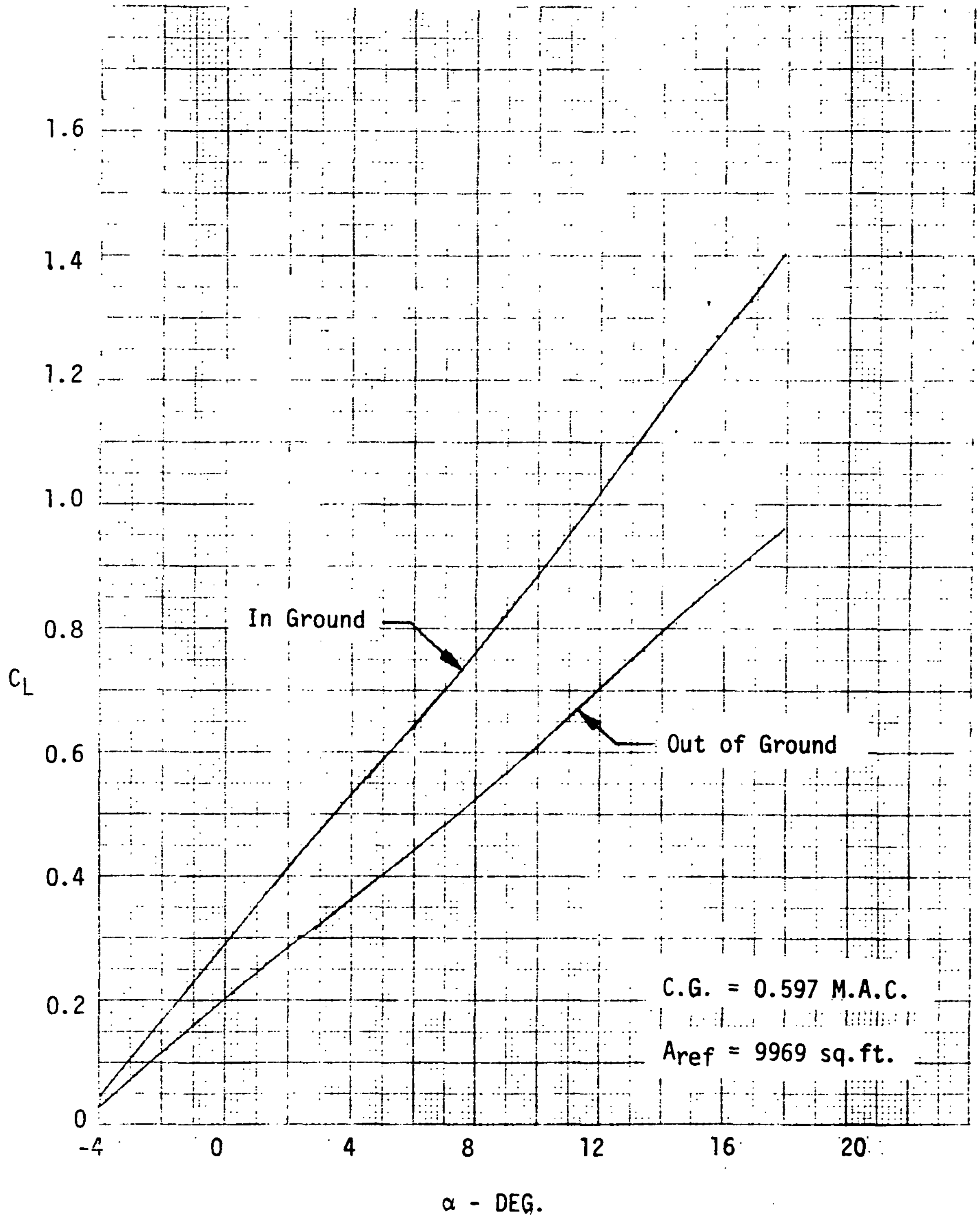

Figure VI-1A-10 — Variation of C_L with α for Reference Configuration with 20° Flaps

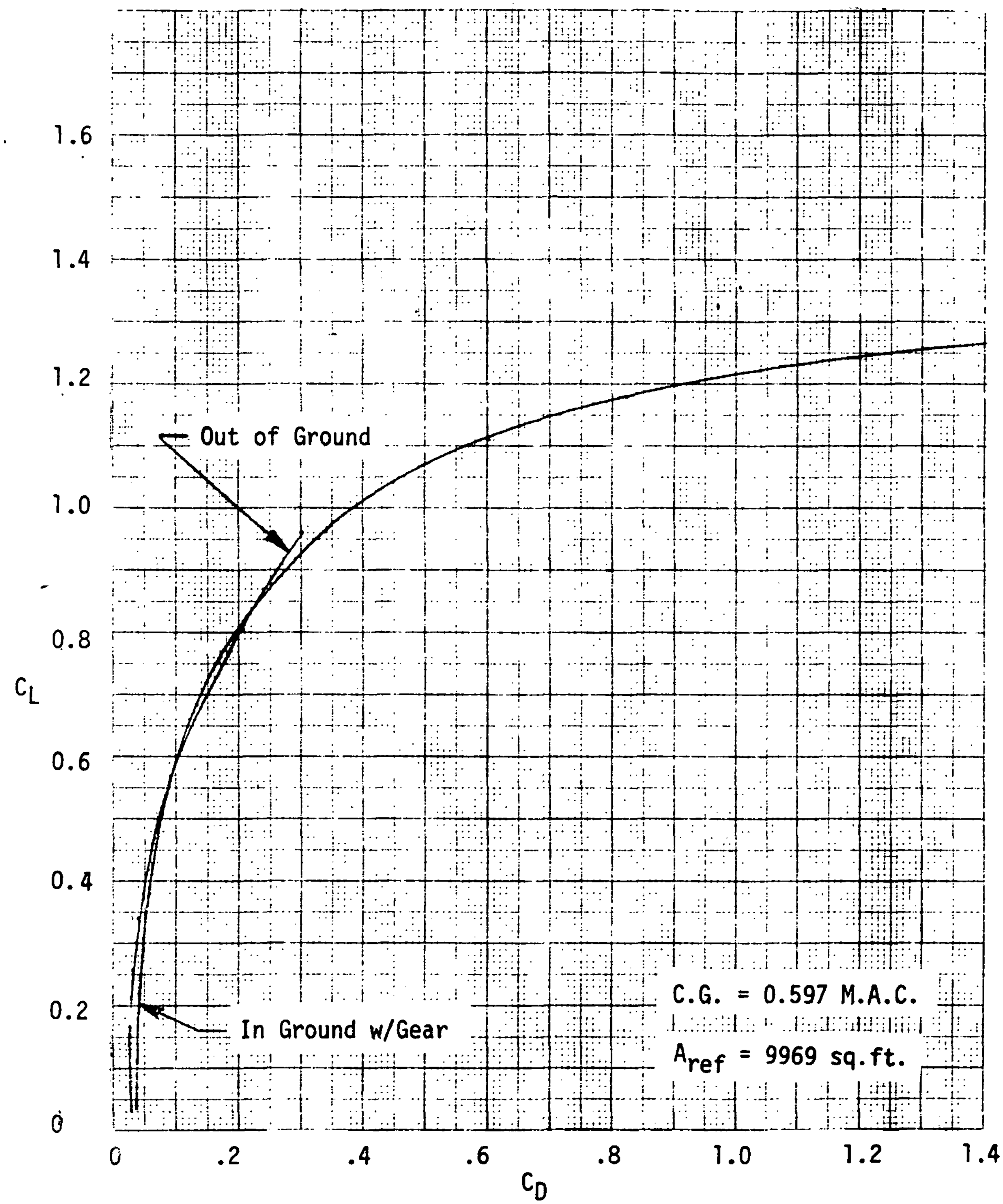

Figure VI-1A-11 - Drag Polar for Reference Configuration with 20° Flaps

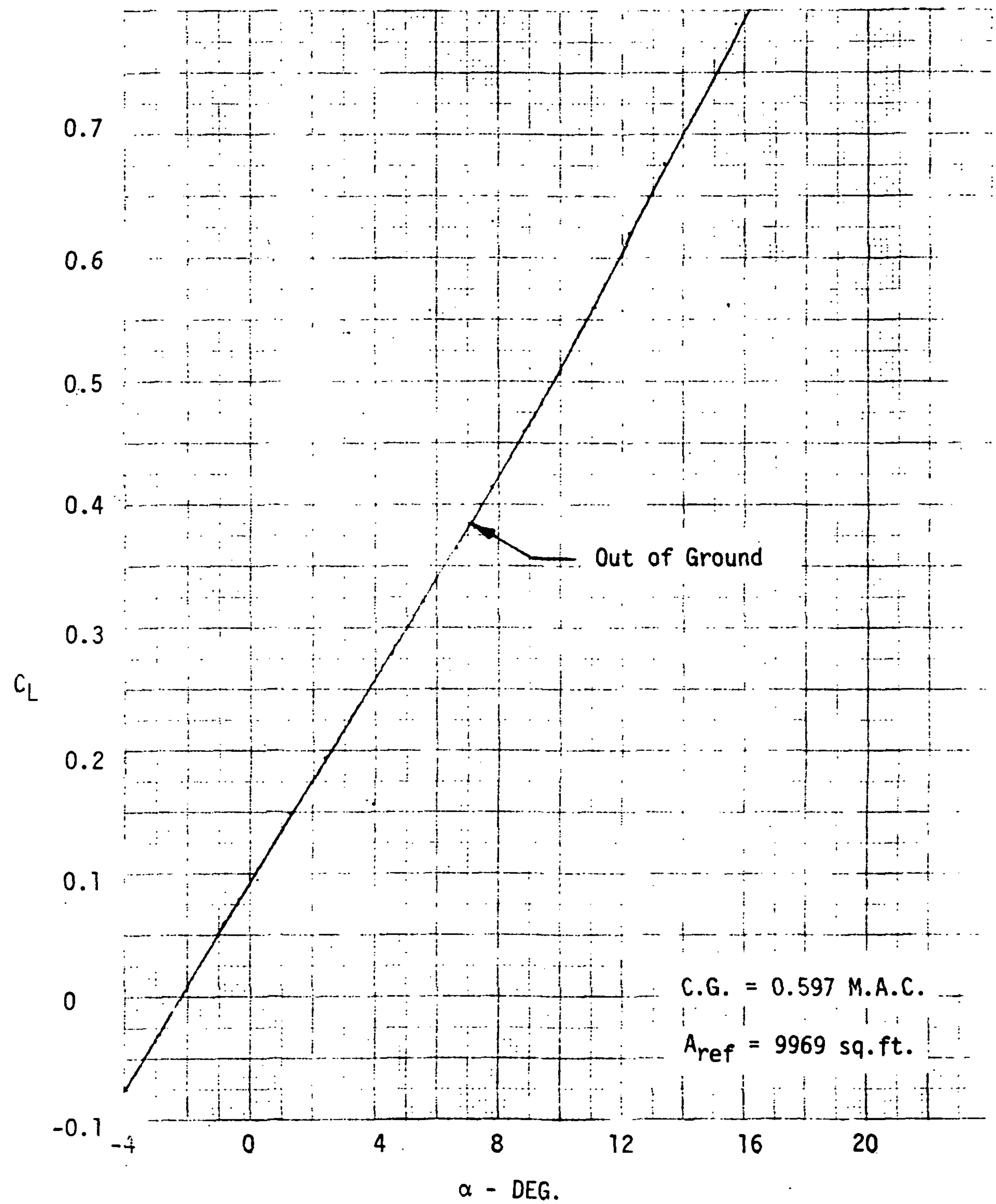

Figure VI-1A-12 - Variation of C_L with α for Reference Configuration with 5° Flaps

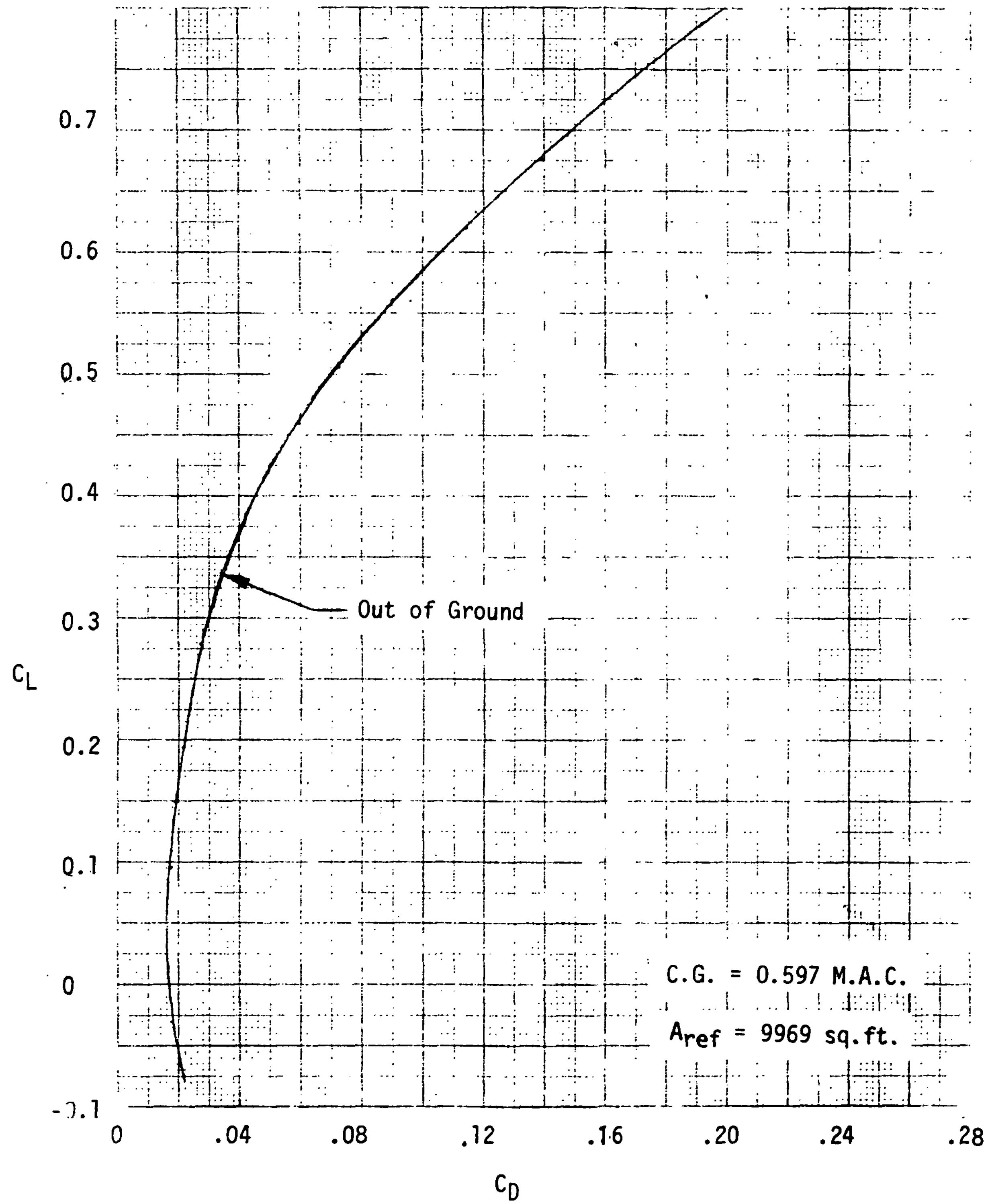

Figure VI-1A-13 - Drag Polar for Reference Configuration with 5° Flaps

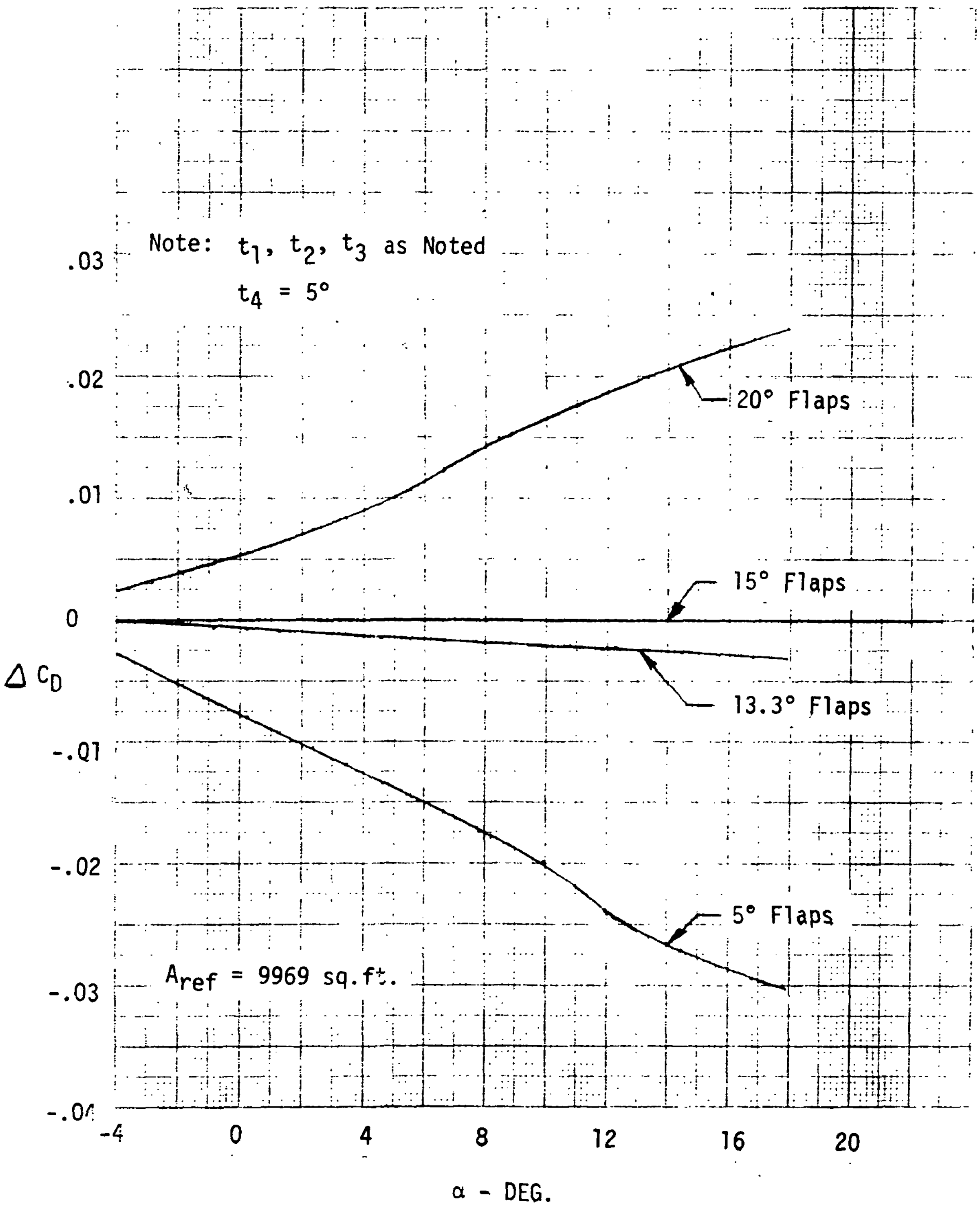

Figure VI-1A-14 — Effect of Trailing Edge Flap Deflection on Drag of Reference Configuration

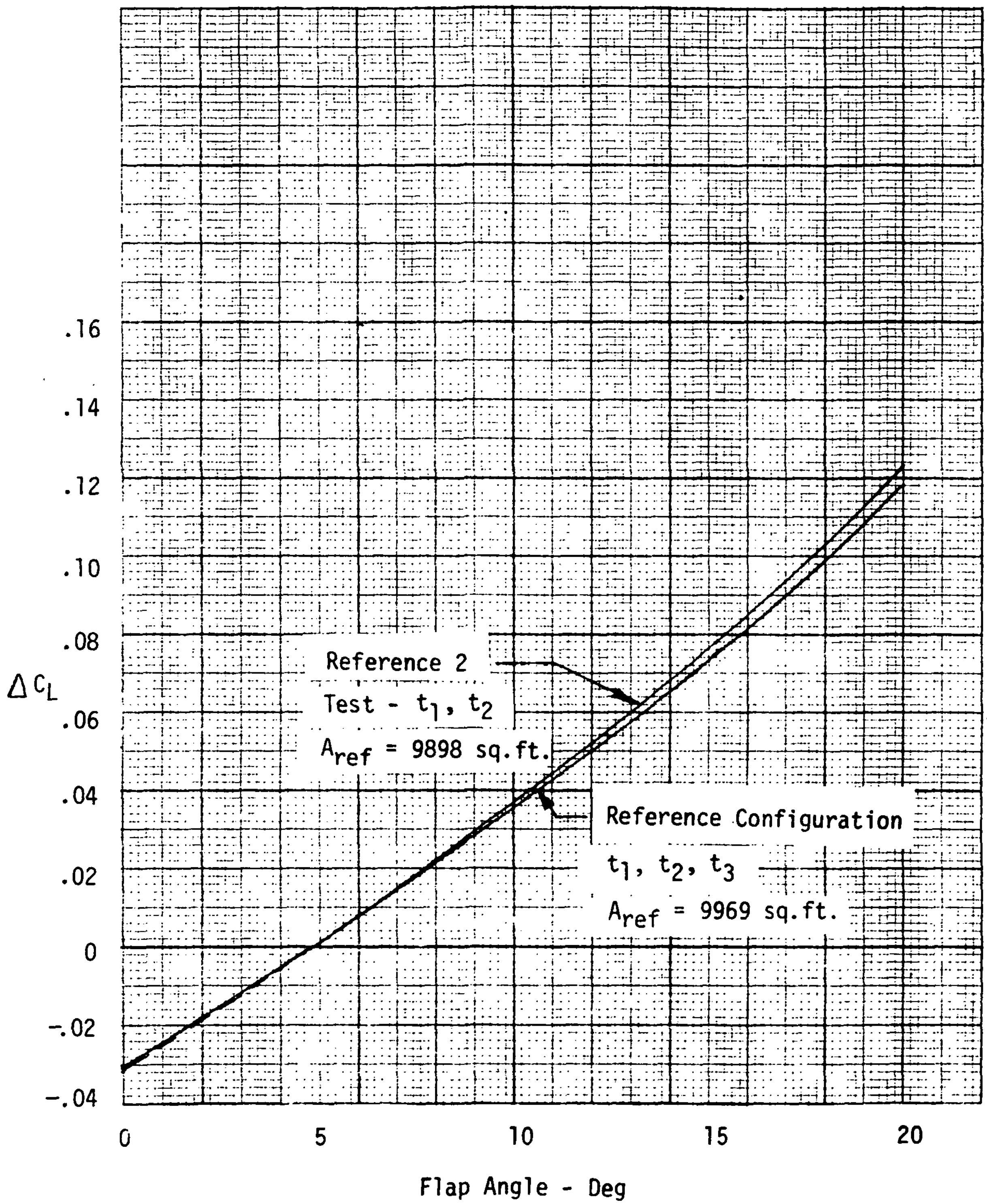

Figure VI-1A-15 — Effect of Trailing Edge Flap Deflection on Lift for Reference Configuration

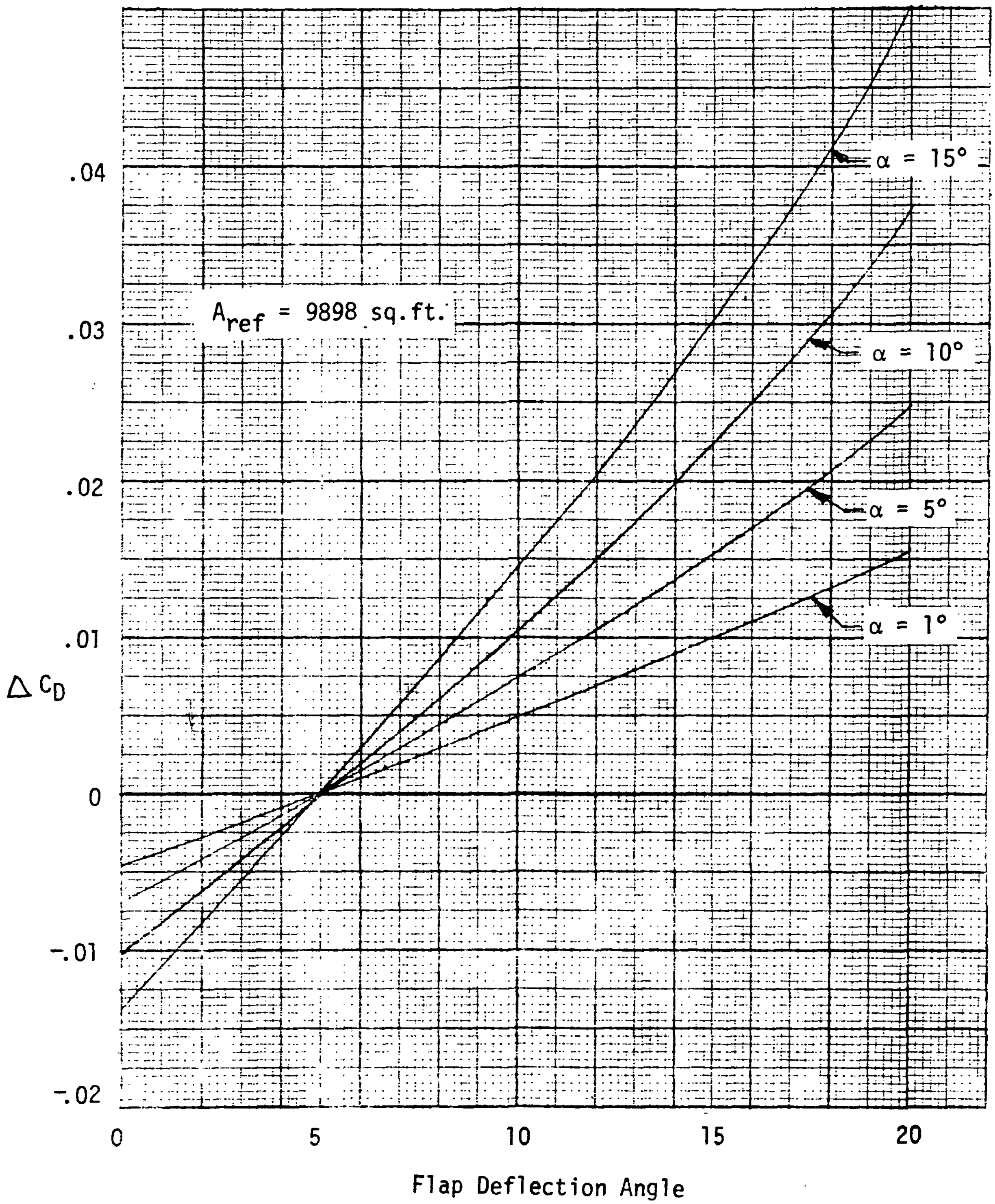

Figure VI-1A-16 - Effect of Flap Deflection Angle on Drag for t_1 and t_2 of Reference 2 Test Model

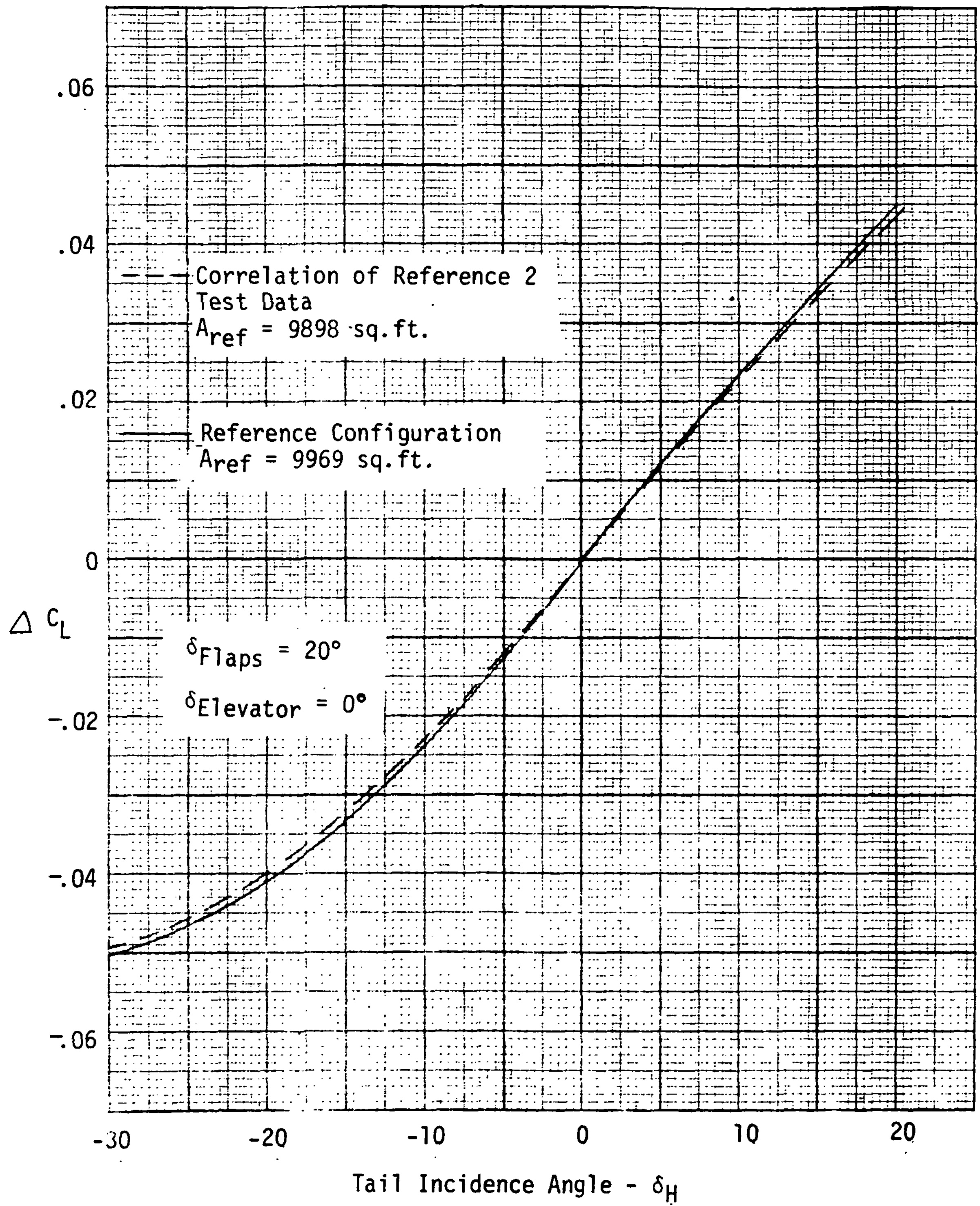

Figure VI-1A-17 – Effect of Tail Incidence Angle on Lift of Reference Configuration

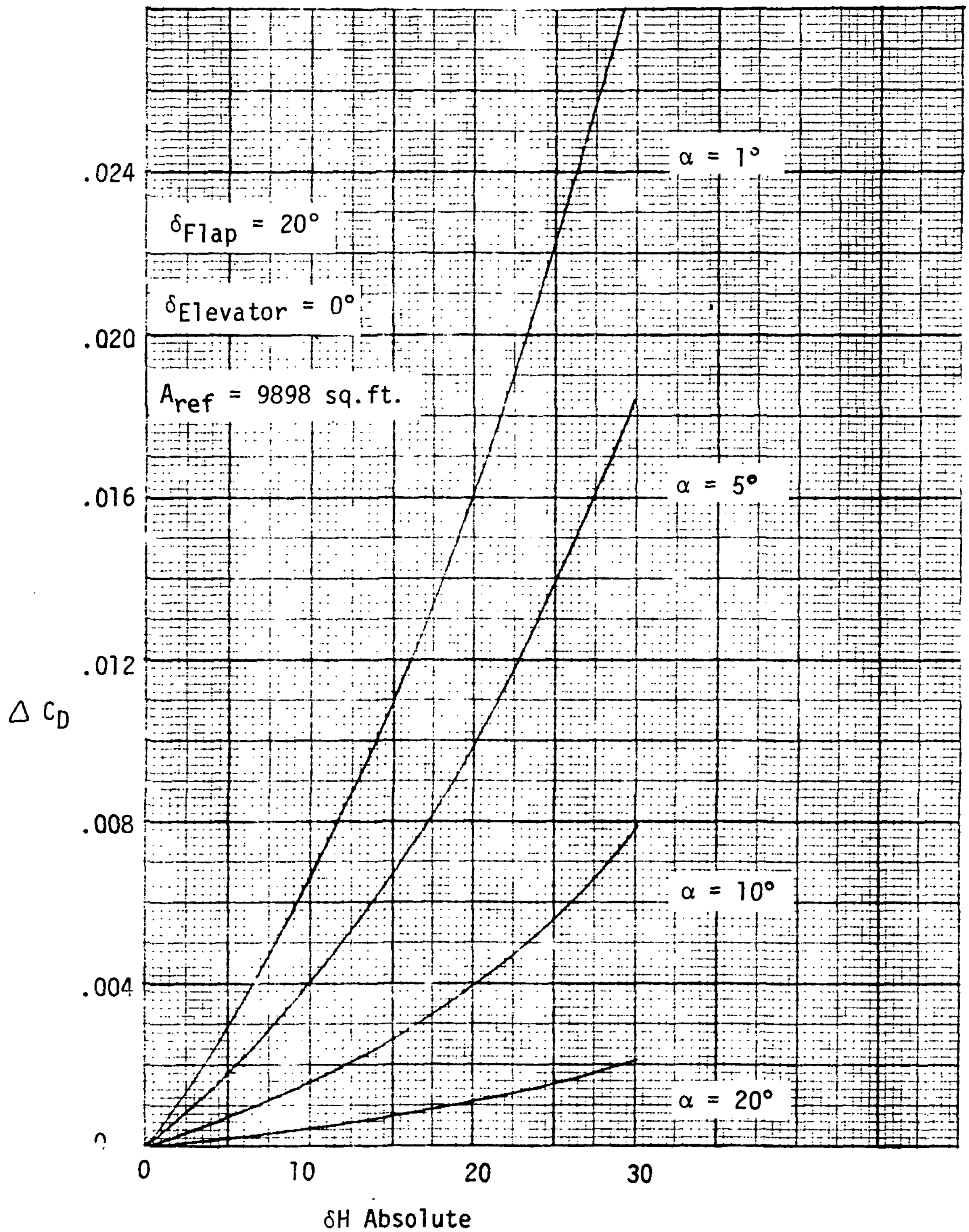

Figure VI-1A-18 - Effect of Tail Incidence Angle on Drag of Reference 2 Test Model

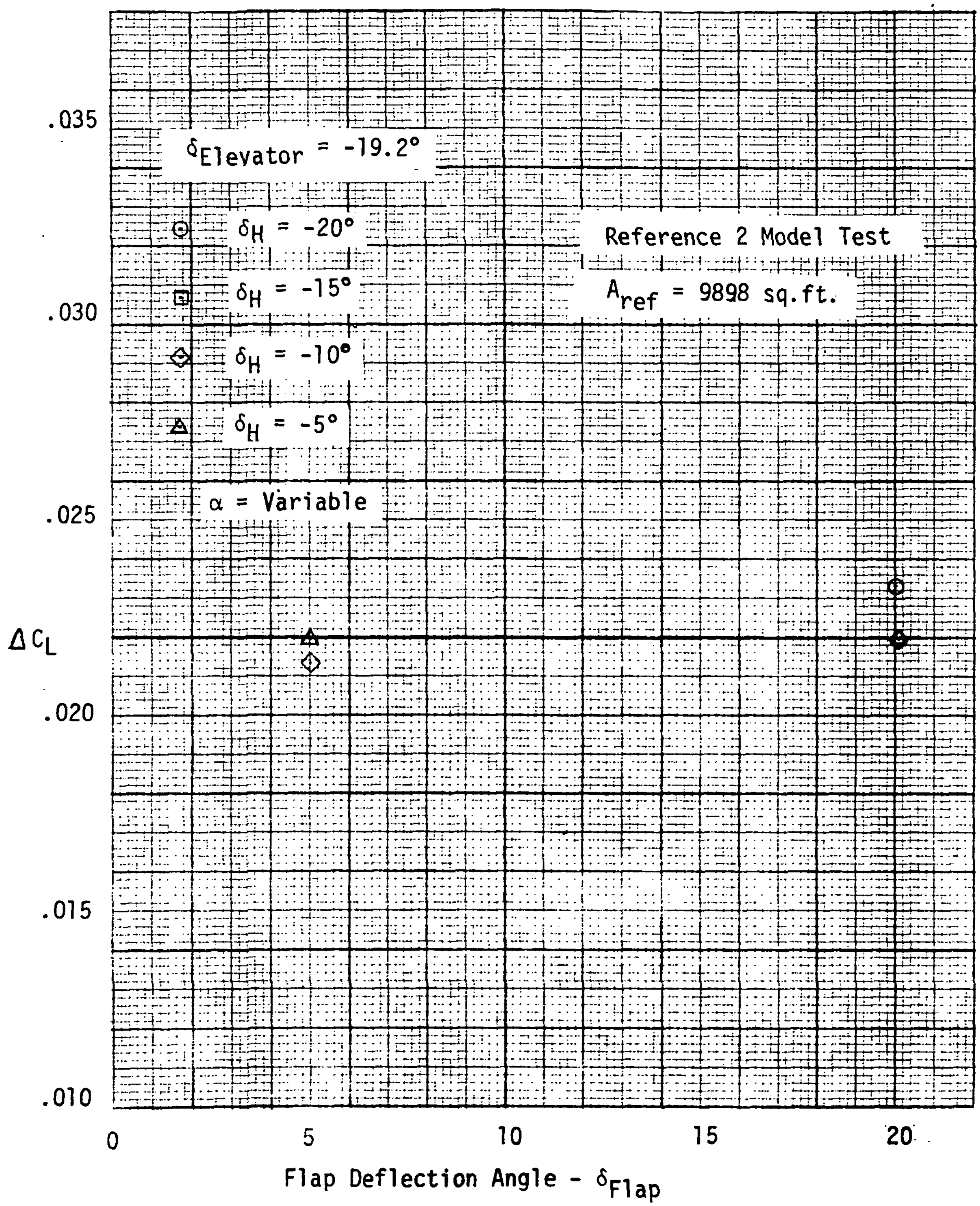

Figure VI-1A-19 — Variation of Elevator Lift with Trailing Edge Flap Angle

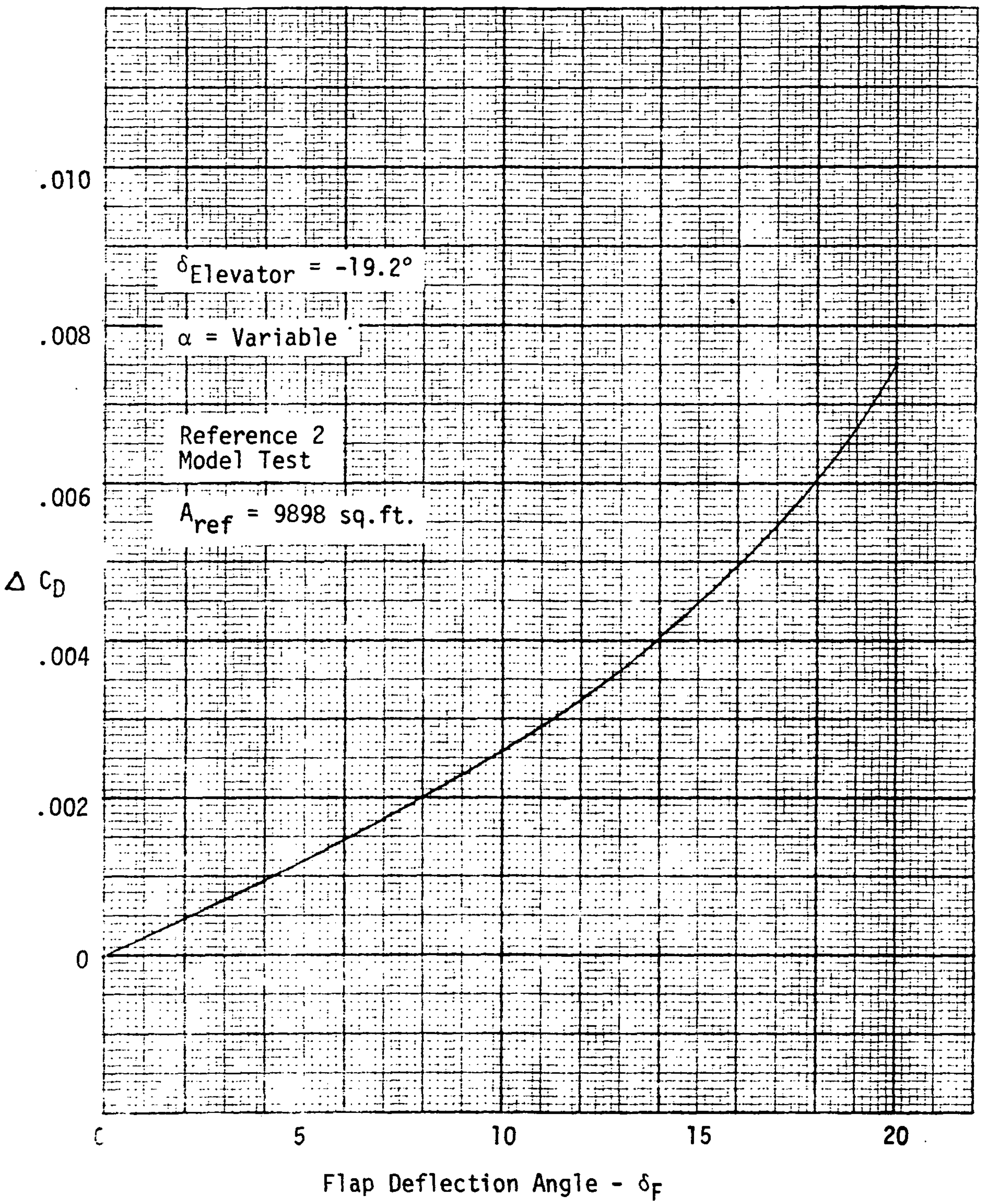

Figure VI-1A-20 — Variation of Elevator Drag with Trailing Edge Flap Angle

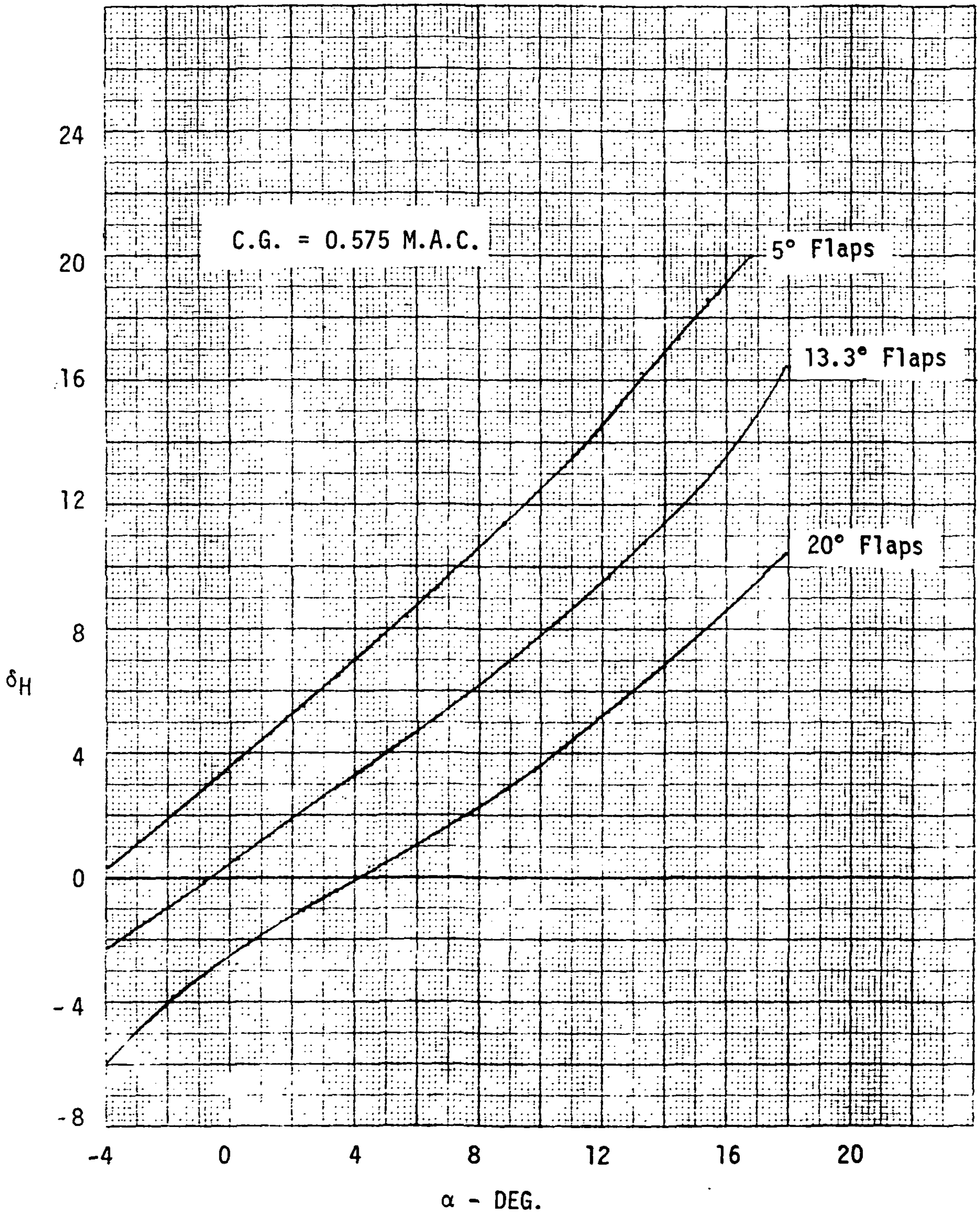

Figure VI-1A-21 — Variation of Tail Incidence Angle with Angle of Attack During Take-Off

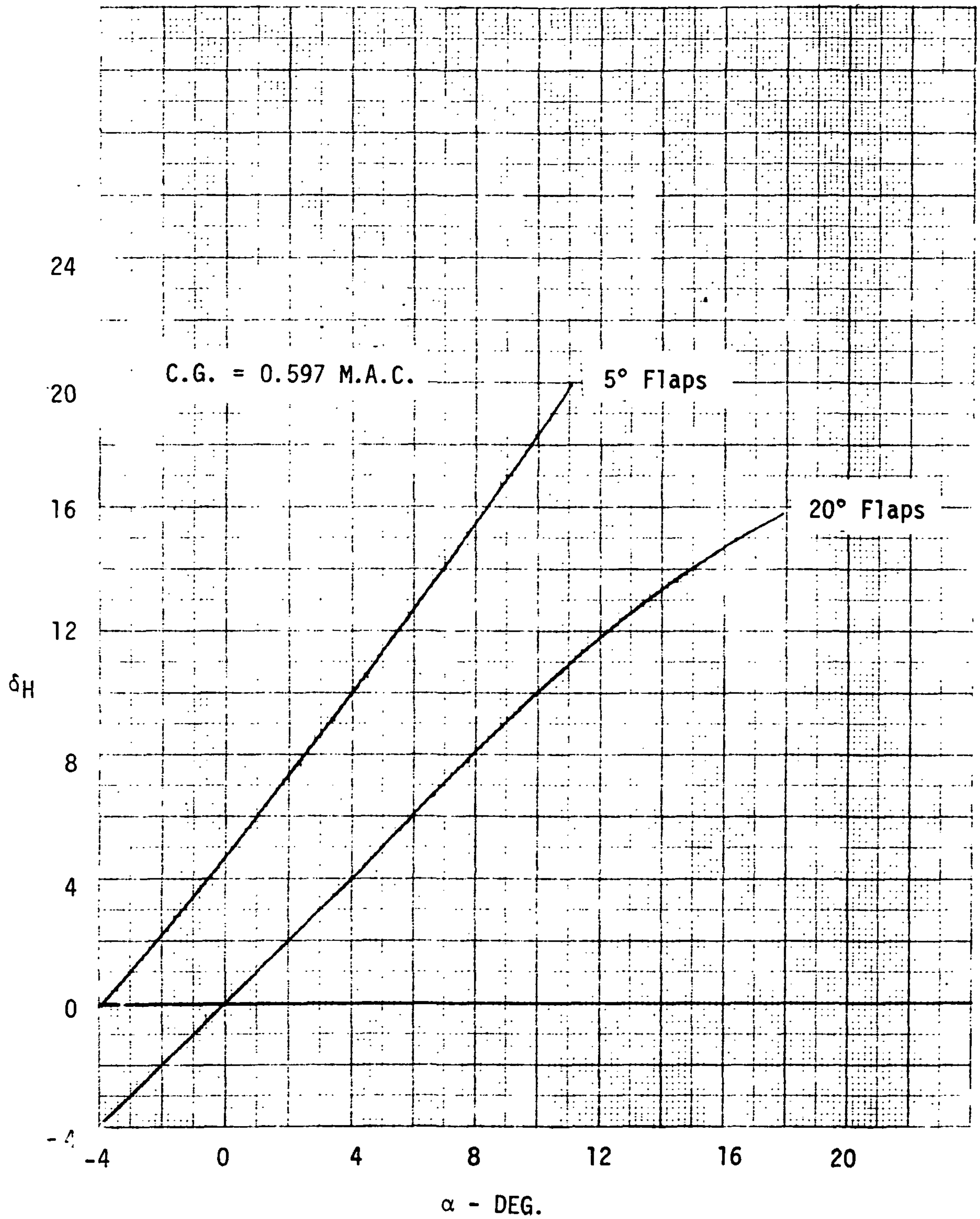

Figure VI-1A-22 — Variation of Tail Incidence Angle with Angle of Attack During Landing

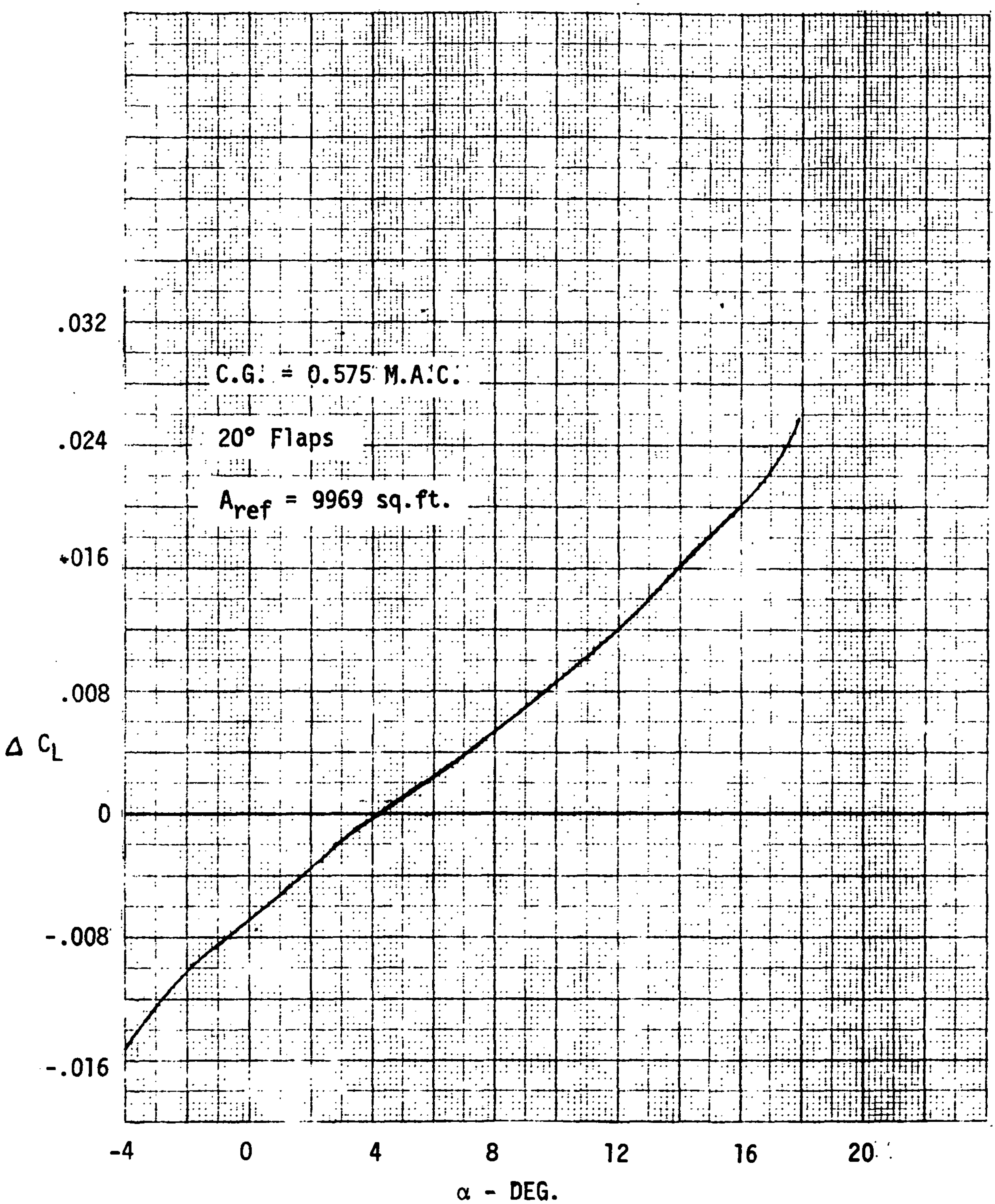

Figure VI-1A-23 — Variation of Tail Lift with Angle of Attack for Reference Configuration

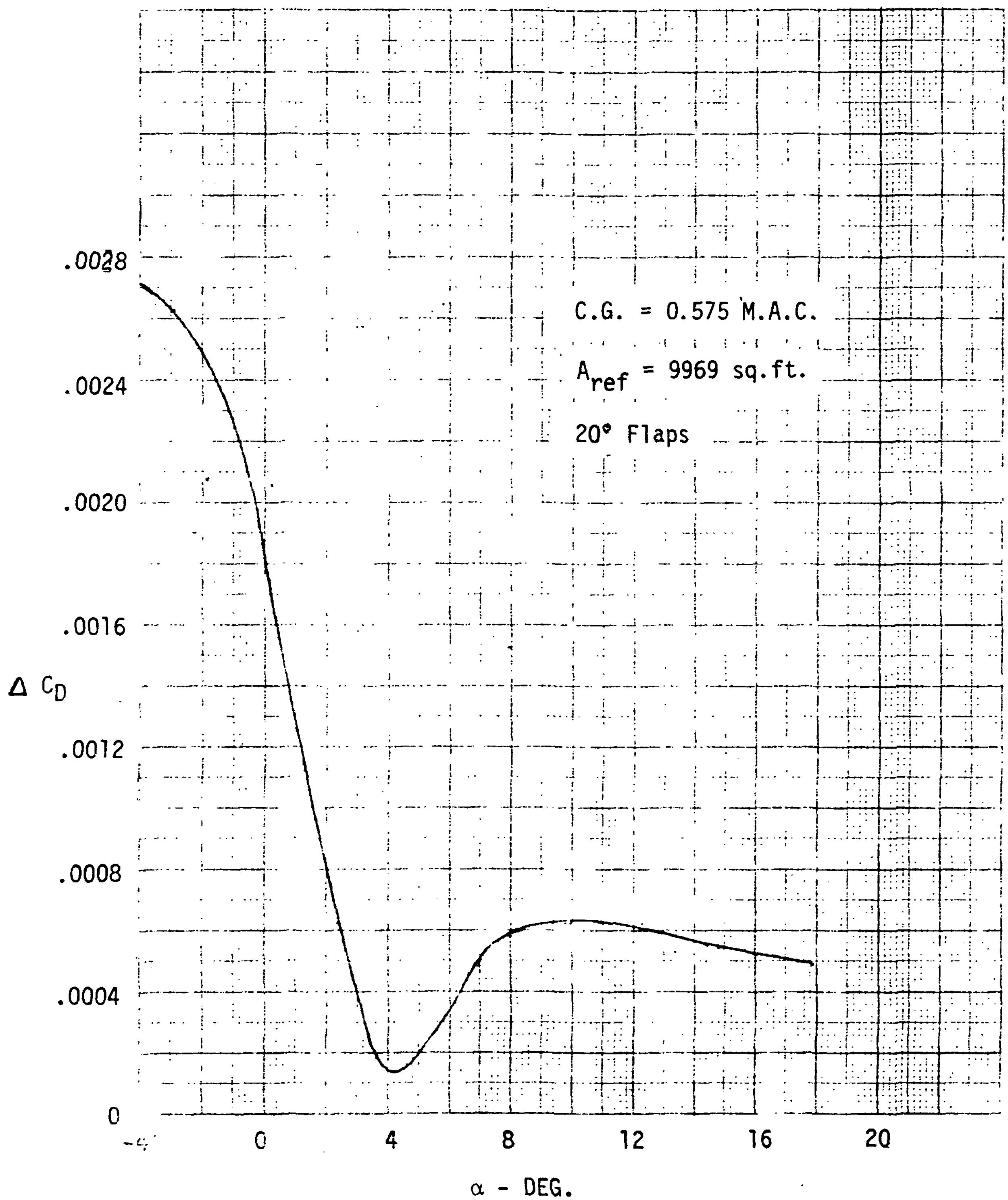

Figure VI-1A-24 — Variation of Tail Drag with Angle of Attack for Reference Configuration

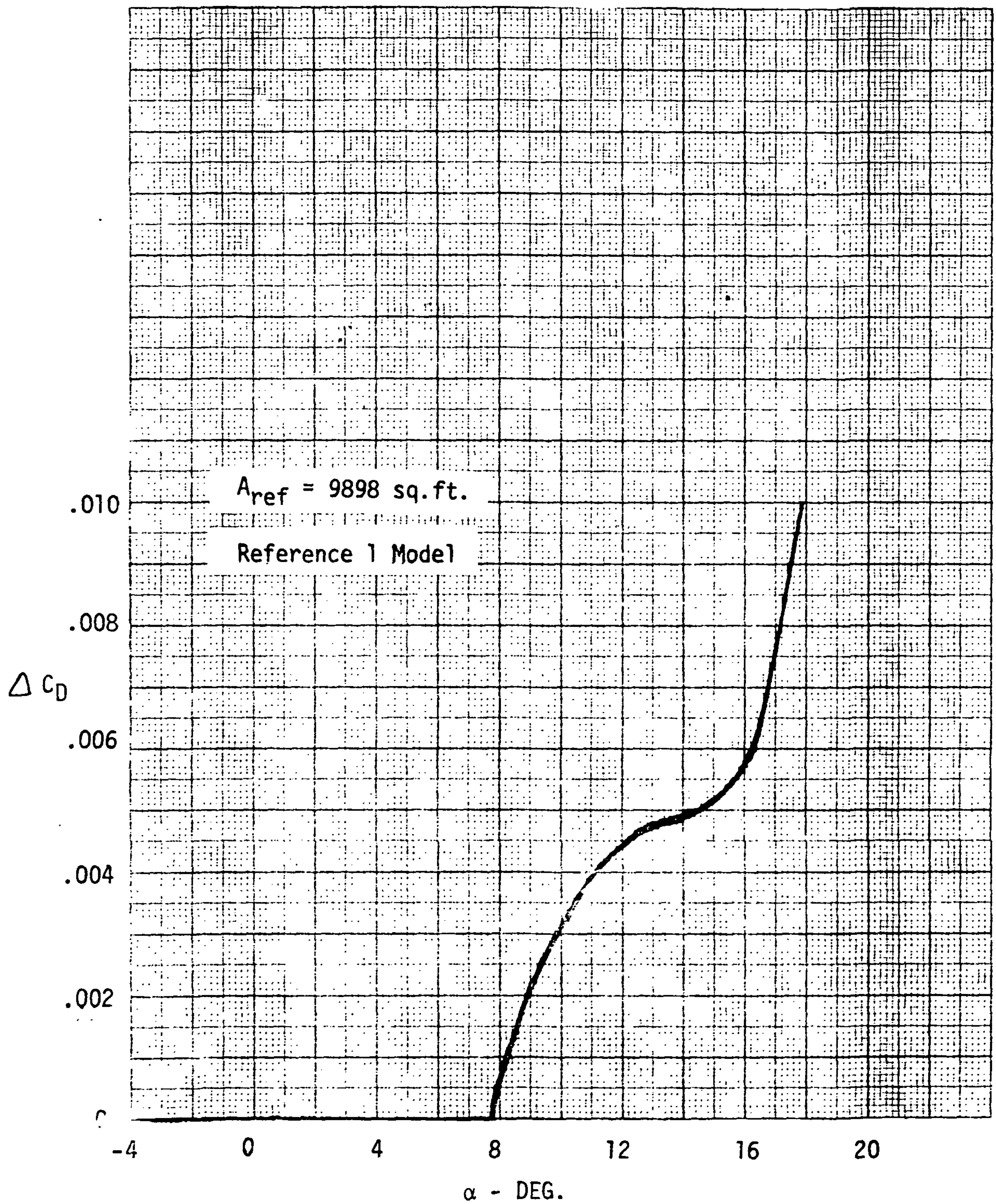

Figure VI-1A-25 — Effect of Angle of Attack on Drag of Outboard Vertical Fins

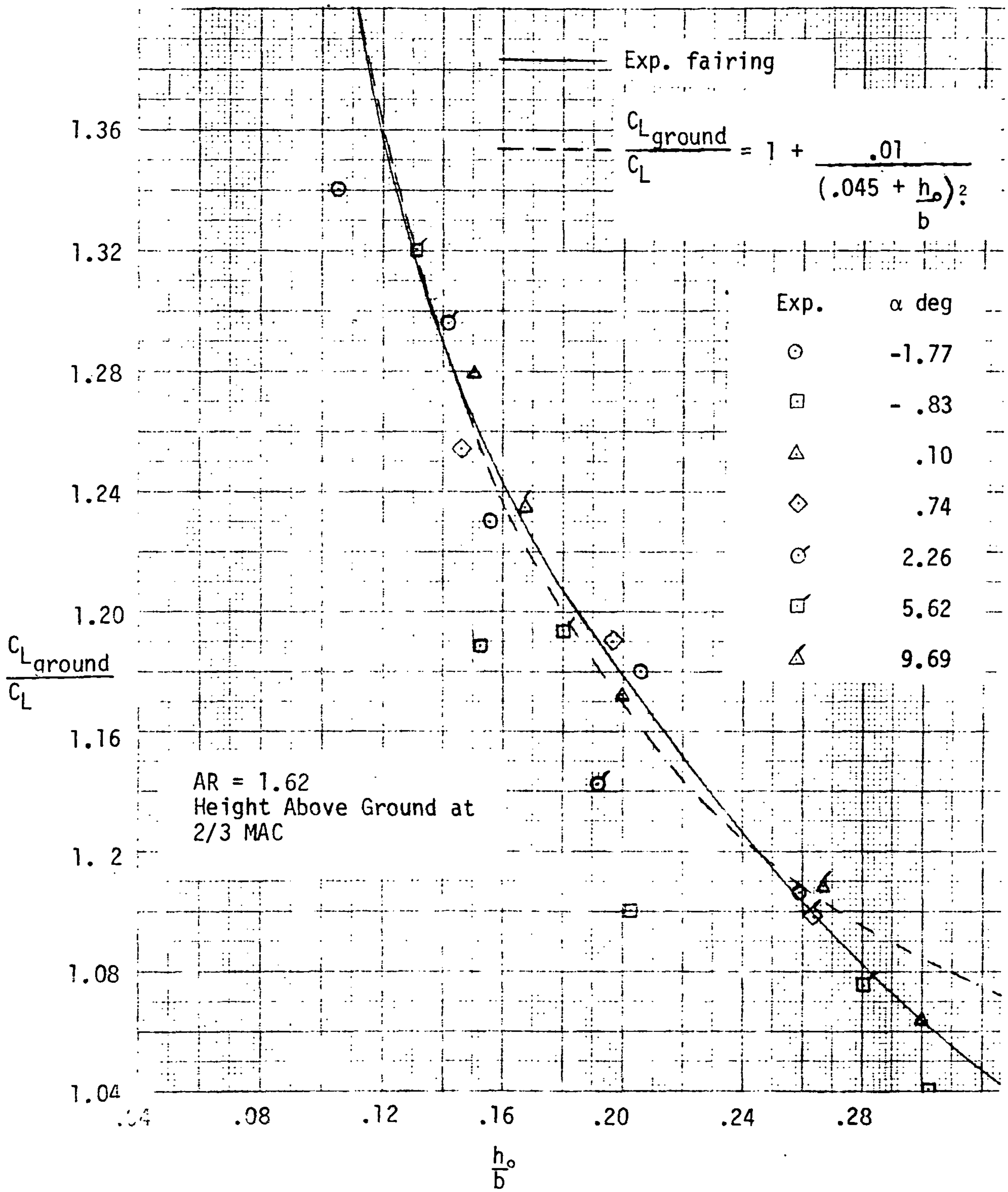

Figure VI-1A-26 — Ground Induced Lift for Arrow Wing Aircraft.

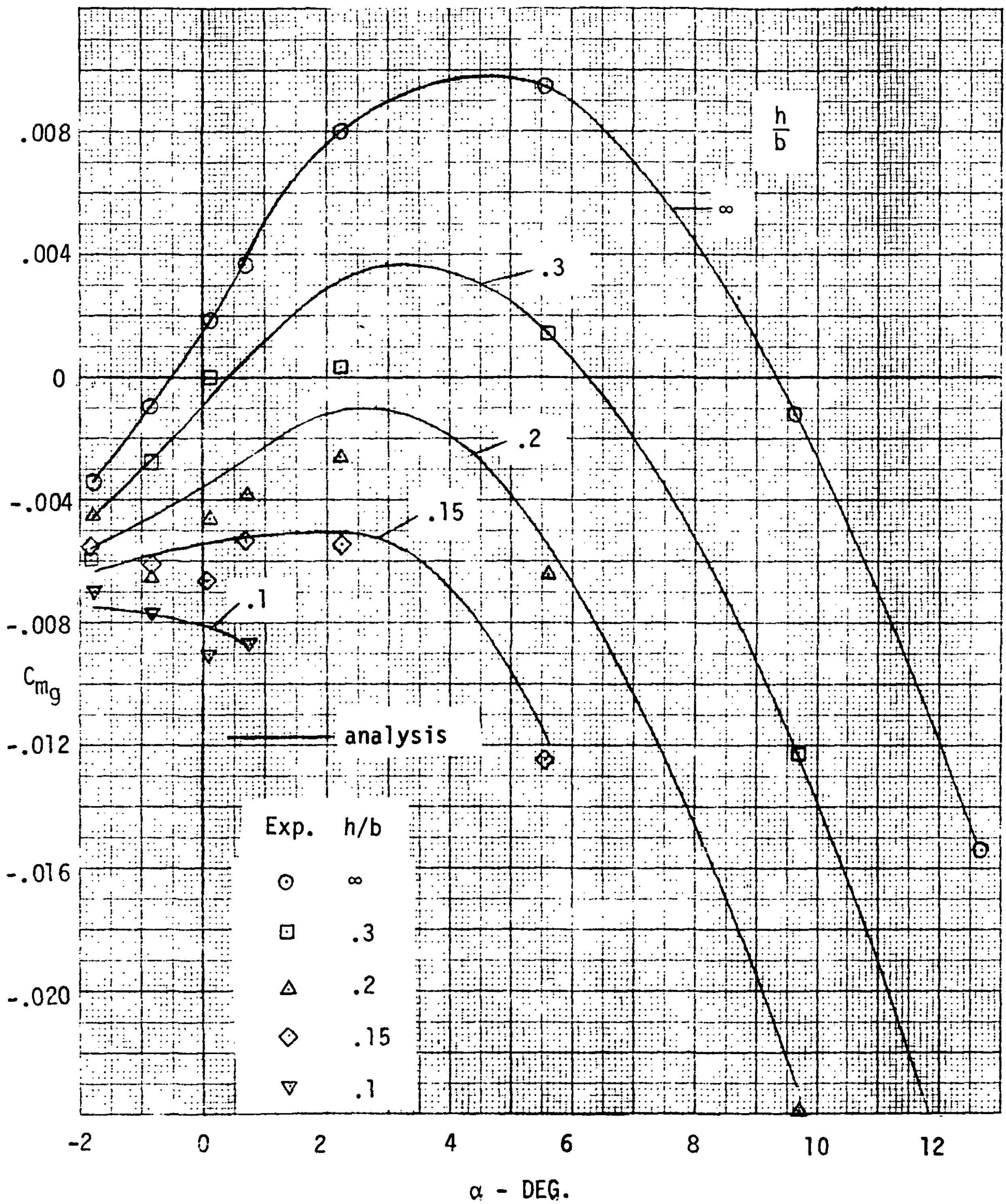

Figure VI-1A-27 — Arrow Wing Configuration Pitching Moment Coefficient near Ground. Correlation of Analysis with Experiment.

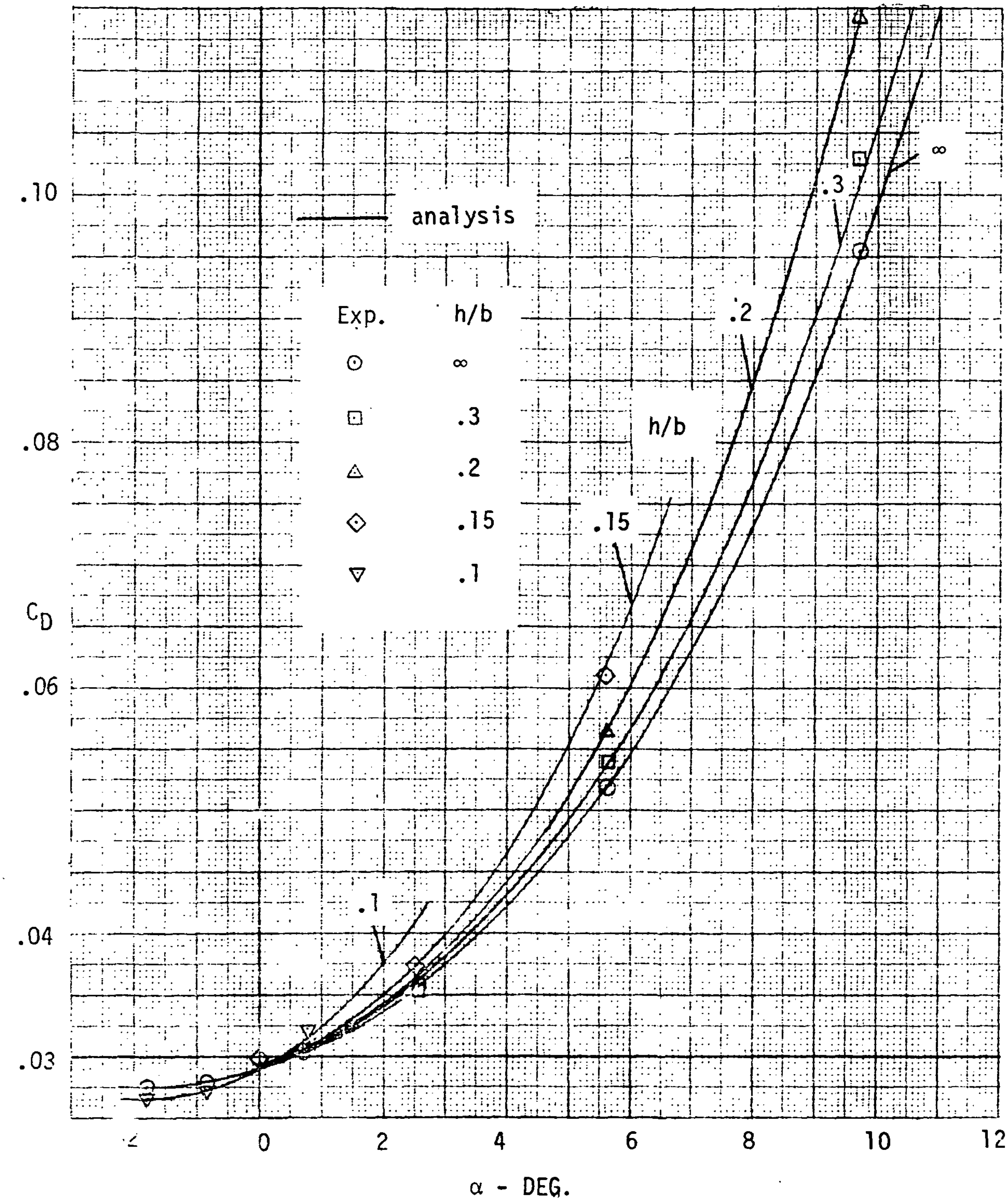

Figure VI-1A-28 — Arrow Wing Configuration Drag Coefficient near Ground. Correlation of Analysis with Experiment.

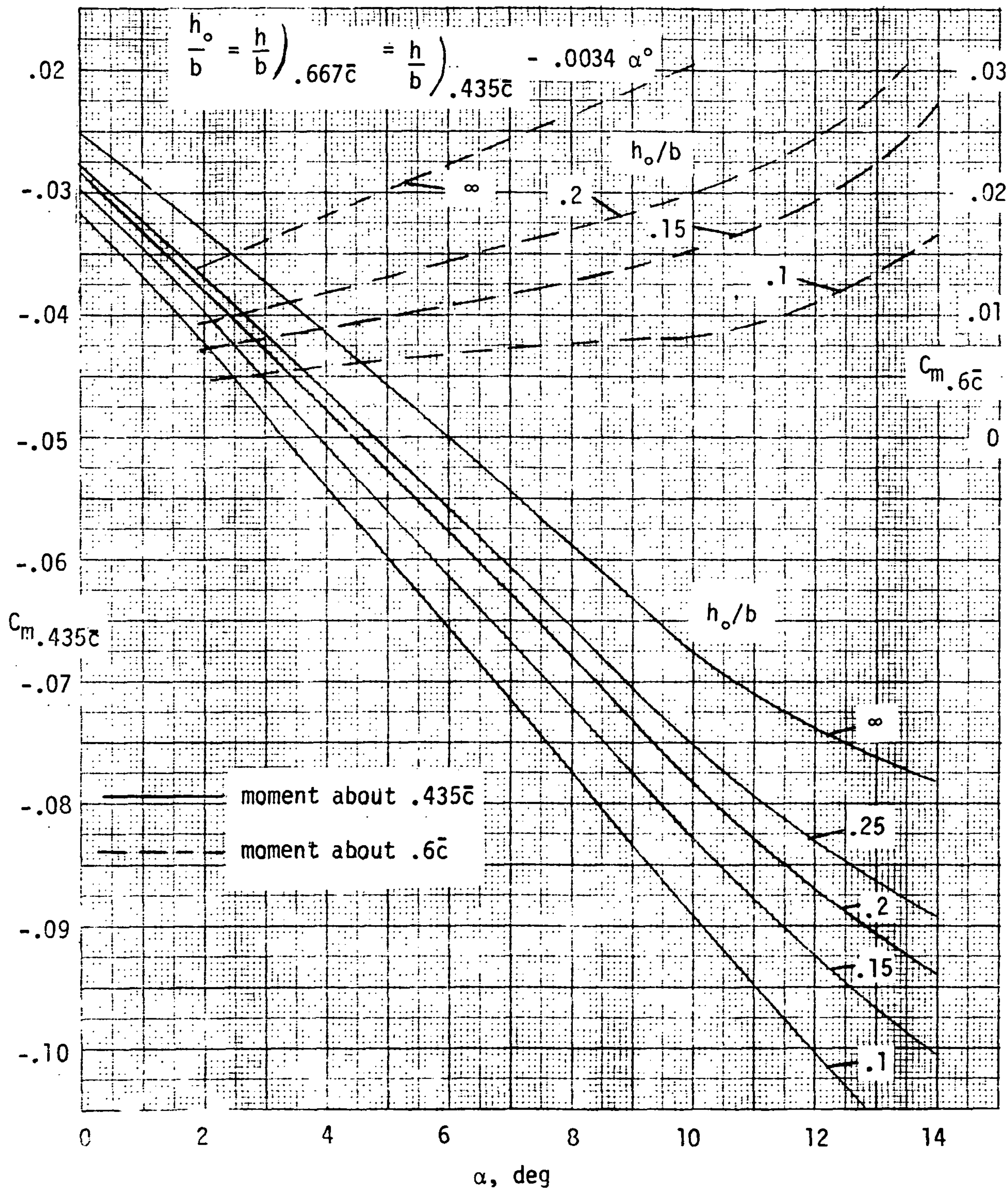

Figure VI-1A-29 — Reference Configuration Pitching Moment Coefficient near Ground.

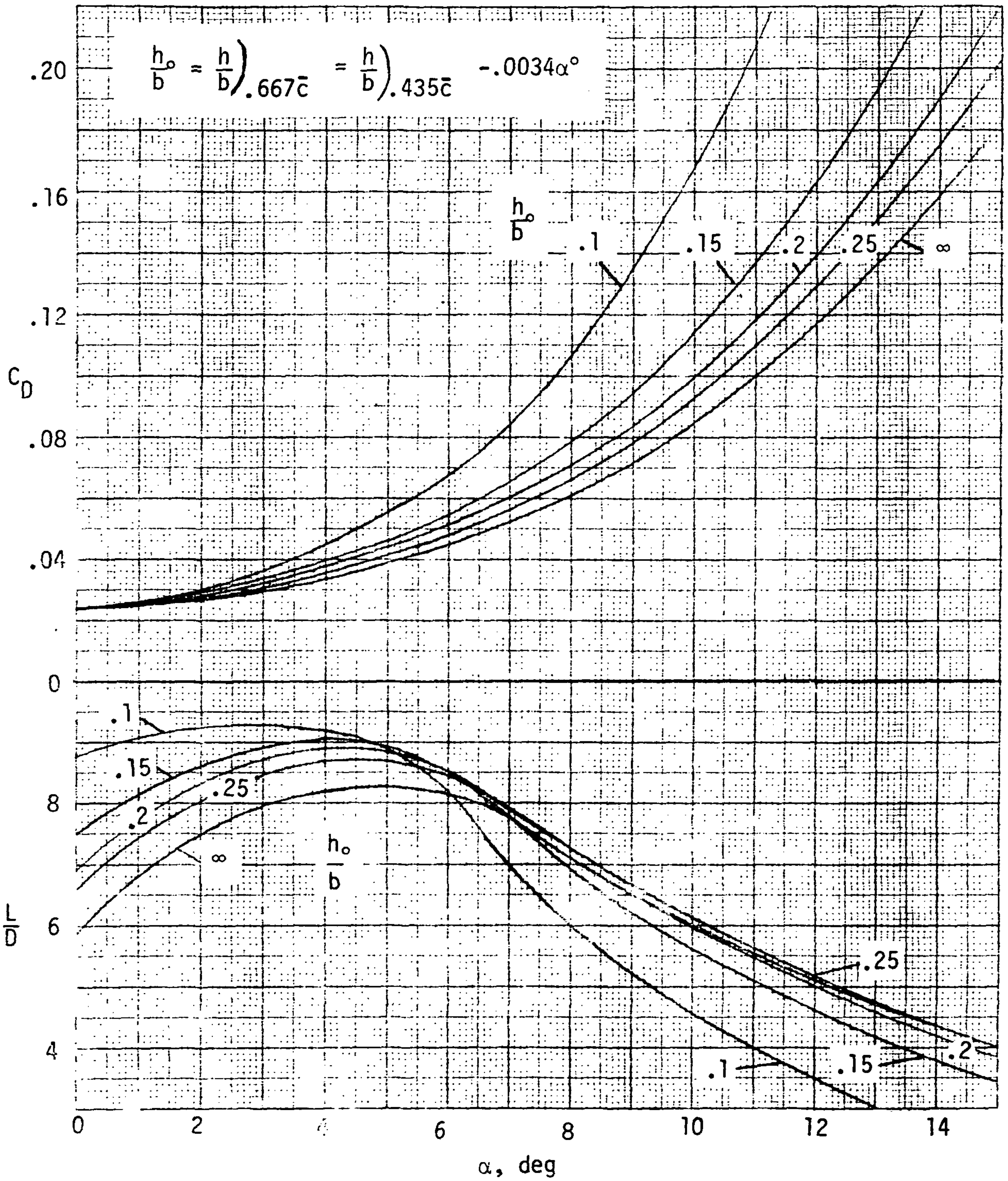

Figure VI-1A-30 -- Reference Configuration Drag Coefficient and L/D Ratio Near Ground.

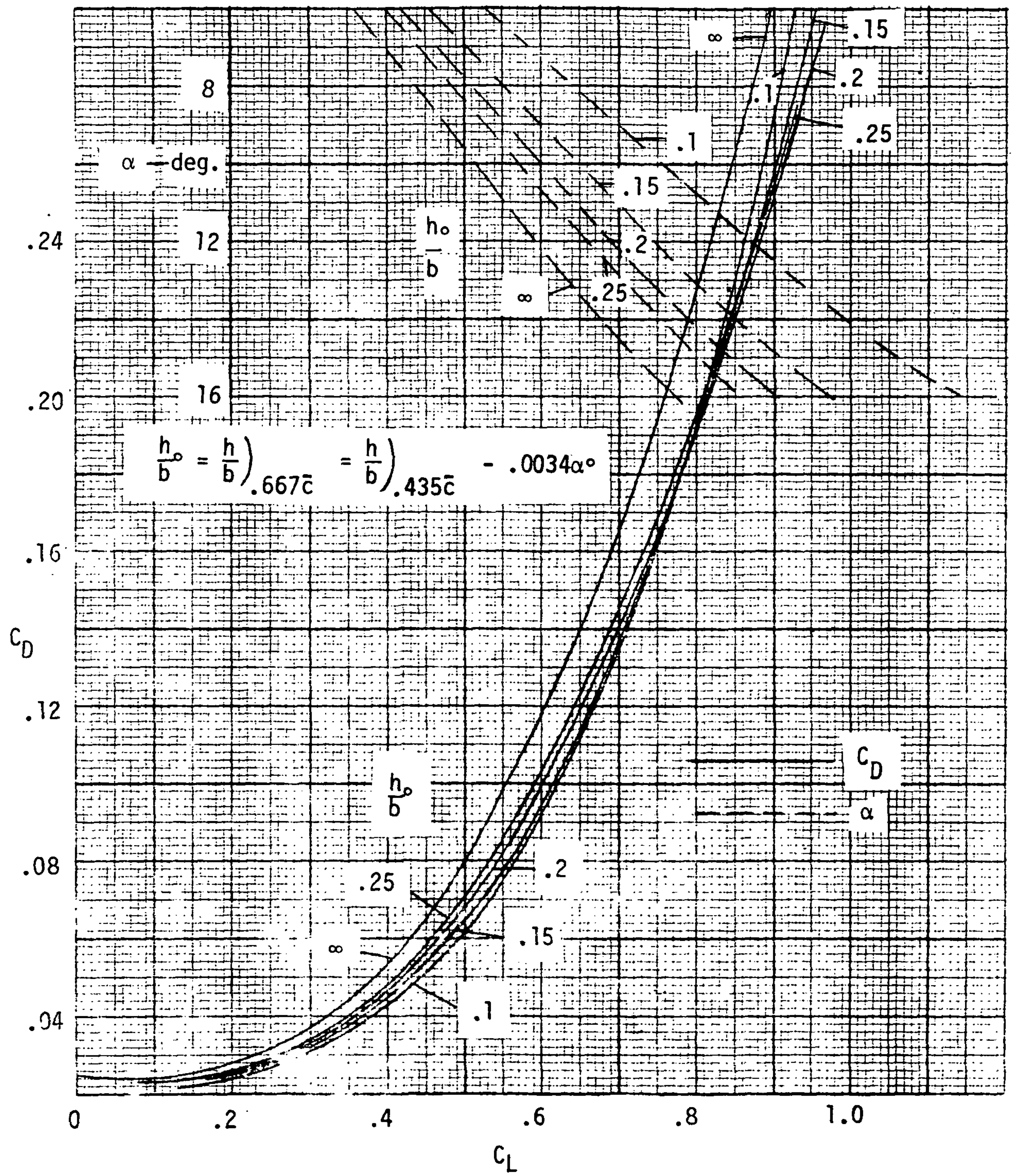

Figure VI-1A-31 Reference Configuration Drag Polar and C_L~α Curve Near Ground.

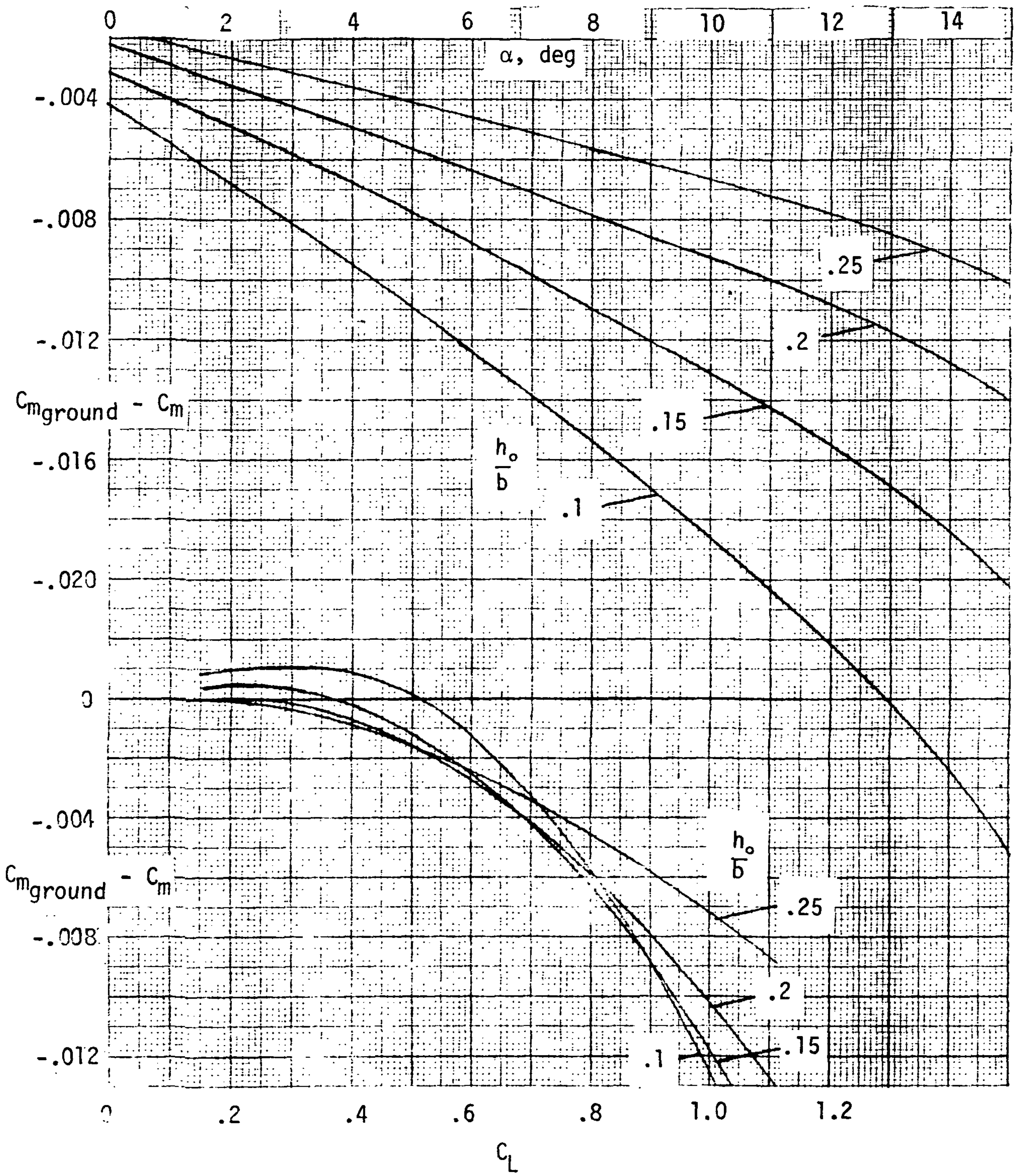

Figure VI-1A-32 - Reference Configuration Change in Pitching Moment Coefficient Due to Ground Effect

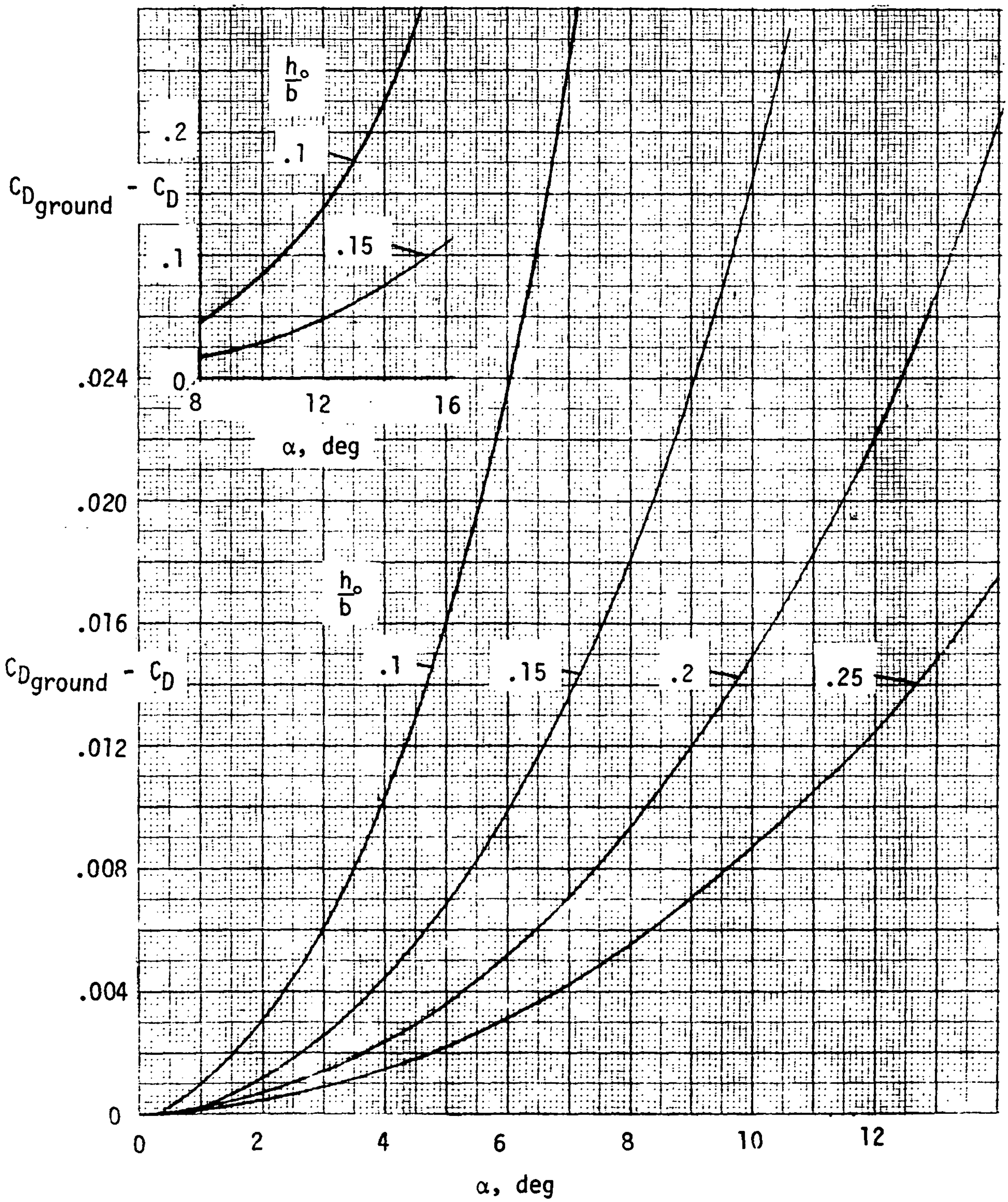

Figure VI-1A-33 — Reference Configuration Change in Drag Coefficient Due to Ground Effect.

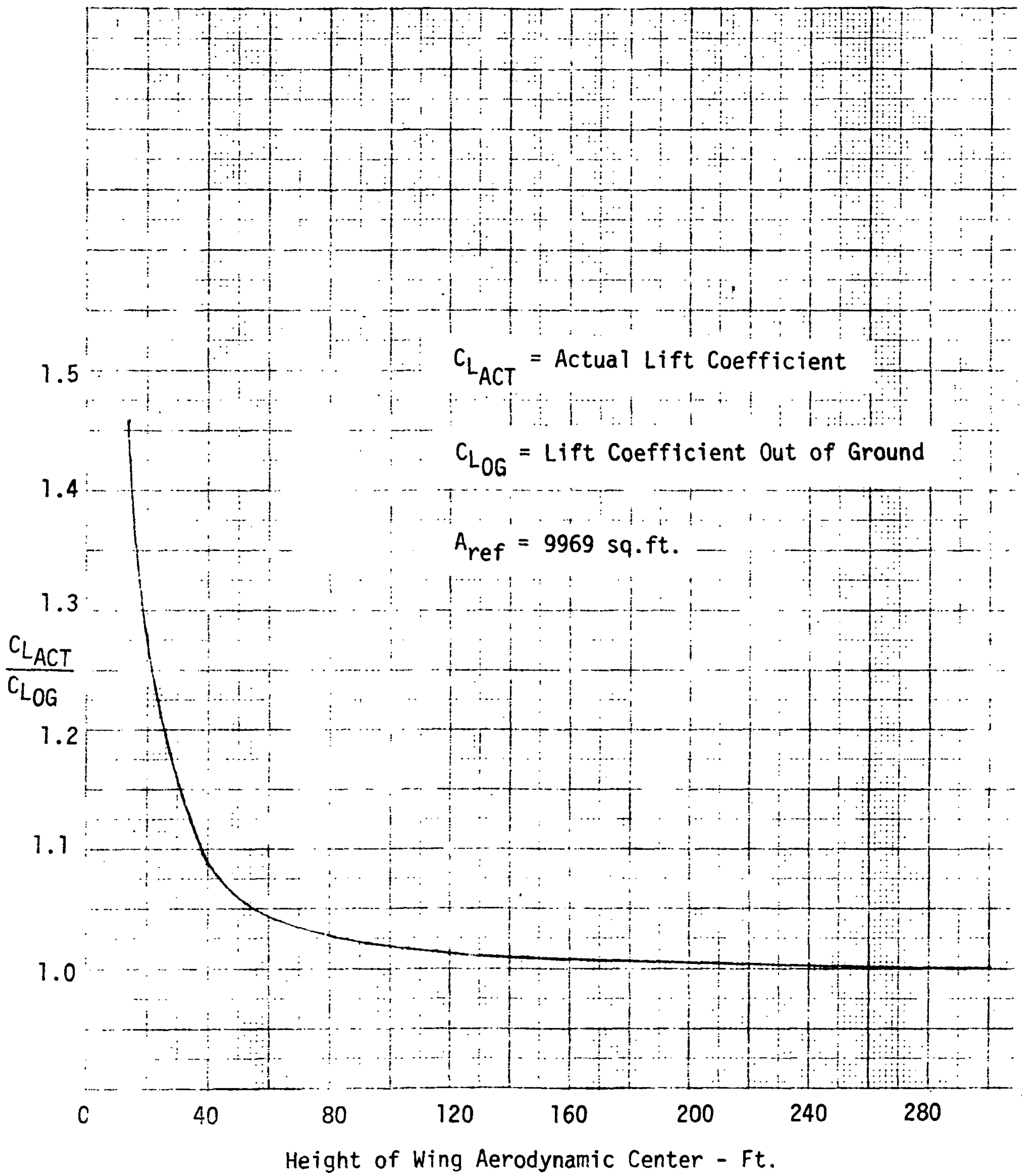

Figure VI-1A-34 — Effect of Wing Height on Lift for Reference Configuration

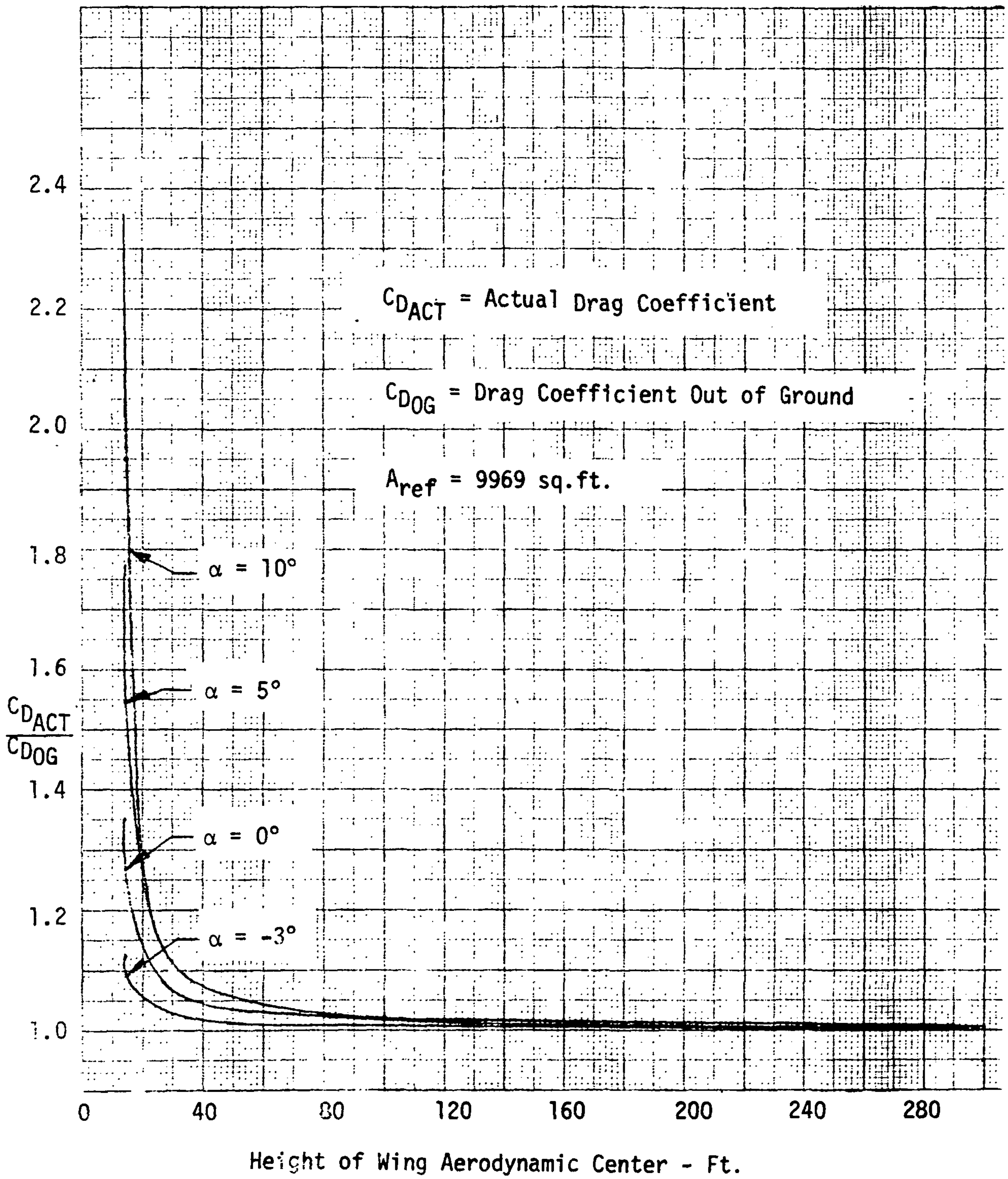

Figure VI-1A-35 — Effect of Wing Height on Drag of Reference Configuration

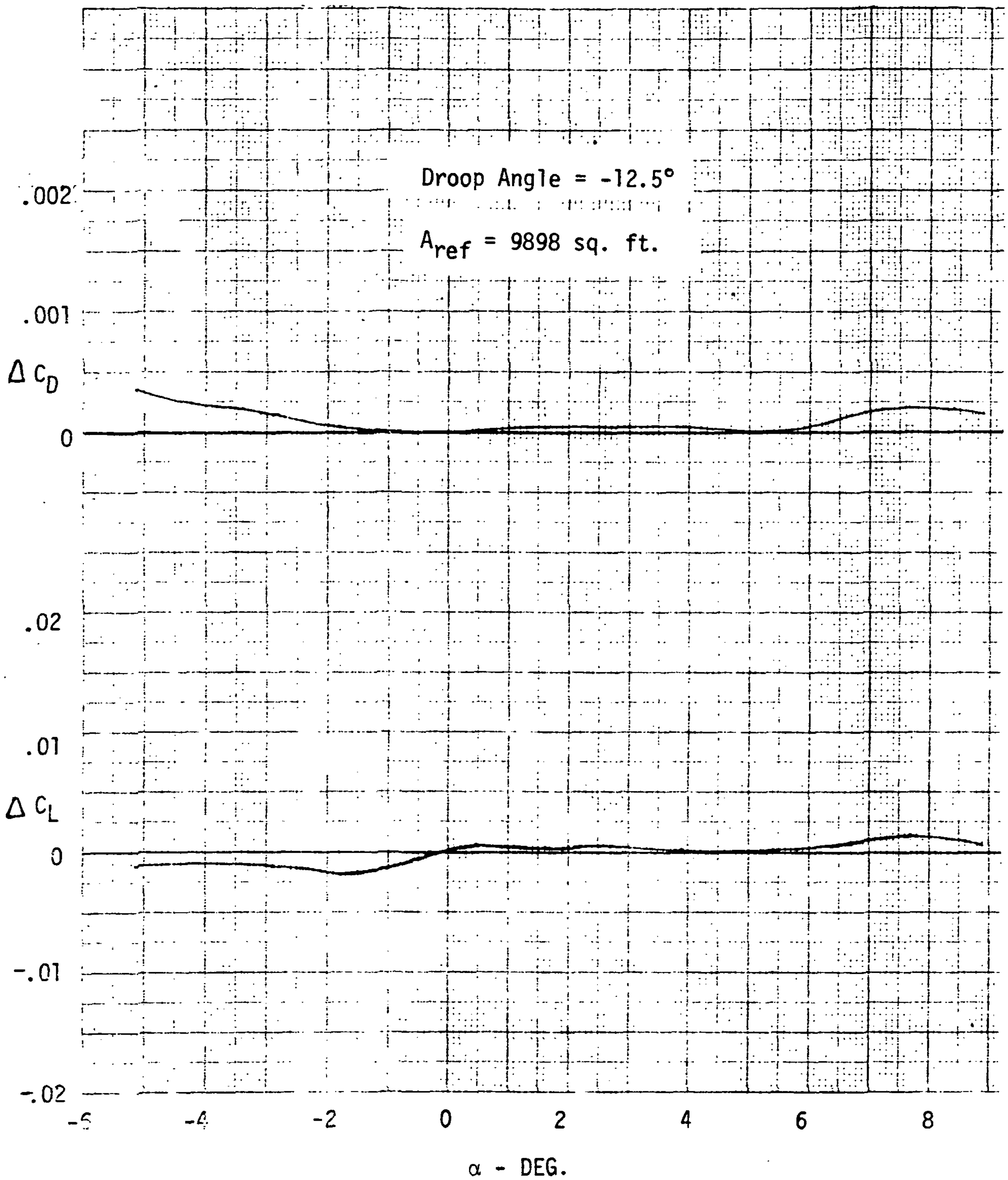

Figure VI-1A-36 — Effect of Nose Droop on Lift and Drag

VI-1B AERODYNAMICS

VI-1B HIGH SPEED AERODYNAMICS

INTRODUCTION

Recent advances in low speed aerodynamic technologies have resulted in wing configurations that exhibit significant improvements to that of the Boeing 969-336C (Reference VI-1B-1). Changes which were incorporated into the Reference Configuration wing to improve the aerodynamic characteristics consisted of a new wing planform to improve the longitudinal stability and low speed performance characteristics, and a supersonic twist and camber distribution optimization including favorable nacelle-wing interference effects to reduce trim drag at cruise. Other changes from the 969-336C SST configuration which affect the high speed aerodynamic characteristics include an increased fuselage size, changes to the wing thickness distribution, and a new and larger engine nacelle configuration. The theoretical aerodynamic methods used to derive the estimated high speed lift and drag performance of the Reference Configuration are an improved version of those used in the late 1960's (Reference VI-1B-2). The basis and methods used are outlined. High speed drag polar and the maximum lift-to-drag ratio behavior achieved are presented for the Reference Configuration.

SUMMARY

The 969-336C SST configuration developed by the Boeing Company during the national SST Program (Unpublished Reference VI-1B-1) was used as the basis for the Reference Configuration. The Reference Configuration incorporates changes from the 969-336C configuration primarily to improve low speed performance, and to provide for increases in passenger and fuel capacities, and to facilitate landing gear stowage. The Reference Configuration achieved a maximum lift-to-drag ratio of 8.67 for cruise at Mach 2.7 at an altitude of 60,000 feet. This compares to a value of 8.9 for the same conditions for the 969-336C configuration. The increase in aircraft wave drag associated with the changes from the 969-336C configuration to the Reference Configuration was the major reason for the reduction in the aerodynamic performance.

Reference Data Base

High speed drag polars for the 969-336C SST configuration were developed by the Boeing Company in 1969 as part of the national SST program Reference VI-1B-1 . The main changes from the 969-336C configuration to the Reference Configuration which affect the aerodynamic drag are the increases in the fuselage size and wing spanwise and chordwise thickness distributions, and changes to the engine nacelle geometry and wing planform. The drag polar shapes for the 969-336C SST configuration (Unpublished Reference VI-1B-1) are based on wind tunnel test data and were selected as a logical starting point for the determination of the lift dependent drag behavior for the Reference Configuration. Drag polars for the Reference Configuration were thereby derived by combining the characteristic polar shape, obtained by correcting the lift dependent drag behavior of the 969-336C configuration for differences in wing aspect ratio and reference area, with a zero-lift drag buildup for the Reference Configuration obtained by analytical methods.

High speed drag polars for the 969-336C SST configuration were available from unpublished reference VI-1B-1 for five Mach numbers (M=2.7, 2.3, 1.2, .95, and .6). These polars are presented for three Mach numbers (M=2.7, 1.2, and .6) in Figure VI-1B-1. Propulsion drag and air conditioning drag are handled as a separate aerodynamic drag increment and are not included in the drag polars. A breakdown of zero lift drag items for these polars follows:

Mach No.	.6	1.2	2.7
C_{D_F}	.00571	.00504	.00379
C_{D_W}	0.	.00308	.00176
$C_{D_{Roughness}}$	.00022	.00051	.00021
$C_{D_{Bumps\ \&\ Gullies}}$	0.	.00031	.00027

Table VI-1B-I. Zero Lift Drag Breakdown - 969-336C SST.

<u>Assumptions and Technology Used to Develop Drag Characteristics</u>

The airplane drag was separated into two categories for analysis: (1) lift dependent drag, and (2) zero lift drag. The lift dependent drag behavior was determined for the Reference Configuration by correcting the drag polars of unpublished reference VI-1B-1 (Figure VI-1B-1) for differences in airplane induced drag while the zero lift drag was determined primarily from a buildup of computed friction, wave, and roughness drag increments.

The drag polars of unpublished reference VI-1B-1 (Figure VI-1B-1) provided the basis for the lift dependent drag behavior, or polar shapes, derived for the Reference Configuration. These polar shapes were determined from wind tunnel test data and were corrected to account for the difference in wing aspect ratio on airplane induced drag for the two configurations. (A comparison of wing planforms for the two configurations is shown on Figure VI-1B-2). A correction to account for the change in the wing reference area defined, from 9898 square feet for the 969-336C configuration to 9969 square feet for the Reference Configuration, was also applied.

The major portion of the zero lift drag was determined from a buildup of the computed friction, wave, and roughness drag components. The Reference Configuration did not require a drag penalty for landing gear and pod bumps and gullies or trim drag at cruise. The zero drag penalty for landing gear and pod bumps and gullies is in keeping with the increased wing thickness of the Reference Configuration, which eliminates the need for landing gear bumps, and a method of fairing the wing trailing edge which eliminates the other bumps and gullies. The zero trim drag at cruise is based on the capability to design the wing with the proper camber and twist distribution and to optimize the nacelle position to result in a zero pitching moment for trim at the cruise condition. The cruise polar (M=2.7) of the Reference Configuration benefits from a zero lift drag coefficient reduction of .0002 relative to that of the 969-336C configuration due to this effect. No other changes in trim drag relative to the 969-336C configuration were considered or investigated.

Figure VI-1B-3 illustrates the breakdown of the cruise polar as described above for the 969-336C configuration used for the drag basis. Here the reduction in trim drag mentioned above is indicated as an increment in the zero lift drag. The drag remaining after the zero lift drag and lift induced drag components are accounted for is indicated as ΔC_{D_P} and is attributed to camber and separated flow effects. The similar breakdown for the cruise polar of the Reference Configuration is illustrated in Figure VI-1B-4.

Skin friction and wave drag solutions were obtained by means of NASA computer programs. A computer plot of the geometry representation of the Reference Configuration used in these programs is illustrated in Figure VI-1B-5. A list of the computer programs used is contained at the end of this section. References VI-1B-3 and VI-1B-4 document the programs used for the wave drag and configuration plots.

Airplane roughness drag for the Reference Configuration was determined at a value of six percent of friction drag at cruise (M=2.7). For Mach numbers below cruise the 969-336C roughness drag values (Unpublished Reference VI-1B-1) were ratioed to provide the Reference Configuration values to the same ratio obtained at the cruise Mach number.

Impact of Configuration Concept on Baseline Drag Characteristics

The Reference Configuration incorporates a number of design changes which result in an increase in aircraft volume relative to the 969-336C configuration. The fuselage length was increased from 295 feet to 315 feet while the width was increased to 140 inches to allow for an increase in passenger seating, from 234 to 292, plus room for optional fuel storage in the aft (tail) region. The inboard wing sections were thickened and the point of maximum thickness shifted aft to 75% chord to provide an additional ten inches wing depth for gear stowage without bumps on the wing in the vicinity of wing station 114 (for both structural and aerodynamic considerations). Finally, the engine size was increased from an airflow of 633 pounds per second to 800 pounds per second and a new "D" engine nacelle configuration was adopted. The effect of these changes on the nacelle net cross section area distribution is shown in Figure VI-1B-6. As a result of all of the changes, the aircraft volume was increased resulting in increases in aircraft friction and wave drag. A summary of the increases in skin friction and wave drag coefficients attributed to these changes is made in Table VI-1B-II below for the cruise condition at an altitude of 60,000 feet. The coefficients shown are based on a common reference area of 9898 square feet. The values listed for the incremental changes are considered to be representative values for the effects indicated.

Configuration Change	$\Delta C_{D_F} \times 10^4$	$\Delta C_{D_W} \times 10^4$
Fuselage Size Increase	.2	2.0
Wing Thickness Increase	.3	3.1
Wing Planform Change	.6	.5
Change from 633#/sec nacelle to 800#/sec "D" nacelle	1.1	-2.4
Total	5.2	4.2

Table VI-1B-II. Increases in Skin Friction and Wave Drag at Cruise for Reference Configuration Relative to 969-336C SST.

In addition to the values summarized in Table VI-1B-II, increases in C_{D_F} of 3.0×10^{-4} and C_{D_W} of 1.0×10^{-4} were obtained for the values calculated for the 969-336C configuration relative to the values quoted in Unpublished Reference VI-1B-1. The reason for these differences is unknown.

A comparison of skin friction drag is made in Table VI-1B-III below for Mach numbers of .6, 1.2, and 2.7, for the two configurations. The coefficients shown are based on a common reference area of 9898 square feet. The reason for the differences between the values calculated for the 969-336C configuration and those quoted in Unpublished Reference VI-1B-1 is unknown.

Configuration	Source	C_{D_F}	(S_{REF} = 9898 ft^2)	
Mach No.		.6	1.2	2.7
Altitude		7,500 ft	34,300 ft	60,000 ft
969-336C	Ref. 1	.00571	.00504	.00379
	Calculated	.005654	.005307	.004091
Reference	Calculated	.005971	.005603	.004320

Table VI-1B-III. Skin Friction Drag Coefficient (C_{D_F}) Comparison.

The aircraft wave drag is a function of the longitudinal distributions of area along Mach angle cuts. The integrated average area distributions for a Mach number of 2.7 are compared in Figure VI-1B-7 for the total aircraft and for the aircraft fuselages alone. (The difference in the characteristic shape of the fuselage area distributions arises to some extent from the difference in the cross section shape of the two fuselage configurations, which is circular for the Reference Configuration and non-circular for the 969-336C configuration.) The effect of the increased volume of the Reference Configuration is apparent in this figure. The Reference Configuration fuselage area distribution was contoured to provide a near-optimum shape for the Mach 2.7 total integrated average area distribution shown in Figure VI-1B-7. An increase in wave drag would be expected for the Reference Configuration as a result of the increase in volume. In Figure VI-1B-8, the wave drag, based on a common reference area of 9898 square feet, is plotted as a function of aircraft volume. The effects of the changes to the 969-336C configuration leading to the Reference Configuration are mapped on this figure. The total drag polars for the 969-336C and Reference Configuration are compared for Mach numbers of .6, 1.2, and 2.7, and a common reference area of 9898 ft^2 in Figures VI-1B-9 through VI-1B-11.

Reference Configuration High Speed Aerodynamic Characteristics

High speed drag polars used for range performance computation of the Reference Configuration are presented. The propulsion and air conditioning drag are also shown. Maximum lift-to-drag ratio performance is compared with that of the 969-336C configuration for Mach numbers above .6.

High speed drag polars are presented for the Reference Configuration in Figures VI-1B-12 through VI-1B-14 for subsonic (M=.6), transonic (M=1.2), and supersonic cruise (M=2.7), Mach numbers. They are also presented in tabulated form in Table VI-1B-IV for Mach numbers of .6, .8, .95, 1.05, 1.2, 1.4, 1.6, 1.8, 2.2, 2.4, and 2.7. These polars are based on the Reference Configuration reference area of 9969 square feet. Lift coefficients achieved for the conditions presented and the lift coefficients required to obtain the maximum lift-to-drag ratios are indicated on the figures. A correction factor was applied to the cruise polar to account for the change in friction drag for altitudes above 60,000 feet when used for mission range performance computations. This correction factor was: $dC_D/dh = .037151 \times 10^{-6}/ft$. The propulsion drag and air conditioning drag used for the Reference Configuration mission range performance is presented as a function of Mach number in Figure VI-1B-15. These drag increments must be added to the drag polars

(Figures VI-1B-13 through VI-1B-15 and Table VI-1B-IV) to obtain the total aircraft drag used for performance analysis.

The maximum lift-to-drag ratio performance is presented for the Reference Configuration for Mach numbers of .6 and above in Figure VI-1B-16. The 969-336C maximum lift-to-drag ratio performance is also included on this Figure for comparison purposes. These curves represent the maximum lift-to-drag ratios obtained using the total drag including propulsion and air conditioning drag. The reduction in the maximum lift-to-drag ratio performance relative to the 969-336C configuration is a result of the increased skin friction and wave drag associated with the increases in wing thickness and fuselage size incorporated into the Reference Configuration design concept.

LIST OF SYMBOLS

A	Wing Aspect Ratio
$\bar{c}$	Wing Mean Aerodynamic Chord - in.
C_D	Airplane Drag Coefficient
$C_{D_{Bumps\ \&\ Gullies}}$	Airplane Drag Coefficient Due to Bumps & Gullies
C_{D_f}	Airplane Friction Drag Coefficient
C_{D_i}	Airplane Induced Drag Coefficient
$C_{D_{Roughness}}$	Airplane Roughness Drag Coefficient
C_{D_W}	Airplane Wave Drag Coefficient
C_L	Airplane Lift Coefficient
c.g.	Airplane Center of Gravity
dC_D/dh	Variation in Airplane Drag Coefficient with Altitude - ft.$^{-1}$
h	Altitude - ft.
$(L/D)_{max}$	Airplane Maximum Lift-to-Drag Ratio
M	Mach Number
S_{EQUIV}	Average Equivalent - Body Area for Cuts Taken Along Mach Lines
S_{GROSS}	Airplane Gross wing area - ft.^{2}
S_{NET}	Nacelle Cross Section Area Minus Inlet Capture Area - ft.^{2}
S_{REF}	Airplane Reference Wing Area - ft.^{2}
ΔC_{D_P}	Airplane Lift-Dependent Drag Coefficient Due To Camber, Planform, and Miscellaneous Effects
$\Delta C_{D_{TRIM}}$	Airplane Drag Coefficient Increment Due To Trim

LIST OF TABLES

REFERENCES

Reference No.	Title
VI-1B-1	The Boeing Co.: Mach 2.7 Fixed Wing SST Model 969-336C (SCAT-15F), Document No. D6A-11666-1, dated November 1969.
VI-1B-2	Baals, Donald D; Robins, Warner A., and Harris, Roy V., Jr.: Aerodynamic Design Integration of Supersonic Aircraft, Journal of Aircraft, Vol. 7, No. 5, September-October, 1970, pp. 385-394.
VI-1B-3	Harris, Roy V., Jr.: An Analysis and Correlation of Aircraft Wave Drag, NASA TM X-947, 1964.
VI-1B-4	Craidon, Charlotte B.: Description of a Digital Computer Program for Airplane Configuration Plots, NASA TM X-2074, 1970.

NASA COMPUTER PROGRAMS

Number	Title
D1260	Aircraft Wetted Areas and Reference Lengths
D1266	Airplane Turbulent Skin Friction Drag
D2290	Configuration Plots
D2500	Wave Drag

LIST OF FIGURES

C_L	C_D					
Mach No.	.6	.8	.95	1.05	1.2	1.4
Altitude	7,500 ft.	21,000 ft.	30,000 ft.	32,000 ft.	34,300 ft.	37,800 ft.
.02	.009164	.009466	.011420	.013900	.014684	.013275
.04	.008502	.008700	.010298	.012538	.013409	.012225
.06	.008147	.008256	.009544	.011602	.012593	.011645
.08	.008101	.008134	.009159	.011093	.012234	.011533
.10	.008361	.008335	.009144	.011011	.012334	.011890
.12	.008929	.008858	.009497	.011357	.012891	.012716
.14	.009805	.009703	.010219	.012129	.013906	.014012
.16	.010988	.010871	.011311	.013328	.015378	.015776
.18	.012478	.012361	.012771	.014955	.017309	.018009
.20	.014276	.014173	.014601	.017008	.019697	.020711
.24	.018795	.018764	.019367	.022397	.025848	.027521
.28	.024543	.024645	.025609	.029493		
.32	.031521	.031815				

Table VI-1B-IV - High Speed Drag Polars - Reference Configuration - S_{ref} = 9969 ft^2

C_L	C_D				
Mach N	1.6	1.8	2.2	2.4	2.7
Altitude	41,300 ft.	44,600 ft.	51,500 ft.	55,000 ft.	60,000 ft.
.02	.011642	.010286	.008479	.008108	.008046
.03	.011174	.009922	.008260	.007916	.007844
.04	.010825	.009679	.008173	.007866	.007808
.05	.010596	.009557	.008216	.007958	.007938
.06	.010486	.009557	.008390	.008191	.008234
.07	.010495	.009679	.008694	.008567	.008697
.08	.010623	.009921	.009130	.009085	.009327
.09	.010871	.010286	.009696	.009745	.010122
.10	.011238	.010772	.010393	.010548	.011084
.12	.012329	.012108	.012178	.012578	.013508
.14	.013897	.013929	.014487	.015176	.016597
.16	.015943	.016237	.017319	.018342	.020351
.18	.018465	.019031	.020673	.022076	.024771
.20	.021464	.022310	.024551	.026378	
.24	.028894				

Table VI-1B-IV (Continued) - High Speed Drag Polars - Reference Configuration - S_{ref} = 9969 ft^2

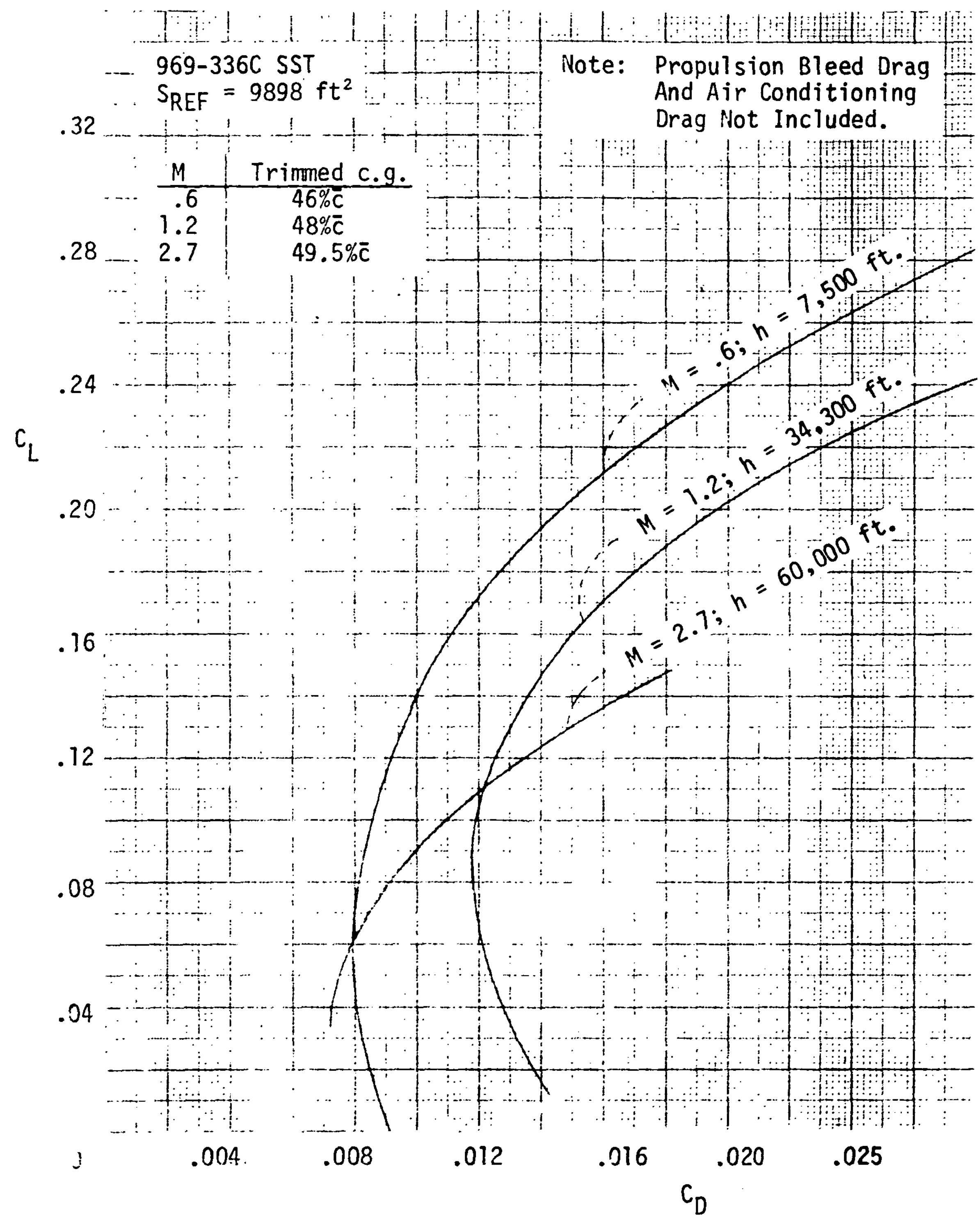

Figure VI-1B-1 Drag Basis - 969-336C High Speed Drag Polars

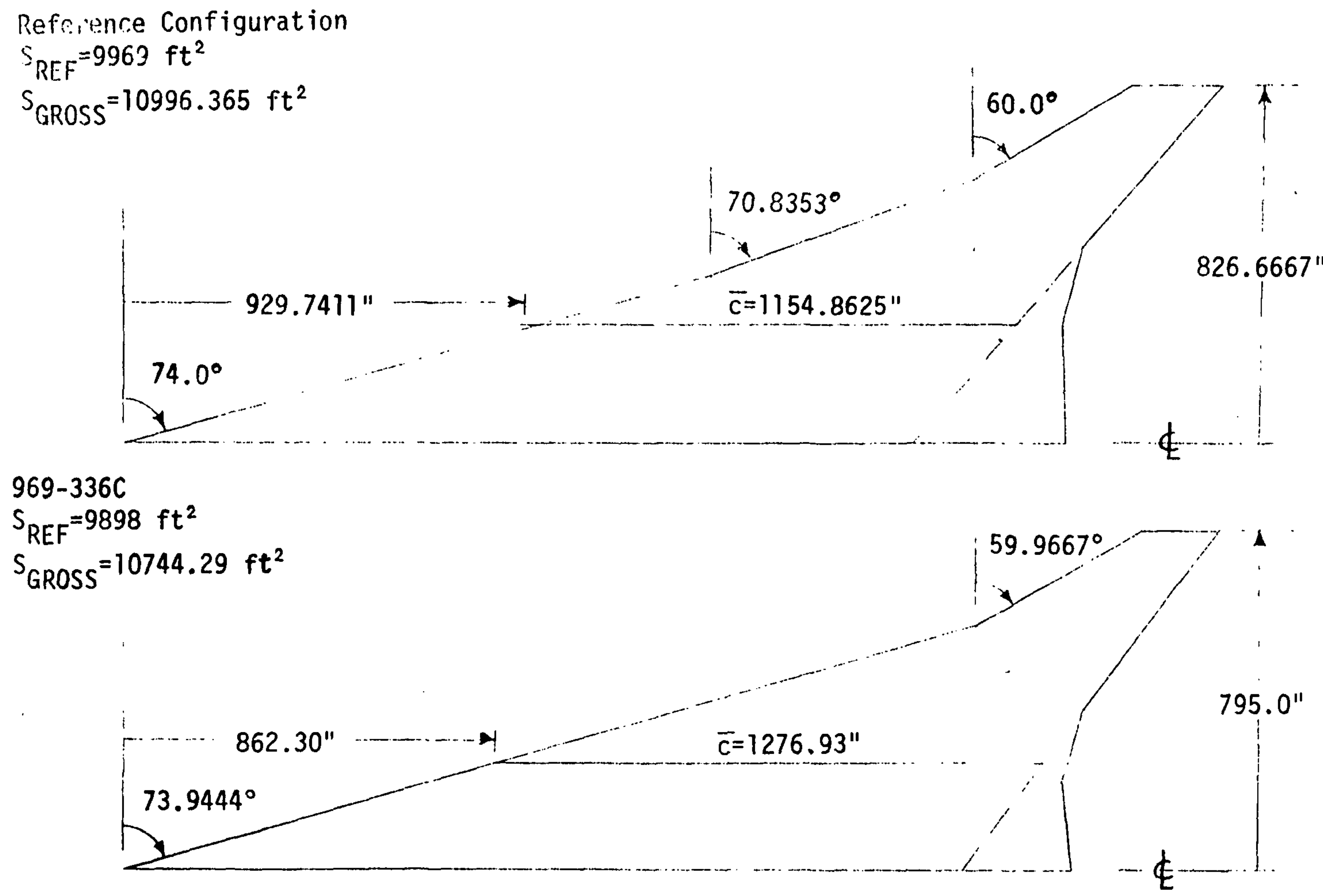

Figure VI-1B-2 Wing Planform Comparison-969-336C SST and Reference Configuration

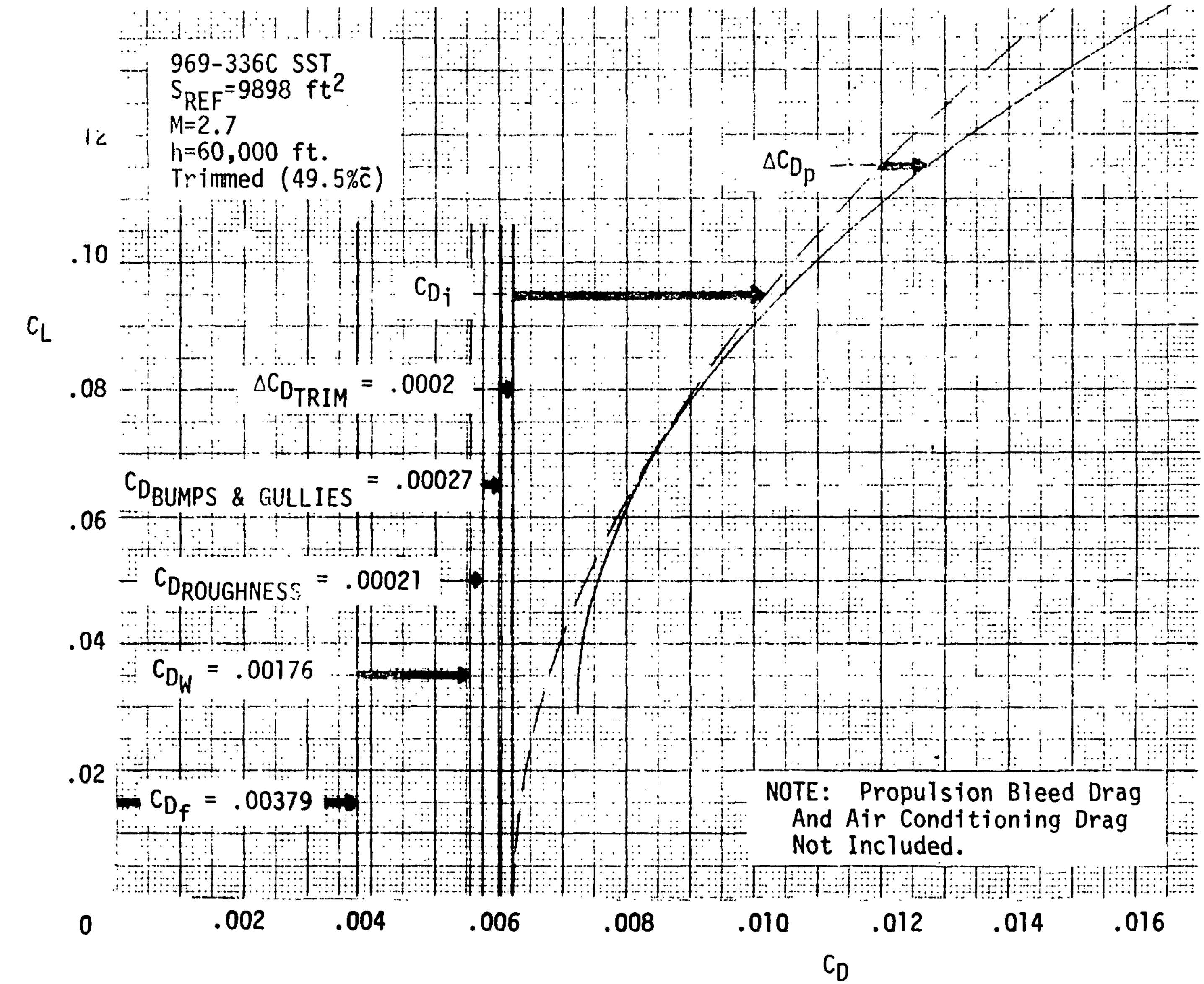

Figure VI-1B-3 Cruise Drag Polar Breakdown - 969-336C SST

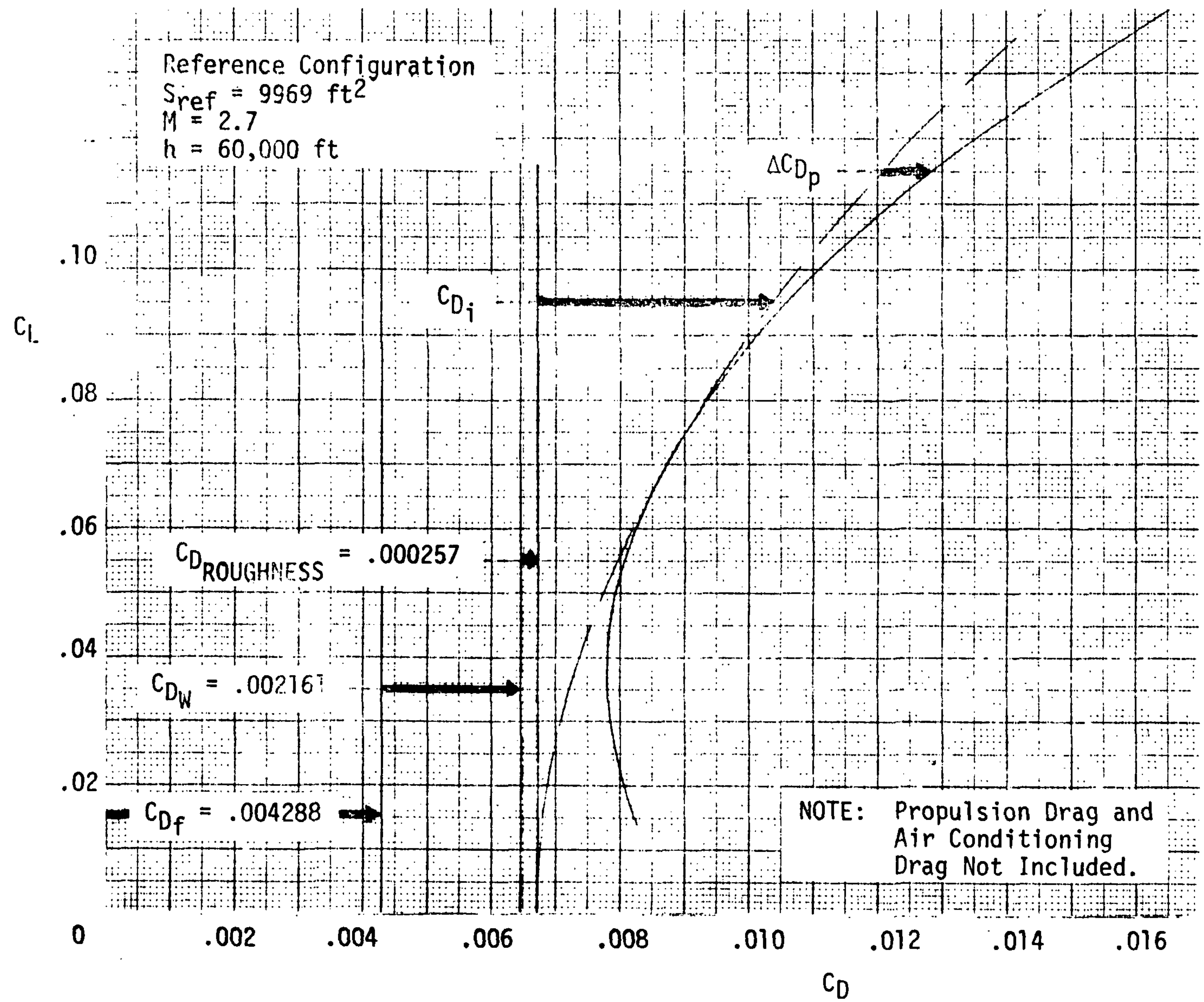

Figure VI-1B-4 Cruise Drag Polar Breakdown - Reference Configuration

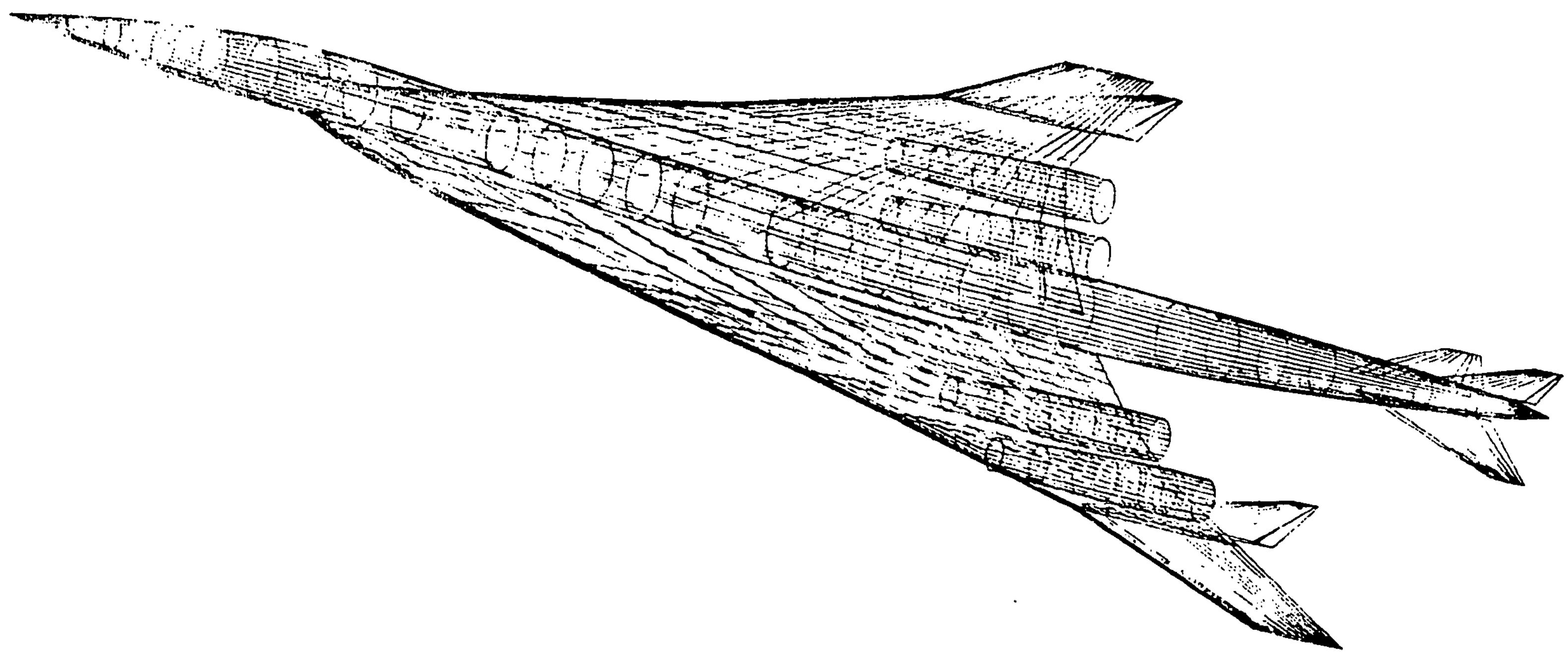

Figure VI-1B-5 Computer Plot - Reference Configuration Geometry

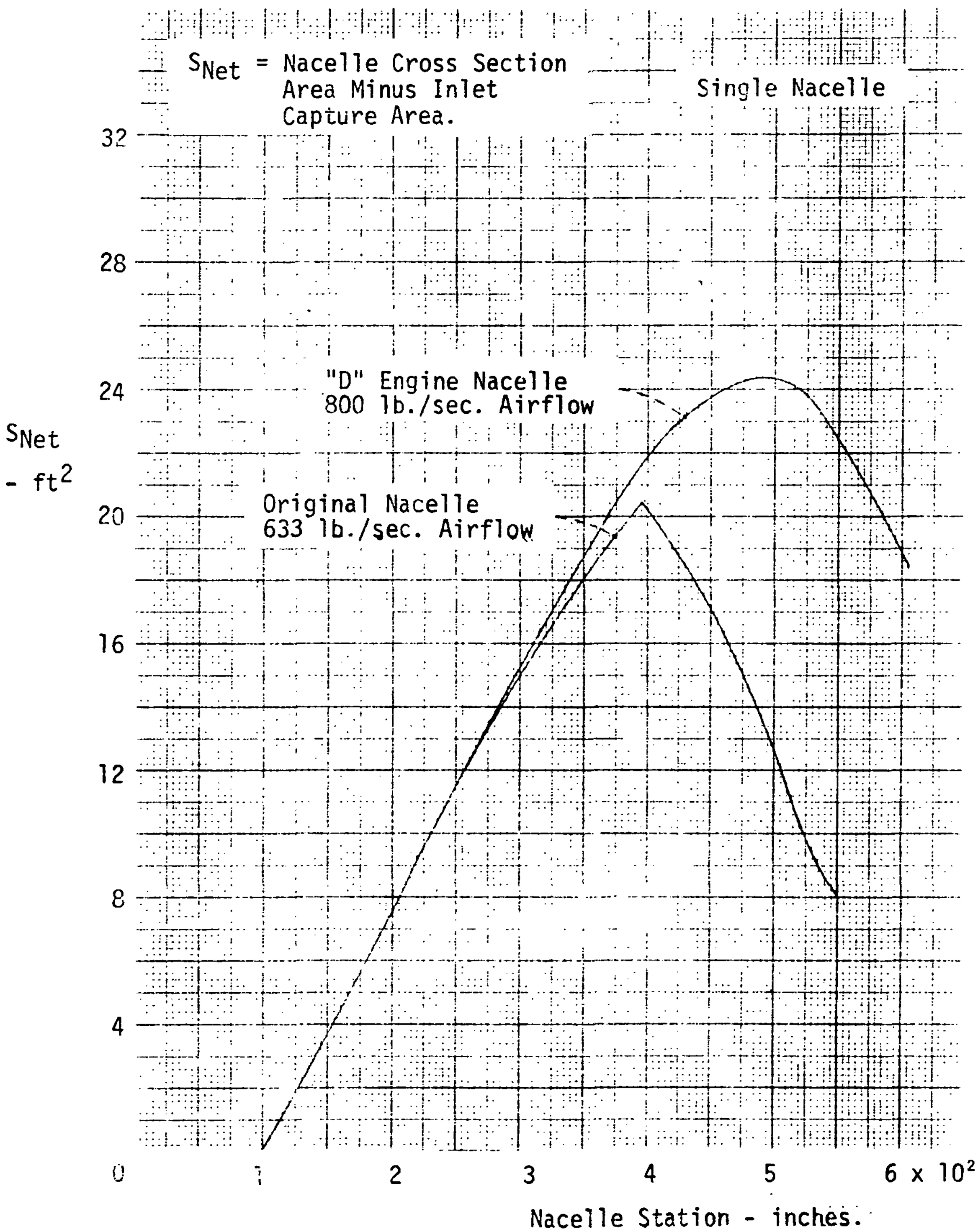

Figure VI-1B-6 Nacelle Net Cross Section Area Distribution Comparison.

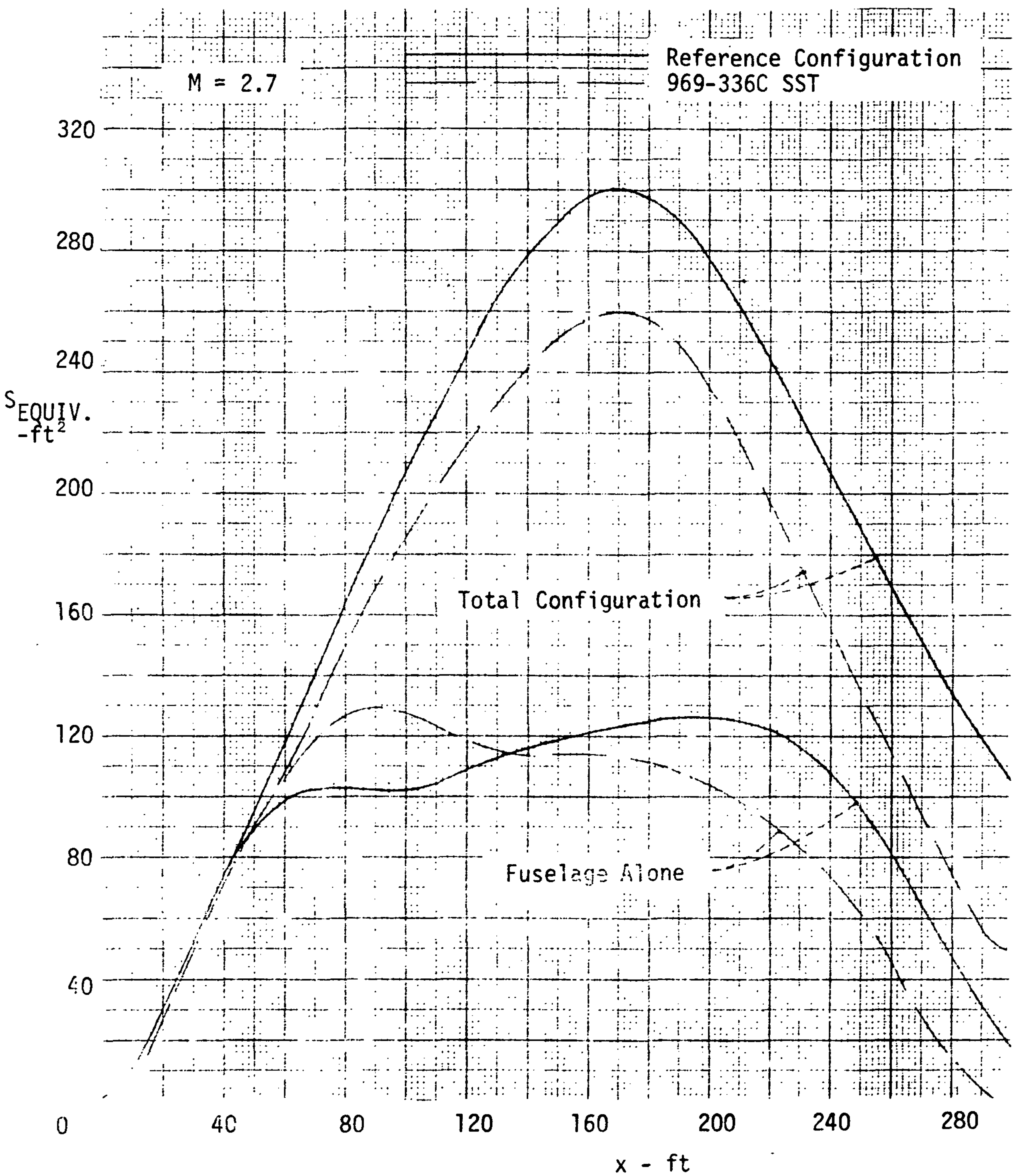

Figure VI-1B-7 Equivalent Area Distribution Comparison At Cruise

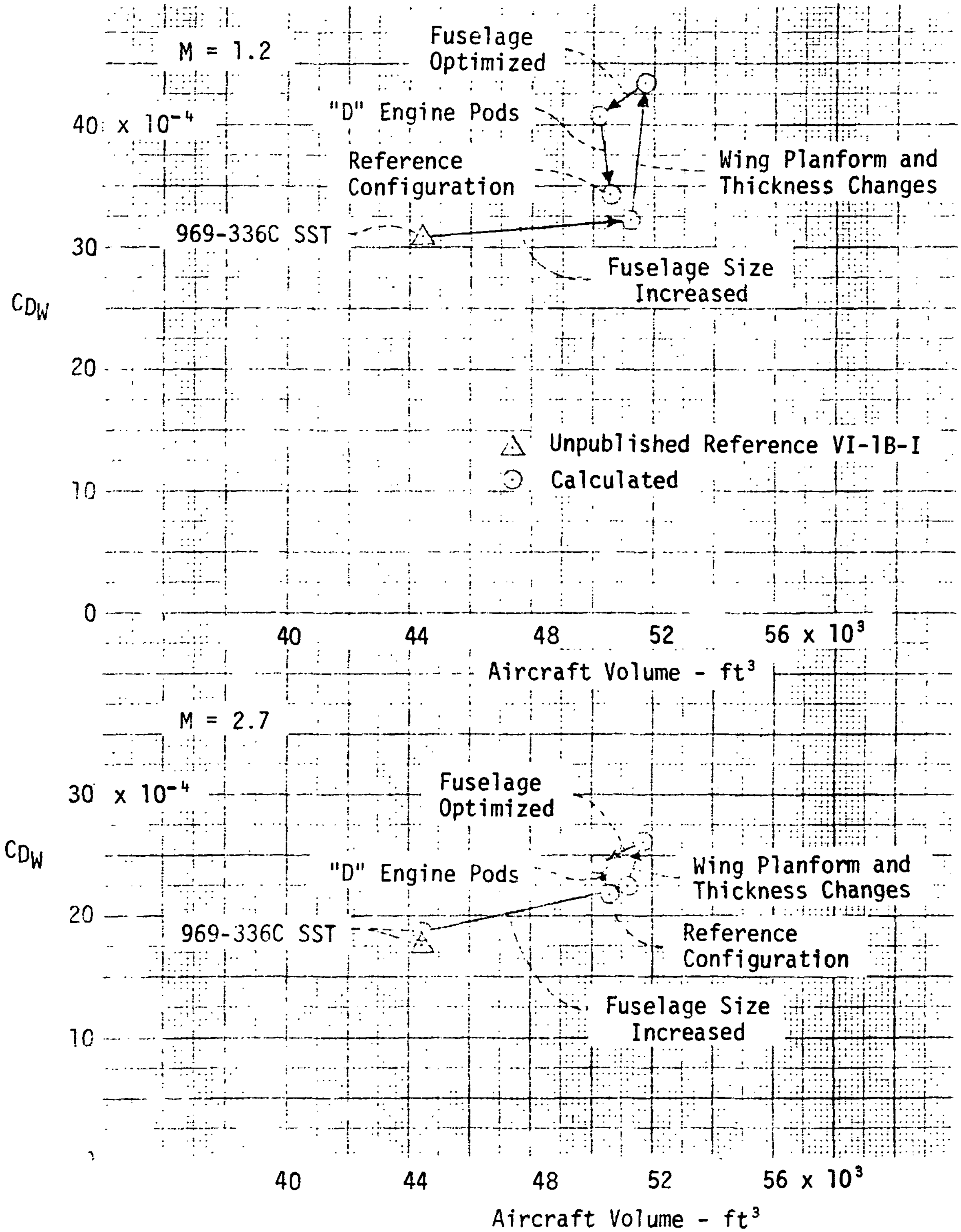

Figure VI-1B-8 Airplane Wave Drag Comparison - S_{ref} = 9898 ft^2

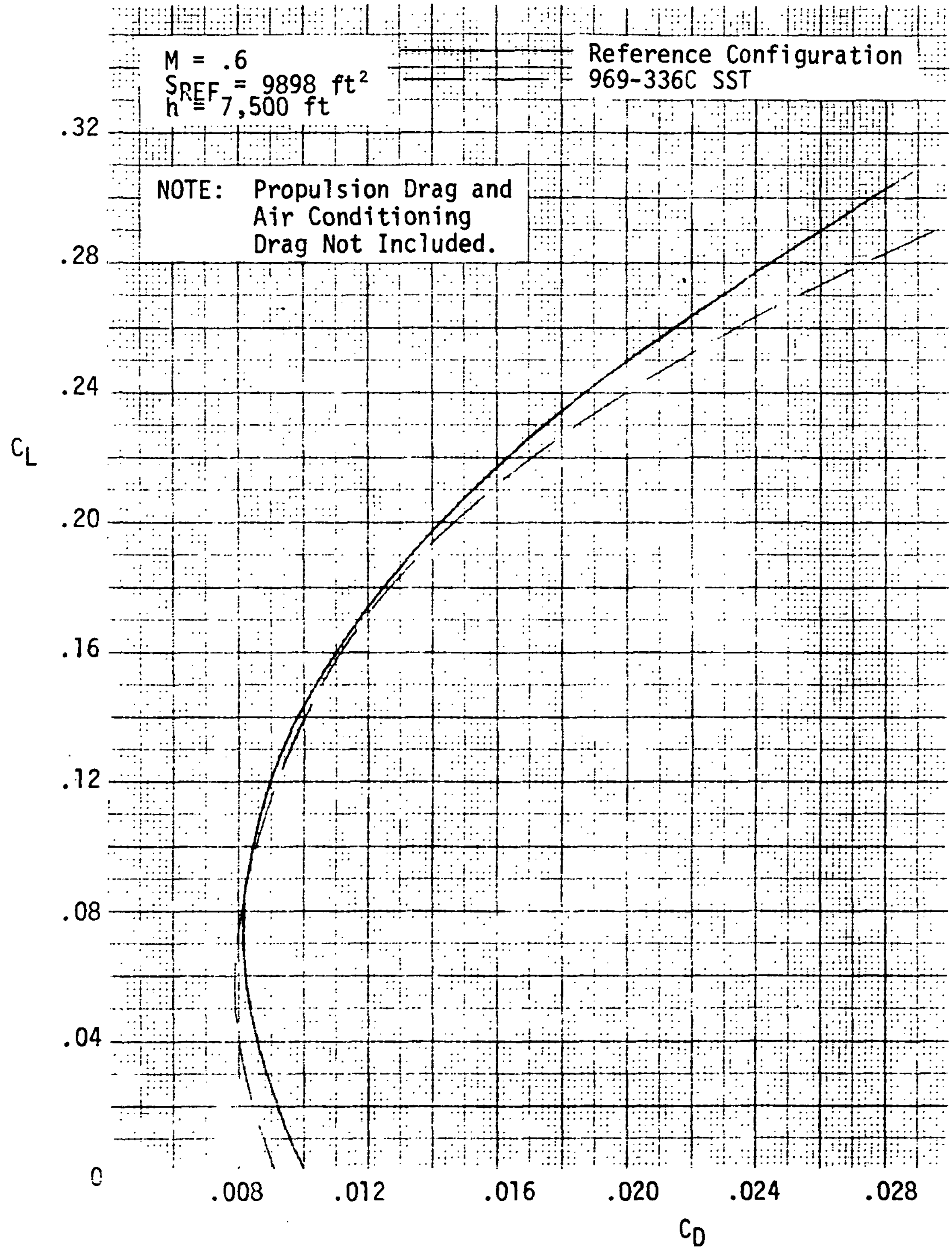

Figure VI-1B-9 Drag Polar Comparison - M = .6.

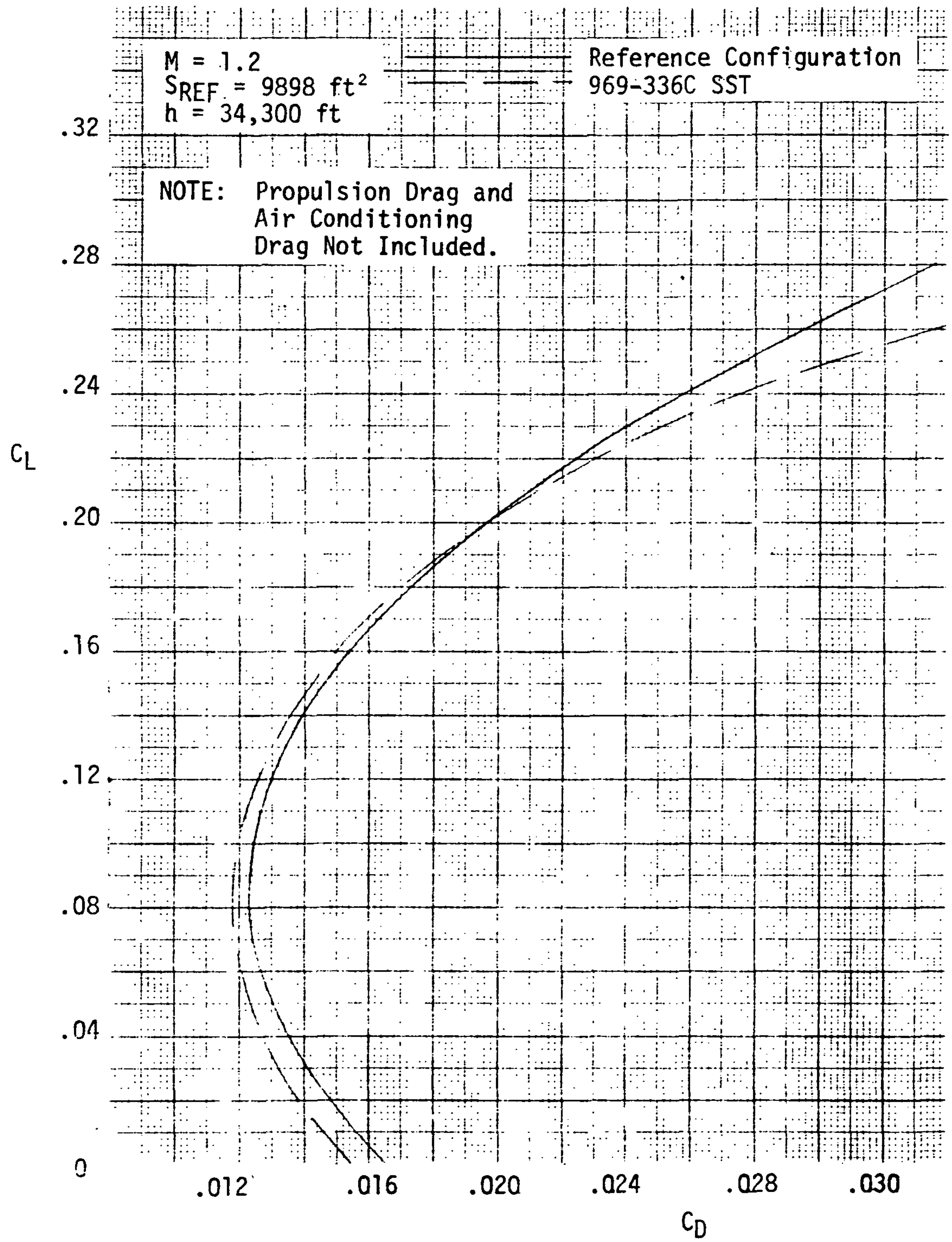

Figure VI-1B-10 Drag Polar Comparison - M = 1.2

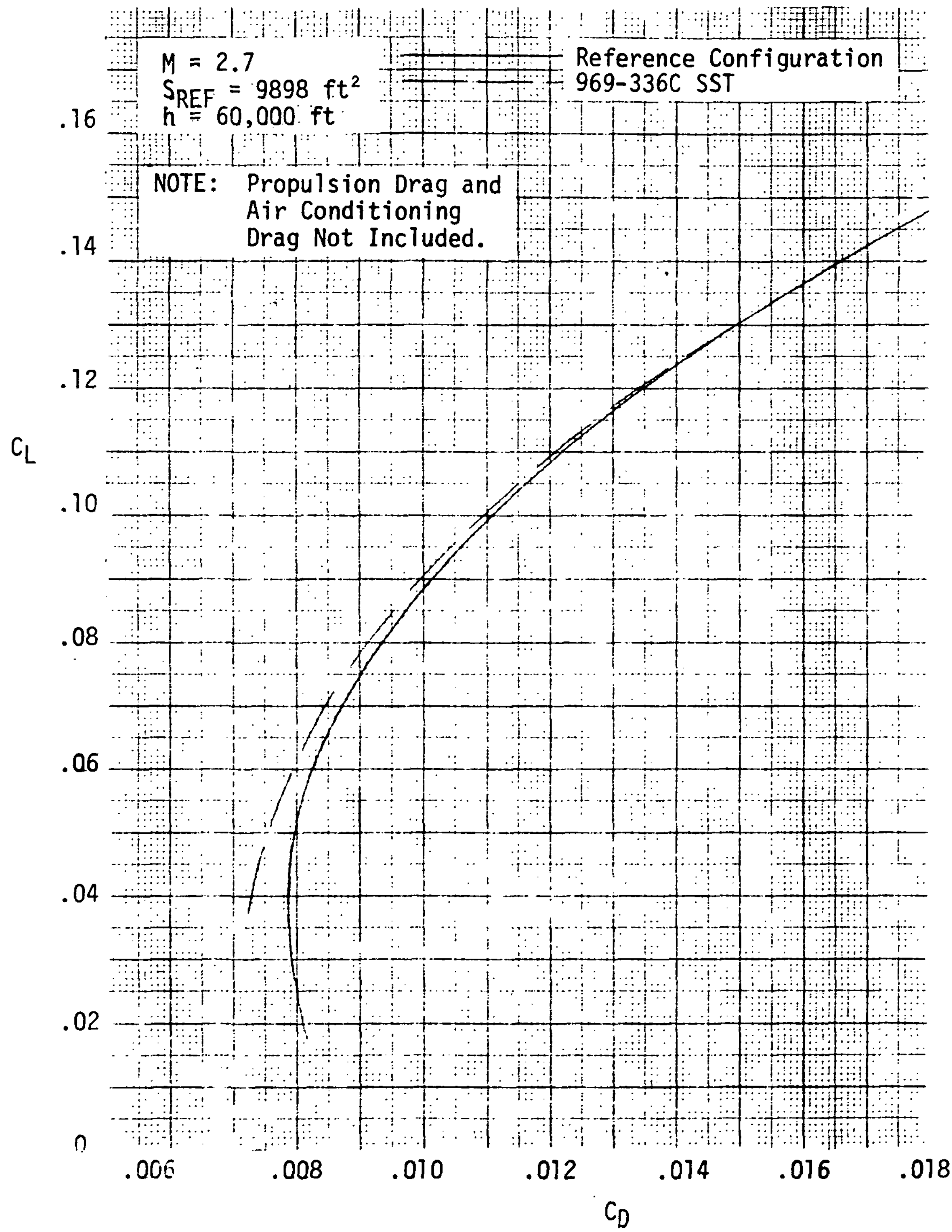

Figure VI-1B-11 Drag Polar Comparison - M = 2.7

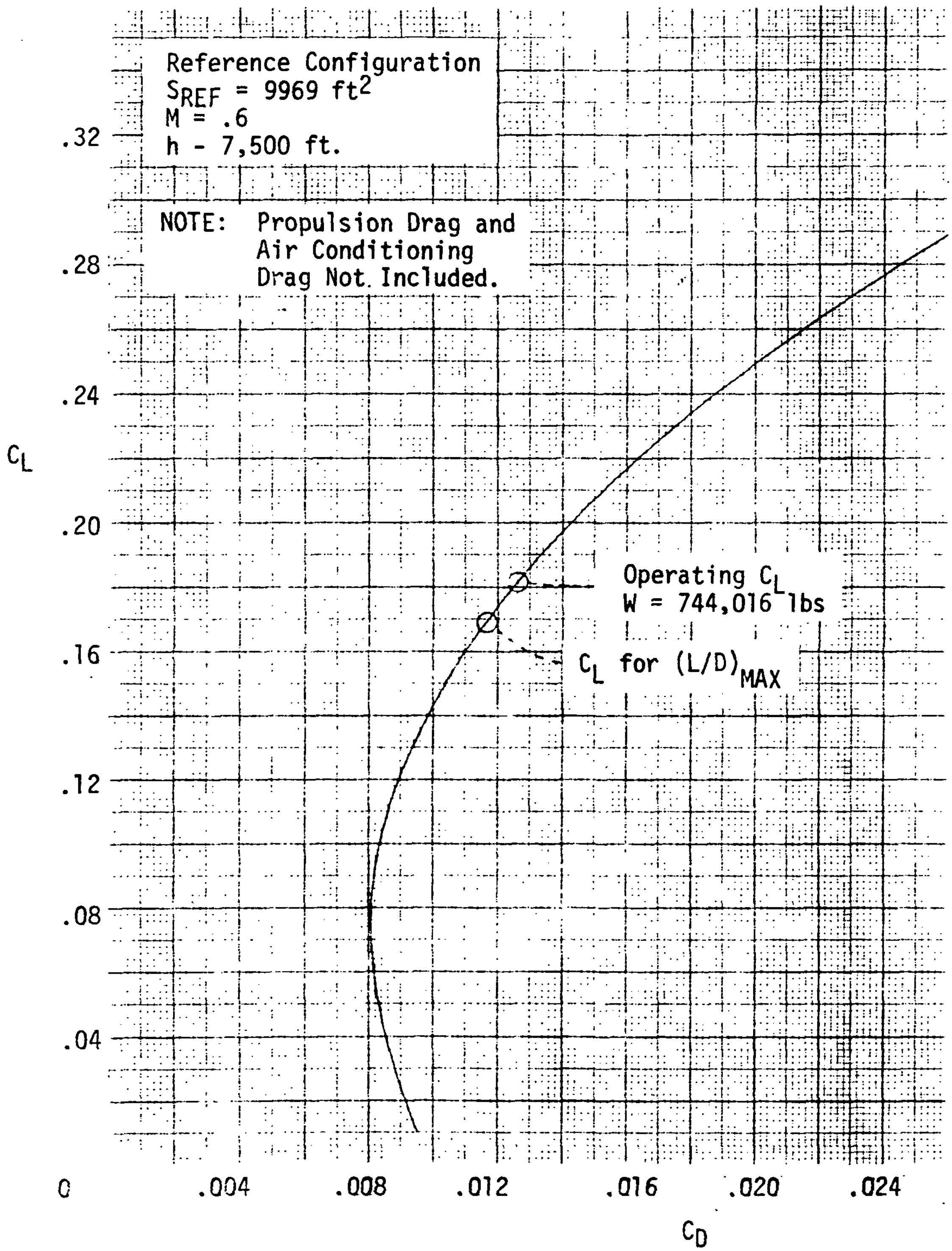

Figure VI-1B-12 Reference Configuration Drag Polar - M = .6.

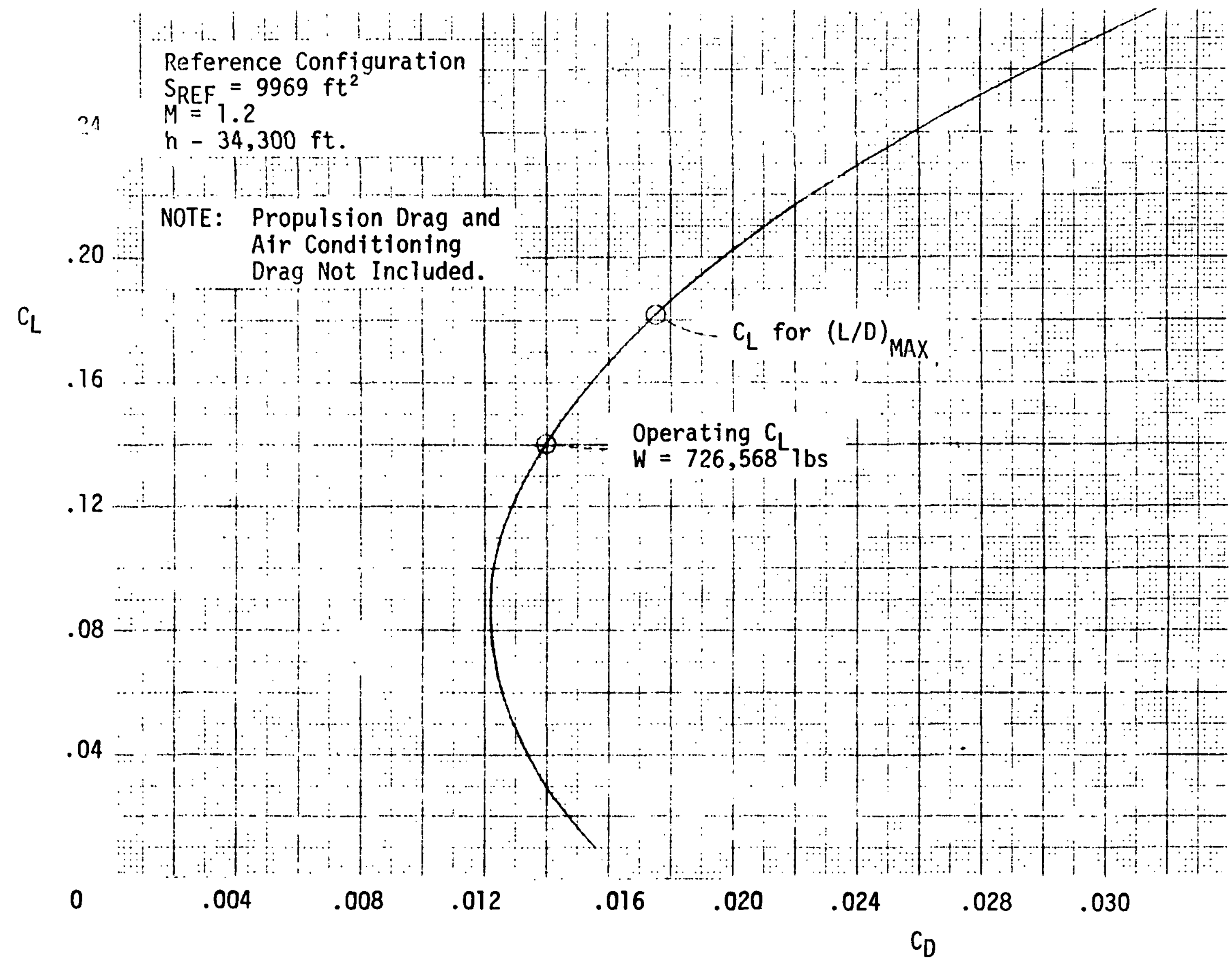

Figure VI-1B-13 Reference Configuration Drag Polar - M = 1.2.

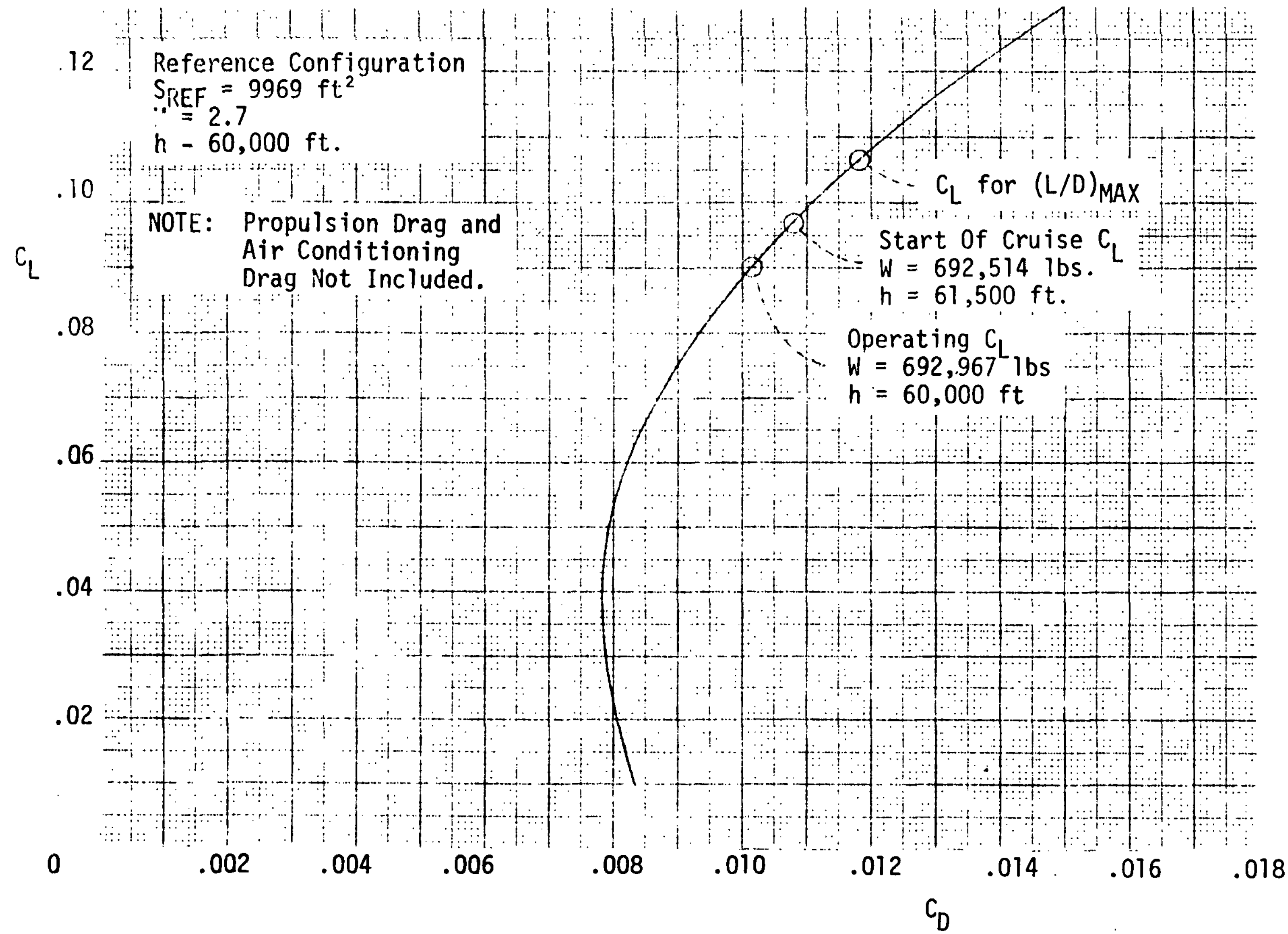

Figure VI-1B-14 Reference Configuration Cruise Drag Polar - M = 2.7.

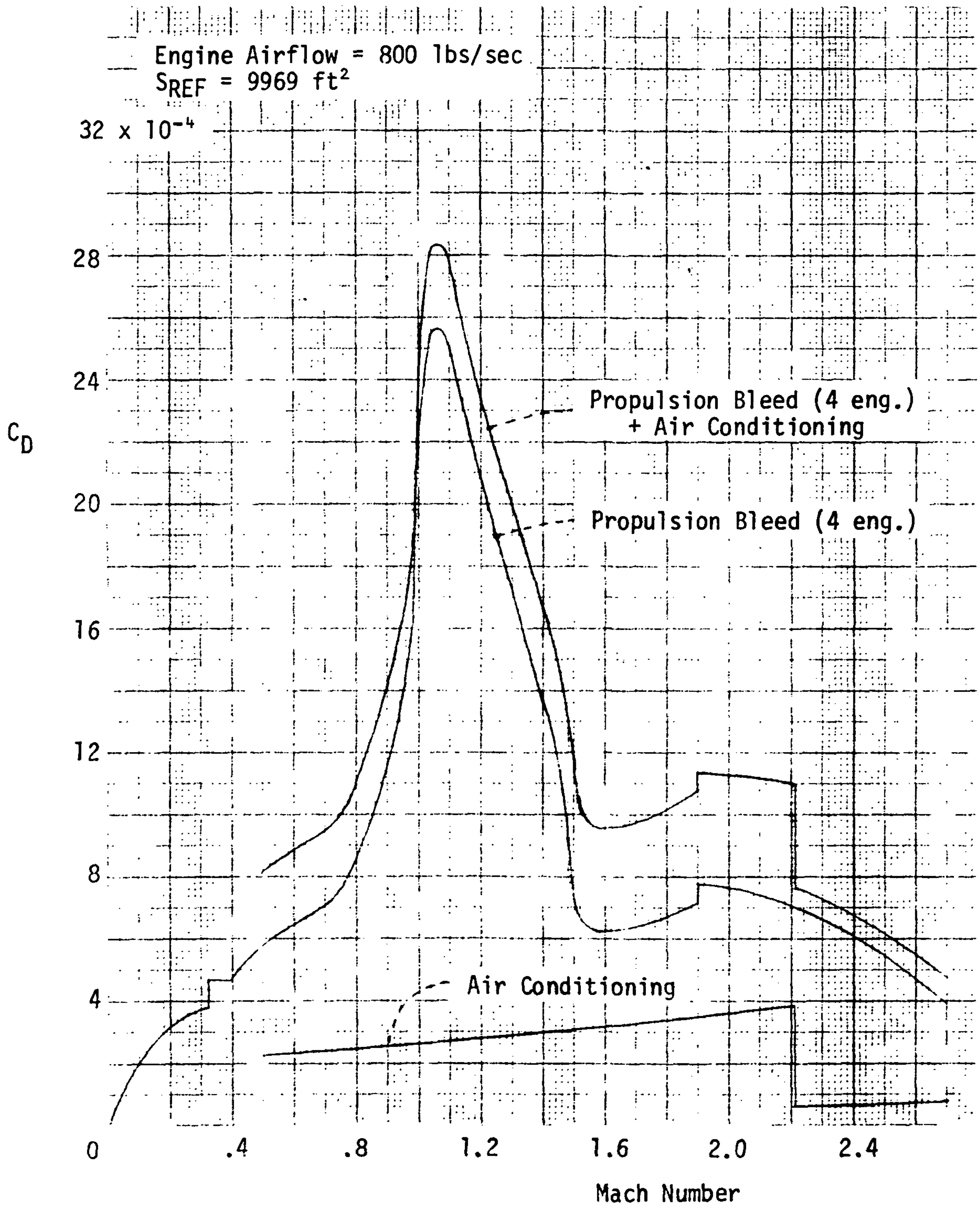

Figure VI-1B-15 Propulsion Bleed And Air Conditioning Drag.

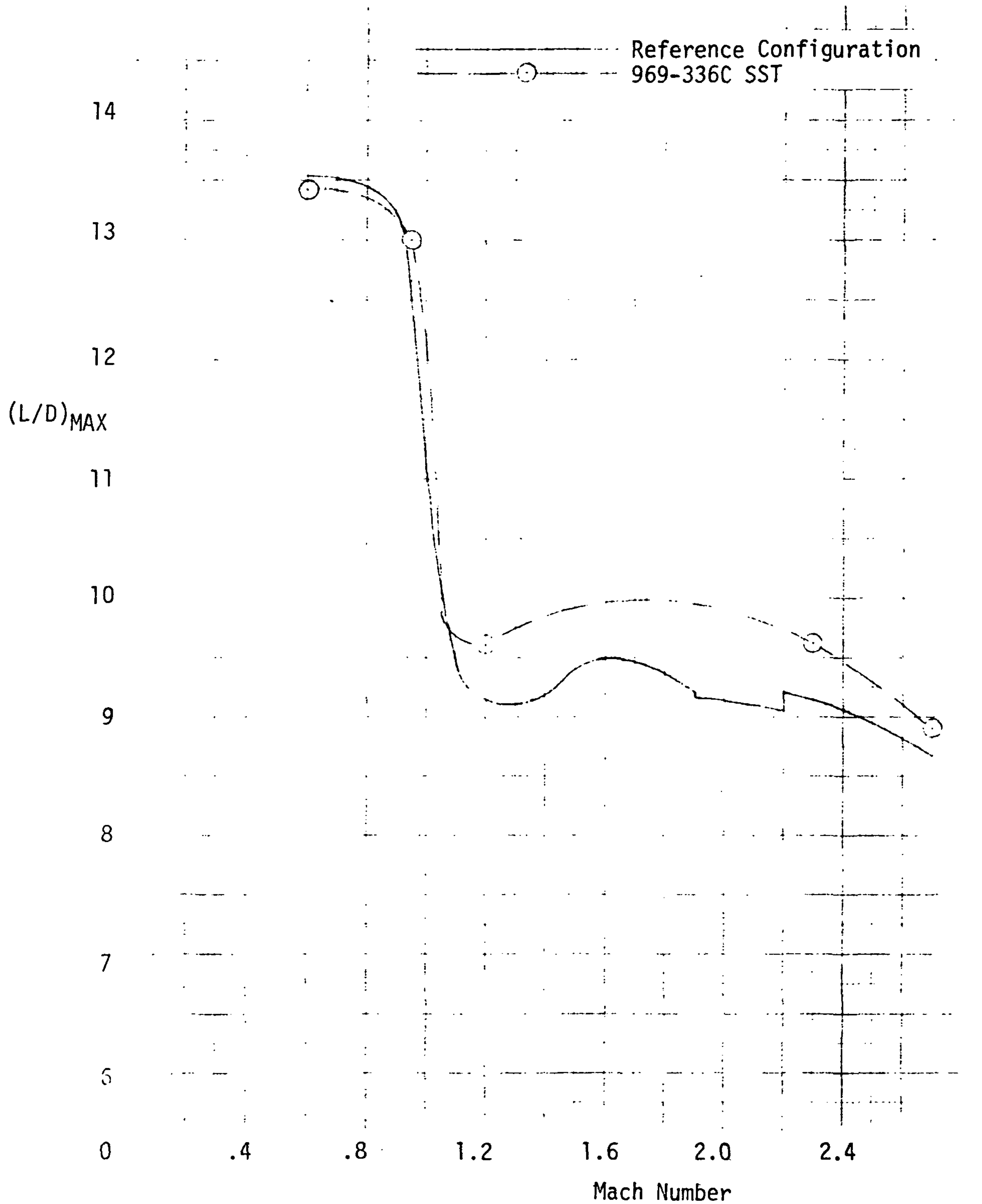

Figure VI-1B-16 Maximum Lift-To-Drag Ratio Performance

VI-1C SONIC BOOM

INTRODUCTION

Sonic boom solutions were computed for the Reference Configuration to provide an indication of the sonic boom pressure levels to be expected for this type aircraft. The methods used are outlined and the results attained are summarized.

SUMMARY

Sonic boom solutions were obtained for start of cruise (M=2.7; h = 61,000 ft.) and climb (M=1.2; h = 35,000 ft.) conditions. Pressure peaks of +2.3 and -2.1 lb./ft^2 were obtained for the start of cruise condition which compares to +2.9 and -3.1 lb./ft.^{2} obtained for the climb condition. An increment in sonic boom overpressure of approximately 1/4 lb./ft.^{2} is attributed to the low speed requirement for wing anhedral.

Sonic Boom Characteristics

Sonic boom solutions were computed by means of NASA computer programs. A list of the programs used is contained at the end of this section. Standard atmosphere, no wind, conditions were assumed with the aircraft in a steady state level flight condition. A tail load of zero was assumed.

The sonic boom signature obtained for a selected mission for the Reference Configuration is presented in Figure VI-1C-1 for the start of cruise weight of 673,605 pounds and altitude of 61,000 feet. The altitude was selected as the start of cruise altitude as determined by the mission-range performance program. Figure VI-1C-1 also shows the equivalent area distribution, AE, and the actual area distribution due to aircraft volume, AV. The equivalent area distribution includes the effect due to the lift distribution and is the primary determining input for the sonic boom signature as computed by the sonic boom computer program.

Figure VI-1C-2 shows the same information for the climb weight of 725,676 pounds at a Mach number of 1.2 and an altitude of 35,000 feet. As indicated, this condition results in a much more severe sonic boom overpressure than that obtained for the start of cruise condition (Figure VI-1C-1).

While optimization for sonic boom was not a consideration for this study, certain effects are known to be beneficial, such as distribution of the lift over a greater length. In the computation of the sonic boom pressure signatures, it became evident that the effect of negative dihedral on the wing was in effect tending to shorten the effective length of the wing. This is due to the high degree of wing sweepback and the fact that the sonic disturbance is propagated along Mach lines. The effect of the wing anhedral was therefore obtained for possible future consideration and is presented in Figure VI-1C-3. The anhedral of the wing is required for low speed stability (C_{l_β}). Figure VI-1C-3 indicates the low speed stability requirement for wing anhedral results in an increase in sonic boom overpressures on the order of 1/4 pound per square foot.

VI-1C

LIST OF FIGURES

Figure No.	Title
VI-1C-1	Sonic Boom - Start of Cruise
VI-1C-2	Sonic Boom - Supersonic Climb Condition
VI-1C-3	Sonic Boom - Effect of Wing Anhedral

LIST OF SYMBOLS

A	Area
A_E	Equivalent Body Area Due To Lift and Volume Effects For Cuts Taken Along Mach Lines
A_V	Equivalent Body Area Due To Volume Effect For Cuts Taken Along Mach Lines
C_{l_β}	Stability Derivative
Δp	Incremental Change In Pressure
Δt	Incremental Change in Time

NASA COMPUTER PROGRAMS

Number	Title
A2994	Sonic Boom
D2340	Lifting Surface
D2500	Wave Drag

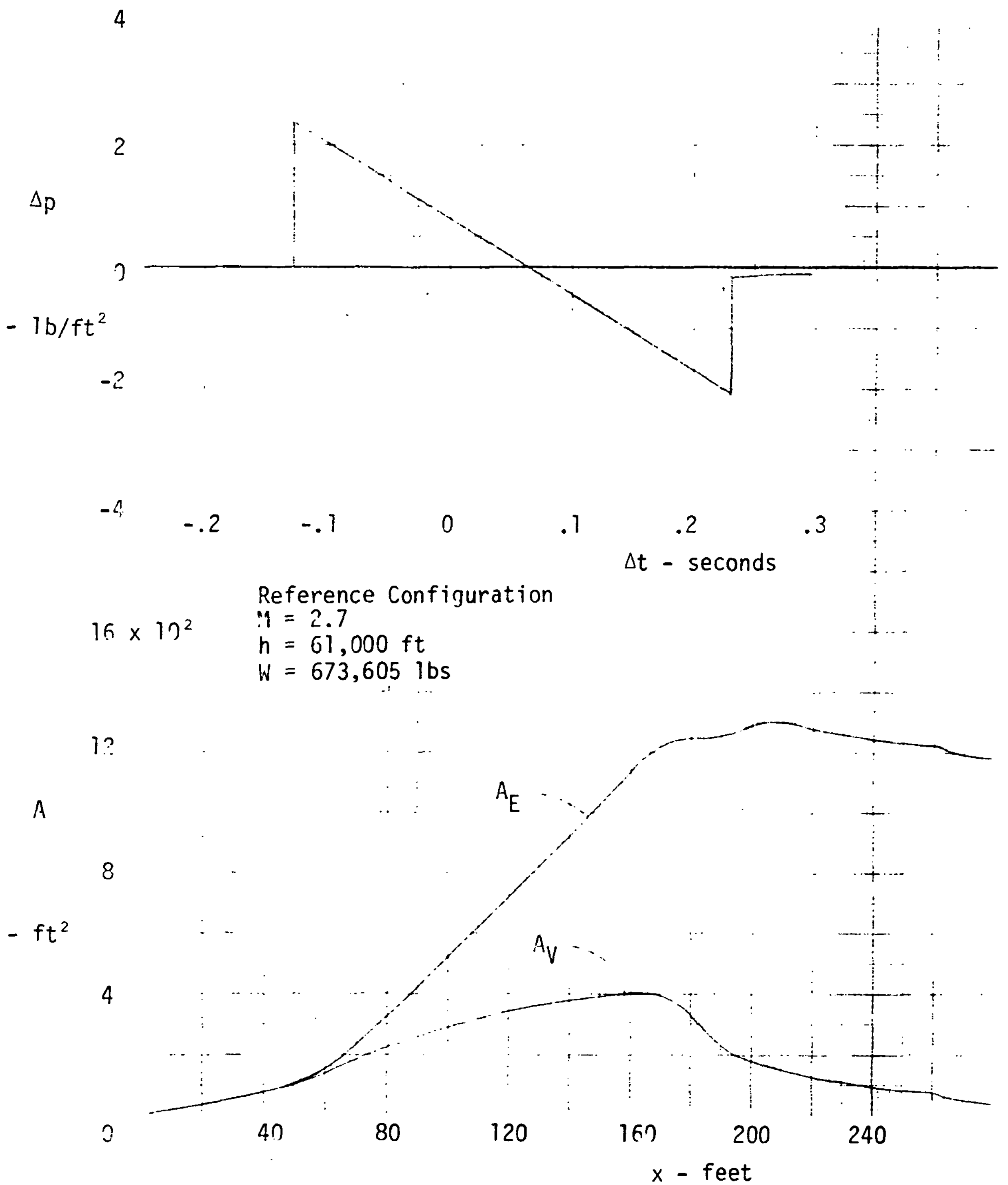

Figure VI-1C-1 Sonic Boom - Start Of Cruise.

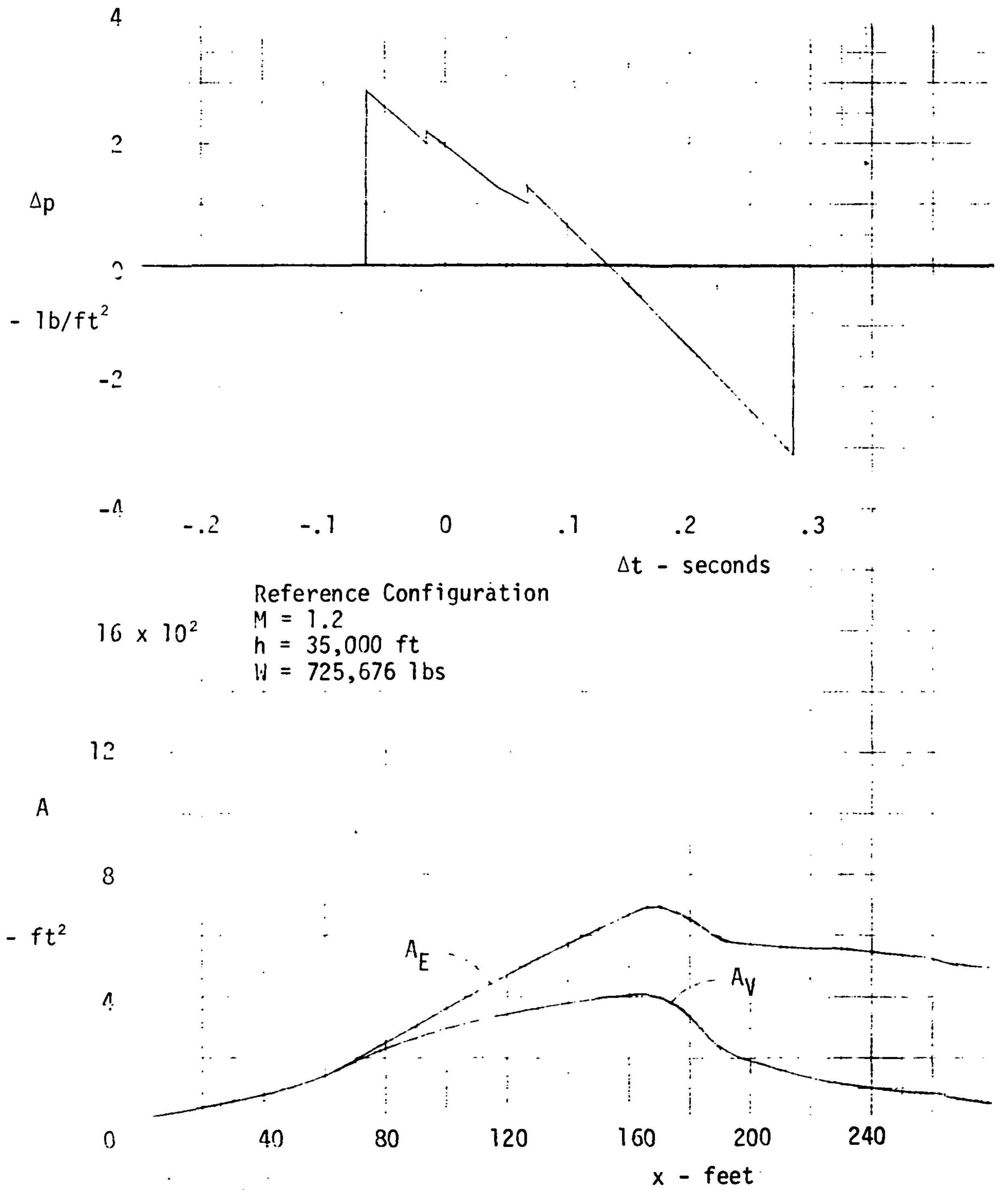

Figure VI-1C-2 Sonic Boom - Supersonic Climb Condition.

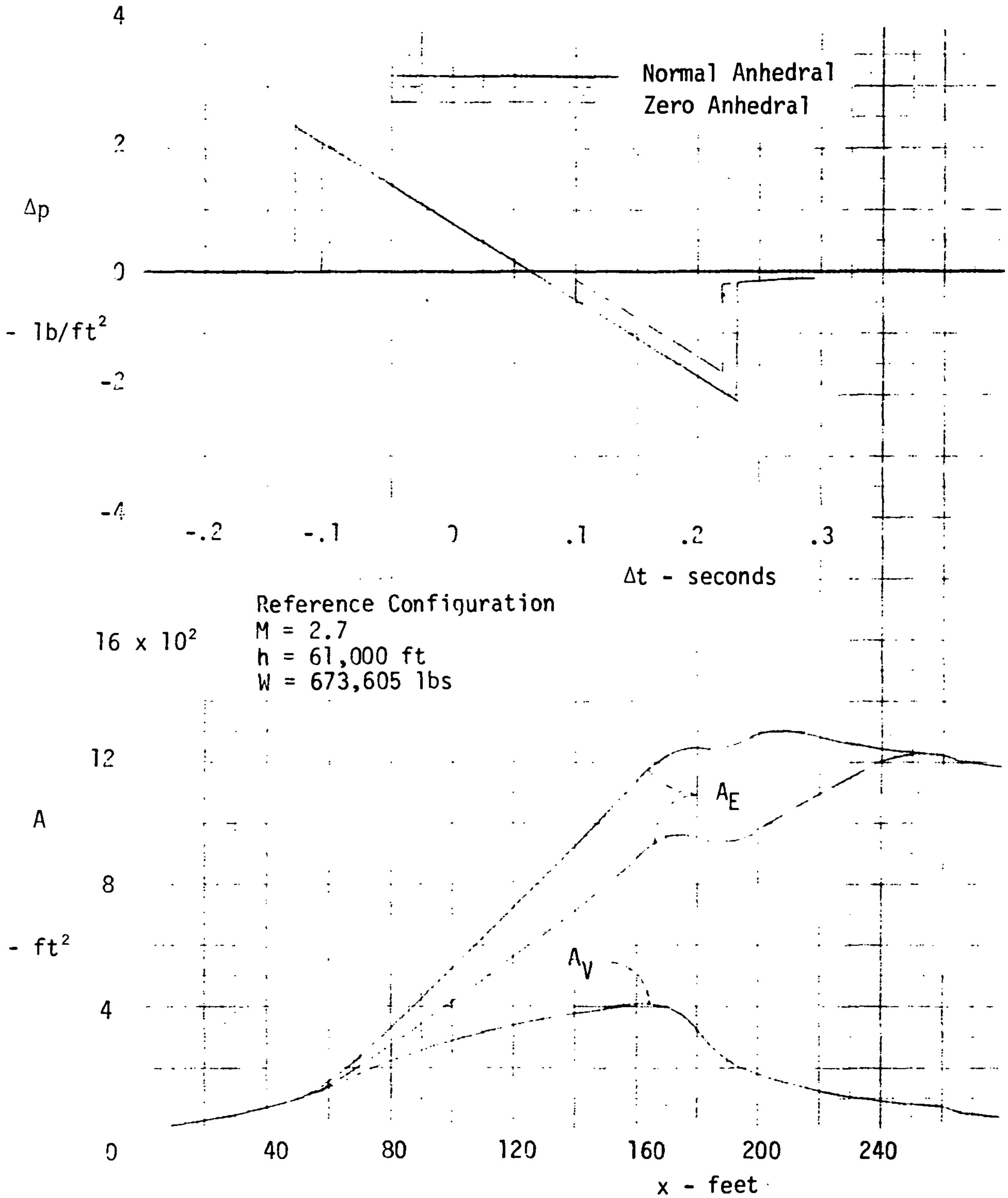

Figure VI-1C-3 Sonic Boom - Effect Of Wing Anhedral

VI-2 STABILITY AND CONTROL

INTRODUCTION

The historical development of the U.S.Supersonic Transport technology development program has been outlined in this report's main Introduction; however, some of the important points, as they affect aircraft stability and control, performance and noise, are reiterated herein.

The Boeing 969-336C configuration, reference VI-2-5, has shown good landing and take-off performance for a stable aircraft by utilizing a lifting canard. However, this high-lift configuration exhibited a substantial pitch-up at a lift coefficient of approximately 0.9 requiring an alpha limiter so that a second trim point was not attained (See Figure VI-2-2).

As the result of an extensive NASA/LRC low speed wind-tunnel development program, significant improvements in longitudinal stability at high angles-of-attack for the take-off and landing modes were achieved by careful attention to wing planform, leading-edge radius, leading-edge high-lift devices and trailing-edge flap location, size and deflection. The significant aerodynamic results to be applied to the Reference Configuration are:

a. A triple-sweep wing planform (Λ_{ref} = 74°/70.5°/60°) with a subsonic leading-edge and increased span.

b. No significant pitch-up present for the selected high-lift configuration.

c. No canard required for aircraft trim.

d. Aft center-of-gravity selected (negative static margin) to minimize landing approach attitude and hence to minimize landing gear length and to maximize trimmed approach lift-to-drag ratio. (Acceptable handling qualities appear to be achievable with a stability augmentation system, SAS, incorporating both pitch rate damping and pitch stiffness functions. However, the SAS has not been adequately defined), and

e. Improved high-lift configuration trimmed lift-to-drag ratios.

The following paragraphs present the various longitudinal stability and control criteria assumed for the reference baseline configuration development, the aerodynamic data base used and the detailed advanced supersonic configuration development. These paragraphs are then followed by analyses describing the establishment of levels of Stability and Control together with the resulting aerodynamic center-of-gravity limits.

SUMMARY

The Reference Configuration described herein was developed from estimated aerodynamic characteristics based on NASA/LRC wind-tunnel data to provide acceptable longitudinal stability and control and performance capability in the take-off and landing modes of flight. These two high-lift modes were selected as the most critical. Based on the criteria that were established, the airplane exhibits significantly improved stability and control characteristics over the Boeing 969-336C airplane. The various configuration changes that were made resulted in a new baseline airplane without a canard and with an aft center-of-gravity position that allowed the aircraft to be

flown unstable such that a trim up-load is required from the aft mounted horizontal tail. The airplane trimmed lift-to-drag ratio was improved over that of the 969-336C configuration.

REFERENCE CONFIGURATION CHARACTERISTICS

Criteria

Several criteria were used to develop the stability and control requirements for the Reference Configuration.

Longitudinal Stability and Control

a. Take-off

°Forward center-of-gravity set by nose-wheel rotation speed consistent with geometry limited maximum lift coefficient, in ground effect

°Control to geometry limit in full ground effect

°No significant pitch-up

°Alpha limit set to provide a Δn_z of 0.15 at the minimum demonstrated speed with one engine inoperative and zero rate-of-climb

b. Landing

°Control to geometry limit in full ground effect

°No significant pitch-up

°Approach speed defined at a lift coefficient of 0.55

°Minimum demonstrated speed defined at a lift coefficient consistent with a 0.5 g(incremental) maneuver from trim at the approach speed, i.e. a lift coefficient of 0.825

°Satisfactory short-period characteristics at approach speed

°Aft center-of-gravity limit based on the ability to provide a nose-down pitching acceleration of 0.1 rad/sec^2 at the minimum demonstrated speed and the maximum landing weight. (This criterion affords acceptable aircraft response rates).

c. Supersonic Cruise

The criteria are incomplete at the time of this study, and consequently not considered in this analysis.

Lateral - Directional Stability and Control

The criteria are incomplete at present, and consequently not considered in this analysis.

Data Base

The high-lift aerodynamic characteristics of the reference concept are based on extensive NASA/LRC wind tunnel tests, references VI-2-1, -2, -3 and -4. These wind-tunnel data, in coefficient form, are based on the original SCAT-15F-9898 dimensions of span, reference mean aerodynamic chord and reference wing area. Therefore, when using these wind-tunnel results corrections had to be applied to make these data compatible with the Reference Configuration geometry. In addition, these data were modified to account for shortened fuselage forebody, extended aft fuselage, modified wing leading-edge high-lift devices, wing trailing-edge geometry, trailing-edge flap location and size, downwash at the tail and horizontal tail size.

The Reference Configuration concept wing is scaled up from the wing presented in reference VI-2-3 but with modified trailing-edge planform geometry, see Figures VI-2-1A, 1B. However, when using the wind tunnel test model (9898 model reference geometry) longitudinal force and moment coefficient data of reference VI-2-3, corrections had to be made to convert these data to the actual wind tunnel model reference configuration as follows:

$$C_F = C_{F_{ND(NASA\ DATA)}} \frac{S_{NR(NASA\ REF)}}{S_{R(REF)}} = C_{F_{ND}} \times \frac{1282.78}{1388.016} = 0.92418\ C_{F_{ND}}$$

$$C_m = C_{m_{ND}} \frac{S_{NR}\ \bar{c}_{NR}}{S_R\ \bar{c}_R} = C_{m_{ND}} \times \frac{1282.78 \times 38.31}{1388.016 \times 37.174} = 0.95242\ C_{m_{ND}}$$

$$(dCm/dC_F) = (dCm/dC_F)_{ND} \frac{\bar{c}_{NR}}{\bar{c}_R} = (dCm/dC_F)_{ND} \times \frac{38.31}{37.174} = 1.0306\ (dCm/dC_F)_{ND}$$

Assuming the wing from reference VI-2-3 was 0.03 scale, the Reference Configuration aircraft wing span became 137.77 feet with a reference wing area of 9969 ft^2 and reference mean aerodynamic chord of 1154.86 inches (see Figure V-2). The moment reference for the test data of reference VI-2-3 is 0.4556 $\bar{c}_{9898\ ref}$ which when converted to the actual Reference Configurations reference mean aerodynamic chord became 0.4436 $\bar{c}_{ref}$.

The modified trailing-edge planform geometry has been accounted for by estimated trailing-edge flap contributions due to location and size.

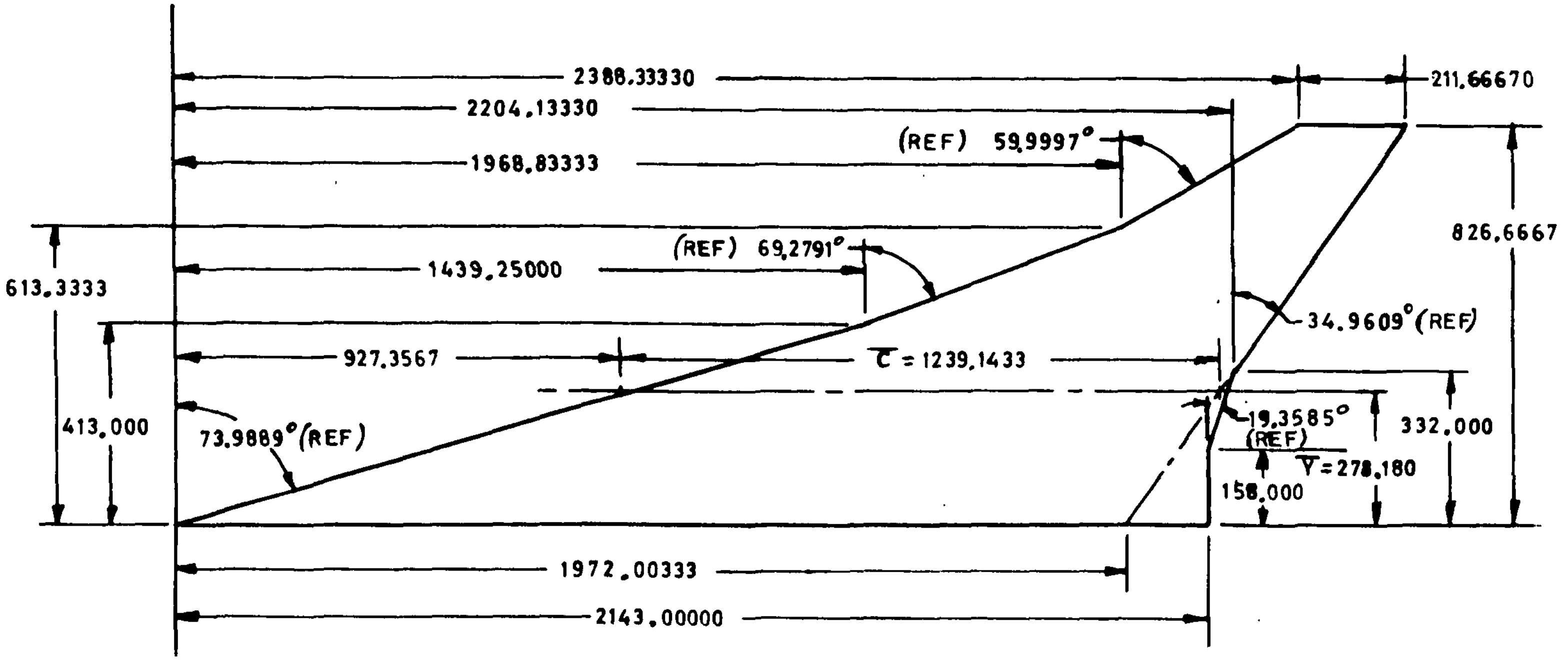

FULL-SCALE PLANFORM OF REF. VI.2-3 CONFIGURATION

Figure VI-2-1A - Wing Planform Definition Data

WING AREA - FT^2	"X"-IN	$\bar{C}$-IN	$\bar{Y}$-IN
REF —9969.000	929.7411	1154.8625	278.0021
GROSS-10996.365	889.2009	1343.0684	265.3174
SCAT-15F-9898-REF	861.4087	1274.3550	248.8898

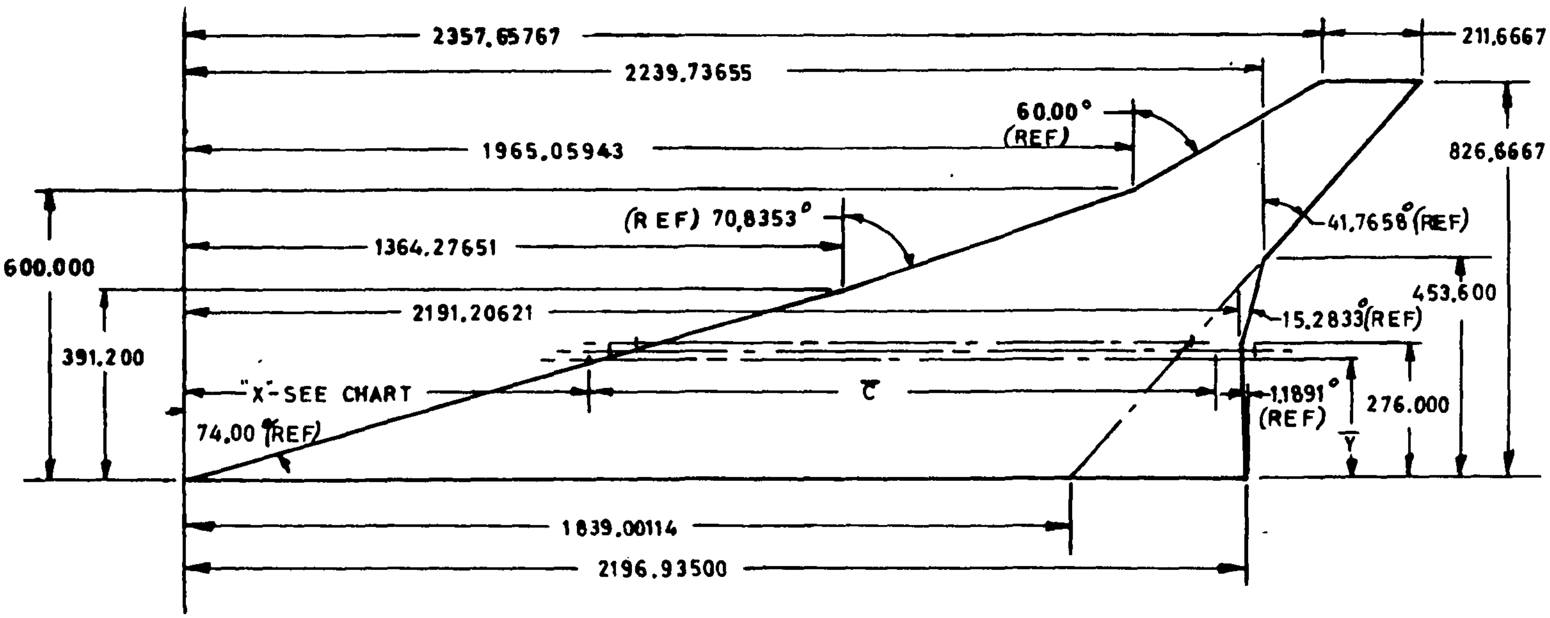

PLANFORM OF REFERENCE AIRPLANE CONFIGURATION

Figure VI-2-1B - Wing Planform Definition Data

Configuration Development

The Reference Configuration was developed from the original Boeing model 969-336C using estimations based on extensive NASA/LRC wind-tunnel data. The significant longitudinal aerodynamic features of the 969-336C from reference VI-2-5 are:

a. A highly swept (Λ_{ref} = 74°/60°) wing planform with a subsonic leading-edge.

b. A folding canard used for trim at low speeds and retracted at high speeds.

c. An apex slot which opens when the leading-edge flaps are deflected.

d. Leading-edge flaps which are used as control devices at high angles-of-attack, and

e. An all-moving horizontal tail with a geared elevator.

Figure VI-2-2 presents the 969-336C free-air stability data, with and without a canard, from reference VI-2-6 Figures 11 and 12. The main purpose of the canard was to trim out the trailing-edge flap contribution to pitching moment. Although, for a stable aircraft, the trimmed lift-to-drag ratio can be improved by use of a canard, there was an associated reduction in airplane stability and the severe pitch-up was present in both configurations.

A wind-tunnel test development program was initiated by the NASA/LRC to improve the arrow-wing supersonic transport high-lift configuration stability characteristics at high angle-of-attack with an aft fuselage mounted horizontal tail. The wind-tunnel testing has

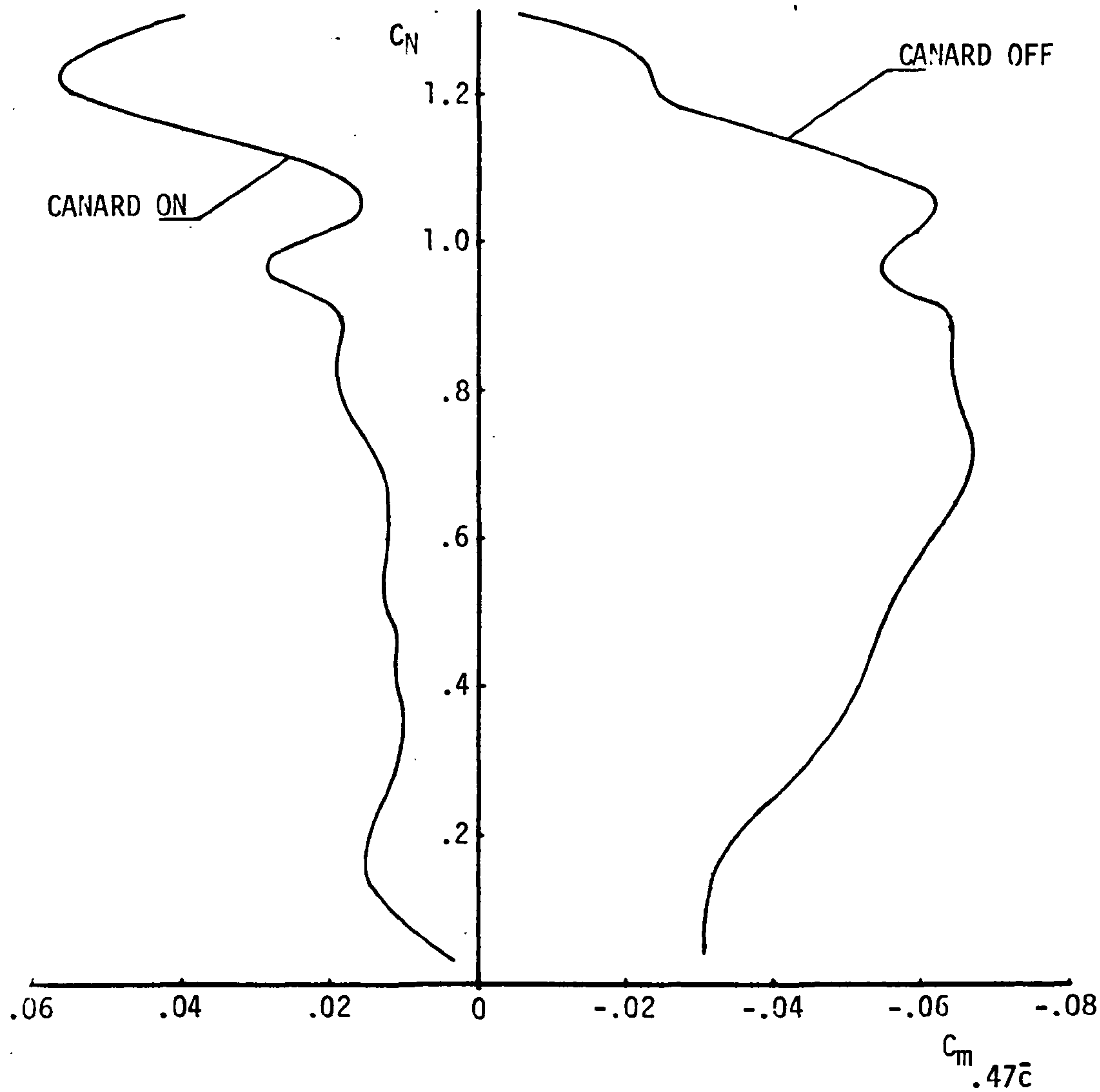

Figure VI-2-2 - Boeing Model 969-336C High-Lift Configuration, Out of Ground Effect resulted in a high-lift configuration with much improved stability characteristics (near linear variation of C_m with C_L) to high angles-of-attack (32 degrees is limit of test data shown) and increased negative C_{m_0}, without a canard. These favorable effects have resulted from wing planform and leading-edge radius changes, modified deflection of the leading and trailing-edge flaps and size of these high-lift devices. It has been assumed that the favorable pitching moment characteristics of a wing having a 1% leading-edge radius can be achieved with the Reference Configuration employing a 0.5% leading-edge radius.

As the level of airplane stability is increased, i.e., the slope dCm/dC_L becomes more negative, the airplane can be trimmed at a farther aft center-of-gravity location. Increasing both the stability and negative C_{m_0}, by large trailing-edge flap size and deflection, and allowing the aircraft to fly unstable, enables the airplane to be trimmed at an even farther aft center-of-gravity position requiring an up-load from the horizontal tail (improved lift-to-drag ratio). It was therefore rationalized that a configuration employing an aft fuselage mounted tail could produce take-off and landing approach trimmed lift-to-drag ratios at least as high as those of the 969-336C with a forebody canard. It therefore remained to define the center-of-gravity range, resulting from a given high-lift configuration, as determined by the selected stability and control criteria.

The effect of reduced lateral-directional stability is not considered in this report and additional wind-tunnel tests are presently being planned to study the configuration changes necessary to improve the apparent lateral-directional stability problems without degrading the acceptable longitudinal characteristics. Reference VI-2-3 illustrates the effect, on lateral-directional stability, of the high-lift leading and trailing-edge flap devices.

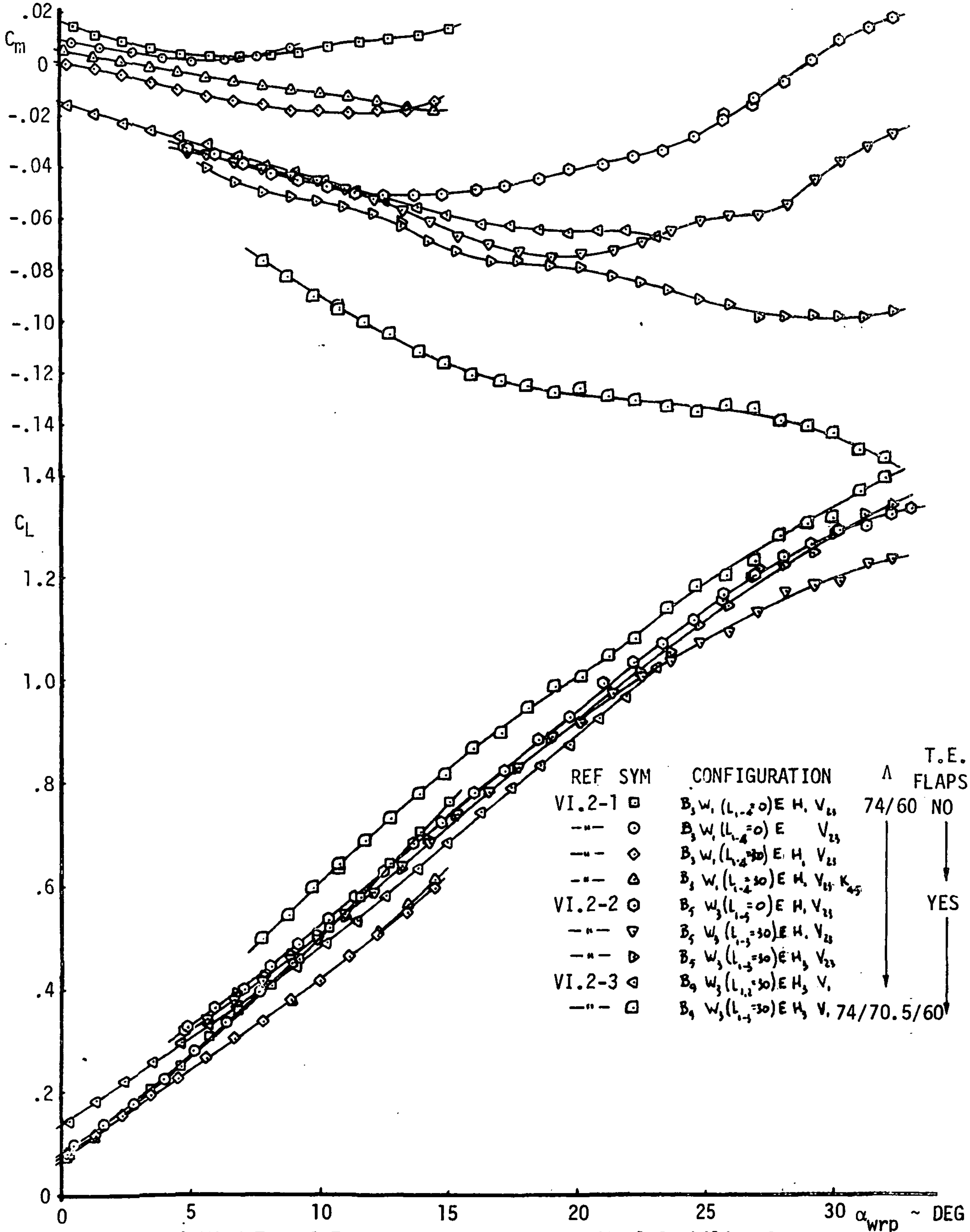

Figure VI-2-3-A Wind-Tunnel Test Development Longitudinal Stability Summary in the High-Lift Configuration

A configuration development summary stability plot is presented on Figure VI-2-3. These data clearly indicate the improvement in stability characteristics as the arrow-wing was developed toward the Reference Configuration. (Increased negative dCm/dα to high angles-of-attack). Figure VI-2-4 presents three (3) sets of arrow-wing wind-tunnel test stability data plotted in the SCAT-15F-9898 reference system. The three (3) curves are identified from NASA/LRC 7 x 10 foot high-speed wind-tunnel tests as follows:

Curve 1: $E_2N_2B_9H_3V_1W_3$ $[(L_{1,2} = 30°)(L_{3-5} = 0°)]$ T_6L_6
$t_{1_f} = t_2 = t_3 = 15°$, $t_4 = 0°$, $\Lambda_{ref} = 74°/60°$ (reference VI-2-3, run no. 21)

Curve 2: Same as curve 1 except $\Lambda_{ref} = 74°/70.5°/60°$ (reference VI-2-3, run no. 30)

Curve 3: $E_2N_2B_9H_3V_1W_3$ $[(L_{1-3} = 30°)(L_{4,5} = 0°)]$ T_6L_6
$t_{1_f} = t_2 = t_3 = 20°$, $t_4 = 5°$, $\Lambda_{ref} = 74°/70.5°/60°$
(reference VI-2-3, run no. 72)

The improvements illustrated by the test data in curve 3 of Figure VI-2-4 provided an acceptable base from which to make adjustments due to any further configuration changes. These changes are illustrated in Figure VI-2-5 and present three (3) sets of stability data, also plotted in the SCAT-15F-9898 reference system. Curve 1 is a replot of curve 3 of Figure VI-2-4 and curves 2 and 3 are based on configuration adjustments as follows:

Curve 2: Same as curve 1 except the trailing-edge flaps are sized to represent those indicated on the Reference Configuration layout, see Figure V-2. References VI-2-7 and -8 were used to obtain the increments in lift and pitching moment due to the trailing-edge flap modification.

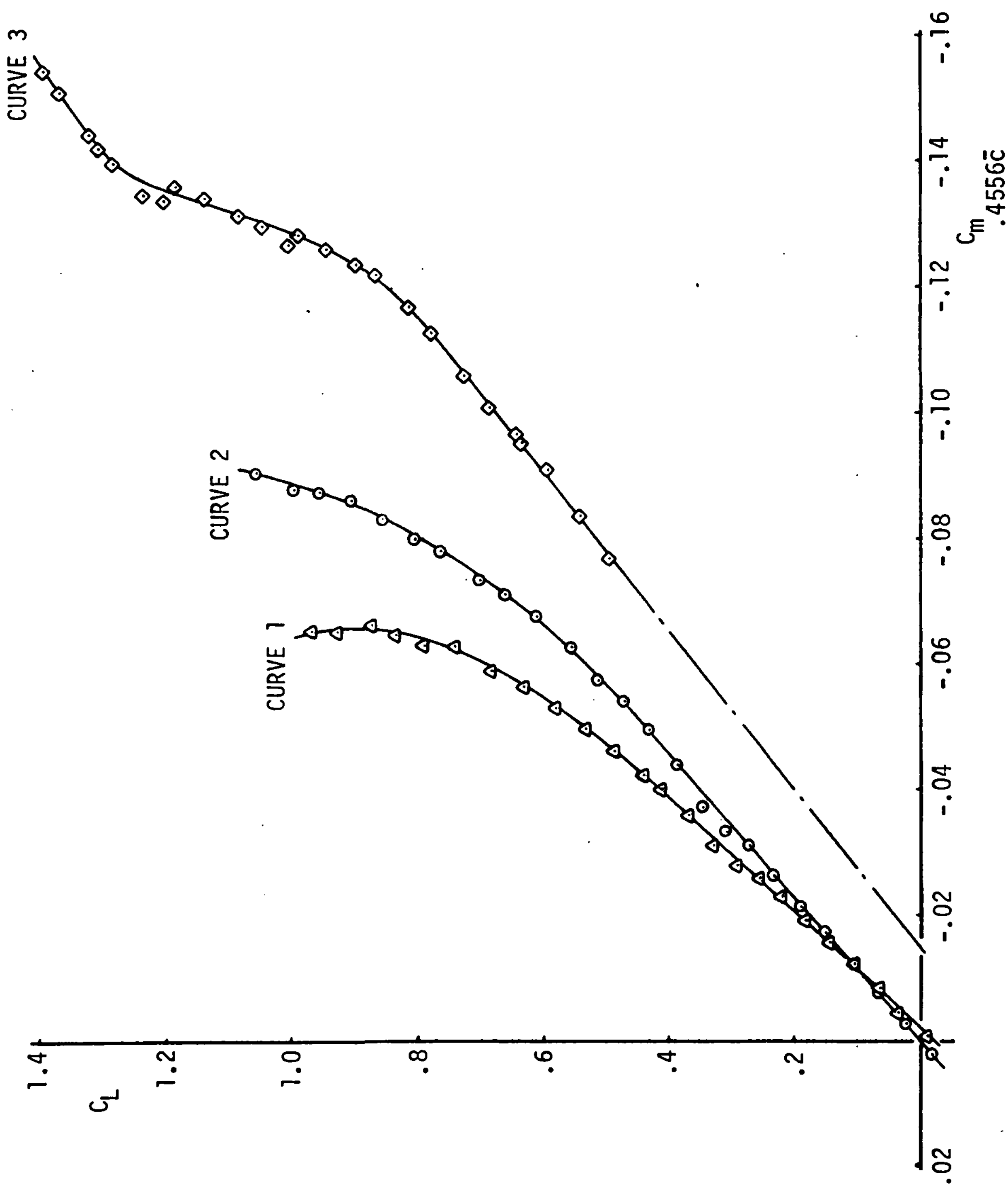

Figure VI-2-4-A Longitudinal Stability Summary of the High-Lift Configuration Development from Reference VI.2-3

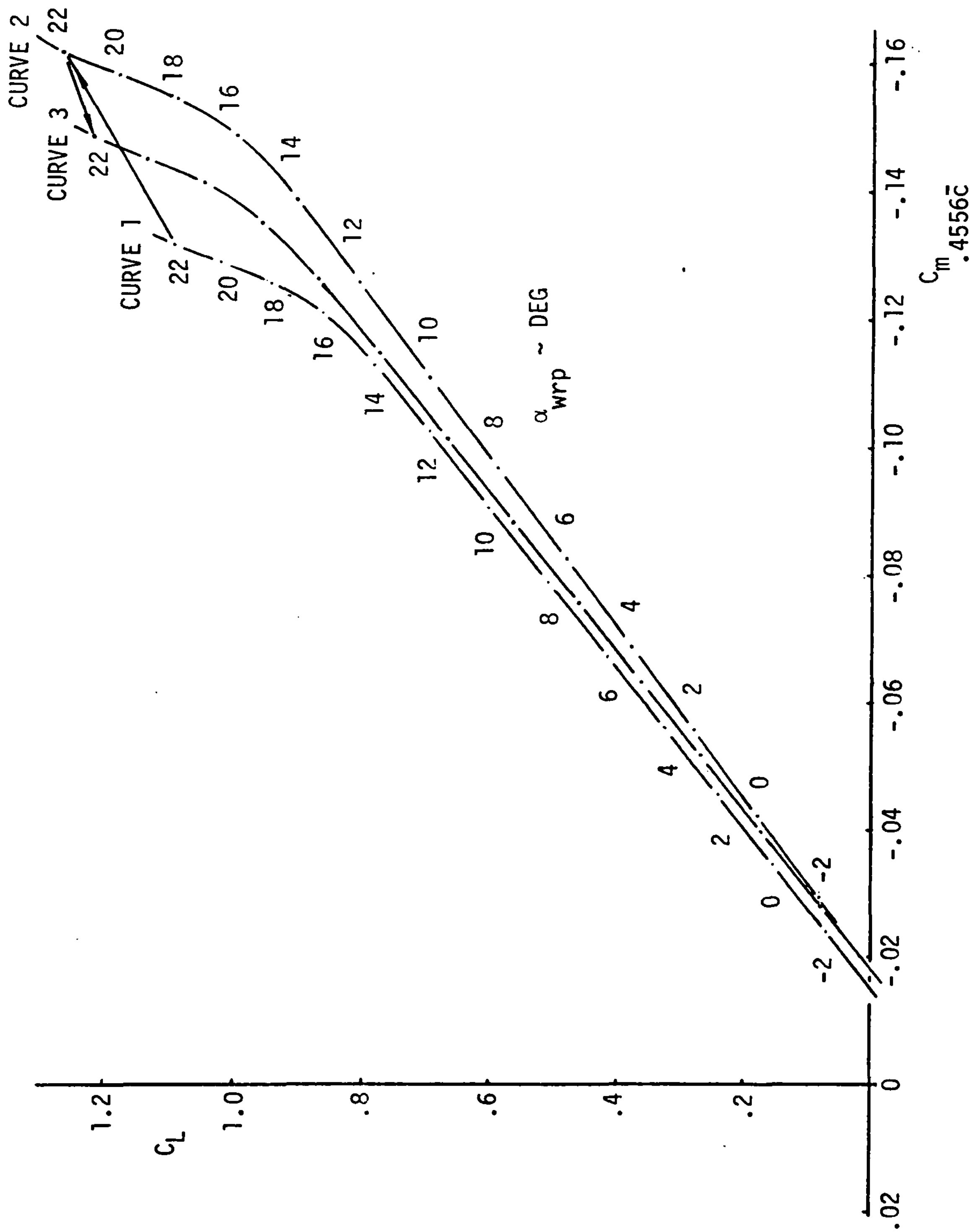

Figure VI-2-5-High-Lift Configuration Longitudinal Stability as Affected by Modifications to the High-Lift Devices

Curve 3: Same as curve 2 except L_3 is returned to 0°, (i.e. $L_{1,2}$ = 30°, L_{3-5} = 0°). The effect of the change in leading-edge devices was derived from a comparison between reference VI-2-3, run no. 21 and reference VI-2-2, run no. 151. (Elimination of one of the leading-edge flap segments provided a mechanically simpler configuration.)

Reference VI-2-9 indicates that, to obtain maximum landing performance, the aft center-of-gravity should be at approximately 0.60 to 0.65 $\bar{c}$, based on the SCAT-15F-9898 reference system. A preliminary weight and balance study ascertained that the probable center-of-gravity range was from 0.50 to 0.60 $\bar{c}$. To obtain the most rearward center-of-gravity, indicated above, the aft fuselage was extended ten (10) ft. Approximately half of the normal fuel reserves could then be carried in an aft fuselage fuel tank which would allow the center-of-gravity to be readily moved to any aft position as dictated by performance, static balance and stability and control requirements.

The Reference Configuration fuselage now became 315 foot long ($lt/\bar{c}$ = 1.232) so adjustments to the level of tail-on stability were estimated. References VI-2-3 and -4 indicated changes in stability due to fuselage length and horizontal tail position changes. The downwash data that was generated from reference VI-2-3 indicated a $d\varepsilon/d\alpha$ = 0.905 and from reference VI-2-4 a $d\varepsilon/d\alpha$= 0.565. As aerodynamic theory would indicate a $d\alpha/d\varepsilon$ of 1 at the trailing-edge to 0.85 at infinity, for an aspect ratio 1.62 wing, the determined value of 0.565 was ignored. Reference VI-2-8 was used to estimate the values of downwash slope at the two tested tail lengths and the estimated value at the longest tail arm was expressed as a percentage of that estimated for the shorter tail arm. This percentage was estimated to be 95.8.

	Reference VI-2-3	Reference VI-2-4
$(l_t/\bar{c})_{aero}$	0.917	1.163
$d\varepsilon/d\alpha$	0.905	0.867(0.905 x 0.958)

Using the values of $d\varepsilon/d\alpha$, in combination with the measured tail contributions to stability, values of q_t/q were calculated and plotted at the two respective test values of $l_t/\bar{c}$. Using a faired curve between these two points, values of $d\varepsilon/d\alpha$ and q_t/q were established for an $l_t/\bar{c}$ of 1.232. Using the value of tail-off dCm/dC_L from reference VI-2-4, and estimating the tail contribution to stability at an $l_t/\bar{c}$ of 1.232, a tail-on value of dCm/dC_L was determined. The change in total airplane stability, between the measured level (reference VI-2-4) and the estimated level for the Reference Configuration, was estimated to be -0.0056. By a comparison of the tests from references VI-2-2 and -3 a ΔC_{m_o} was established for changes in fuselage forebody length (B_5 to B_9). This trend was used to establish a ΔC_{m_o} of 0.0045 for the Reference Configuration forebody length. Using these estimated values of C_{m_o} and $\Delta(dCm/dC_L)$, and applying them to curve 3 of Figure VI-2-5, the stability plot presented on Figure VI-2-6 was generated. All data to this point are presented in the SCAT-15F-9898 reference system.

An illustration of the improvements made in the Reference Configuration are shown in Figure VI-2-7 where a comparison between the modified SCAT-15F configuration and the Reference Configuration is presented. At a given lift coefficient the following effects are noted:

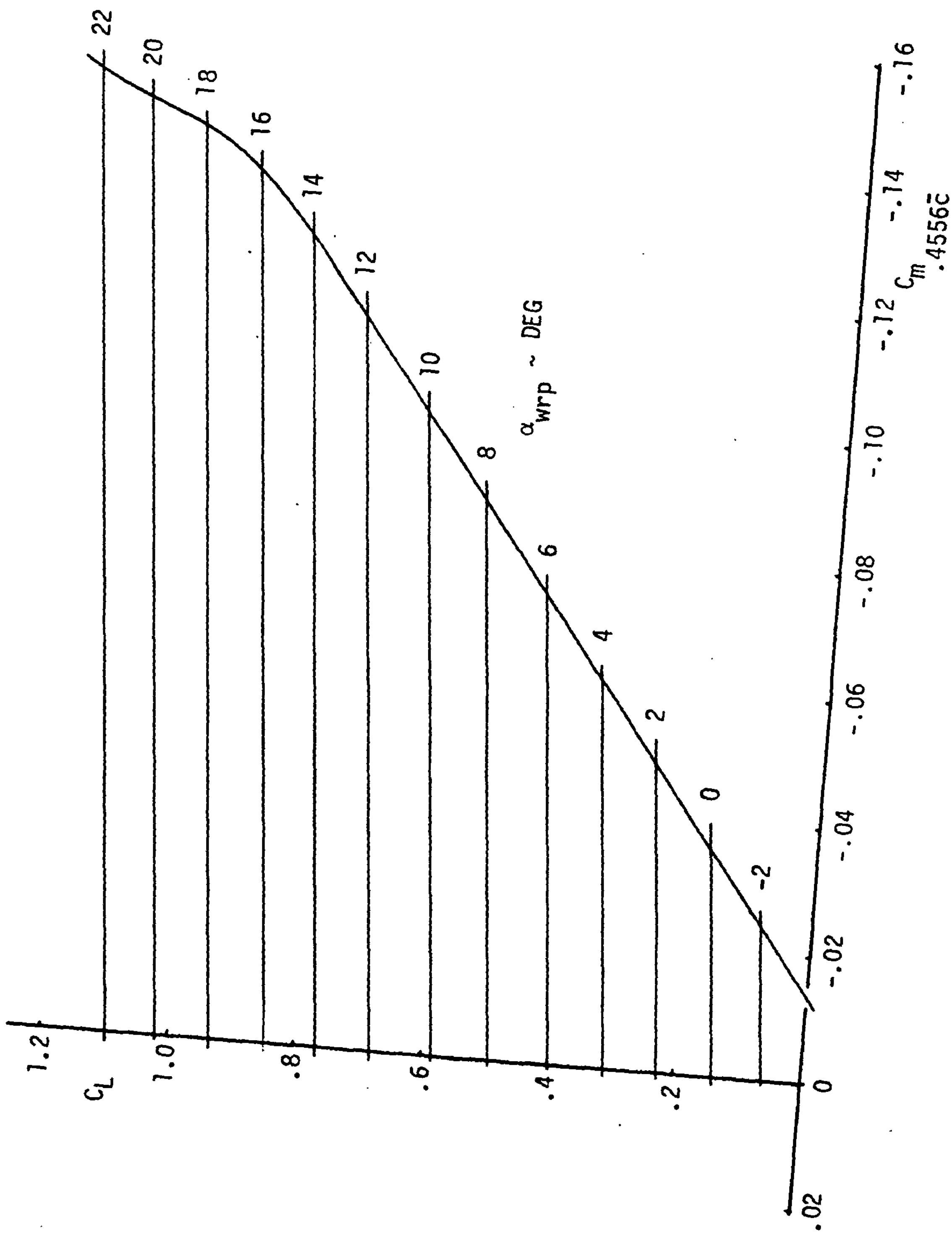

Figure VI-2-6-High-Lift Configuration Longitudinal Stability as Modified by Fuselage Length Change

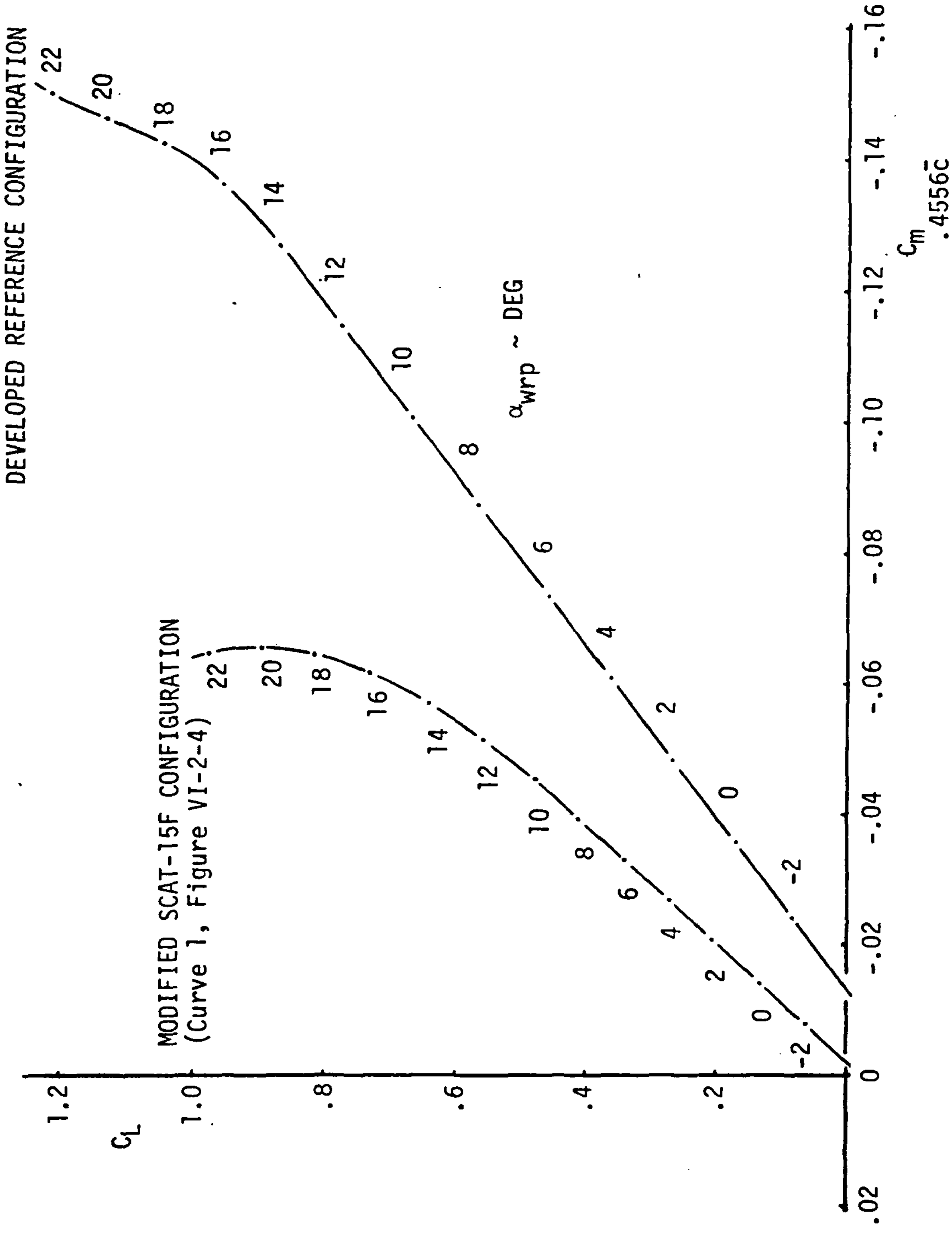

Figure VI-2-7- A Summary of the Change in Longitudinal Stability Due to Configuration Modifications

°more negative pitching moment, and

°lower trimmed angle-of-attack

These effects are highly desirable in maximizing the take-off and landing approach performance and minimizing the main landing gear length.

Static Stability and Control

In the following paragraphs the same high-lift configuration is used for both the take-off and landing approach modes of flight. No assessment of the resulting stability levels is made in this section of the report.

Static Longitudinal Stability and Control, Out of Ground Effect

Longitudinal control power capability was estimated for the Reference Configuration high-lift configuration using data from reference VI-2-4. Various combinations of tail incidence, i_t, and elevator deflection, δ_e, indicated that the maximum control effectiveness occurred at an $i_t/\delta_e = \pm 20°/22.5°$. The resulting maximum control deflection data were plotted and faired to produce the following tabulated results at an $l_t/\bar{c}$ of 1.163 in the SCAT-15F-9898 reference system:

C_N	ΔC_m $(i_t/\delta_e = -20°/-22.5°)$	ΔC_m $(i_t/\delta_e = +20°/+22.5°)$
0	.0545	-.0552
0.2	.0547	-.0553
0.4	.0556	-.0563
0.6	.0568	-.0580
0.8	.0575	-.0600
1.0	.0578	-.0617
1.2	.0578	-.0624

The tail maximum lift coefficient, developed at an i_t/δ_e of -20°/-22.5°, was checked at $C_L = 0$ by dividing the delta pitching moment, from the tail-off to the fully deflected tail values, by the horizontal tail volume coefficient. The maximum lift coefficient was calculated to be 1.44. The exposed wind-tunnel tail mean aerodynamic chord length was 7.835 inches, and at the test Reynold's Number (RN) of 1.23×10^6 per foot, gave a model tail RN of 0.803×10^6. The Reference Configuration full-scale tail RN, at nose-wheel lift-off, was estimated to be a minimum of 32.3×10^6. The variation of two-dimensional maximum lift coefficient with RN, from the data of reference VI-2-10, is presented on Figure VI-2-8. Using the noted RN variation, presented by these curves, indicated that a full-scale maximum lift coefficient of 1.864 was achievable.

The wind-tunnel model exposed horizontal tail area was 0.4275 ft^2 and assuming the model was 0.03 scale produced a full scale horizontal tail area of 475 ft^2. Correcting this area due to the 15 degree anhedral angle results in an exposed full scale projected tail area of 458 ft^2.

The estimated data that were presented on Figure VI-2-6, including the tail-off stability, were now converted to the Reference Configuration reference system, as outlined in the Data Base section, for horizontal tail areas of 458 and 916 ft^2 respectively (Figure VI-2-9). The establishment of the noted alpha and center-of-gravity limits will be discussed in the section on Aerodynamic Center-of-Gravity Limits.

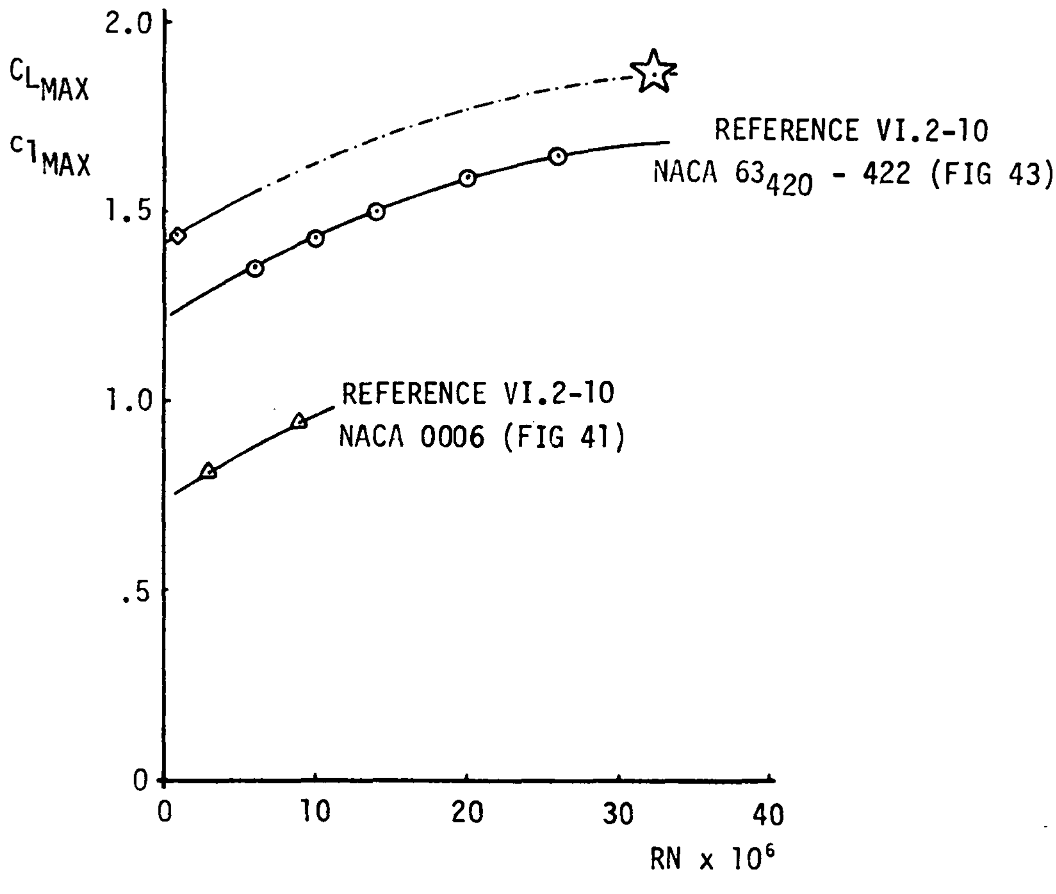

Figure VI-2-8 – The Variation of Maximum Lift Coefficient with Reynold's Number

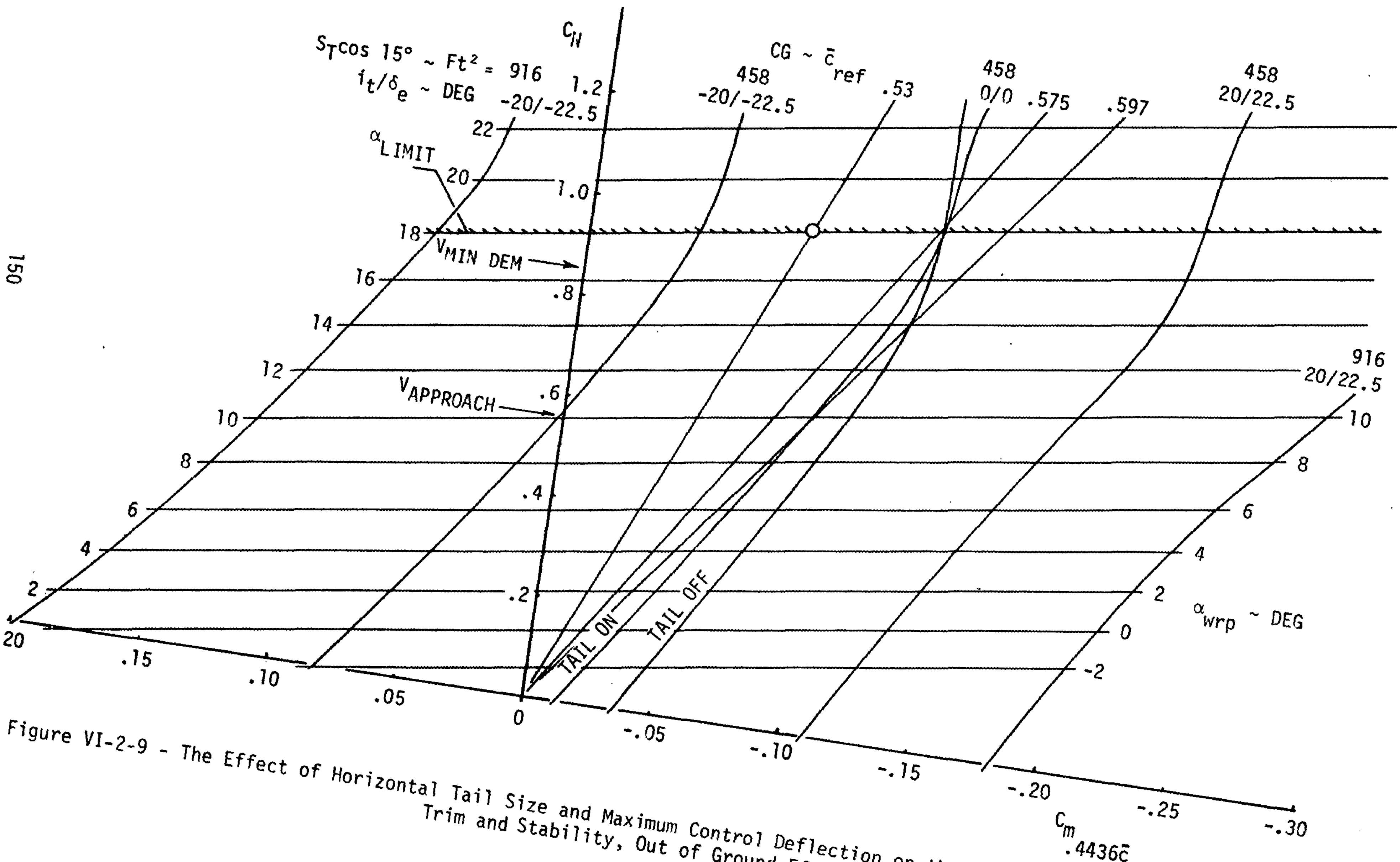

Figure VI-2-9 - The Effect of Horizontal Tail Size and Maximum Control Deflection on the Reference Configuration Trim and Stability, Out of Ground Effect

Static Longitudinal Stability and Control, In Ground Effect

The high-lift configuration tail-off pitching moment curve and horizontal tail contribution to stability of Figure VI-2-9 were adjusted due to the presence of the ground. These ground effects were obtained from Section VI-1A (see also references VI-2-7 and -11). The free-air horizontal tail maximum control contributions were also adjusted due to ground effects producing the in-ground-effect high-lift configuration stability and maximum control curves of Figure VI-2-10 for the two noted horizontal tail sizes. It should be recognized that these data reflect the effect of aircraft rotation, on the ground, about the main landing gear at all the presented angles-of-attack. In reality, once the aircraft starts to rotate, it will become airborne and the ground induced effects will start to diminish, resulting in no pitch-up being present. These data are therefore pessimistic in terms of the stability level at angles-of-attack greater than approximately 4 degrees. They do, however, serve to establish the minimum nose-wheel lift-off angle-of-attack (-3.2 degrees).

Supersonic Aerodynamic Center Location

An investigation of supersonic stability was undertaken to approximate the position of the Reference airplane's aerodynamic center. The test data of references VI-2-12 and -13 (SCAT-15F-9898) were used and the stability slopes at low values of lift coefficient were established. These data were corrected to the Reference Configuration's reference system and converted to aerodynamic center location and are presented in Figure VI-2-11. The method of reference VI-2-14 was used to establish an aerodynamic center shift due to

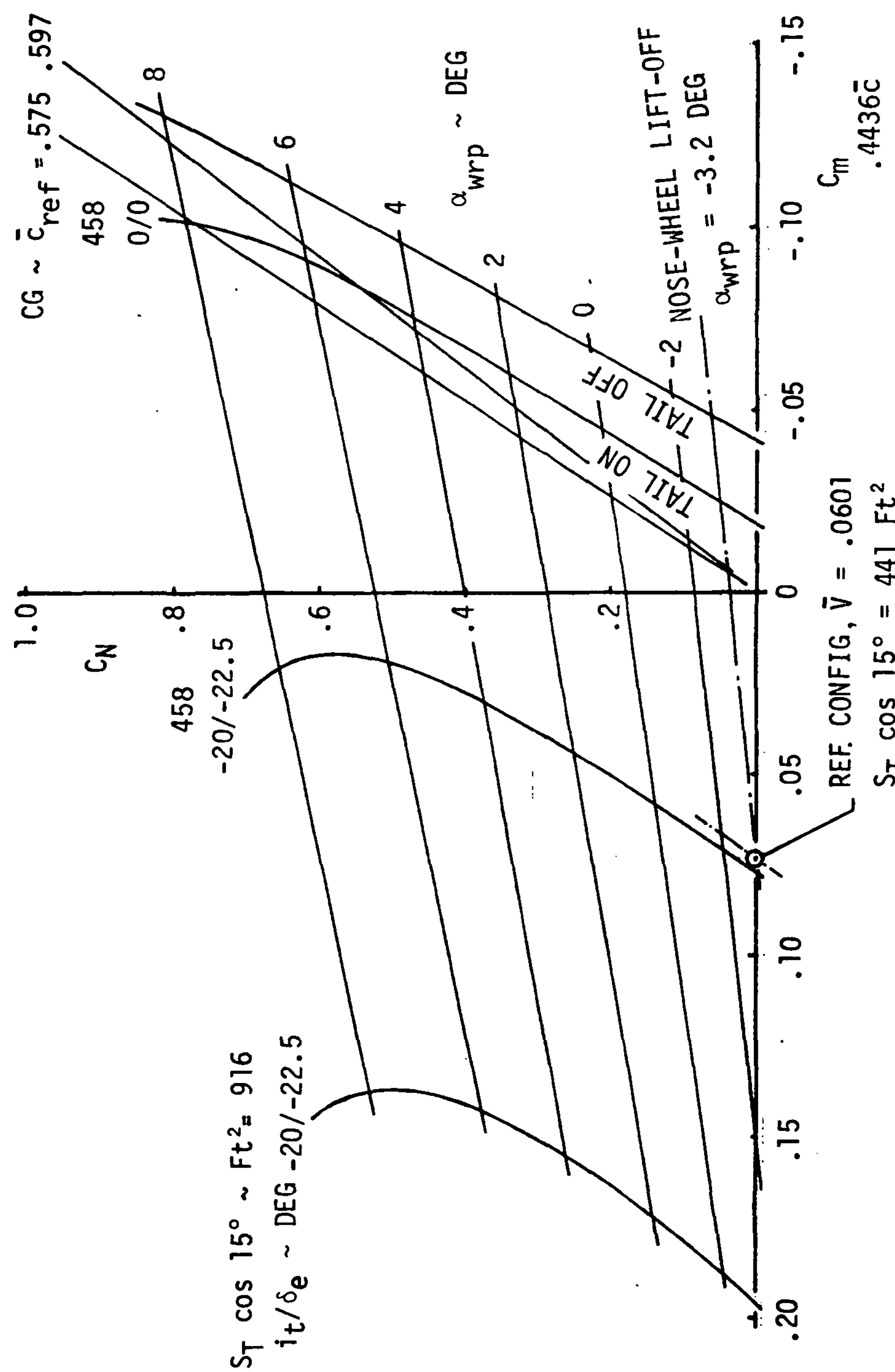

Figure VI-2-10 - The Effect of Horizontal Tail Size and Maximum Control Deflection on the Reference Configuration Trim and Stability, In Ground Effect planform differences between the SCAT-15F-9898 and the Reference concept airplane. The aerodynamic center shift was estimated to be approximately 4% aft due to the planform change and is presented on Figure VI-2-11. Assuming that the 'rigid' model shape tested at M=2.7 is the actual flexible airplane shape for that Mach number, and using flexibility factors from reference VI-2-5, the flexible airplane aerodynamic center was estimated and is presented on Figure VI-2-12. The M=2.7 aerodynamic center is estimated to be located at $0.5925\bar{c}_{ref}$ which is further forward than the take-off and landing aft center-of-gravity limit ($0.597\bar{c}_{ref}$).

The cruise performance calculations assumed 'zero' trim drag, i.e. the horizontal tail was set at its maximum lift-to-drag ratio incidence providing an upload on the tail. The test data of references VI-2-12 and -13 were used to obtain the values of the tail-on zero-lift pitching moment coefficient at zero degrees tail setting for Mach numbers of 1.2, 2.3, and 2.7. These values were converted to the Reference Configuration reference system and are plotted on Figure VI-2-13. The horizontal tail contribution to pitching moment from zero incidence was established at the tail setting for maximum tail lift-to-drag ratio and then corrected for reference system, horizontal tail arm and tail area. These values were used to establish the residual pitching moment that would have to be trimmed by correct location of the cruise center-of-gravity and are also plotted on Figure VI-2-13. The resulting center-of-gravity position for 'zero' trim drag is plotted on Figure VI-2-12 and illustrates essentially a constant location of $0.56\bar{c}_{ref}$. Additional analyses

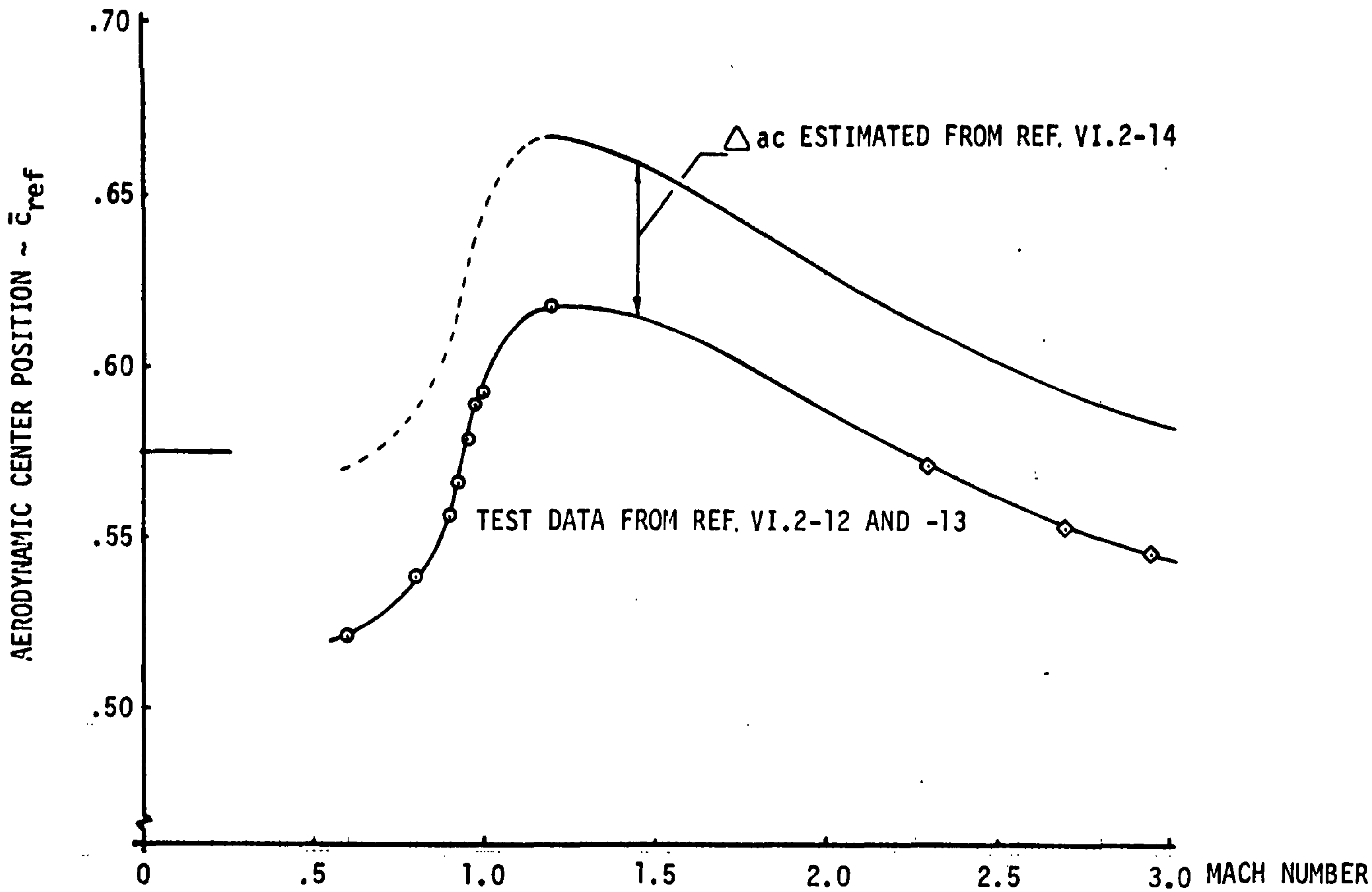

Figure VI-2-11 – Rigid Airplane Aerodynamic Center Position

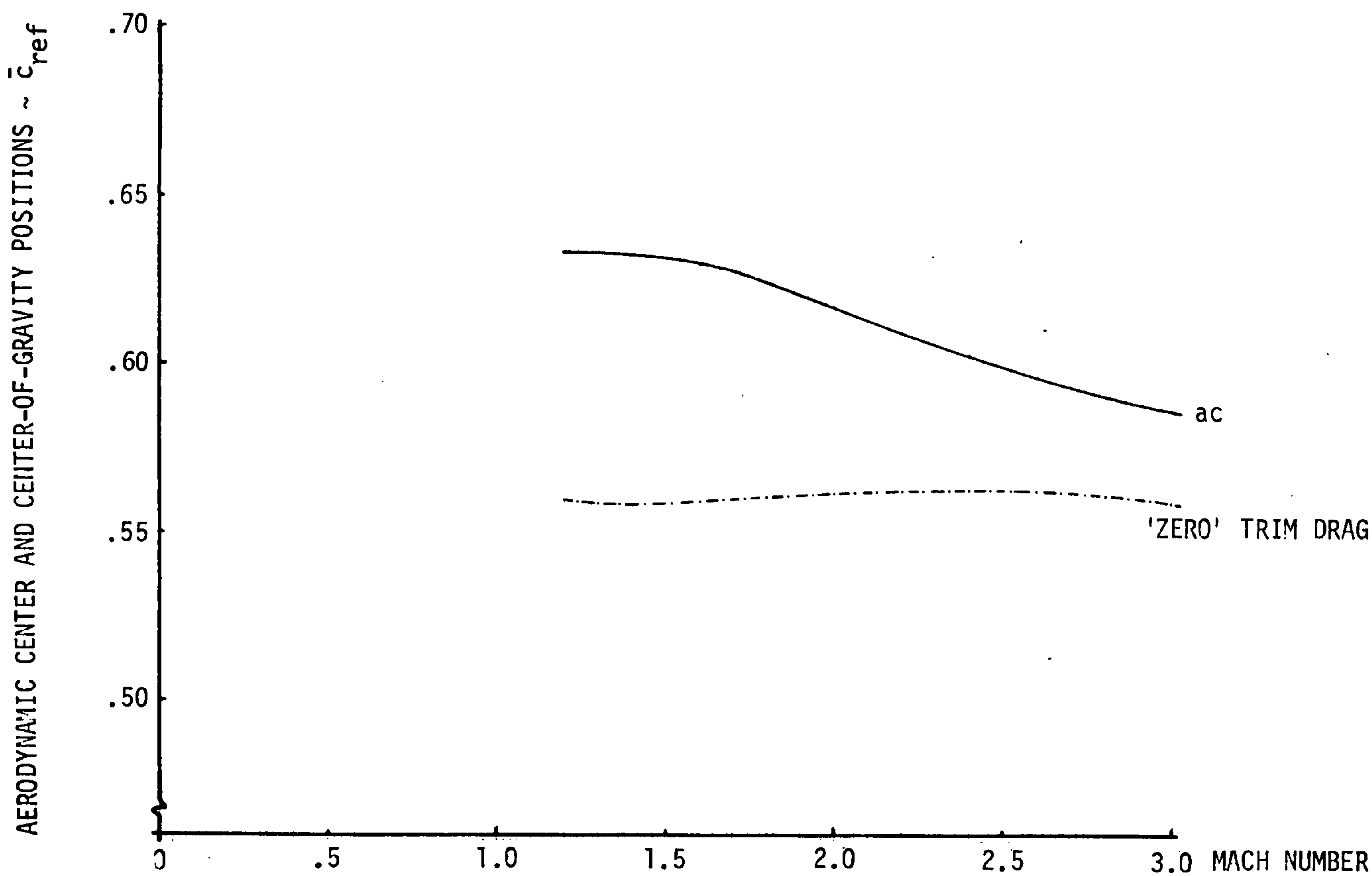

Figure VI-2-12-Flexible Airplane Aerodynamic Center and 'Zero' Trim Drag Center-of-Gravity Positions

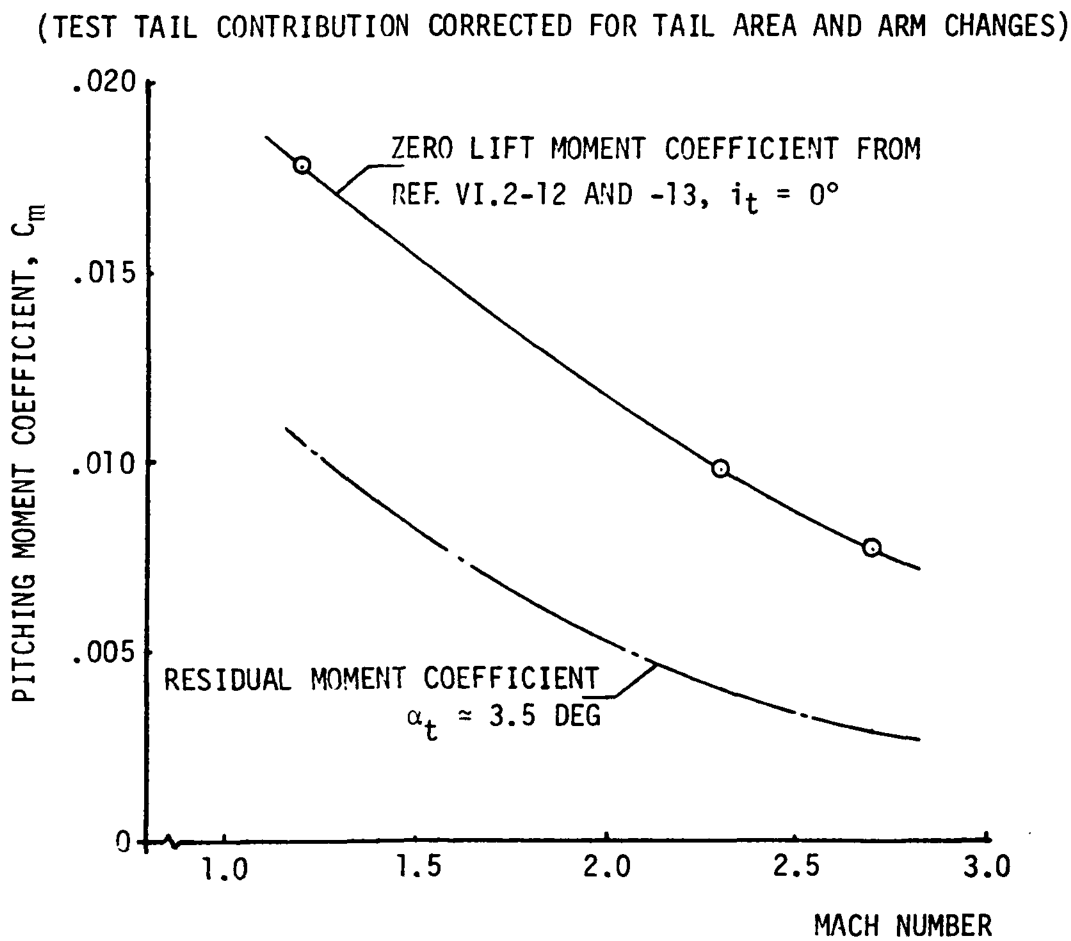

Figure VI-2-13 – Supersonic Pitching Moment Data are required to determine the most desirable level of supersonic cruise static margin. A positive static margin is desired in 1 g flight at M=2.7 to compensate for loss of stability due to structural flexibility at the required 2.5g maneuver condition. If the desired level at M=2.7 is less than the approximate $.03\bar{c}$ shown on Figure VI-2-12, then a redefinition of the wing camber and twist is required to provide the proper cruise design zero-lift pitching moment. Additional static margin can be provided by the ability to manage fuel.

Aerodynamic Center-of-Gravity Limits

The aerodynamic take-off, landing and in-flight center-of-gravity limits have been established based on the previously developed Criteria. These limits result from initial estimations of the Reference Configuration design gross weight, maximum landing weight and pitching moment of inertia, thrust-to-weight ratio and geometry limited airplane maximum lift coefficient, in ground effect. The finalized values of these items may be different from those presented below and the effect of the differences will be discussed in the last section. The estimated data are as follows:

- °Design Gross Weight = 776,000 lb
- °Maximum Landing Weight = 500,000 lb($I_y \simeq 48.4 \times 10^6$ slugs ft^2)
- °Thrust-to-Weight Ratio = 0.34
- °Take-off Lift Coefficient, in ground effect = 0.648

°Approach Speed Lift Coefficient = 0.55

°Minimum Demonstrated Speed Lift Coefficient = 0.825

°Center-of-Gravity Range = 26 inches

In-Flight Limits

Refering to Figure VI-2-9, and noting the maximum trim capability for $\pm\ i_t/\delta_e = \pm\ 20°/22.5°$ at the minimum demonstrated V, the following results are obtained:

a. Aft C.G. Trim Limits, OGE, $V_{min\ dem}$:

S_T cos 15° ~ ft^2	458	916
$l_t/\bar{c}$	1.361	1.361
$\bar{V} = l_t/\bar{c}.S_T/S$	.0624	.1248
C_m $.4436\bar{c}_{ref}$	-.218	-.3053(i_t/δ_e = 20°/22.5°)
$\Delta C_{m_{\ddot{\theta}}}$	.083	.083($\ddot{\theta}$ = -0.1 rad/sec^2)
ΣC_m	-.135	-.2223
dCm/dC_N	-.1584	-.2613
∴CG ~ $\bar{c}_{ref}$	.6020	.7049

b. Fwd CG Trim Limits, OGE, $V_{min\ dem}$:

$\bar{V}$	.0624	.1248
C_m $.4436\bar{c}_{ref}$	-.0333	.0622(i_t/δ_e = -20°/-22.5°)
dCm/dC_N	-.0391	.073
∴CG ~ $\bar{c}$ ref	.4827	.3706

Using the assumed approach lift coefficient of 0.55, the following neutral stability data are presented:

c. Neutral Stability CG, OGE, $V_{approach}$:

$\bar{V}$	.0624	.1248
dCm/dC_N	-.1317	-.1653
$\therefore CG \sim \bar{c}_{ref}$	.5763	.6089

Nose-Wheel Rotation Limits

The significant parameters in the computation of the forward center-of-gravity position based on nose-wheel rotation requirements are:

°Wing-body C_{m_0}, in ground effect

°Horizontal tail maximum lift coefficient, in ground effect

°Take-off maximum airplane lift coefficient, in ground effect

°Gear location aft of most aft center-of-gravity position

°Center-of-gravity range

Take-off gross weight affects the take-off speed and thrust-to-weight ratio, the aircraft acceleration capability, and hence take-off distance. Thrust-to-weight ratio also has a second order effect on the forward center-of-gravity position.

Based on Figure VI-2-10 the horizontal tail maximum lift coefficient is computed to be 1.896, in ground effect. Checking the landing gear location, based on turn-over limitations, gave a minimum distance of 55 inches aft of the most aft center-of-gravity ($0.597\bar{c}_{ref}$). For the two horizontal tail volume coefficients assumed, the forward centers-of-gravity were calculated. These results, including the estimated center-of-gravity locations computed in the previous paragraphs, are presented on Figure VI-2-14. It can be seen that for the assumed exposed projected horizontal tail area of 441 ft^2, for

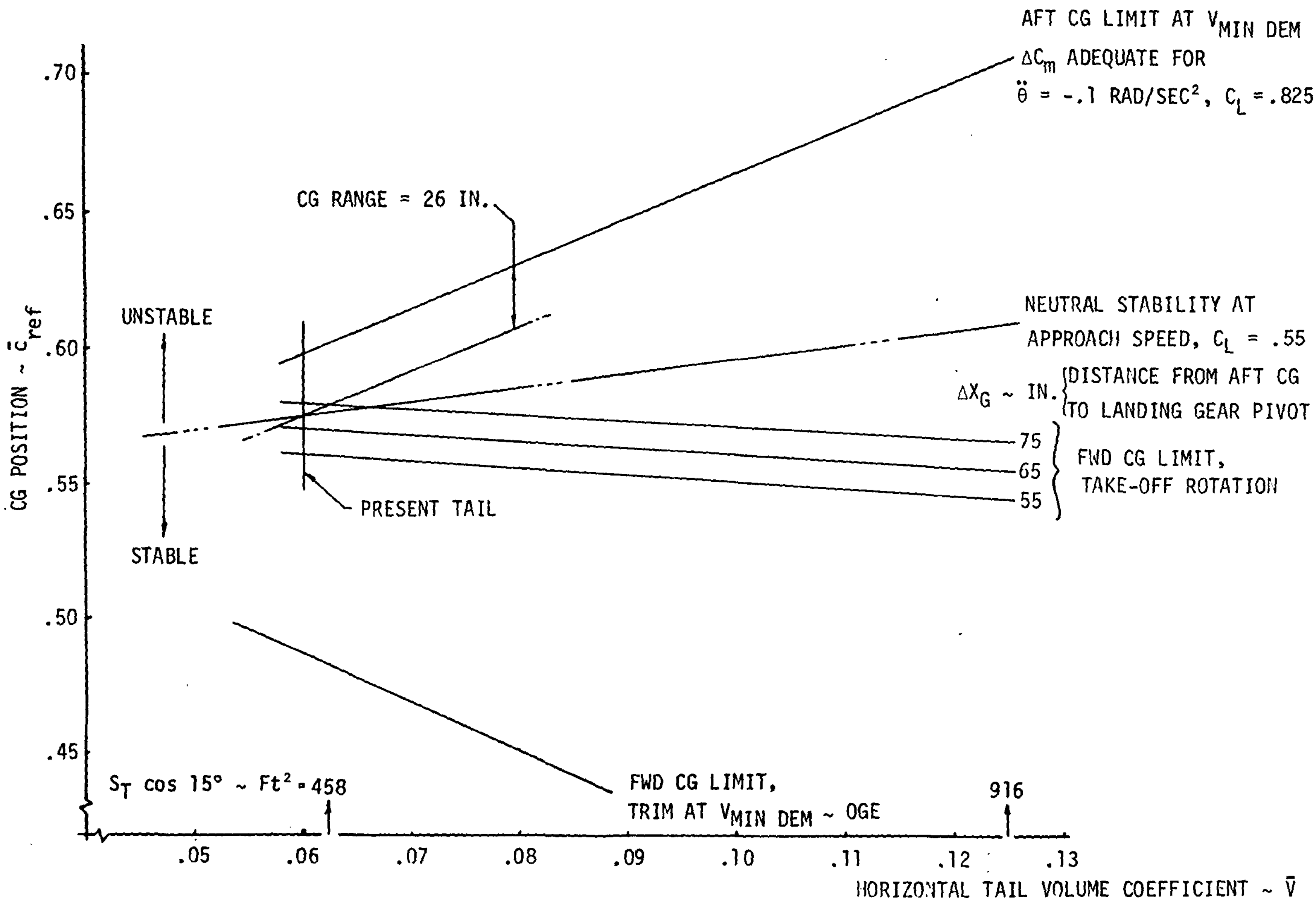

Figure VI-2-14 — Center-of-Gravity Limits for Take-off and Landing the Reference airplane, there is more than 26 inches of center-of-gravity range available. This result allows the landing gear to be located farther aft than the assumed 55 inches.

Two additional incremental distances were assumed, namely 65 and 75 inches, and the resulting forward centers-of-gravity recalculated. It can be seen that, with the presently assumed horizontal tail size (441 ft^2) and a 26 inch center-of-gravity range, the landing gear can be located aft of the most aft limit by 70 inches. Based on these results the most forward and aft take-off limits are established as follows:

$$\text{Most aft} = 0.597\ \bar{c}_{ref}$$

$$\text{Most forward} = 0.575\ \bar{c}_{ref}$$

Alpha Limit at the Most Forward In-Flight Limit

No significant pitch-up is present for the Reference airplane high-lift configuration; however, an alpha limiter is recommended on the basis of rate-of descent criteria. Based upon a zero rate-of-climb condition with one engine inoperative at the minimum demonstrated speed and most forward in-flight center-of-gravity position (0.53 $\bar{c}_{ref}$), an alpha limit of 18 degrees was established. The selected forward center-of-gravity position provides a minimum upset margin of 0.15 g's to manage gust induced disturbances and a minimum approach condition performance level. (Trimmed lift-to-drag ratio of 5:1).

Recommended Aerodynamic Center-of-Gravity Envelope

The recommended aerodynamic center-of-gravity envelope is presented on Figure VI-2-15 as a function of airplane gross weight. Assuming the 18 degree alpha limit, the gust margin is 0.15 g's at 0.53 $\bar{c}_{ref}$ and greater than 0.15 g's at farther aft centers-of-gravity. The recommended cruise range of from 0.53 to 0.56 $\bar{c}_{ref}$ may require fuel management reevaluation and/or wing camber changes.

Figure VI-2-16 presents the variation of trimmed airplane lift-to-drag ratio and angle-of-attack, as a function of center-of-gravity position, for the landing approach condition.

Longitudinal Dynamic Stability

Only the Reference airplane high-lift approach configuration was examined for dynamic longitudinal stability characteristics. The effect of flying during landing at neutral and unstable conditions (0.575 and 0.597 $\bar{c}_{ref}$ respectively), was established by conducting a simple controls fixed short-period dynamic analysis. This was achieved by examination of the roots of the airplane characteristic equation of motion and reviewing the solutions against some known handling qualities criteria. Present and proposed FAR's, references VI-2-15 and -16 give no quantitative requirements for stability, therefore the criteria of references VI-2-17 and -18 were selected. The inherent airframe characteristics were found to be unacceptable, when compared against the selected criteria, indicating the need for some form of stability augmentation system (SAS). Based on the Boeing development of a Hardened SAS concept, reference VI-2-19, three (3) levels of pitch-rate

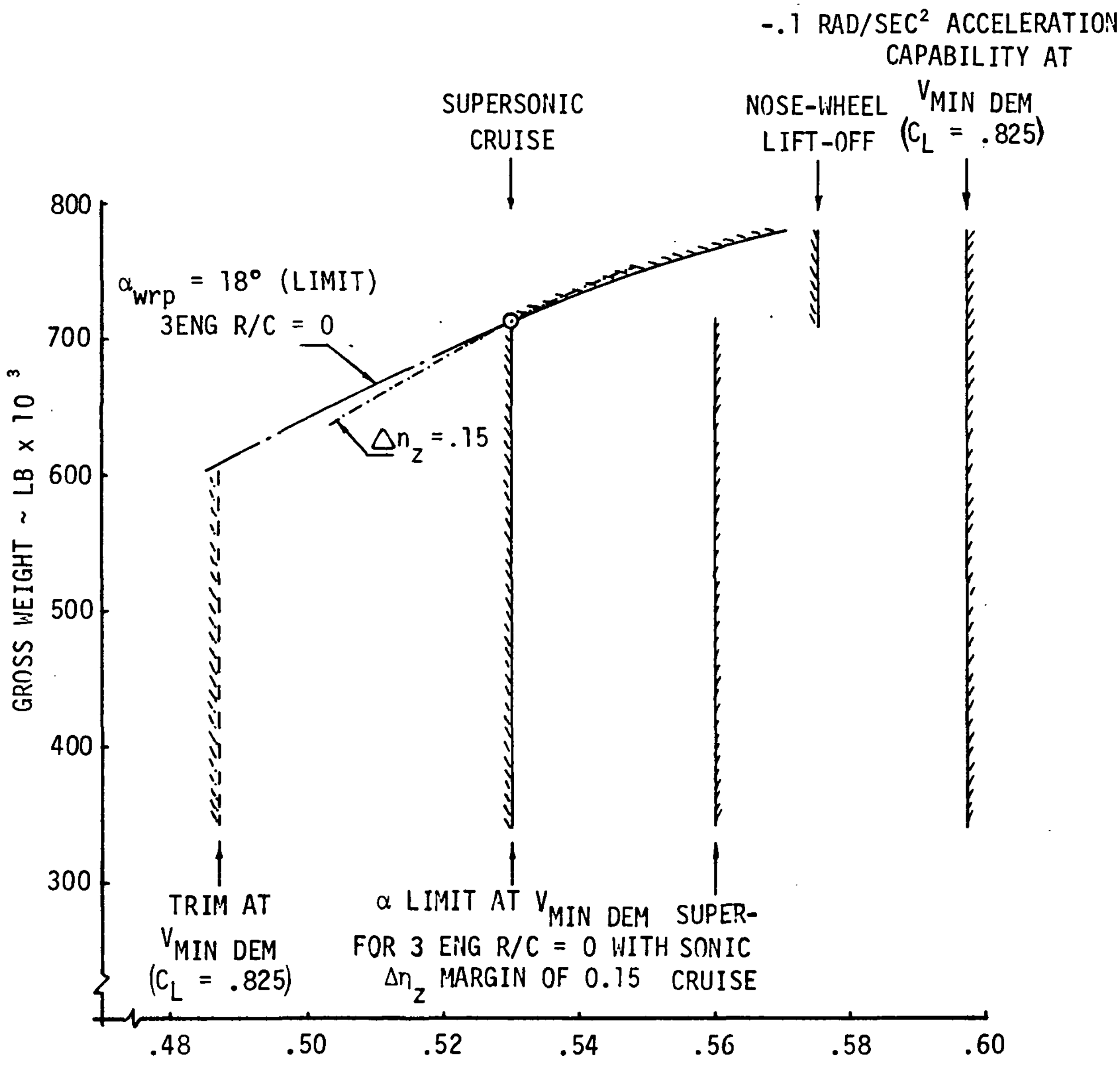

	CG LIMITS FWD	CG LIMITS AFT
TAKE-OFF:	.575$\bar{c}$	.597$\bar{c}$
LANDING:	.53$\bar{c}$	.597$\bar{c}$
CRUISE:	*.53$\bar{c}$	.56$\bar{c}$

*SEE ABOVE FIGURE

LE MAC = STN 1438.5

MAC = 1154.86 IN.

Figure VI-2-15 - Aerodynamic Center-of-Gravity Envelope

$C_{L_{APPROACH}} = .55$

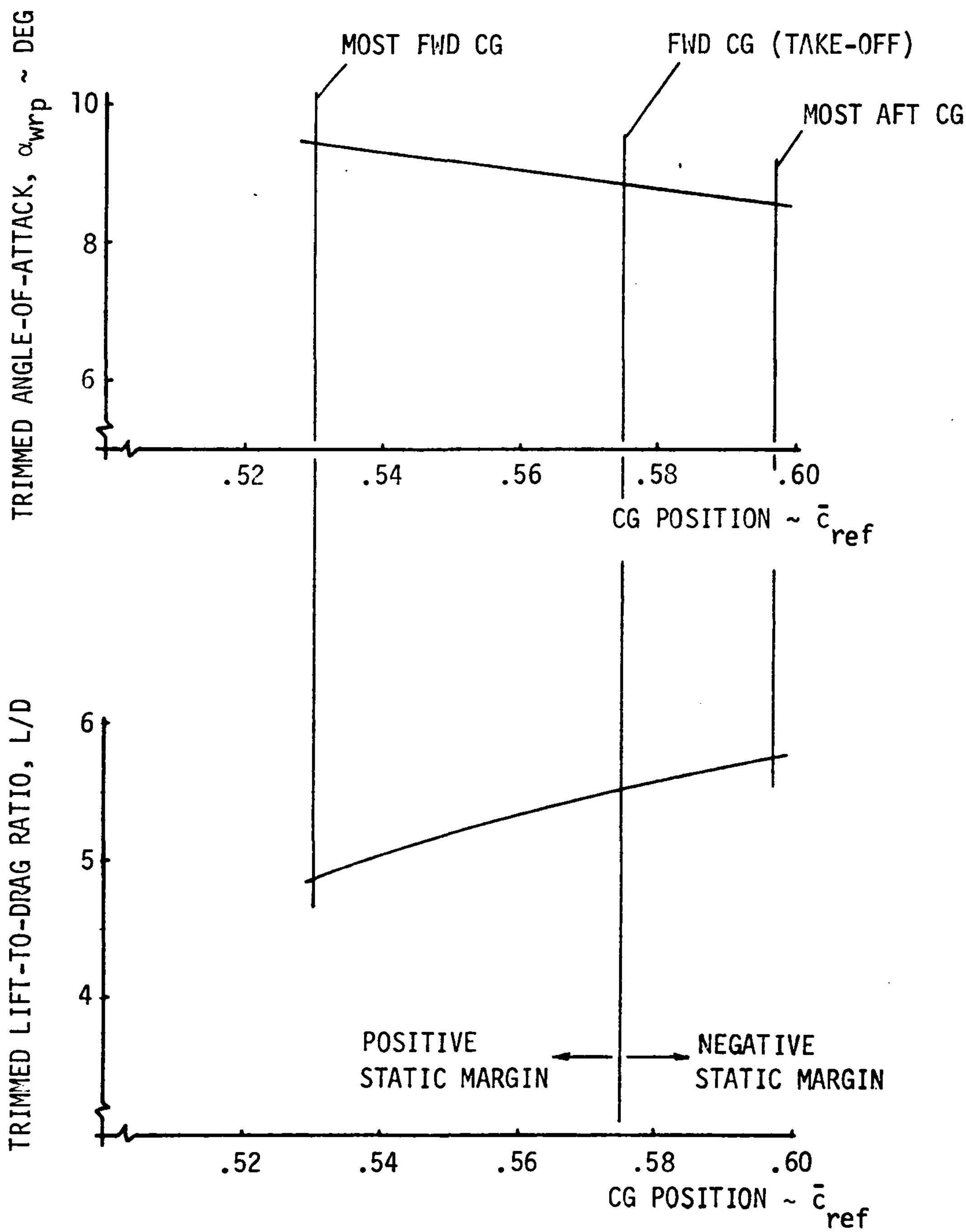

Figure VI-2-16 – Landing Approach Configuration Trim Data damping were investigated. This analysis assumed a perfect SAS, i.e., with no system dynamics or lags, and just examined the roots resulting from the modified characteristic equations of motion. The results are presented on Figures VI-2-17 and -18 for the selected center-of-gravity locations, 0.575 and 0.597 $\bar{c}_{ref}$ respectively. Based on these results it is indicated that artificial pitch stiffness, ΔM_{α}, is required in order to increase the short-period undamped natural frequency, which in turn will reduce the damping ratio.

Reference VI-2-18 requires a damping ratio no greater than 1.3 for acceptable handling qualities under normal (non-emergency) flight conditions. An arbitrary pitch stiffness gain of one (1) degree of horizontal tail incidence per degree angle-of-attack was chosen and combined with a pitch-rate gain of three (3) degrees of horizontal tail incidence per degree per second pitch rate and checked at the aft center-of-gravity of 0.597 $\bar{c}_{ref}$. This result is also presented on Figures VI-2-17 and -18 and shows much improved short-period characteristics indicating the requirement for a SAS incorporating both pitch-rate and stiffness functions. Gain scheduling appears to be required for supersonic flight due to the fact that the airplane will be flown with a positive static margin in 1 g flight at M=2.7. The results that are plotted on Figures VI-2-17 and -18 are tabulated below:

W = 500000 LB $C_{L_{TRIM}} = .55$

3 DEG GLIDE SLOPE

SYM	CG ~ $\bar{c}_{ref}$
△	.575
⊙	.597

NEUTRAL POINT = $.575\bar{c}_{ref}$

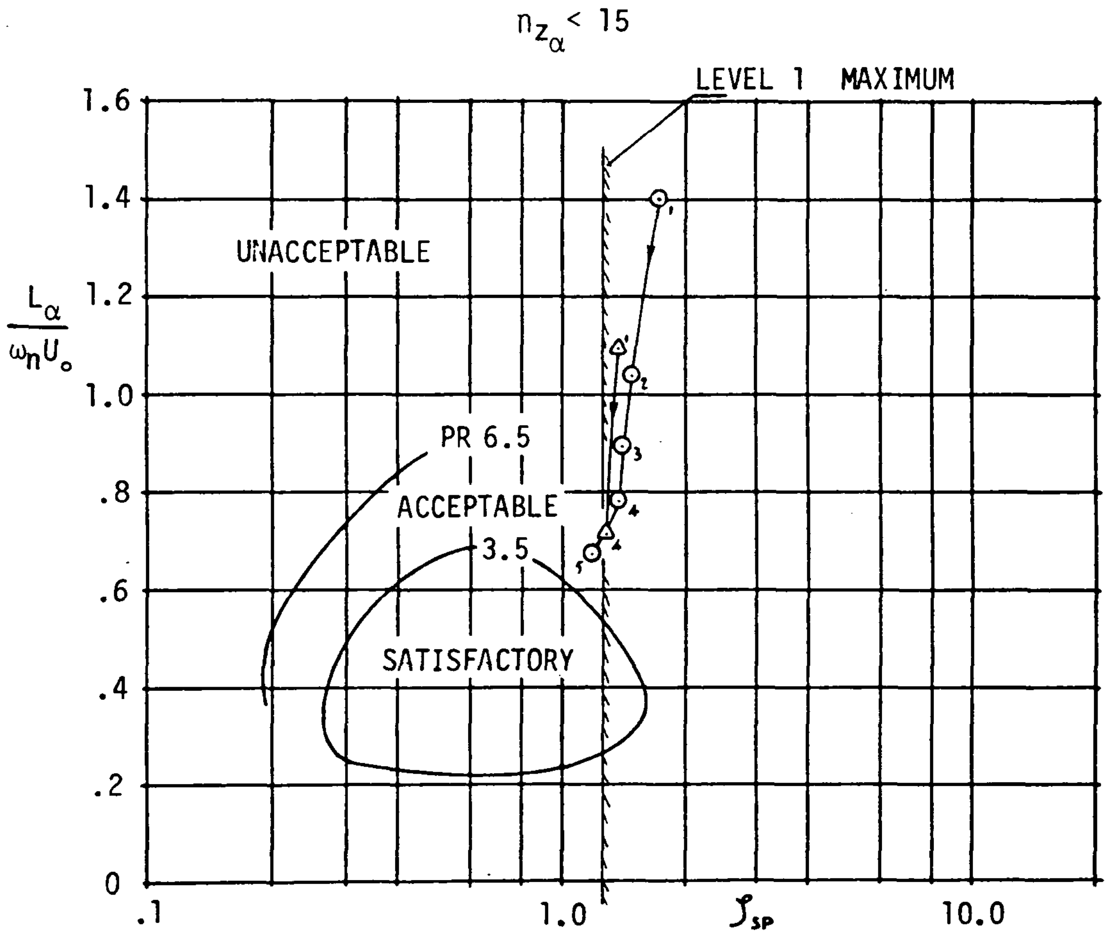

	SUBSCRIPT	1	2	3	4	5
SAS GAINS	$K_{\dot{\theta}}$	0	1	2	3	3
	K_α	0	0	0	0	1

Figure VI-2-17 – Longitudinal Short Period Stability Characteristics Approach Configuration

W = 500000 LB $C_{L_{TRIM}}$ = .55

3 DEG GLIDE SLOPE

NEUTRAL POINT = .575 $\bar{c}_{ref}$

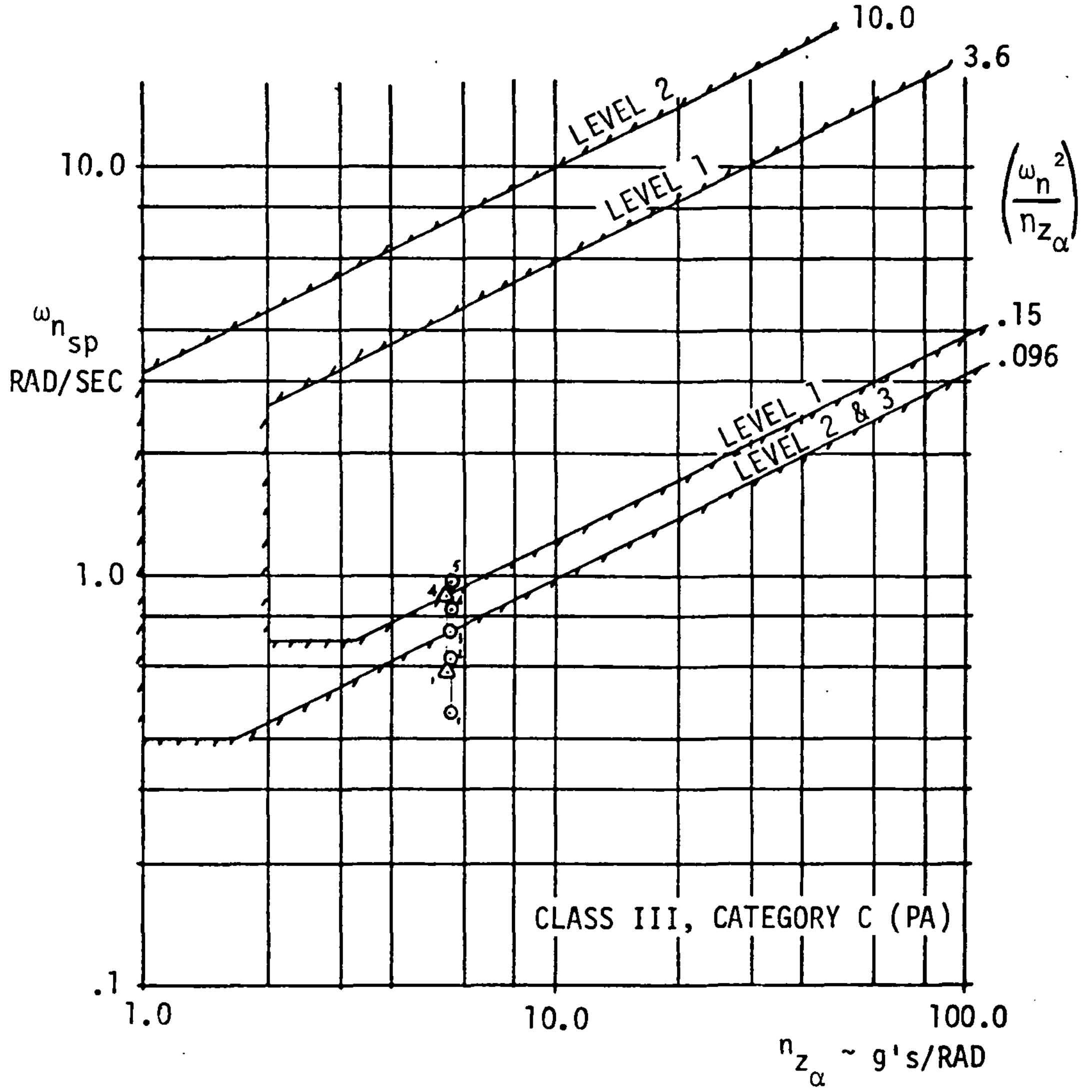

FOR DEFINITION OF SYMBOLS, SEE FIGURE VI.2-17

Approach Configuration

Figure VI-2-18 – Longitudinal Short Period Stability Characteristics

CG ~ $\bar{c}$	.575	.575	.597	.597	.597	.597	.597
U_o ~ ft/sec	276.5	→	→	→	→	→	→
$K_{\dot{\theta}}$ ~ deg/deg/sec	0	3	0	1	2	3	3
K_α ~ deg/deg	0	0	0	0	0	0	1
$-L_\alpha$ ~ ft/sec^2	176.1	176.1	178.9	178.9	178.9	178.9	178.9
$-L_\alpha/U_o$ ~ 1/sec	.637	.637	.647	.647	.647	.647	.647
$n_{z_\alpha} = -L_\alpha/g$	5.46	5.46	5.56	5.56	5.56	5.56	5.56
Static margin ~ $\bar{c}$	0	0	- .022	-.022	-.022	-.022	-.022
ω_n ~ rad/sec	.582	.896	.463	.624	.782	.829	.964
$-L_\alpha/U_o\omega_n$	1.093	.712	1.40	1.038	.89	.781	.672
ζ_{SP}	1.418	1.328	1.76	1.523	1.456	1.421	1.223

<u>Effect of Changes in Operating Conditions on the Reference Airplane Configuration Development</u>

Since the Reference Configuration take-off and landing trim calculations were initially estimated some performance parameter changes have taken place. The significant terms that have been changed are as follows:

°The noise limited take-off power thrust-to-weight ratio changed from 0.34 to <u>0.27</u>

°the take-off lift coefficient changed from 0.648 to <u>0.531</u>

The combined effects of these two parameters result in the capability of moving the main landing gear aft by an additional 17 inches for the same horizontal tail size (441 ft^2). This would then allow the main landing gear struts to be slightly shorter.

LIST OF SYMBOLS

ac	aerodynamic center
$B_{3,5,9}$	fuselage designation
$\bar{c}$	mean aerodynamic chord, ft or inches
C_F	force coefficient, $\frac{\text{Force}}{qs}$
CG	center of gravity
C_L	lift coefficient, $\frac{\text{Lift}}{qs}$
c_l	two-dimensional lift coefficient
C_m	pitching moment coefficient, $\frac{\text{Pitching Moment}}{qs\bar{c}}$
C_{m_o}	zero-lift pitching moment coefficient
$C_{m_{\ddot{\theta}}}$	pitching moment coefficient necessary to produce a given $\ddot{\theta}$
C_N	normal force coefficient in stability axis system
E_2	engine nacelle designation
g	gravitational constant, assumed to be 32.2 ft/sec^2
$H_{1,3}$	horizontal tail designation
i_t	tail incidence setting, degrees
K_α	stability augmentation pitch-attitude gain
$K_{\dot{\theta}}$	stability augmentation pitch-rate gain, seconds
$L_{1,2,3,4,5,6}$	wing leading-edge flap designation
LEMAC	leading-edge of the mean aerodynamic chord, fuselage station
l_t	horizontal tail arm from moment reference, ft or inches
L_α	dimensional variation of lift with angle-of-attack, ft/sec^2
M	Mach number

VI-2 (Continued)

LIST OF SYMBOLS

MAC	mean aerodynamic chord, ft or inches
M_{α}	dimensional variation of pitching moment with angle-of-attack, sec^{-2}
N_2	notch at wing-fuselage junction
n_z	normal acceleration, ft/sec^2
$n_{z_{\alpha}}$	normal acceleration per radian angle-of-attack, g's/radian
OGE	out of ground effect
q	free-stream dynamic pressure, lb/ft^2
q_t	local dynamic pressure at the horizontal tail, lb/ft^2
S	wing area, ft^2
S_T	exposed horizontal tail area, ft^2
T_6	wing-tip geometry designation
U_o	free-stream trimmed airspeed, ft/sec
$V_{1,23}$	vertical tail designation
$\bar{V}$	horizontal tail volume coefficient
W	airplane gross weight, lb
W_3	wing leading-edge designation
α	angle-of-attack, degrees or radians
α_{wrp}	angle-of-attack with reference to the wing reference plane,
α_t	horizontal tail angle-of-attack, degrees
Δ	increment
δ_e	elevator deflection, degrees

VI-2 (Continued)

LIST OF SYMBOLS

$d\varepsilon/d\alpha$	rate-of-change of downwash at the tail with angle-of-attack
$dCm/d\alpha$	rate-of-change of pitching moment coefficient with angle-of-attack, radian^{-1}
dCm/dC_L	rate-of-change of pitching moment coefficient with lift coefficient
dCm/dC_N	rate-of-change of pitching moment coefficient with normal force coefficient
ζ_{SP}	longitudinal short-period damping ratio
$\ddot{\theta}$	pitching acceleration, radians/sec^2
Λ	wing leading-edge sweep angle, degrees
ω_n	longitudinal short-period undamped natural frequency, radians/sec

REFERENCES

Reference No.	Title
VI-2-1	Unpublished Data.
VI-2-2	Unpublished Data.
VI-2-3	Unpublished Data.
VI-2-4	Unpublished Data.
VI-2-5	The Boeing Co.; "Mach 2.7 Fixed Wing SST Model 969-336C (SCAT-15F), Document No. D6A-11666-1, dated November 1969.
VI-2-6	Unpublished Data.
VI-2-7	DeYoung, J.; "Ground-Induced Lift of Arrow Wing Aircraft," Memorandum V-19000/3NASA-436, dated 27 July 1973. (Unpublished)
VI-2-8	USAF Stability and Control DATCOM, "Stability and Control Methods," Air Force Flight Dynamics Laboratory, Ohio, dated October 1960, Revised November 1965.
VI-2-9	Unpublished Data.
VI-2-10	Abbott, I. H., and von Doenhoff, A. E.; "Summary of Airfoil Date," NACA TR 824, dated 1945.
VI-2-11	DeYoung, J.; "Lift, Drag and Moment Near Ground of AST Aircraft," Memorandum V-19000/3AVO-096, dated 24 August 1973. (Unpublished)
VI-2-12	Unpublished data.
VI-2-13	Unpublished Data.
VI-2-14	Middleton, W. D., and Carlson, H. W.; "A Supersonic Lifting Surface Program, No. D 2340." (Unpublished)
VI-2-15	Federal Aviation Regulations - Part 25, "Airworthiness Standards, Transport Category Airplanes, Rules Service Co., dated 1 October 1972.

REFERENCES (Continued)

Reference No.	Title
VI-2-16	Dept. of Transportation, FAA, "Tentative Airworthiness Standards for Supersonic Transports," dated 1 January 1971.
VI-2-17	Shomber, H. A., and Gertsen, W. M.; "Longitudinal Handling Qualities Criteria: An Evaluation," Journal of Aircraft, Vol. 4, No. 4, dated 1967.
VI-2-18	Anon; "Flying Qualities of Piloted Airplanes," Military Specification MIL-F-008785 A (USAF), dated 31 October 1968.
VI-2-19	Tomlinson, L. R.; "SST Longitudinal Control System Design and Design Processes, Hardened Stability Augmentation Design," Report No. FAA-SS-73-1 (Boeing D6-60285), dated June 1973.

LIST OF FIGURES

LIST OF FIGURES (Continued)

VI-3 PROPULSION

INTRODUCTION

In previous studies airplane-propulsion integration has proved to be the single most difficult design problem with supersonic transport type airplanes. Even when high specific thrust engine cycles (afterburning turbojets-which produce the highest cruise efficiency) have been used, the payload fraction has proved to be marginally acceptable from an economic point of view (Reference VI-3-1). The adoption of special regulatory rules, in the areas of noise, reserve fuel requirements, and subsonic overland legs to avoid sonic boom can only make the airplane-propulsion integration problem more difficult. These rules can have as much or more influence on the choice of the engine cycle than the basic airplane mission performance requirements. It was deemed desirable, therefore, to define a reference study engine which would develop the highest possible specific thrust and still be capable of meeting the minimum acceptable noise requirements (Federal Aviation Regulations part 36). The resulting reference airplane configuration will then form a solid basis for future trade studies on the influence of these special rules.

The type of engine selected for this study is a non-afterburning single spool turbojet. Performance data, for this type of engine, was provided for use in the Reference Configuration mission range and noise studies, by means of a computer program developed by the NASA Langley Research Center (LRC). This program provides engine performance data for a single spool turbojet engine with or without afterburning using a cycle match procedure. It is the same computer program as that used to generate the data of Reference VI-3-2.

SUMMARY

Results of this study indicate that the engine is sized by take-off community noise requirements, and that the use of a variable geometry turbine results in an engine which is 8 percent smaller than one employing a fixed geometry turbine. In addition, the variable geometry turbine engine will provide significant fuel savings relative to the fixed geometry turbine engine at part throttle operation corresponding to subsonic holding conditions.

The initial results of this study indicate the desirability to determine the performance gains, if any, to be realized with a completely variable geometry single spool turbojet engine, that is both the compressor and the turbine employ variable geometry.

Engine Performance Computation Procedures

For completeness of this report a summary of the operation characteristics of the program cited in the introduction, has been extracted from Reference VI-3-2, modified as it pertains to this study and presented below. The parameters discussed are identified with Sketch (a).

The LRC single spool turbojet performance program calculates design-point-cycle performance and then uses the computed value of turbine-entrance corrected flow at design $(W_4 \sqrt{\theta_4}/\delta_4)_d$ to define, by flow matching, all possible operating points of a given design cycle through a desired Mach number, altitude, and power-level range. The program conducts a step-by-step thermodynamic progression from the undisturbed free-stream condition, to the air intake, through the individual engine components, to the exhaust nozzle.

The exhaust nozzle employed in this program is a completely variable convergent-divergent nozzle which fully expands the exhaust gas to ambient pressure at design, at all off design and at all part power operating conditions. With input to the program of the parameters listed in Table VI-3-I, the program will compute the performance parameters presented in Tables VI-3-II, -III, and -IV. The nondissociated thermodynamic properties of gases from Reference VI-3-3 were used in the flow-process calculation. The present study uses the combustion-products tables for a fuel with a hydrogen-carbon ratio of 2 to simulate JP-4 jet-fuel performance.

The nondimensionalized compressor-map characteristics shown in Figure VI-3-1 were used for all engine designs to retain the parametric identity of the study to the maximum degree possible. Each design-point value of compressor ratio CPRD was established on the map, as shown by the target symbol in Figure VI-3-1(a), at a point along the 100-percent corrected-speed curve (N_{corr}), 10 percent of CPRD below the surge value. Off-design compressor-operating points were established by iteration along constant corrected-speed lines until the resulting turbine-entrance corrected flow was matched with the design value; off-design corrected speed was defined by Mach number, altitude, and engine desired-power level.

Definition of operating points by turbine-corrected flow match was required because a map of turbine work and flow characteristics was not included in the program. The quantities that could compromise constant, corrected turbine-entrance flow as the matching parameter are (1) turbine-entrance Mach number less than unity, (2) unknown changes in effective turbine-entrance flow area, and (3) variation in γ_4 and the gas constant R_4 due to changes in turbine-entrance temperature (TET) and gas constituency from the design values. Only condition (3) was considered to have important influences; examination of the effects of γ_4 and R_4 variations from design indicated a maximum variation in corrected flow of less than two percent of design value when TET was varied from high values at design to very low values at off-design partial power. The variation in compressor corrected inlet flow with Mach number and associated altitude resulting from the present flow-match procedure is presented in Figure VI-3-2 for the range of conditions studied.

Control of the operating modes of any engine with a fixed[1] geometry turbine can be accomplished by giving values to two and solving for the third of the following parameters: compressor physical rotational speed, turbine-entrance temperature, and exhaust-nozzle-throat area. For maximum power at all off-design conditions, compressor rotational speed was set at 100 percent of design, turbine-entrance temperature was set at a design value, and the required nozzle-throat and corresponding exit areas were calculated. Partial power was defined by a schedule of compressor rotational speed and ratio of nozzle-throat area to maximum-power throat area (see Figure VI-3-3). Engine control specified in this manner required computer program loops to satisfy flow matching at both the turbine-entrance and nozzle throat by varying turbine-entrance temperature.

NOTE:

1 A fixed geometry turbine is one in which the flow area can not be changed from its design value.

Alteration to the computer program logic to provide for the concept of a variable[2] geometry turbine was made. Upon solution of the compressor-turbine operating point required by flow matching at maximum power, the turbine-entrance area was reduced to maintain constant corrected turbine-entrance flow and the exhaust-nozzle-throat area required to pass the internal flow was calculated. The program recognizes a maximum variation in turbine area. To solve for this limit, iteration of turbine-entrance temperature and area is conducted until the limiting input area value is obtained, or a limiting minimum nozzle pressure ratio is reached.

The present study was conducted with the air-inlet total-pressure recovery schedule with Mach number shown in Figure VI-3-4. This schedule is considered typical of fully variable internal-external compression inlets. The exhaust nozzle was assumed to fully expand the internal flow to ambient pressure with a gross-thrust coefficient of 0.985. The schedule for controlling partial-power engine operation (Figure VI-3-3) is similar to that for a recent turbojet (GE4) designed for supersonic speeds.

Engine Parameters

The scope of this study was such that it did not permit the optimization of each airplane/engine combination. Therefore, to maintain simplicity, each of

NOTE:

2 Variable geometry turbine as used in this study is defined as a turbine in which the flow area can be varied from its design value by means of opening or closing the stators (turbine nozzles).

the baseline engines was designed to have a compressor pressure ratio (CPRD) of 15:1 and a maximum turbine-entrance temperature (TETD) of 3060°R at standard day atmospheric conditions. Thrust variation between engines of a type (fixed or variable geometry turbine) is achieved by varying sea level static corrected airflow (W_{corr}). All engine performance data (of a type) are therefore scalable directly with thrust with the exception of exhaust gas velocity (V_8) which remains constant.

The scale factors for engine performance are given below:

$$F_{g_r} = F_{g_b}\ (F_{N_r}/F_{N_b})\quad \text{Take-off}$$

$$F_{N_r} = F_{N_b}\ (F_{N_r}/F_{N_b})\quad \text{Take-off}$$

$$RD_r = RD_b\ (F_{N_r}/F_{N_b})\quad \text{Take-off}$$

$$W_{f_r} = W_{f_b}\ (F_{N_r}/F_{N_b})\quad \text{Take-off}$$

$$V_{8_r} = V_{8_b}$$

$$A_{8_r} = A_{8_b}\ (F_{N_r}/F_{N_b})\quad \text{Take-off}$$

$$W_{8_r} = W_{8_b}\ (F_{N_r}/F_{N_b})\quad \text{Take-off}$$

The scale factors for thrust (F_g), ram drag (RD) and fuel flow (W_f) were incorporated directly within the missions analysis computer program, explained elsewhere in this report, to generate the engine performance data for the particular airplane and mission desired.

Take-off, maximum climb and maximum cruise performance levels were established at the maximum design power level. Idle performance was defined as that performance which resulted with the engine operating at its minimum operational thrust level, as determined by the computer program.

Selection of Engine Size

The engine size selected for the Reference Configuration was the smallest engine that would provide the following:

1. Sufficient thrust at start cruise (maximum weight) for the airplane to cruise at the desired cruise altitude and Mach number. (Standard +8°C Day)
2. Sufficient thrust to achieve a take-off balanced field length of 10,500 feet or less.
3. After take-off, following the clearance of the 35 foot obstacle, the engine must provide sufficient thrust to continue to climb at a 3 percent gradient (4 engine airplane) with the critical engine inoperative, and the remaining three engines operating at take-off power.
4. The engine must be capable of providing sufficient thrust at take-off power (derated by limiting exhaust jet velocity to 2400 feet per second) to effect a normal four engine take-off in 10,500 feet on a simple hot day of standard +10°C.

The result of the engine sizing procedure established that the noise criteria, item 4 above, was the most critical, that is, it required the largest engine.

Early studies of jet engines have established the prime noise source of a turbojet engine as its exhaust jet velocity. This means that the lower the exhaust velocity the lower the engine noise. The exhaust velocity can be reduced by means of a jet noise suppressor or part power operation (reduced throttle). Both of these techniques result in a reduction in thrust and thus require larger engines.

A plot of predicted jet suppressor effectiveness as a function of exhaust jet velocity has been extracted from Reference VI-3-4 and reproduced as Figure VI-3-5. Although this plot shows that the expected reductions in jet noise at the nominal take-off jet velocity of 3000 ft/sec is significant, there is no prediction as to the associated thrust loss. It is conceivable that the thrust loss could be as high as 10 or 12 percent.

One technique for reducing jet velocity without reducing the engine thrust or increasing engine size is to vary the airflow through the engine. This can be accomplished by means of variable geometry components such as the compressor and/or turbine. The LRC single spool turbojet computer program, as previously stated, has the capability of producing performance for an engine with a variable geometry turbine.

The effect of a variable geometry turbine on engine performance is shown on Figure VI-3-6, in comparison with a fixed geometry turbine engine. These engines were sized to the same maximum take-off thrust. The variable geometry turbine permits the engine to develop 7.8% more power at the desired exhaust jet velocity, or a 7.8% smaller engine to meet the same take-off noise requirements.

An additional advantage of the variable geometry turbine engine is to provide a reduction in fuel consumption compared to the fixed geometry turbine when operating at reduced power. This comparison is shown for typical holding conditions on Figure VI-3-7.

It has been established that turbojet engines provide the highest supersonic cruise efficiency and since the single spool turbojet engine with a variable geometry turbine also offers improved subsonic performance, both in lower fuel consumption and reduced noise, it was selected as a desirable type of engine to meet the requirements of the Reference Configuration. The Reference Configuration would have the following design characteristics:

overall compressor pressure ratio of 15:1

turbine-entrance temperature of 3060°R

uninstalled corrected compressor airflow of 800 lbs/sec

An engine with these design characteristics would provide an uninstalled net engine thrust of 82,800 lbs, at sea level static standard day conditions with no service airbleed or power extraction.

The weights of this reference engine were ratioed to those of the 633 lbs/sec engine, used on the Boeing 336C supersonic study airplane.

Engine Performance

Standard day engine performance data, without service airbleed or power extraction, for the selected engine was generated for use in mission studies. Performance data for a simple hot day of standard +8° Celsius was also generated for hot day mission studies and are presented on Tables VI-3-II and VI-3-III, respectively.

Similar data were generated for simple hot day atmospheric conditions of standard +10°Celsius for use in noise and engine sizing studies. These data are presented on Table VI-3-IV. As shown on Tables VI-3-II, -III, and -IV the parameters of gross engine thrust, ram drag and fuel flow are used in mission and take-off studies. The parameters of net engine thrust (the difference between gross engine thrust and ram drag), exhaust gas flow, exhaust gas (jet) velocity and nozzle area are used for noise studies. The remaining parameters are used for identification.

Engine performance data was not penalized for service airbleed or power extraction since this effect amounted to approximately a 1% increase in cruise fuel flow or a 1% decrease in range at maximum cruise power. This increment was considered to be well within the range of accuracy for initial studies. The effects of propulsion drag (due to inlet spillage, nozzle boattail and air conditioning discharge) are normally included as an aerodynamic drag increment in the performance section (VI-6). Should these effects, however, be included with those of service airbleed and power extraction and charged to the engine performance, the result is to increase the specific fuel consumption at Mach 2.7 cruise, from 1.31 to 1.39 at constant thrust.

Maximum take-off performance for the Reference Configuration is shown on Figure VI-3-8 for atmospheric condition of standard and standard +10°C days. This data is valid for both fixed and variable geometry turbine engines. Also, shown on Figure VI-3-8 is derated (with an exhaust jet velocity of 2400 ft/sec) take-off performance for both fixed and variable geometry turbine engines at atmospheric conditions of standard and standard +10°C days. These data are presented for altitudes of sea level, 2000 and 4000 feet.

Idle performance, for both fixed and variable geometry turbine engines at atmospheric conditions of standard and standard +10°C days, is shown on Figure VI-3-9.

LIST OF SYMBOLS

A	area, ft^2
Fg	gross thrust, lbs
F_N	net thrust, lbs = Fg - RD
JP-4	jet fuel
M	Mach number
N	rotational speed, percent of design value
N_{corr}	corrected rotational speed, $N/\sqrt{\theta}$, percent
p	pressure, lb/ft^2
R	gas constant
RD	ram drag, lbs
T	temperature, °Rankine
V	velocity, ft/sec
W	weight flow, lb/sec
W_{corr}	corrected weight flow, $W\sqrt{\theta}/\delta$, lb/sec
W_f	fuel flow, lbs/hr
γ	ratio of specific heats
δ	ratio of total pressure to standard sea-level pressure
η	efficiency
θ	ratio of total temperature to standard sea-level temperature

LIST OF SYMBOLS (Continued)

Subscripts:

b	baseline
d	design
P	airplane
r	required
sls	sea-level static conditions
t	stagnation or total conditions
0	free stream station
1	compressor inlet
2	compressor outlet
4	combustor outlet (turbine nozzle entrance)
5	turbine outlet
7	exhaust-nozzle throat
8	exhaust-nozzle exit

Stations 0 through 8: See Sketch (a)

Abbreviations:

Alt	altitude, feet
CPR	operating compressor pressure ratio, $P_{t,2}/P_{t,1}$
PRD	design compressor pressure ratio, $(P_{t,2}/P_{t,1})_d$
TSFC	thrust specific fuel consumption, lb/hr/lb
TET	turbine entrance stagnation temperature, °Rankine
TETD	design turbine-entrance stagnation temperature, °Rankine

REFERENCES

Reference No.	Title
VI-3-1	The Boeing Company: Mach 2.7 Fixed Wing SST Model 969-336C (SCAT-15F), Document No. D6A-11666-1, dated November 1969.
VI-3-2	Keith, Arvid L., Jr.; Effects of Variable Turbine Area on Subsonic Cruise Performance of Turbojet Designed for Supersonic Application. NASA TN D-5962, October 1970.
VI-3-3	Hall, Eldon W.; and Weber, Richard J.: Tables and Charts for Thermodynamic Calculations Involving Air and Fuels Containing Boron, Carbon, Hydrogen, and Oxygen. NACA RM #56B27, 1956.
VI-3-4	Foss, Richard L., and Bragdon, Ellwood L.: Propulsion Technology Advances Needed for a Quiet Supersonic Transport. Society of Automotive Engineers Paper No. 730898, October 1973.

LIST OF FIGURES

LIST OF TABLES

TABLE VI-3-I - PROGRAM INPUT

Flight condition (standard day):	
Altitude	0 to stratosphere
Mach number	0. to 3.6
Power setting	Maximum and partial
Compressor:	
Design pressure ratio	4 to 30
Design efficiency	0.875
Maximum rotational speed, percent	100
Combustor:	
Maximum design turbine-entrance temperatures, °R	2260 to 3460
Combustion efficiency	0.98
Design combustor total-pressure ratio	0.95
Fuel sensible energy, Btu/LB (JP-4 fuel)	1600
Fuel total enthalpy, Btu/LB (JP-4 fuel)	20,000
Initial liquid-fuel temperature, °R	350
Turbine:	
Polytropic efficiency	0.90
Cooling air, percent	0
Nozzle:	
Tailpipe total-pressure ratio	0.95
Gross thrust coefficient	0.985
Static-pressure ratio	1.0

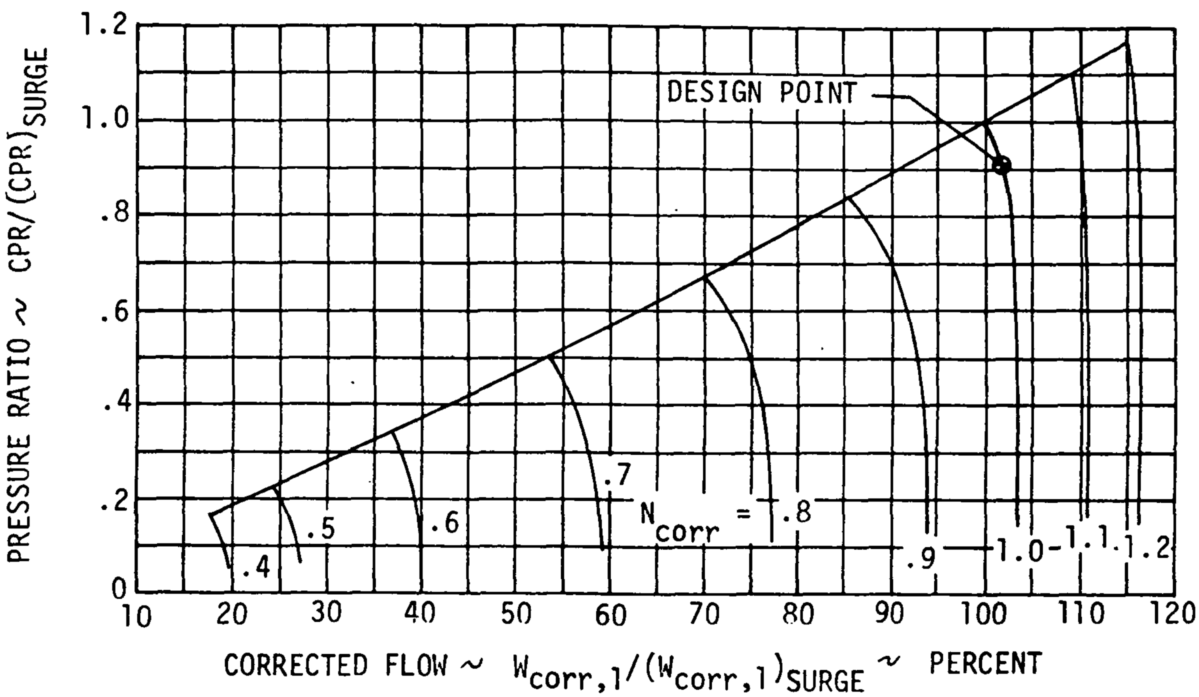

(a) Pressure Ratio as a Function of Corrected Flow

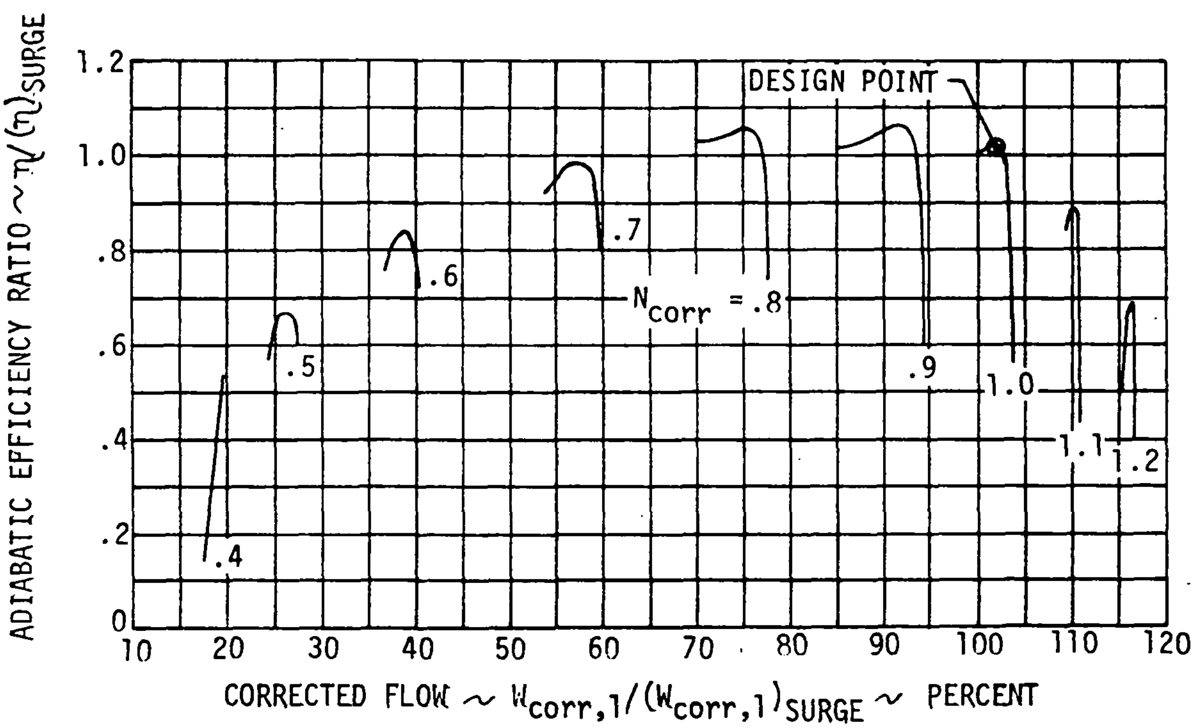

(b) Efficiency as a Function of Corrected Flow

FIGURE VI-3-1 - Nondimensional Compressor Map

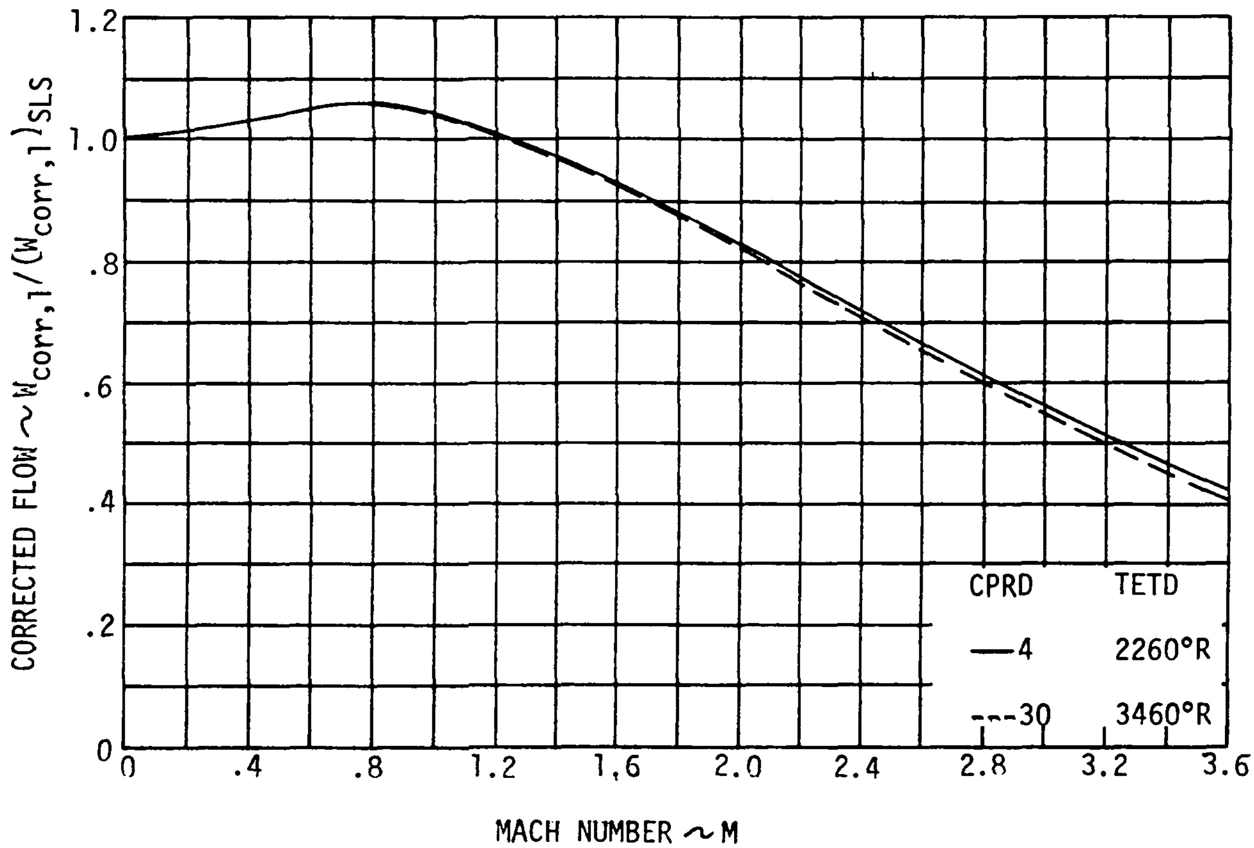

FIGURE VI-3-2 = Variation of Compressor Inlet Flow with Mach Number for Range of Design Engines

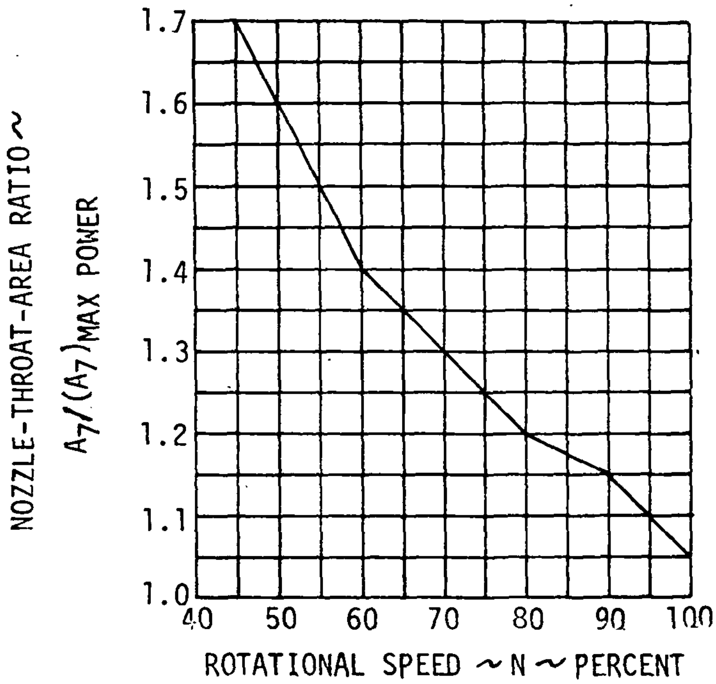

FIGURE VI-3-3 - Schedule of Ratio of Exhaust Nozzle - Throat Area Used for Partial Power Control

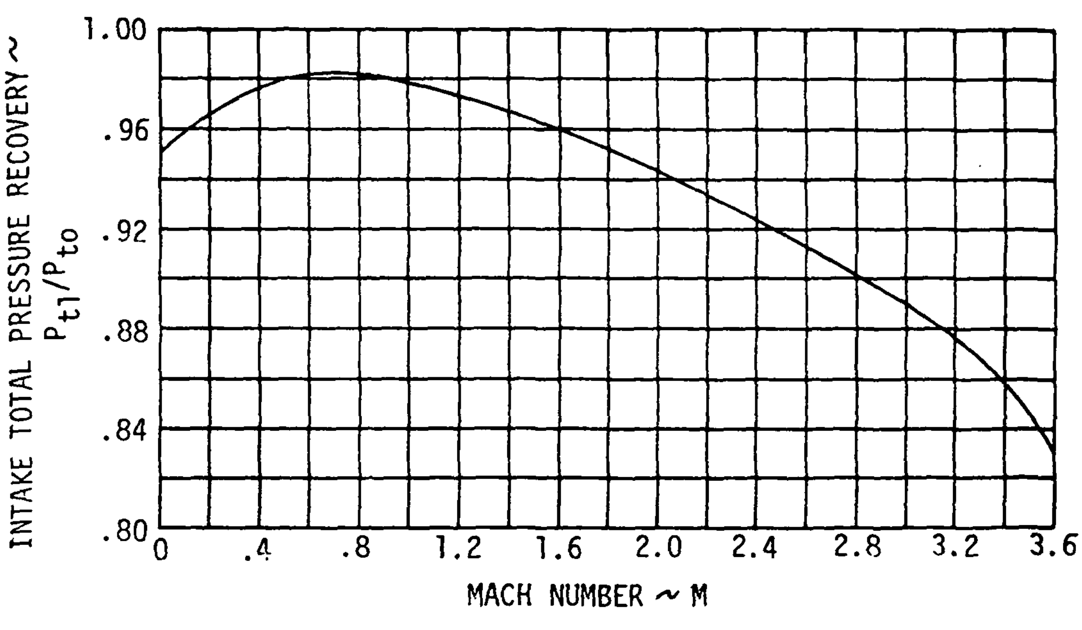

FIGURE VI-3-4 - Schedule of Air-Inlet Total-Pressure Recovery Used for All Engine Designs

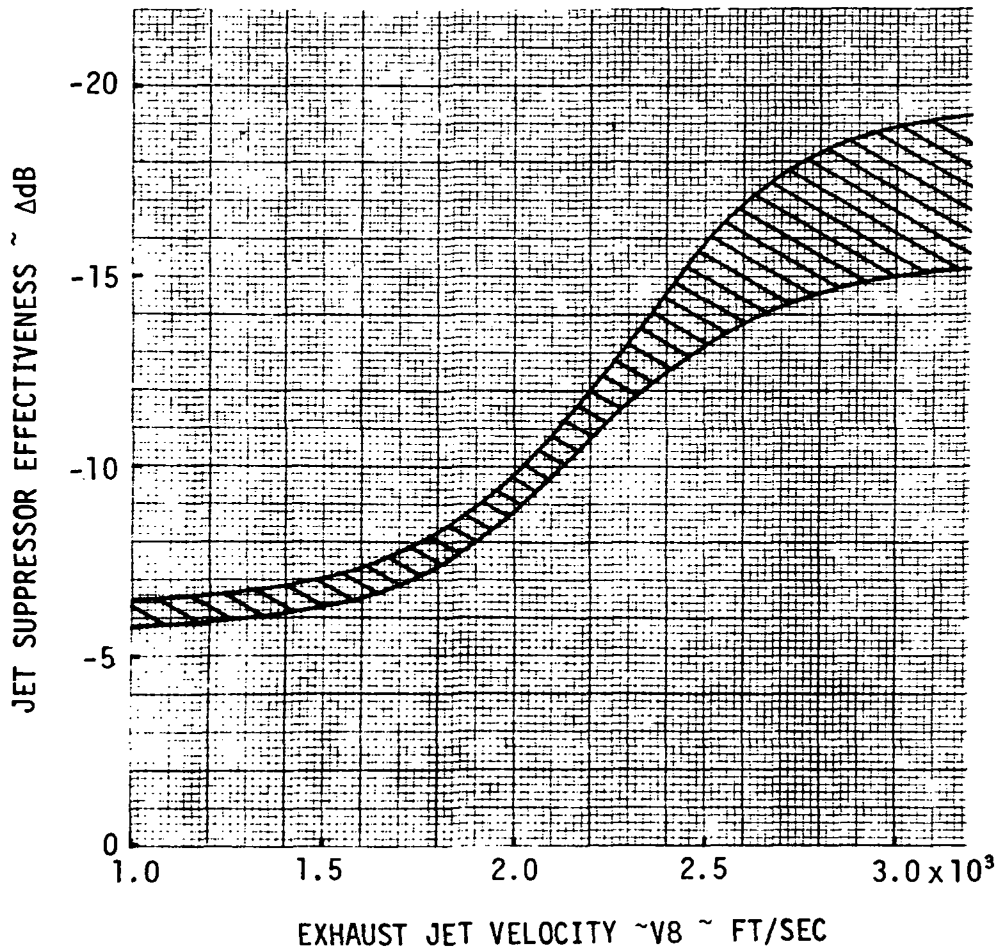

FIGURE VI-3-5 - Predicted Jet Noise Suppressor Effectiveness

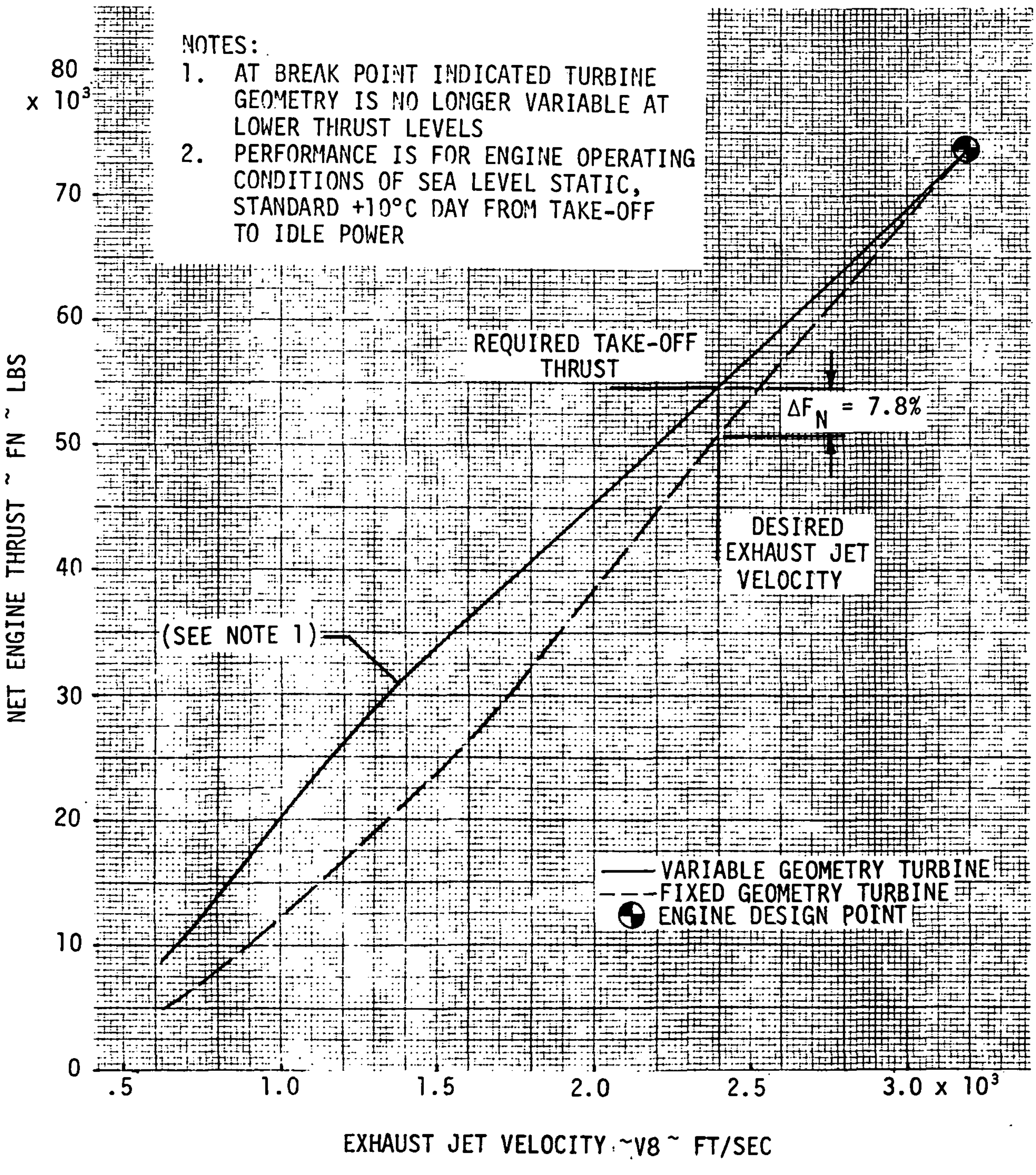

FIGURE VI-3-6 - Thrust Variation with Exhaust Jet Velocity for Fixed and Variable Geometry Turbine Engines

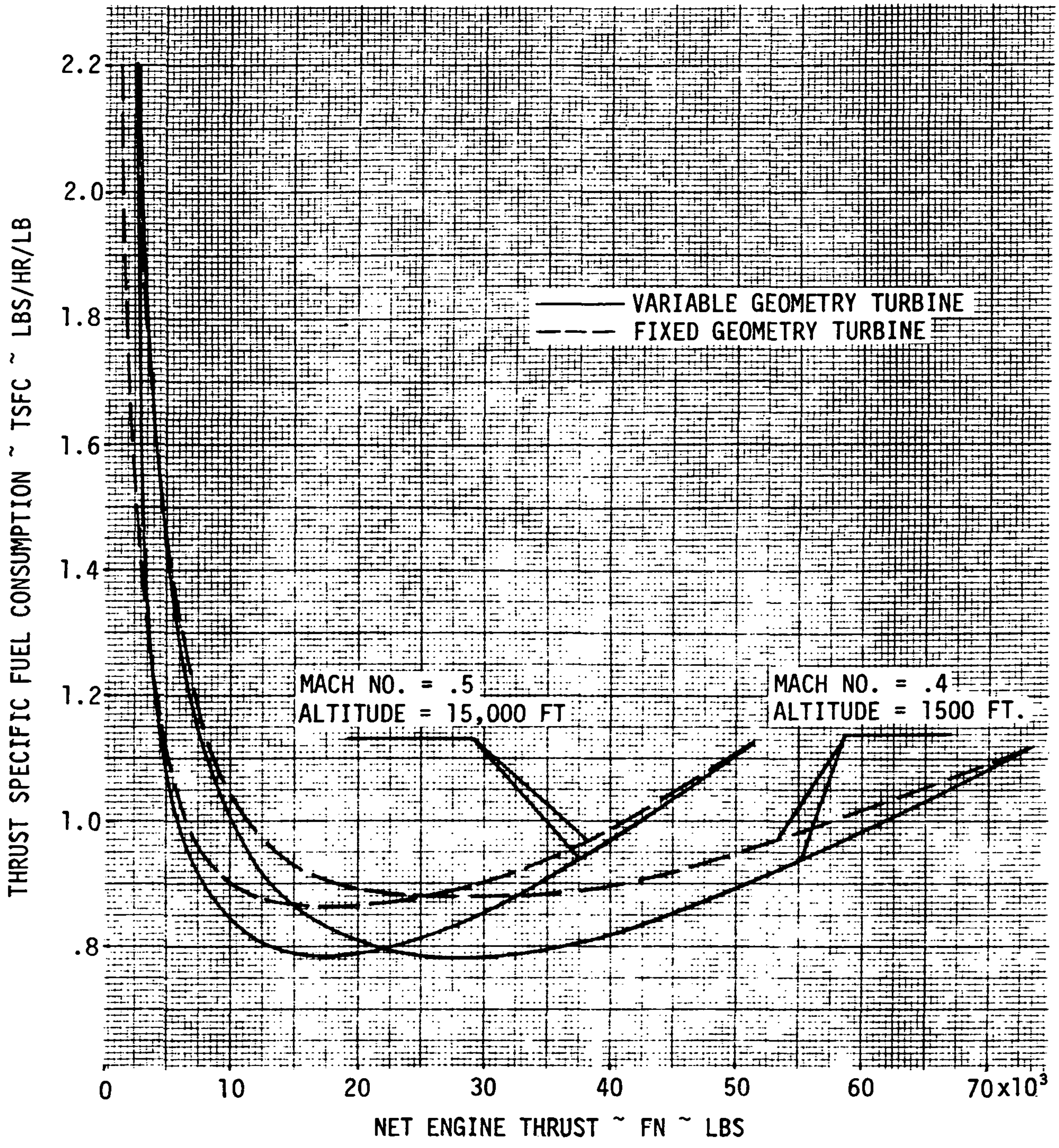

FIGURE VI-3-7 - Comparison of Thrust Specific Fuel Consumption at Typical Holding Conditions - Standard Day

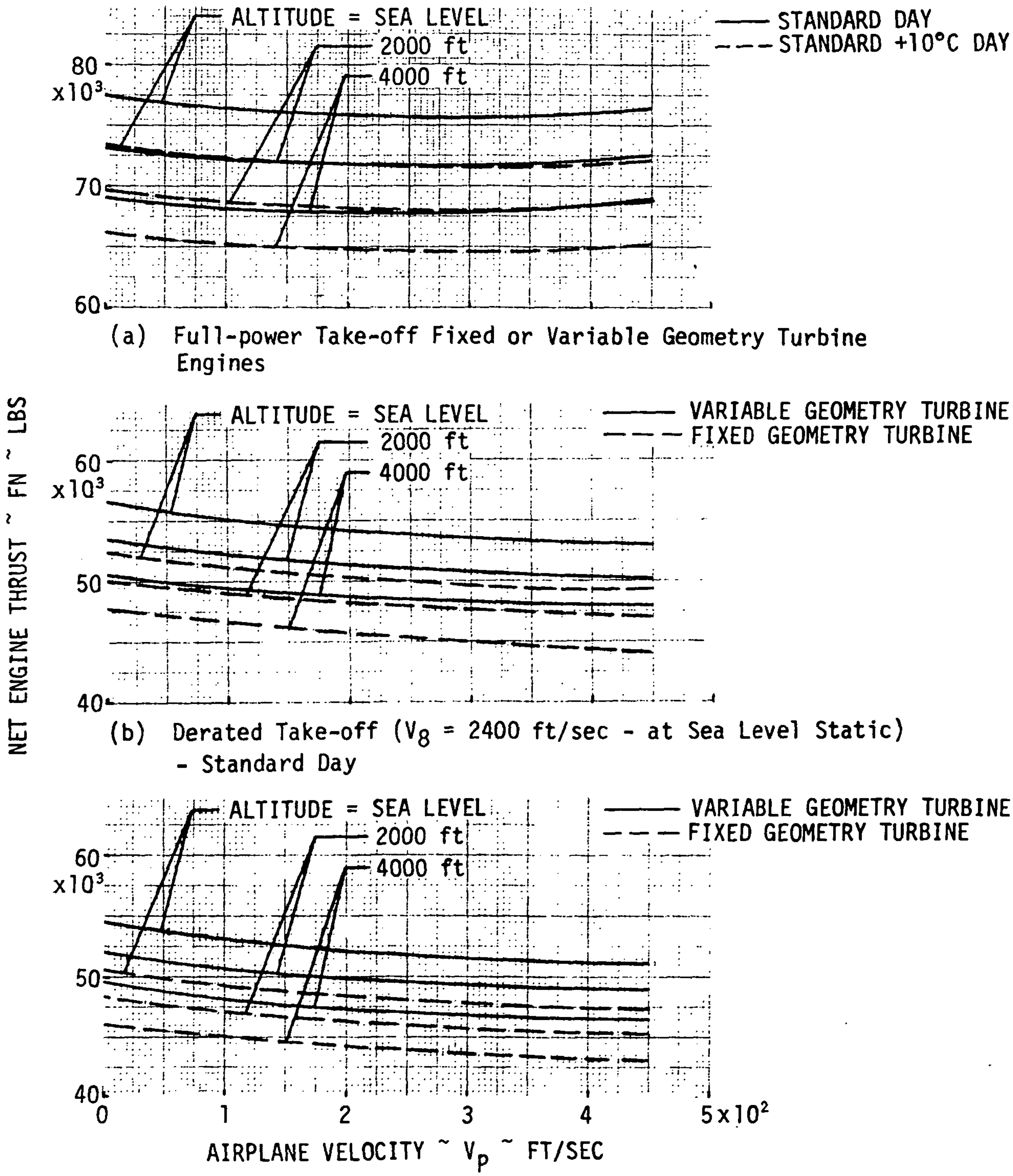

(a) Full-power Take-off Fixed or Variable Geometry Turbine Engines

(b) Derated Take-off (V_8 = 2400 ft/sec - at Sea Level Static) - Standard Day

(c) Derated Take-off (V_8 = 2400 ft/sec - at Sea Level Static) - Standard +10°C Day

FIGURE VI-3-8 - Take-off Thrust Comparison Fixed and Variable Geometry Turbine Engines

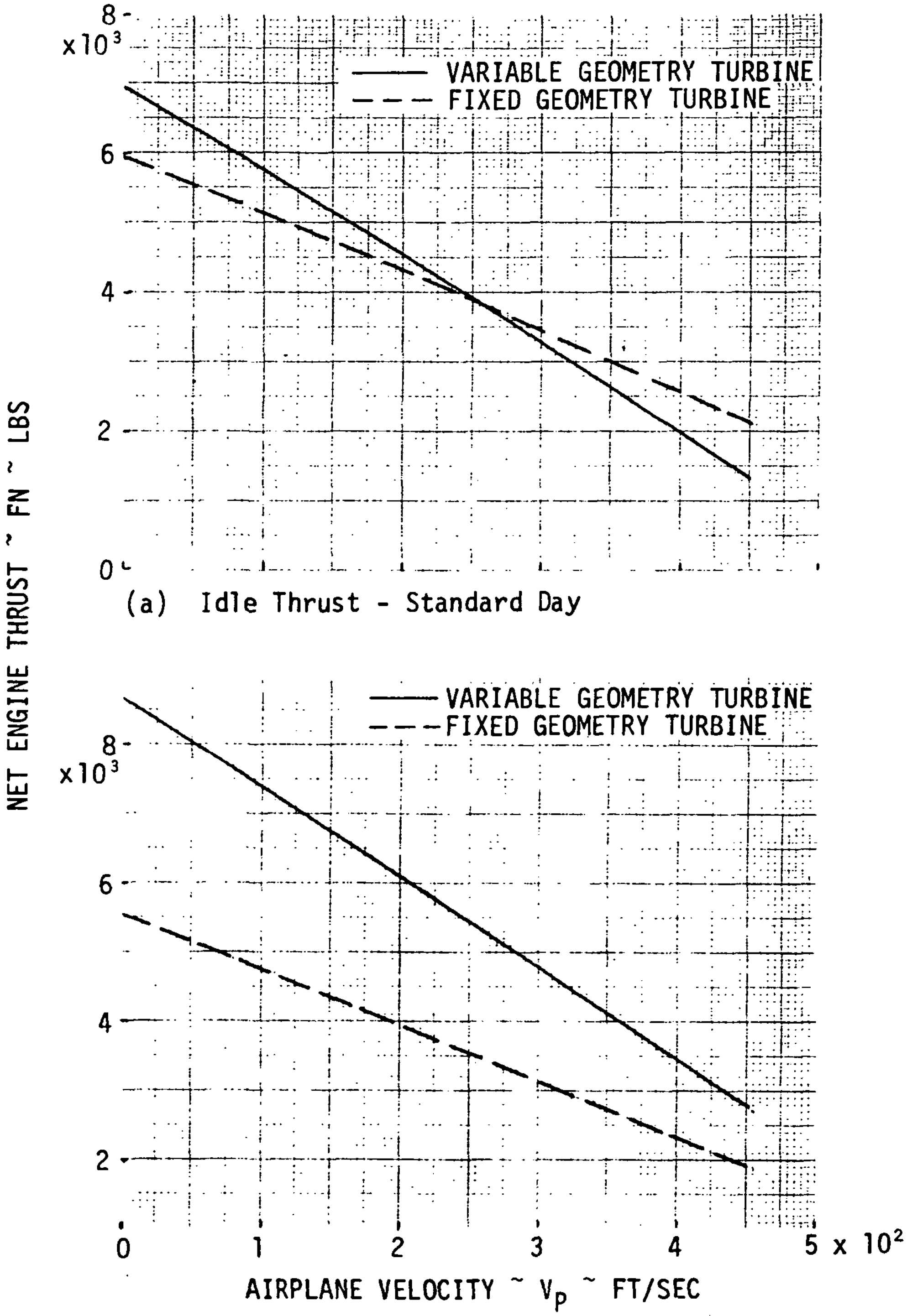

(a) Idle Thrust - Standard Day

(b) Idle Thrust - Standard +10°C Day

FIGURE VI-3-9 - Idle Thrust Comparison Fixed and Variable Geometry Turbine Engines

TABLE VI-3-II

JP4 FUELED ENGINE PERFORMANCE
VARIABLE GEOMETRY TURBINE

MAXIMUM CLIMB AND MAXIMUM CRUISE PERFORMANCE
STANDARD DAY

MACH NO.	ALTITUDE FEET	TURB. IN TEMP. (R)	GROSS THRUST (LBS)	RAM DRAG (LBS)	TOTAL FUEL FLOW (LBS/HR)	JET VELOCITY (FT/SEC)	NOZZLE EXIT AREA (SQ FT)	EXHAUST GAS FLOW (LBS/SEC)
0.00	0.0	3060	77614.6	0.0	78163.3	3243.2	10.123	781.7
0.00	5000.0	3060	67204.5	0.0	67636.7	3274.4	10.252	670.4
.40	0.0	3060	88112.1	11704.4	85759.1	3319.3	10.700	867.1
.40	5000.0	3060	76842.5	9901.7	74738.2	3361.4	10.841	746.7
.40	15000.0	3060	56841.8	6917.4	55268.7	3428.3	11.165	541.6
.60	0.0	3060	98954.1	19368.6	93284.8	3380.3	11.331	956.2
.60	5000.0	3060	86294.7	16375.1	81308.2	3425.1	11.453	823.0
.60	15000.0	3060	64813.5	11578.4	61018.3	3504.2	11.868	604.1
.60	25000.0	3060	46489.3	7835.5	43844.4	3567.2	12.255	425.7
.80	0.0	3060	114137.6	29154.9	103329.3	3455.4	12.155	1078.9
.80	5000.0	3060	99502.5	24680.1	90202.4	3495.6	12.326	929.8
.80	15000.0	3060	75417.6	17549.1	68368.4	3588.5	12.770	686.5
.80	25000.0	3060	54415.5	11932.7	49480.0	3656.9	13.213	486.0
.80	36152.0	3060	36227.4	7437.4	33080.4	3719.2	13.845	318.2
1.00	15000.0	3060	89098.5	25396.7	77378.1	3664.1	13.975	794.3
1.00	25000.0	3060	65512.1	17505.1	57101.3	3753.2	14.526	570.1
1.00	36152.0	3060	43452.5	10870.0	38168.0	3816.8	15.170	371.9
1.00	45000.0	3060	28447.3	7116.3	24987.7	3816.8	15.170	243.5
1.20	25000.0	3060	79075.6	24860.2	65883.9	3830.6	16.164	674.3
1.20	36152.0	3060	53648.1	15696.0	45083.4	3918.2	16.968	447.2
1.20	45000.0	3060	35122.1	10275.8	29515.0	3918.2	16.968	292.8
1.40	36152.0	3060	65968.3	22066.1	52984.5	4001.1	19.113	538.6
1.40	45000.0	3060	43187.8	14446.2	34687.7	4001.1	19.113	352.6

TABLE VI-3-II (CONTINUED)

MAXIMUM CLIMB AND MAXIMUM CRUISE PERFORMANCE (CONTINUED)
STANDARD DAY

MACH NO.	ALTITUDE FEET	TURB. IN TEMP. (R)	GROSS THRUST (LBS)	RAM DRAG (LBS)	TOTAL FUEL FLOW (LBS/HR)	JET VELOCITY (FT/SEC)	NOZZLE EXIT AREA (SQ FT)	EXHAUST GAS FLOW (LBS/SEC)
1.80	36152.0	3060	100785.0	41963.2	73289.6	4140.1	24.762	795.2
1.80	45000.0	3060	65981.5	27472.3	47980.9	4140.1	24.762	520.6
1.80	55000.0	3060	40896.2	17027.6	29739.2	4140.1	24.762	322.7
2.00	45000.0	3060	80894.3	36913.5	55793.9	4201.4	28.115	628.9
2.00	55000.0	3060	50139.3	22879.5	34581.8	4201.4	28.115	389.8
2.00	65000.0	3060	31091.2	14187.5	21444.0	4201.4	28.115	241.7
2.40	55000.0	3060	74475.8	39794.3	45762.6	4314.9	36.035	563.8
2.40	65000.0	3060	46182.1	24676.3	28377.2	4314.9	36.035	349.6
2.40	75000.0	3060	28124.1	15164.5	17195.9	4304.0	35.642	213.4
2.70	55000.0	3060	98190.7	58135.4	54757.2	4388.7	42.955	730.8
2.70	65000.0	3060	60887.6	36049.5	33954.7	4388.7	42.955	453.2
2.70	75000.0	3060	37010.9	22100.5	20515.5	4380.0	42.385	276.0
3.00	55000.0	3060	127355.2	82450.9	63864.5	4467.5	50.412	931.2
3.00	65000.0	3060	78972.5	51127.5	39602.1	4467.5	50.412	577.4
3.00	75000.0	3060	48009.8	31349.0	23881.7	4458.6	49.777	351.7

TABLE VI-3-II (CONTINUED)

MAXIMUM CRUISE AND PART POWER PERFORMANCE
STANDARD DAY

MACH NO.	ALTITUDE FEET	TURB. IN TEMP. (R)	GROSS THRUST (LBS)	RAM DRAG (LBS)	TOTAL FUEL FLOW (LBS/HR)	JET VELOCITY (FT/SEC)	NOZZLE EXIT AREA (SQ FT)	EXHAUST GAS FLOW (LBS/SEC)
.40	5000.0	3060	76842.5	9901.7	74738.2	3361.4	10.841	746.7
.40	5000.0	2785	70975.1	9901.7	64156.5	3117.0	10.658	743.8
.40	5000.0	2509	64514.8	9901.7	53361.6	2844.7	10.489	740.8
.40	5000.0	2234	57070.7	9901.7	42391.2	2526.9	10.436	737.7
.40	5000.0	1958	47312.3	9901.7	30673.5	2104.1	10.814	734.5
.40	5000.0	1700	35662.0	9901.7	19898.7	1592.5	12.223	731.5
.40	5000.0	1689	35134.3	9904.5	19494.6	1568.7	12.335	731.6
.40	5000.0	1611	30956.0	9612.8	16614.0	1425.4	12.685	709.4
.40	5000.0	1536	26785.8	9316.9	13991.0	1273.6	13.260	687.0
.40	5000.0	1436	21268.9	8713.8	10836.5	1082.3	13.939	641.9
.40	5000.0	1366	16997.8	7947.9	8771.4	948.8	14.173	585.1
.40	5000.0	1298	13219.4	7170.4	7051.9	818.3	14.525	527.7
.40	5000.0	1246	9884.2	6331.1	5806.7	693.1	15.070	465.8
.40	5000.0	1194	7134.8	5484.6	4772.5	577.7	15.635	403.4
.60	15000.0	3060	64813.5	11578.4	61018.3	3504.2	11.868	604.1
.60	15000.0	2785	60064.7	11578.4	52467.9	3260.3	11.612	601.8
.60	15000.0	2509	54777.0	11578.4	43745.1	2985.3	11.385	599.3
.60	15000.0	2234	48743.1	11578.4	34880.3	2667.4	11.252	596.9
.60	15000.0	1958	40939.8	11578.4	25399.3	2250.3	11.496	594.3
.60	15000.0	1700	31842.6	11578.4	16679.0	1757.4	12.577	591.8
.60	15000.0	1690	31468.2	11583.9	16369.0	1736.2	12.659	592.0
.60	15000.0	1597	28278.9	11345.2	13847.4	1594.7	12.850	579.2
.60	15000.0	1516	24761.1	10996.8	11547.0	1441.9	13.221	560.9
.60	15000.0	1400	19588.2	10295.4	8540.6	1219.9	13.816	524.5
.60	15000.0	1316	15708.4	9462.4	6613.5	1065.1	14.037	481.7
.60	15000.0	1237	12116.1	8556.5	5027.6	909.1	14.426	435.3
.60	15000.0	1170	9006.8	7595.2	3861.4	761.7	14.998	386.3

TABLE VI-3-II (CONTINUED)

MAXIMUM CRUISE AND PART POWER PERFORMANCE (CONTINUED)

STANDARD DAY

MACH NO.	ALTITUDE FEET	TURB. IN TEMP. (R)	GROSS THRUST (LBS)	RAM DRAG (LBS)	TOTAL FUEL FLOW (LBS/HR)	JET VELOCITY (FT/SEC)	NOZZLE EXIT AREA (SQ FT)	EXHAUST GAS FLOW (LBS/SEC)
.80	15000.0	3060	75417.6	17549.1	68368.4	3588.5	12.770	686.5
.80	15000.0	2785	69950.4	17549.1	58633.3	3341.5	12.473	683.8
.80	15000.0	2509	63876.1	17549.1	48702.2	3063.7	12.201	681.0
.80	15000.0	2234	56960.4	17549.1	38609.7	2743.3	12.017	678.2
.80	15000.0	1958	48083.4	17549.1	27837.3	2326.0	12.203	675.2
.80	15000.0	1700	37837.1	17549.1	17933.3	1837.8	13.184	672.5
.80	15000.0	1690	37418.3	17554.1	17590.7	1817.2	13.261	672.6
.80	15000.0	1611	33548.8	17024.7	14922.2	1681.5	13.386	651.7
.80	15000.0	1530	29648.0	16506.1	12357.3	1534.1	13.653	631.3
.80	15000.0	1407	23647.0	15431.1	8849.3	1310.5	14.053	589.4
.80	15000.0	1307	18350.6	14084.9	6322.5	1115.2	14.430	537.5
.80	15000.0	1223	14282.1	12706.1	4588.8	962.7	14.572	484.6
.80	15000.0	1151	10437.6	11213.4	3285.8	797.6	15.189	427.4
1.00	36152.0	3060	43452.5	10870.0	38168.0	3816.8	15.170	371.9
1.00	36152.0	2785	40457.9	10870.0	32917.2	3567.7	14.741	370.4
1.00	36152.0	2509	37141.2	10870.0	27560.3	3288.5	14.323	368.9
1.00	36152.0	2234	33399.7	10870.0	22116.2	2969.4	13.970	367.4
1.00	36152.0	1958	28647.9	10870.0	16279.8	2558.2	13.941	365.8
1.00	36152.0	1700	23308.5	10870.0	10909.1	2089.9	14.551	364.3
1.00	36152.0	1689	23091.4	10873.8	10714.2	2070.0	14.604	364.4
1.00	36152.0	1589	21189.4	10682.7	9093.1	1935.7	14.513	357.6
1.00	36152.0	1489	19191.2	10488.0	7521.8	1787.7	14.565	350.7
1.00	36152.0	1370	15914.2	9819.0	5566.3	1585.4	14.471	327.9
1.00	36152.0	1270	13231.4	9135.3	4136.1	1418.1	14.300	304.8
1.00	36152.0	1170	10450.3	8293.7	2864.8	1234.8	14.197	276.4
1.00	36152.0	1062	7684.1	7434.9	1728.1	1013.8	14.644	247.6
1.00	36152.0	977	5445.3	6503.0	1009.1	821.9	15.194	216.4

TABLE VI-3-II (CONTINUED)

MAXIMUM CRUISE AND PART POWER PERFORMANCE (CONTINUED)
STANDARD DAY

MACH NO.	ALTITUDE FEET	TURB. IN TEMP. (R)	GROSS THRUST (LBS)	RAM DRAG (LBS)	TOTAL FUEL FLOW (LBS/HR)	JET VELOCITY (FT/SEC)	NOZZLE EXIT AREA (SQ FT)	EXHAUST GAS FLOW (LBS/SEC)
2.70	65000.0	3060	60887.6	36049.5	33954.7	4388.7	42.955	453.2
2.70	65000.0	2785	56568.8	36049.5	27305.4	4094.1	41.336	451.3
2.70	65000.0	2509	51803.1	36049.5	20525.7	3764.9	39.711	449.4
2.70	65000.0	2234	46435.9	36049.5	13637.4	3389.2	38.273	447.5
2.70	65000.0	1958	39977.7	36049.5	6536.2	2930.8	37.782	445.6

TABLE VI-3-III

JP4 FUELED ENGINE PERFORMANCE

VARIABLE GEOMETRY TURBINE

MAXIMUM CLIMB AND MAXIMUM CRUISE PERFORMANCE

STANDARD + 8 C DAY

MACH NO.	ALTITUDE FEET	TURB. IN TEMP. (R)	GROSS THRUST (LBS)	RAM DRAG (LBS)	TOTAL FUEL FLOW (LBS/HR)	JET VELOCITY (FT/SEC)	NOZZLE EXIT AREA (SQ FT)	EXHAUST GAS FLOW (LBS/SEC)
0.00	0.0	3060	74339.5	0.0	75096.9	3202.8	10.024	758.2
0.00	5000.0	3060	65088.0	0.0	65538.0	3249.7	10.145	654.2
.40	0.0	3060	84711.9	11547.6	82598.4	3280.1	10.620	843.6
.40	1500.0	3060	81385.4	10990.0	79317.7	3294.2	10.653	807.0
.40	5000.0	3060	74002.6	9771.0	72004.5	3328.2	10.724	726.3
.40	15000.0	3060	55137.7	6865.0	53566.8	3403.2	11.058	529.2
.60	0.0	3060	94770.5	19016.4	89443.7	3343.7	11.185	925.8
.60	5000.0	3060	83197.5	16188.2	78409.2	3389.0	11.367	801.9
.60	15000.0	3060	62549.3	11428.2	58854.3	3479.6	11.702	587.2
.60	25000.0	3060	44614.4	7702.3	42081.0	3541.2	12.036	411.5
.80	0.0	3060	109871.7	28753.9	99373.2	3420.2	12.035	1049.3
.80	5000.0	3060	95817.9	24338.0	86768.0	3463.2	12.186	903.7
.80	15000.0	3060	72326.8	17267.6	65525.2	3552.3	12.606	665.1
.80	25000.0	3060	52509.0	11799.8	47682.1	3628.8	13.053	472.6
.80	36152.0	3060	34787.0	7321.9	31735.4	3694.9	13.588	307.5
1.00	15000.0	3060	85268.7	24919.5	73940.5	3629.7	13.756	767.3
1.00	25000.0	3060	62393.4	17128.2	54342.3	3715.1	14.274	548.6
1.00	36152.0	3060	41732.2	10702.6	36580.3	3792.1	14.892	359.5
1.00	45000.0	3060	27321.1	7006.7	23948.2	3792.1	14.892	235.3
1.20	25000.0	3060	75121.3	24244.5	62450.7	3794.7	15.823	646.6
1.20	36152.0	3060	51258.8	15387.7	42974.2	3889.6	16.630	430.5
1.20	45000.0	3060	33557.9	10073.9	28134.1	3889.6	16.630	281.8
1.40	36152.0	3060	62575.9	21521.8	50082.0	3963.9	18.703	515.6
1.40	45000.0	3060	40966.9	14089.8	32787.4	3963.9	18.703	337.6

TABLE VI-3-III (CONTINUED)

MAXIMUM CLIMB AND MAXIMUM CRUISE PERFORMANCE (CONTINUED)
STANDARD + 8 C DAY

MACH NO.	ALTITUDE FEET	TURB. IN TEMP. (R)	GROSS THRUST (LBS)	RAM DRAG (LBS)	TOTAL FUEL FLOW (LBS/HR)	JET VELOCITY (FT/SEC)	NOZZLE EXIT AREA (SQ FT)	EXHAUST GAS FLOW (LBS/SEC)
1.80	36152.0	3060	95221.3	40713.5	68756.9	4107.0	24.092	757.3
1.80	45000.0	3060	62339.1	26654.1	45013.5	4107.0	24.092	495.8
1.80	55000.0	3060	38638.5	16520.6	27899.9	4107.0	24.092	307.3
2.00	45000.0	3060	76356.5	35756.3	52193.9	4170.7	27.304	598.0
2.00	55000.0	3060	47326.8	22162.2	32350.5	4170.7	27.304	370.6
2.00	65000.0	3060	29347.1	13742.7	20060.4	4170.7	27.304	229.8
2.40	55000.0	3060	70131.3	38435.9	42490.3	4285.8	34.908	534.5
2.40	65000.0	3060	43488.2	23833.9	26348.1	4285.8	34.908	331.4
2.40	75000.0	3060	26582.2	14689.7	16022.4	4277.4	34.583	203.0
2.70	55000.0	3060	92353.5	56005.2	50584.9	4365.3	41.472	691.0
2.70	65000.0	3060	57268.0	34728.6	31367.5	4365.3	41.472	428.5
2.70	75000.0	3060	35027.4	21409.2	19057.1	4358.5	41.076	262.5
3.00	55000.0	3060	119533.6	79227.5	58563.1	4445.9	48.589	878.2
3.00	65000.0	3060	74122.3	49128.7	36314.7	4445.9	48.589	544.6
3.00	75000.0	3060	45261.3	30230.7	21987.9	4439.9	48.053	333.0

TABLE VI-3-III (CONTINUED)

MAXIMUM CRUISE AND PART POWER PERFORMANCE

STANDARD + 8 C DAY

MACH NO.	ALTITUDE FEET	TURB. IN TEMP. (R)	GROSS THRUST (LBS)	RAM DRAG (LBS)	TOTAL FUEL FLOW (LBS/HR)	JET VELOCITY (FT/SEC)	NOZZLE EXIT AREA (SQ FT)	EXHAUST GAS FLOW (LBS/SEC)
.40	5000.0	3060	74002.6	9771.0	72004.5	3328.2	10.724	726.3
.40	5000.0	2785	68238.2	9771.0	61698.4	3081.1	10.566	723.4
.40	5000.0	2509	61928.1	9771.0	51184.9	2807.5	10.415	720.5
.40	5000.0	2234	54649.6	9771.0	40500.6	2487.8	10.386	717.5
.40	5000.0	1958	45056.5	9771.0	29103.9	2060.2	10.825	714.4
.40	5000.0	1700	33506.0	9771.0	18627.4	1538.3	12.406	711.5
.40	5000.0	1687	32879.9	9774.7	18157.3	1509.2	12.554	711.6
.40	5000.0	1614	28980.4	9479.2	15537.2	1372.9	12.923	689.5
.40	5000.0	1542	25114.5	9187.3	13145.0	1228.5	13.518	667.8
.40	5000.0	1449	19937.1	8554.5	10298.7	1048.3	14.182	621.2
.40	5000.0	1378	15758.4	7790.7	8301.8	910.3	14.538	565.5
.40	5000.0	1317	12364.4	7006.8	6792.4	794.4	14.756	508.4
.40	5000.0	1264	9160.8	6174.3	5587.8	668.1	15.390	447.9
.40	5000.0	1217	6563.0	5328.8	4661.9	554.7	16.054	386.5
.60	15000.0	3060	62549.3	11428.2	58854.3	3479.6	11.702	587.2
.60	15000.0	2785	57931.5	11428.2	50535.3	3235.5	11.458	584.8
.60	15000.0	2509	52785.9	11428.2	42048.7	2960.0	11.245	582.5
.60	15000.0	2234	46915.9	11428.2	33424.1	2641.7	11.126	580.1
.60	15000.0	1958	39337.4	11428.2	24210.1	2224.8	11.381	577.5
.60	15000.0	1700	30407.8	11428.2	15737.2	1726.8	12.538	575.2
.60	15000.0	1690	30032.8	11431.3	15436.5	1705.3	12.624	575.3
.60	15000.0	1609	26811.9	11109.1	13134.2	1568.1	12.819	558.5
.60	15000.0	1528	23356.1	10769.5	10912.1	1410.3	13.271	540.9
.60	15000.0	1413	18484.7	10081.8	8079.4	1193.7	13.877	505.8
.60	15000.0	1330	14632.8	9212.7	6221.7	1034.8	14.152	461.9
.60	15000.0	1255	11381.9	8317.5	4799.6	892.0	14.430	416.8
.60	15000.0	1191	8380.2	7355.1	3713.7	743.0	15.090	368.4

TABLE VI-3-III (CONTINUED)

MAXIMUM CRUISE AND PART POWER PERFORMANCE (CONTINUED)
STANDARD + 8 C DAY

MACH NO.	ALTITUDE FEET	TURB. IN TEMP. (R)	GROSS THRUST (LBS)	RAM DRAG (LBS)	TOTAL FUEL FLOW (LBS/HR)	JET VELOCITY (FT/SEC)	NOZZLE EXIT AREA (SQ FT)	EXHAUST GAS FLOW (LBS/SEC)
.80	15000.0	3060	72326.8	17267.6	65525.2	3552.3	12.606	665.1
.80	15000.0	2785	66984.8	17267.6	56079.9	3303.0	12.338	662.4
.80	15000.0	2509	61107.4	17267.6	46444.7	3025.4	12.074	659.8
.80	15000.0	2234	54388.7	17267.6	36653.0	2703.9	11.910	657.0
.80	15000.0	1958	45703.4	17267.6	26217.5	2282.2	12.154	654.1
.80	15000.0	1700	35564.7	17267.6	16626.4	1783.2	13.295	651.5
.80	15000.0	1690	35173.8	17272.9	16300.9	1763.3	13.370	651.6
.80	15000.0	1613	31486.4	16754.5	13788.4	1628.7	13.529	631.5
.80	15000.0	1531	27704.5	16248.0	11316.3	1479.1	13.852	611.8
.80	15000.0	1409	21713.2	15111.4	7981.4	1248.0	14.407	568.3
.80	15000.0	1315	16974.6	13774.7	5776.3	1071.2	14.709	517.6
.80	15000.0	1235	13066.0	12379.6	4200.7	918.0	14.974	464.9
.80	15000.0	1162	9461.9	10902.6	2978.7	755.2	15.671	409.2
1.00	36152.0	3060	41732.2	10702.6	36580.3	3792.1	14.892	359.5
1.00	36152.0	2785	38823.3	10702.6	31498.2	3541.7	14.491	358.1
1.00	36152.0	2509	35633.9	10702.6	26313.6	3263.8	14.074	356.6
1.00	36152.0	2234	32013.0	10702.6	21044.5	2944.3	13.739	355.2
1.00	36152.0	1958	27401.2	10702.6	15403.0	2531.3	13.747	353.6
1.00	36152.0	1700	22221.8	10702.6	10212.9	2061.2	14.393	352.1
1.00	36152.0	1689	21993.4	10707.3	10010.4	2039.5	14.455	352.2
1.00	36152.0	1589	20112.5	10520.5	8432.0	1900.3	14.419	345.7
1.00	36152.0	1506	18135.7	10235.2	7066.4	1763.0	14.480	336.0
1.00	36152.0	1385	15016.2	9584.0	5192.7	1560.8	14.400	314.2
1.00	36152.0	1285	12366.9	8861.3	3814.0	1391.6	14.210	290.3
1.00	36152.0	1181	9649.8	8036.1	2586.1	1198.5	14.242	263.0
1.00	36152.0	1076	7032.2	7170.5	1541.8	979.7	14.733	234.5

TABLE VI-3-III (CONTINUED)

MAXIMUM CRUISE AND PART POWER PERFORMANCE (CONTINUED)

STANDARD + 8 C DAY

MACH NO.	ALTITUDE FEET	TURB. IN TEMP. (R)	GROSS THRUST (LBS)	RAM DRAG (LBS)	TOTAL FUEL FLOW (LBS/HR)	JET VELOCITY (FT/SEC)	NOZZLE EXIT AREA (SQ FT)	EXHAUST GAS FLOW (LBS/SEC)
2.70	65000.0	3060	57268.0	34728.6	31367.5	4365.3	41.472	428.5
2.70	65000.0	2785	53184.6	34728.6	25065.2	4070.7	39.916	426.8
2.70	65000.0	2509	48675.4	34728.6	18639.6	3741.2	38.358	425.0
2.70	65000.0	2234	43591.4	34728.6	12111.2	3364.8	36.986	423.2
2.70	65000.0	1958	37457.5	34728.6	5397.0	2904.1	36.621	421.3

TABLE VI-3-IV

JP4 FUELED ENGINE PERFORMANCE
VARIABLE GEOMETRY TURBINE

TAKEOFF AND PART POWER PERFORMANCE
STANDARD + 10 C DAY

MACH NO.	ALTITUDE FEET	TURB. IN TEMP. (R)	GROSS THRUST (LBS)	RAM DRAG (LBS)	TOTAL FUEL FLOW (LBS/HR)	JET VELOCITY (FT/SEC)	NOZZLE EXIT AREA (SQ FT)	EXHAUST GAS FLOW (LBS/SEC)
0.00	0.0	3060	73550.7	0.0	74357.3	3192.6	10.000	752.5
0.00	0.0	2785	67657.1	0.0	63674.5	2948.4	9.880	749.5
0.00	0.0	2509	61138.3	0.0	52776.8	2675.2	9.789	746.5
0.00	0.0	2234	53576.1	0.0	41702.0	2354.0	9.839	743.4
0.00	0.0	1958	43455.8	0.0	29894.3	1917.8	10.435	740.1
0.00	0.0	1700	30880.1	0.0	19041.0	1368.4	12.530	737.1
0.00	0.0	1691	30395.5	0.0	18699.5	1346.7	12.667	737.2
0.00	0.0	1629	26846.1	0.0	16396.5	1227.8	13.098	714.2
0.00	0.0	1570	23397.5	0.0	14320.1	1105.5	13.719	691.3
0.00	0.0	1492	18765.2	0.0	11747.8	955.4	14.317	641.6
0.00	0.0	1429	14843.6	0.0	9803.4	830.9	14.739	583.5
0.00	0.0	1377	11682.1	0.0	8333.3	728.4	14.993	523.8
0.00	0.0	1334	8596.4	0.0	7132.1	616.3	15.654	460.9
.10	0.0	3060	74893.2	2620.6	75379.3	3204.5	10.073	763.4
.10	0.0	2785	68906.7	2620.6	64540.8	2960.1	9.949	760.4
.10	0.0	2509	62286.8	2620.6	53484.3	2686.5	9.853	757.3
.10	0.0	2234	54613.8	2620.6	42248.2	2365.3	9.897	754.2
.10	0.0	1958	44360.3	2620.6	30269.6	1929.8	10.480	750.9
.10	0.0	1700	31649.5	2620.6	19259.6	1382.5	12.532	747.8
.10	0.0	1691	31152.1	2621.4	18905.5	1360.5	12.668	747.9
.10	0.0	1628	27496.3	2541.2	16538.3	1239.6	13.103	724.5
.10	0.0	1568	23961.2	2461.6	14400.5	1115.9	13.716	701.4
.10	0.0	1488	19164.2	2285.4	11756.3	961.9	14.337	650.7
.10	0.0	1426	15255.5	2079.4	9821.0	842.0	14.668	591.8
.10	0.0	1371	11868.9	1867.0	8268.0	729.8	15.063	531.2
.10	0.0	1328	8844.8	1642.8	7057.9	618.1	15.696	467.4

TABLE VI-3-IV (CONTINUED)

TAKEOFF AND PART POWER PERFORMANCE (CONTINUED)

STANDARD + 10 C DAY

MACH NO.	ALTITUDE FEET	TURB. IN TEMP. (R)	GROSS THRUST (LBS)	RAM DRAG (LBS)	TOTAL FUEL FLOW (LBS/HR)	JET VELOCITY (FT/SEC)	NOZZLE EXIT AREA (SQ FT)	EXHAUST GAS FLOW (LBS/SEC)
.20	0.0	3060	77172.9	5369.9	77058.1	3223.2	10.201	782.1
.20	0.0	2785	71022.5	5369.9	65950.9	2978.1	10.071	779.0
.20	0.0	2509	64224.2	5369.9	54620.4	2703.9	9.969	775.8
.20	0.0	2234	56355.0	5369.9	43105.8	2382.4	10.003	772.6
.20	0.0	1958	45911.9	5369.9	30834.2	1949.5	10.552	769.2
.20	0.0	1700	32895.4	5369.9	19555.4	1402.5	12.571	766.1
.20	0.0	1690	32419.1	5371.6	19176.4	1382.0	12.682	766.2
.20	0.0	1626	28543.6	5207.7	16711.0	1256.0	13.150	742.3
.20	0.0	1565	24944.6	5045.1	14485.1	1133.7	13.706	718.7
.20	0.0	1484	19828.5	4679.9	11737.6	972.2	14.388	666.2
.20	0.0	1420	15771.2	4257.4	9744.5	850.4	14.712	605.8
.20	0.0	1365	12326.7	3820.2	8189.9	740.9	15.021	543.4
.20	0.0	1319	9128.0	3360.8	6929.1	623.8	15.715	478.0
.30	0.0	3060	80001.4	8296.7	79076.2	3244.3	10.366	805.5
.30	0.0	2785	73645.1	8296.7	67631.0	2998.3	10.229	802.3
.30	0.0	2509	66668.0	8296.7	55955.7	2725.3	10.106	799.1
.30	0.0	2234	58545.0	8296.7	44090.9	2403.1	10.129	795.8
.30	0.0	1958	47715.4	8296.7	31452.4	1967.3	10.688	792.2
.30	0.0	1700	34415.6	8296.7	19837.6	1424.7	12.638	789.0
.30	0.0	1690	33856.9	8299.4	19446.1	1401.4	12.781	789.2
.30	0.0	1625	29778.3	8047.1	16852.1	1272.1	13.255	764.6
.30	0.0	1561	25972.6	7796.7	14523.4	1145.9	13.836	740.3
.30	0.0	1478	20605.6	7221.3	11658.3	982.3	14.490	685.2
.30	0.0	1411	16362.9	6568.3	9555.1	858.0	14.788	622.9
.30	0.0	1357	12740.8	5887.5	7998.6	745.5	15.133	558.2
.30	0.0	1308	9418.3	5176.9	6712.6	626.9	15.817	490.8

TABLE VI-3-IV (CONTINUED)

TAKEOFF AND PART POWER PERFORMANCE (CONTINUED)
STANDARD + 10 C DAY

MACH NO.	ALTITUDE FEET	TURB. IN TEMP. (R)	GROSS THRUST (LBS)	RAM DRAG (LBS)	TOTAL FUEL FLOW (LBS/HR)	JET VELOCITY (FT/SEC)	NOZZLE EXIT AREA (SQ FT)	EXHAUST GAS FLOW (LBS/SEC)
.40	0.0	3060	83709.4	11485.3	81683.4	3270.1	10.583	836.2
.40	0.0	2785	77098.3	11485.3	69794.2	3023.8	10.434	832.9
.40	0.0	2509	69771.0	11485.3	57666.1	2747.5	10.315	829.5
.40	0.0	2234	61337.5	11485.3	45341.2	2425.4	10.320	826.1
.40	0.0	1958	50088.5	11485.3	32221.7	1989.4	10.865	822.4
.40	0.0	1700	36321.1	11485.3	20166.6	1448.5	12.777	819.1
.40	0.0	1690	35733.1	11489.2	19748.6	1424.7	12.919	819.2
.40	0.0	1621	31417.7	11142.0	16973.6	1292.7	13.379	793.9
.40	0.0	1557	27334.9	10796.8	14521.5	1161.5	13.997	768.7
.40	0.0	1470	21562.4	9978.6	11461.2	992.1	14.644	709.9
.40	0.0	1403	17129.2	9071.4	9353.5	867.3	14.936	645.1
.40	0.0	1348	13306.2	8121.1	7768.1	752.8	15.273	577.3
.40	0.0	1296	9832.5	7134.6	6448.3	633.3	15.909	507.1

TABLE VI-3-IV (CONTINUED)

TAKEOFF AND PART POWER PERFORMANCE (CONTINUED)
STANDARD + 10 C DAY

MACH NO.	ALTITUDE FEET	TURB. IN TEMP. (R)	GROSS THRUST (LBS)	RAM DRAG (LBS)	TOTAL FUEL FLOW (LBS/HR)	JET VELOCITY (FT/SEC)	NOZZLE EXIT AREA (SQ FT)	EXHAUST GAS FLOW (LBS/SEC)
0.00	2000.0	3060	69852.2	0.0	70510.4	3212.7	10.047	710.2
0.00	2000.0	2785	64297.6	0.0	60434.8	2968.9	9.920	707.4
0.00	2000.0	2509	58162.4	0.0	50156.3	2696.5	9.818	704.5
0.00	2000.0	2234	51048.3	0.0	39710.9	2376.5	9.854	701.6
0.00	2000.0	1958	41566.1	0.0	28566.7	1943.6	10.408	698.5
0.00	2000.0	1700	29857.8	0.0	18321.8	1401.9	12.361	695.7
0.00	2000.0	1690	29378.6	0.0	17976.1	1379.2	12.496	695.8
0.00	2000.0	1626	25901.5	0.0	15698.5	1255.2	12.925	674.0
0.00	2000.0	1565	22565.0	0.0	13670.3	1129.6	13.528	652.5
0.00	2000.0	1484	18100.6	0.0	11162.1	974.2	14.147	606.9
0.00	2000.0	1422	14431.7	0.0	9340.8	853.6	14.469	552.3
0.00	2000.0	1367	11330.0	0.0	7870.2	745.3	14.756	496.6
0.00	2000.0	1322	8402.1	0.0	6695.0	627.7	15.466	437.3
.10	2000.0	3060	71116.4	2456.3	71473.8	3224.5	10.119	720.4
.10	2000.0	2785	65473.8	2456.3	61252.4	2980.4	9.988	717.6
.10	2000.0	2509	59244.3	2456.3	50825.2	2707.8	9.882	714.7
.10	2000.0	2234	52027.0	2456.3	40228.6	2387.7	9.911	711.7
.10	2000.0	1958	42419.5	2456.3	28924.3	1955.4	10.454	708.6
.10	2000.0	1700	30583.3	2456.3	18532.4	1415.6	12.368	705.7
.10	2000.0	1690	30149.7	2457.0	18177.6	1395.3	12.471	705.8
.10	2000.0	1624	26507.8	2382.0	15830.4	1266.3	12.936	683.8
.10	2000.0	1562	23091.7	2307.5	13742.9	1139.5	13.530	661.9
.10	2000.0	1481	18496.7	2147.4	11180.3	981.5	14.158	615.6
.10	2000.0	1418	14737.0	1954.7	9323.7	859.4	14.480	560.1
.10	2000.0	1360	11492.5	1758.0	7794.7	745.5	14.838	503.6
.10	2000.0	1316	8576.8	1548.3	6638.4	631.8	15.460	443.4

TABLE VI-3-IV (CONTINUED)

TAKEOFF AND PART POWER PERFORMANCE (CONTINUED)
STANDARD + 10 C DAY

MACH NO.	ALTITUDE FEET	TURB. IN TEMP. (R)	GROSS THRUST (LBS)	RAM DRAG (LBS)	TOTAL FUEL FLOW (LBS/HR)	JET VELOCITY (FT/SEC)	NOZZLE EXIT AREA (SQ FT)	EXHAUST GAS FLOW (LBS/SEC)
.20	2000.0	3060	73250.1	5031.6	73048.0	3242.8	10.247	737.8
.20	2000.0	2785	67504.8	5031.6	62576.3	3000.3	10.097	734.9
.20	2000.0	2509	61060.0	5031.5	51894.0	2724.9	9.998	731.9
.20	2000.0	2234	53662.3	5031.6	41038.1	2404.7	10.017	728.9
.20	2000.0	1958	43863.9	5031.6	29460.5	1974.3	10.531	725.7
.20	2000.0	1700	31804.7	5031.6	18818.2	1437.4	12.386	722.8
.20	2000.0	1690	31282.9	5033.1	18449.6	1413.6	12.527	722.9
.20	2000.0	1623	27492.9	4879.9	15997.3	1282.3	12.987	700.3
.20	2000.0	1558	23949.1	4727.9	13802.9	1153.7	13.563	678.0
.20	2000.0	1476	19131.6	4396.0	11168.0	991.9	14.207	630.0
.20	2000.0	1412	15240.7	4001.2	9254.8	868.5	14.510	573.2
.20	2000.0	1352	11844.5	3596.6	7675.6	751.2	14.883	515.0
.20	2000.0	1307	8840.7	3166.7	6503.3	636.9	15.479	453.4
.30	2000.0	3060	75881.3	7770.2	74931.0	3263.4	10.411	759.5
.30	2000.0	2785	69901.0	7770.2	64146.1	3018.1	10.266	756.5
.30	2000.0	2509	63330.9	7770.2	53144.3	2745.5	10.135	753.5
.30	2000.0	2234	55698.6	7770.2	41963.7	2424.6	10.144	750.4
.30	2000.0	1958	45550.8	7770.2	30046.0	1991.7	10.665	747.1
.30	2000.0	1700	33163.7	7770.2	19092.0	1456.0	12.492	744.0
.30	2000.0	1690	32618.2	7772.6	18703.2	1431.8	12.632	744.1
.30	2000.0	1621	28647.6	7536.8	16131.7	1297.8	13.093	721.0
.30	2000.0	1555	24927.5	7302.9	13847.0	1166.3	13.684	698.1
.30	2000.0	1470	19824.6	6780.6	11071.5	999.8	14.330	647.7
.30	2000.0	1402	15699.0	6170.6	9059.1	870.4	14.680	589.2
.30	2000.0	1346	12304.9	5539.7	7560.0	760.1	14.940	528.8
.30	2000.0	1297	9096.7	4875.6	6329.5	638.6	15.637	465.3

TABLE VI-3-IV (CONTINUED)

TAKEOFF AND PART POWER PERFORMANCE (CONTINUED)

STANDARD + 10 C DAY

MACH NO.	ALTITUDE FEET	TURB. IN TEMP. (R)	GROSS THRUST (LBS)	RAM DRAG (LBS)	TOTAL FUEL FLOW (LBS/HR)	JET VELOCITY (FT/SEC)	NOZZLE EXIT AREA (SQ FT)	EXHAUST GAS FLOW (LBS/SEC)
.40	2000.0	3060	79523.9	10772.7	77514.9	3289.5	10.641	789.7
.40	2000.0	2785	73289.6	10772.7	66294.4	3043.6	10.484	786.5
.40	2000.0	2509	66391.2	10772.7	54848.3	2768.4	10.354	783.4
.40	2000.0	2234	58428.4	10772.7	43216.4	2446.4	10.352	780.1
.40	2000.0	1958	47914.9	10772.7	30826.1	2015.1	10.844	776.7
.40	2000.0	1700	35033.0	10772.7	19439.6	1479.4	12.650	773.5
.40	2000.0	1685	34234.8	10777.9	18864.3	1445.3	12.845	773.7
.40	2000.0	1619	30332.0	10451.0	16297.7	1321.5	13.202	749.7
.40	2000.0	1552	26298.7	10127.9	13899.0	1183.2	13.856	726.0
.40	2000.0	1461	20709.7	9384.9	10868.1	1006.4	14.538	672.2
.40	2000.0	1393	16413.7	8536.6	8846.5	877.3	14.873	611.1
.40	2000.0	1337	12844.8	7652.5	7341.1	766.1	15.120	547.7
.40	2000.0	1286	9503.2	6730.4	6081.2	644.6	15.758	481.6

TABLE VI-3-IV (CONTINUED)

TAKEOFF AND PART POWER PERFORMANCE (CONTINUED)

STANDARD + 10 C DAY

MACH NO.	ALTITUDE FEET	TURB. IN TEMP. (R)	GROSS THRUST (LBS)	RAM DRAG (LBS)	TOTAL FUEL FLOW (LBS/HR)	JET VELOCITY (FT/SEC)	NOZZLE EXIT AREA (SQ FT)	EXHAUST GAS FLOW (LBS/SEC)
0.00	4000.0	3060	66284.1	0.0	66806.3	3232.7	10.096	669.7
0.00	4000.0	2785	61052.7	0.0	57310.7	2989.3	9.962	667.1
0.00	4000.0	2509	55281.3	0.0	47623.9	2717.7	9.850	664.4
0.00	4000.0	2234	48595.6	0.0	37779.6	2398.9	9.870	661.7
0.00	4000.0	1958	39712.4	0.0	27269.8	1969.1	10.387	658.8
0.00	4000.0	1700	28811.9	0.0	17606.8	1434.4	12.211	656.1
0.00	4000.0	1690	28402.6	0.0	17270.3	1413.9	12.311	656.2
0.00	4000.0	1622	24940.1	0.0	15015.2	1281.6	12.772	635.6
0.00	4000.0	1560	21773.7	0.0	13042.2	1155.9	13.318	615.3
0.00	4000.0	1476	17414.1	0.0	10586.9	991.5	14.002	573.7
0.00	4000.0	1414	13919.7	0.0	8857.2	870.6	14.297	522.3
0.00	4000.0	1354	10860.5	0.0	7366.5	754.2	14.653	470.4
0.00	4000.0	1310	8141.0	0.0	6272.1	641.5	15.217	414.5
.10	4000.0	3060	67472.8	2300.2	67713.6	3244.4	10.169	679.3
.10	4000.0	2785	62206.7	2300.2	58081.5	3003.0	10.016	676.6
.10	4000.0	2509	56299.5	2300.2	48255.5	2728.8	9.914	673.9
.10	4000.0	2234	49516.7	2300.2	38269.8	2410.0	9.928	671.1
.10	4000.0	1958	40553.7	2300.2	27610.1	1982.5	10.418	668.2
.10	4000.0	1700	29549.0	2300.2	17809.4	1450.4	12.192	665.4
.10	4000.0	1690	29064.3	2300.8	17464.3	1426.5	12.329	665.5
.10	4000.0	1621	25509.3	2230.7	15137.8	1292.4	12.786	644.7
.10	4000.0	1558	22242.7	2160.9	13112.2	1164.0	13.345	624.1
.10	4000.0	1473	17816.6	2015.8	10619.3	1000.3	13.997	581.8
.10	4000.0	1410	14225.6	1835.9	8844.9	877.3	14.293	529.6
.10	4000.0	1349	11094.6	1653.7	7344.9	759.9	14.652	476.9
.10	4000.0	1305	8295.5	1457.6	6228.4	644.7	15.241	420.3

TABLE VI-3-IV (CONTINUED)

TAKEOFF AND PART POWER PERFORMANCE (CONTINUED)

STANDARD + 10 C DAY

MACH NO.	ALTITUDE FEET	TURB. IN TEMP. (R)	GROSS THRUST (LBS)	RAM DRAG (LBS)	TOTAL FUEL FLOW (LBS/HR)	JET VELOCITY (FT/SEC)	NOZZLE EXIT AREA (SQ FT)	EXHAUST GAS FLOW (LBS/SEC)
.20	4000.0	3060	69467.7	4710.5	69188.1	3262.4	10.296	695.5
.20	4000.0	2785	64013.9	4710.5	59323.3	3018.2	10.152	692.8
.20	4000.0	2509	58041.9	4710.5	49259.9	2747.7	10.015	690.0
.20	4000.0	2234	51089.5	4710.5	39032.9	2428.6	10.019	687.1
.20	4000.0	1958	41860.1	4710.5	28118.8	1998.7	10.515	684.1
.20	4000.0	1700	30626.6	4710.5	18084.9	1468.3	12.255	681.3
.20	4000.0	1685	29925.2	4712.4	17581.7	1434.4	12.446	681.5
.20	4000.0	1619	26402.4	4568.7	15280.4	1306.3	12.853	660.2
.20	4000.0	1554	22988.8	4426.3	13173.2	1174.8	13.426	639.2
.20	4000.0	1468	18396.0	4125.6	10603.2	1009.4	14.063	595.3
.20	4000.0	1402	14606.0	3757.4	8728.1	880.4	14.399	541.9
.20	4000.0	1344	11490.8	3382.0	7284.8	769.8	14.645	487.6
.20	4000.0	1295	8501.8	2980.9	6114.0	646.3	15.362	429.7
.20	4000.0	1253	6179.2	2575.3	5208.5	543.7	15.890	371.2
.30	4000.0	3060	71907.5	7270.7	70943.1	3282.1	10.460	715.6
.30	4000.0	2785	66289.2	7270.7	60788.3	3037.7	10.306	712.8
.30	4000.0	2509	60079.9	7270.7	50429.1	2764.3	10.176	709.9
.30	4000.0	2234	52937.5	7270.7	39901.6	2445.7	10.163	707.0
.30	4000.0	1958	43435.0	7270.7	28672.3	2015.6	10.649	703.9
.30	4000.0	1700	31899.4	7270.7	18349.6	1486.4	12.362	701.0
.30	4000.0	1685	31179.4	7273.8	17828.8	1452.5	12.550	701.2
.30	4000.0	1617	27515.1	7052.6	15425.0	1323.0	12.946	679.3
.30	4000.0	1550	23907.2	6833.9	13209.7	1187.2	13.541	657.8
.30	4000.0	1460	18973.6	6361.6	10445.4	1013.0	14.212	611.8
.30	4000.0	1396	15186.7	5790.9	8643.9	891.1	14.460	556.7
.30	4000.0	1335	11801.6	5207.9	7112.1	770.3	14.830	500.5
.30	4000.0	1286	8764.0	4587.8	5949.5	649.5	15.474	440.8

TABLE VI-3-IV (CONTINUED)

TAKEOFF AND PART POWER PERFORMANCE (CONTINUED)

STANDARD + 10 C DAY

MACH NO.	ALTITUDE FEET	TURB. IN TEMP. (R)	GROSS THRUST (LBS)	RAM DRAG (LBS)	TOTAL FUEL FLOW (LBS/HR)	JET VELOCITY (FT/SEC)	NOZZLE EXIT AREA (SQ FT)	EXHAUST GAS FLOW (LBS/SEC)
.40	4000.0	3060	75341.0	10073.2	73348.2	3309.9	10.674	743.5
.40	4000.0	2785	69430.7	10073.2	62790.7	3062.3	10.524	740.6
.40	4000.0	2509	62953.8	10073.2	52020.8	2787.9	10.383	737.6
.40	4000.0	2234	55481.6	10073.2	41076.1	2467.2	10.367	734.5
.40	4000.0	1958	45601.3	10073.2	29409.6	2036.8	10.840	731.3
.40	4000.0	1700	33649.0	10073.2	18686.7	1509.1	12.522	728.3
.40	4000.0	1686	32934.7	10077.7	18161.2	1476.7	12.697	728.5
.40	4000.0	1616	29102.5	9772.6	15615.4	1346.7	13.061	705.9
.40	4000.0	1546	25205.6	9471.3	13257.0	1204.4	13.697	683.6
.40	4000.0	1457	20034.5	8796.9	10426.8	1031.5	14.307	634.4
.40	4000.0	1385	15780.6	8007.2	8407.3	893.1	14.710	577.2
.40	4000.0	1327	12380.2	7189.8	6927.6	780.6	14.924	518.1
.40	4000.0	1273	9069.5	6330.0	5688.3	649.7	15.713	456.0
.40	4000.0	1230	6542.5	5452.2	4805.9	544.1	16.271	392.7

VI-4 WEIGHT ANALYSIS

INTRODUCTION

The objective of the weight analysis is to establish a realistic design gross weight in selection of a conceptual supersonic configuration which will serve as a reference for current and future advanced technology evaluations. The design goal was to achieve a Reference Configuration having the mission capability of flying four thousand (4000) nautical miles at Mach 2.7 cruise speed while carrying two hundred ninety two passengers with baggage.

Historically, the genealogy of the Reference Configuration can be traced back to the NASA SCAT-15. A derivative, the Boeing 969-336C, characterized by fixed "arrow" wing geometry and forebody mounted retractable canards became the baseline model for additional investigations. Through extensive wind tunnel testing conducted by NASA/LRC, advanced low speed aerodynamic concepts were developed specifically for incorporation into the 969-336C model.

The configuration changes resulting from application of these concepts to the 969-336C indicated that major weight reductions were possible. From a structural weight viewpoint, the most significant of these changes were:

- °Deletion of canard system
- °Deletion of portions of wing leading edge High Lift Systems
- °Shifting center-of-gravity aft resulting in decreased landing gear strut length

Accepting the structural design of the 969-336C, incorporating the advanced aerodynamic concepts, and taking advantage of the ensuing weight savings led to a modified version of the 969-336C without canards. This version became the statistical weight base from which the computer generated Reference Configuration would evolve.

SUMMARY

The structural weight analysis is based on a strength designed all titanium primary structure. Design features and construction techniques for major components are:

- °Wing and aerodynamic surfaces - stresskin titanium skin/core sandwich panels
- °Fuselage - titanium skin/stringer/frame construction
- °Two-strut main landing gear and single strut nose gear structure - high strength steel
- °Engines - 800 lb/sec mass flow dry turbojets oversized to meet noise requirements

The weight development of the Reference Configuration is summarized as follows:

- °Establishment of a statistical weight base for computerized methods using the 969-336C prototype (having a 316650 lb operating wt. and a 635000 lb gross wt.) for correlation.
- °Incorporation of OW and GW changes from prototype to production 969-336C (increased OW from 315650 to 326650 lbs and GW from 635000 to 750000 lbs) enabling valid comparison with Reference Configuration

- °Incorporation of advanced aerodynamic concepts and other changes resulting in weight reductions (21566 lbs)
- °Generation of weights and sizing of Reference Configuration through computerized methods resulting in OW increases (46056 lbs) and a new OW of 351140 lbs with a GW of 762000 lbs.

The net results indicate increases of 1.6% in gross weight and 7.5% in operating weight which are due primarily to growths of 25% in payload and 10% in propulsion (engine oversizing to meet FAR 36 noise criterion). A comparative summary of these results appears in Table VI-4-1.

A graph indicating the gross weight breakdown, expressed in percentages, of the production 969-336C in comparison with the Reference Configuration appears as Figure VI-4-1.

Discussion

Methods

One of the prime requisites for attaining valid design evaluations during early conceptual development of an aircraft system, is availability of accurate weight and balance data. Obtaining precise mass data would require a detailed structural weight analysis comparable to the effort expended by the Boeing Company during the National SST program. Analysis of such magnitude is beyond the scope of this study. However, it is possible, after establishing a sound reference base, to produce first level mass data with reasonably adequate confidence levels. These data, while not highly detailed, do reveal trends and serve to isolate, identify, and assess impacts resulting from incorporation of variations in design or technology.

TABLE VI-4-1

CHARACTERISTICS COMPARISON

ITEM	-336C (PRODUCTION)	% CHANGE	REFERENCE CONFIGURATION
[1] DESIGN GROSS WEIGHT	750000	+ 1.6	762000
[1] OPERATING WEIGHT	326650	+ 7.5	351140
[1] PAYLOAD	48906	+25.0	61028
[1] FUEL	374444	- 6.6	349833
[2] MISSION RANGE (N.MI.) (STD DAY)	3790	+ 5.5	4000

1 SEE GROUP WEIGHT SUMMARY

2 DESIGN GOAL IS 4000 NAUTICAL MILES

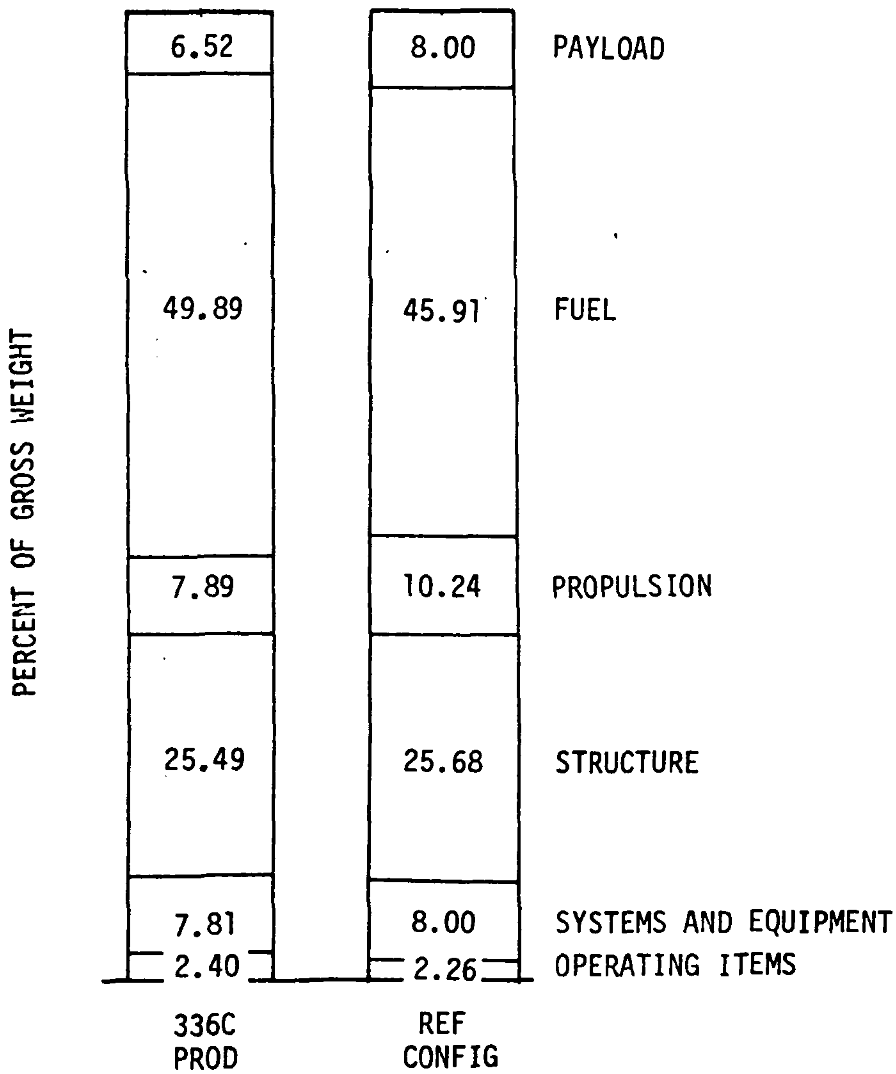

FIGURE-VI-4-1

Design Weight Fractions

For this study, computerized statistical estimating techniques were employed in performing parametric weight and balance evaluations. A basic mass data program was modified and adapted to evaluate supersonic transport aircraft and yield a high correlation with the 969-336C Boeing derivative. All analyses were performed on an identical basis, and variations in design and technology concepts appeared as real value differences. Comparative assessment of specific variations was accomplished and developing trends were evaluated. Selecting an appropriate design gross weight involved a sizing synthesis with an array of aircraft weights ranging from 400 to 850 thousand pounds. The weight data from this sizing program were subjected to mission performance evaluations and the candidate model with the best gross weight/thrust/range match was selected as the point design Reference Configuration.

Materials

In accordance with the design philosophy of retaining the structural concepts of the 969-336C, the Reference Configuration weights represent an all titanium primary airframe structure composed of stresskin sandwich panels for wing and other aerodynamic surfaces, titanium skin-stringer-frame fuselage construction, and high strength steel alloy landing gear structure.

The use of stresskin in the weight base was deemed a conservative approach because of the existence of other advanced materials and construction techniques which promise equal or lighter weights. Of the alternate materials and techniques under consideration, two seem extremely promising. One is a diffusion bonded titanium skin/stringer built-up construction technique pioneered by NASA; the other is a patented process, LID, liquid interface

TABLE VI-4-2

WEIGHT CHANGE SUMMARY

(REFERENCE BOEING DOCUMENT)

DESCRIPTION	-336 PROTOTYPE	ΔWEIGHT	-336C PRODUCTION
OPERATING WEIGHT	316650	+ 11000	326650
PAYLOAD	48900	-	48900
FUEL	270444	+104000	374444
MAXIMUM GROSS WEIGHT	635000		750000

diffusion bonded titanium skin/core sandwich panel. In the NASA process, the continuity of the bond between skin and stringer increases panel buckling resistance, improves flutter characteristics, and enhances fatigue life. The LID process, in comparison to other bonding and brazing techniques, promises improvements in shear strength, resistance to interlaminar separation, and elimination of interface stress corrosion. Specimen panels of both construction techniques are undergoing actual flight testing on YF12 Mach 3 aircraft under auspices of NASA/Edwards.

Because of the considerations mentioned, neither weight disadvantages, such as those reportedly arising from use of aluminum brazed titanium core sandwich, nor weight advantages anticipated from utilization of more exotic materials are reflected in the weights.

Weight Derivation

The statistical weight derivation began with the adoption of the 635000 lb. gross weight 969-336C prototype (Reference VI-4-1) as the reference base for structural weights. The 750000 lb. gross weight 969-336C production version is used in the final weight comparisons because its higher gross weight and similar range makes possible a more valid direct comparison with the Reference Configuration than could be achieved if the prototype were used. Of this 115000 lb. difference in gross weight, 104000 lbs. is fuel and the remaining 11000 lbs. is attributable to operating weight changes. A comparative weight summary listing these differences is presented at Table VI-4-2.

Incorporation of advanced aerodynamic concepts, resulted in the following significant weight reductions.

°Deletion of the canard and provisions yielded a net weight reduction of 5109 lbs.

°Deletion of part of wing L.E. high lift devices resulted in a weight decrease of 6224 lbs.

°A 20 inch decrease in main landing gear strut length resulted in a weight reduction of 5000 lbs.

One item, listed as manufacturing and certification tolerance, was deleted from the reference model as being unaccountable within the accuracy tolerance of the computer generated data during early conceptual evaluations. A list of these weight reductions is presented as Table VI-4-3.

The final phase of weight development was the computerized weight synthesis of the specific Reference Configuration. The results indicate that a 762000 lb. design gross weight is required to achieve the desired payload, range and noise goals.

Of the operating weight increases, the largest single increase (14812 lbs.) occurs in the propulsion group as a result of increased engine size dictated by sizing engines for noise (throttle back). Another propulsion related increase is the 10601 lb. increment for thrust reversers. These and other operating weight increases are presented in Table VI-4-4.

These weight changes in derivation of the operating weight are summarized in Table VI-4-5.

A weight summary listing the weight derivation from the 969-336C prototype through the production version and finally to the Reference Configuration is presented in Table VI-4-6.

TABLE VI-4-3

CHANGE SUMMARY

REDUCTIONS

ITEM/DESCRIPTION		WT~LBS
Wing		4,870
Leading edge flaps - deleted inboard sections and demand system		
Canard		2,950
Canard deleted entirely		
Fuselage		1,409
Deleted canard attachment and stowage provisions		
Landing Gear		5,000
Reduced strut length by 20 inches		
Flight Controls		4,052
L.E. Flap - operating system	3,302	
Canard - operating system	750	
Mfg and Certification Tolerance		3,094
Deleted as unaccountable in conceptual evaluations		
Operating Items		191
Unusable fuel adjustment		
Total Reductions		21,566

TABLE VI-4-4

CHANGE SUMMARY

INCREASES

ITEM/DESCRIPTION		WT~LBS
Wing		4,061
Increased gross weight, area, span, t/c at root, added fixed L.E. in lieu of L.E. flaps		
Horizontal Tail		2,901
Increased area from 456 to 600 ft^2 (exposed area 296 to 441 ft^2) Increased gross weight effects		
Vertical Tail		1,465
Increased gross weight effects		
Fuselage		4,153
Increased width to 5 abreast seating increased length from 295 to 315 ft.		
Landing Gear		4,484
Increased gross weight and improved flotation		
Nacelle		1,603
Increased length and diameter to accommodate larger engines		
Propulsion		18,554
Engines - increased mass flow from 633 to 800 lbs/sec	7,082	
Thrust reversers - added thrust reversers	10,601	
Fuel tanks and plumbing - added aft fuselage and apex tanks	871	
Surface Controls		1,602
Effects of increased gross weight		

TABLE VI-4-4 (continued)

CHANGE SUMMARY

INCREASES

ITEM/DESCRIPTION		WT~LBS
Furnishings and Equipment		3,821
Provisions for 58 additional passengers achieved by 5 abreast seating		
Air Conditioning		310
Increased environmental requirements for additional passengers		
Operating Items		3,102
Cabin attendants - increased from 7 to 10 to accommodate additional passengers	510	
Engine oil - increased for larger engines	123	
Passenger service - increased requirements for additional passengers	1,769	
Cargo containers - larger containers due to increases in body width and depth and baggage requirements	460	
Adjustment for computer deviation	240	
Total Increases		46,056

TABLE VI-4-5

DERIVATION SUMMARY

ITEM/DESCRIPTION	WT~LBS
-336C Production Operating Weight	326,650
Total Reductions	- 21,566
Total Additions	+ 46,056
Reference Configuration O.W. (Computer Generated)	351,140

WEIGHT DERIVATION SUMMARY

ITEM	Ref(VI-4-1) Prototype -336C	LTV Prototype -336C	Ref(VI-4-1) Prototype to Production Changes	LTV Computer Production -336C	Advanced Technol. Changes	A/C Growth Changes	Final ΔWt	LTV Computer Reference Config.
Wing	83,940	84,116	+40	84,156	-4,870	+4,061	-809	83,347
Horizontal Tail	2,370	2,370		2,370		+2,901	+2,901	5,271
Vertical Tail	3,270	3,270		3,270		+1,465	+1,465	4,735
Canard	2,950	2,950		2,950	-2,950	0	-2,950	0
Fuselage	51,570	51,570		51,570	-1,409	+4,153	+2,744	54,314
Landing Gear	28,720	28,731	+750	29,481	-5,000	+4,484	-516	28,965
Nacelle	15,650	15,650	+1,762	17,412		+1,603	+1,603	19,015
Structure Total	(188,470)	(188,657)	(+2,552)	(191,209)	(-14,229)	(+18,667)	(+5,077)	(195,646)
Engines	45,020	45,020	7,730	53,750		+7,082	+7,082	59,832
Thrust Reversers	0	0		0		+10,601	+10,601	10,601
Miscellaneous Systems	1,780	1,780		1,780		0	0	1,780
Fuel System-Tanks and Plumbing	4,530	4,530	+380	4,910		+871	+871	5,781
-Insulation		0		0		0	0	0
Propulsion Total	(51,330)	(51,330)	(+8,110)	(59,440)		(+18,554)	(+18,554)	(77,994)
Surface Controls	12,430	12,431		12,431	-4,052	+1,602	-2,450	9,981
Auxiliary Power	0	0		0		0	0	0
Instruments	3,400	3,400		3,400		0	0	3,400
Hydraulics	5,600	5,600		5.600		0	0	5,600
Electrical	5,050	5,050		5,050		0	0	5,050
Avionics	2,690	2,690		2,690		0	0	2,690
Furnishings and Equipment	21,290	21,290		21,290		+3,821	+3,821	25,111
Air Conditioning	7,890	7,890		7,890		+310	+310	8,200
Anti-icing	210	210		210		0	0	210
Systems and Equipment Total	(58,560)	(58,561)		(58,561)	(-4,052)	(+5,733)	(+1,681)	(60,242)
Mfg and Certif Tolerance	2,980	2,986	+108	3,094	-3,094	0	-3,094	0
Weight Empty	301,340	301,534	+10,770	312,304	-21,375	+42,953	+21,578	333,882
Crew and Baggage-Flight,	(3) 675	(3) 675		(3) 675		0	0	675
-Cabin,	(7) 1,130	(7) 1,130		(7) 1,130		+510	+510	1,640
Unusable Fuel	2,250	2,296	+230	2,526	-191		-191	2,335
Engine Oil	672	672		672		+123	+123	795
Passenger Service	7,083	7,083		7,083		+1,769	+1,769	8,852
Cargo Containers	(5) 2,500	(5) 2,500		2,500		+460	+460	2,960
Adjustment for Computer Deviation		-240		-240		+240	+240	0
Operating Weight	315,650	315,650	+11,000	326,650	-21,566	+46,056	+24,489	351,139
Passengers,	(234)38,610	(234)38,610		(234)38,610		+9,570	+9,570	(292)48,180
Passenger Baggage	10,296	10,296		10,296		+2,552	+2,552	12,848
Cargo	0	0			0	0	0	0
Zero Fuel Weight	364,796	364,796		375,556		+36,611	+36,611	412,167
Mission Fuel	270,444	270,444	+104,000	374,444		-24,611	-24,611	349,833
Design Gross Weight	635,000	635,000	+115,000	750,000		+12,000	+12,000	762,000

TABLE VI-4-6

Balance

Mass balance characteristics are a major parameter influencing design, configuration development, and flying qualities of all aircraft. Because of the broad operational requirements of supersonic aircraft, (flight at subsonic, transonic, and supersonic speeds), the trim and stability requirements are more extensive than those for subsonic applications. Attainment of a design goal fulfilling the trim conditions at the extremes of the operational spectrum, requires a high degree of flexibility in the balance potential of a configuration.

Ensuring this flexibility of operation over a wide C.G. range was accomplished with a combination of design implementations. The primary step in providing the configuration with an aft C.G. potential was to move the wing forward relative to the fuselage while remaining within acceptable forward contour limits of the area distribution curves dictated by the cruise Mach no. area ruling criterion. The next phase involved extending the aftbody section (of the fuselage) by ten (10) feet increasing the overall fuselage length to 315 ft. Thus, the aircraft C.G., at lower gross weights at or near reserve fuel conditions, tends to be aft satisfying the approach stability requirements. Optional fuel tanks are located in the aftbody and wing apex to satisfy the take-off and cruise trim requirements.

With proper fuel management, the aircraft is capable of operating within a C.G. range from 53 to 60 percent of the reference mean aerodynamic chord (MAC = 1154.28 inches). This range is illustrated in Figure VI-4-2.

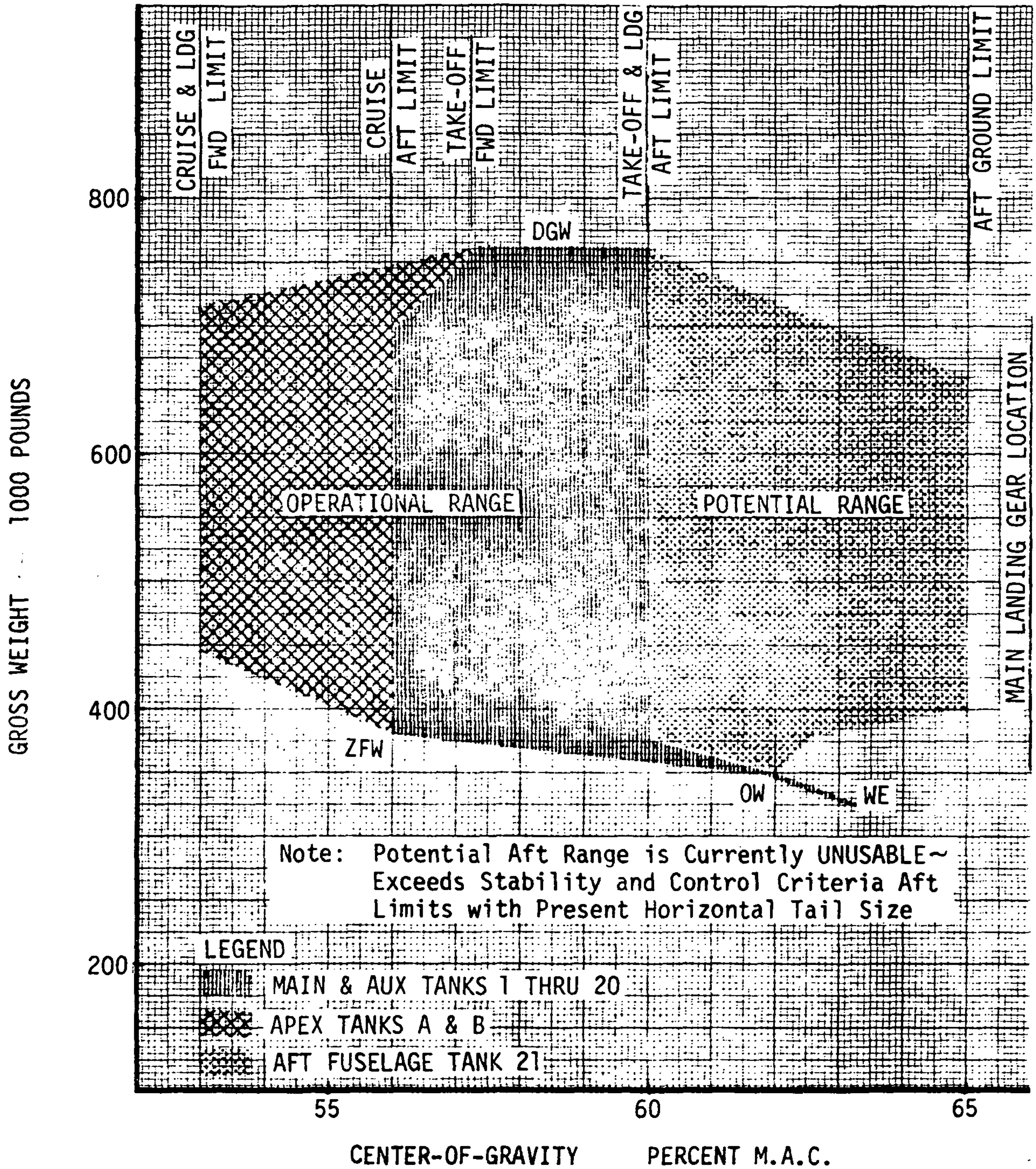

FIGURE-VI-4-2 Operational Center-of-Gravity Envelope

Two potential benefits of the current design illustrate the significant influence that balance can have on weight and warrant discussion.

One potential benefit is the possibility of utilizing the optional fuel tanks as heat transfer reservoirs in thermal management of fuel which has not been addressed in this study.

The second, influence of balance on structural weight, is indicated in this study. Introduction of an advanced aerodynamic concept, making possible the operation of the aircraft at aft C.G. positions and reducing the angles of attack in take-off and landing modes, resulted in a decrease of 20 inches in landing gear strut length. The result of this was a significant weight reduction of 5000 lbs.

Another aspect of influence by balance on design may be illustrated by the following assumption. Most, if not all, current supersonic aircraft (transport) designs have engines mounted on the trailing edge of the wing for a multitude of design reasons. If, for reasons of improving performance or noise abatement, engine sizes were drastically increased, the balance could be measurably affected. The impact of additional weight at an aft position could adversely affect a point design having a limited C.G. operating range either hampering or limiting growth or major changes. Capability of operation over a broad C.G. range, particularly in aft regions, would diminish the impact of such changes, perhaps even absorbing the effects without requiring any major configuration changes.

VI-4

LIST OF REFERENCES

Reference No.	Title
VI-4-1	The Boeing Co.; "Mach 2.7 Fixed Wing SST Model 969-336C (SCAT-15F)," Document No. D6A-11666-1, Dated November 1969.

LIST OF FIGURES

LIST OF TABLES

VI-5 NOISE ANALYSIS

INTRODUCTION

This section presents the predicted noise characteristics of the Reference Configuration for both the takeoff and approach conditions, and for the airframe only. The effective perceived noise levels (EPNL's) were calculated at the FAR 36 (Reference VI-5-1) prescribed noise measurement stations shown in Figure VI-5-1. During takeoff, the effective perceived noise level is normally considerably greater than either the approach noise level or the airframe noise level. In addition to presenting the EPNL at the noise measurement position, community noise profile maps are presented for the takeoff condition with both unsuppressed and suppressed engines. A summary is included of the engine noise prediction method used to obtain the EPNL values.

To reduce the noise levels during takeoff, oversized engines were employed which operate at partial power (Thrust = 54600 lbs/engine rather than 73550 lbs/engine sea level static takeoff) and jet exhaust suppressors were used. These are variable geometry turbine engines with variable geometry exit nozzles. Several takeoff profiles were evaluated to optimize the EPNL at the FAR 36 measurement positions. For a 3 degree approach condition, the engine EPNL was predicted at the FAR 36 prescribed measurement positions.

The overall sound pressure level (OASPL) of the airframe was evaluated at the times the aircraft was nearest the FAR 36 observer measurement stations.

All engine performance, speed of sound calculations, and atmosphere absorption factors for noise attenuation are based on a 77° F day with 70% humidity.

SUMMARY

The takeoff and approach noise levels are presented in Table VI-5-1, along with the overall sound pressure level (OASPL) of the airframe and the amount of engine noise suppression required to meet the FAR 36 requirement of 108 DB. The results of the noise study of the Reference Configuration are briefly as follows:

- °To meet the FAR 36 standards 11.7 DB of engine suppression are required during Takeoff
- °During Takeoff the Airframe noise of 105.6 DB is less than the FAR 36 requirement of 108 DB
- °During approach the airframe noise exceeds the engine noise by 11.1 DB
- °During approach the airframe noise is 0.3 DB less than the FAR 36 requirement of 108 DB
- °A variable geometry turbine yields an engine noise reduction of 3 DB over a fixed geometry turbine during Takeoff

Engine Noise Prediction Method

Prediction of aircraft engine noise at ground observer stations is dependent on the engine performance characteristics and the flight profile. The engine performance characteristics including jet velocity, relative to ambient air and jet area, are used in SAE AIR 876 Method 2 (Reference VI-5-2) for computing maximum passby noise level. This method yields the maximum passby noise level at 200 feet radius for each third octave band level of preferred frequencies at a directivity angle of 135°. Because the directivity angle between the engine and the observer varies with time, it is necessary to obtain the maximum passby noise level over a range of directivity angles. Table VI-5-2 presents the variation of sound pressure level corrections with directivity angle and frequency which are used in this analysis. These values were obtained from Reference VI-5-3. Using these values the variation of engine sound pressure level (SPL) with frequency level and directivity angle is computed.

The flight profile characteristics include the time history of the range and altitude. Thus at a particular time at each observer position, an effective perceived noise level (EPNL) is obtained at the observer position.

Table VI-5-III presents a typical PNL time history prediction and the EPNL during takeoff with observer located near 3.5 nautical miles (21280 ft.) from brake release and at a sideline distance of 0.35 nautical miles (2128 ft.) along the runway centerline. These observer locations are some of the FAR 36 prescribed noise measuring locations.

Takeoff Noise Level

To minimize community noise levels during takeoff, oversized engines were employed which operate at partial power (V_{Jet} = 2400 ft./sec and Thrust = 54600 lbs./engine rather than 73550 lbs./engine at sea level static takeoff on a 77°F day). These engines employ variable geometry in both the turbine and the exit nozzle. Section VI-3 presents the engine performance characteristics. Takeoff profiles were evaluated which use various climb gradients.

A Trade study between climb gradient (altitude) and speed showed that as the aircraft velocity increases the noise level decreases. For this study, the runway length of 10,500 ft. dictated a liftoff velocity of 352 ft./sec. (208 knots) and the velocity at 3.5 nautical miles (21280 ft.) from brake release was 385 ft./sec. (228 knots). At the 3.5 mile point, the C_L is 0.42 and the corresponding L/D is 8.2. The takeoff profile for the Reference Configuration is presented in Figure VI-5-2. At thrust cut-back the effectiveness of the jet suppressor is reduced (Figure VI-3-5) as a result of lower jet velocity (1935 ft./sec.). For this study it was assumed that the flaps could be partially retracted to 5° at 700 ft. altitude. Using this takeoff profile, the variation of effective perceived noise level (EPNL), with distance along the runway centerline and along a sideline position .35 nautical miles (2128 ft.) from the runway centerline are presented in Figures VI-5-3 and VI-5-4 respectively. Also shown on these figures is the FAR 36 allowable noise level and the area where engine noise suppression is required. A comparison of these two figures shows that the maximum EPNL occurs at the runway centerline and not along the sideline. Figure VI-5-5 presents contour plots for specific EPNL values for 120 DB, 115 DB, and 108 DB with no suppression. Figure VI-5-6 presents similar contour plots assuming engine suppression of 11.7 DB.

A noise analysis was conducted using fixed geometry turbine engines with variable geometry exit nozzles over the same flight profile at the same thrust level. With these engines the predicted EPNL was 3.0 DB higher than the variable geometry turbine engines at the FAR 36 prescribed measuring stations.

Approach Noise Level

During approach the noise level was evaluated at the FAR 36 prescribed measuring points which are 1.0 nautical mile (6080 ft.) from the 50 foot obstacle threshold point along the runway centerline and at a sideline distance of 0.25 nautical miles (1520 ft.). Figure VI-5-7 shows the 3° approach profile. During approach the trailing edge flaps t_1, t_2, t_3, and t_4 were deflected to 20°, 20°, 20°, and 5° respectively. A tradeoff of aircraft aerodynamics and airframe noise level dictated the landing velocity to be 269 ft./sec. (159 knots) and a lift coefficient of 0.55 at the 1.0 nautical mile point. The aircraft landing weight is 482,000 lbs. and the L/D is 5.2. With this 3° approach profile the EPNL at the FAR 36 prescribed measuring points were computed to be 96.6 DB on the runway centerline, and 83.7 DB on the sideline.

Airframe Noise Prediction

The airframe overall sound pressure level (OASPL) of the Reference Configuration was computed from equation 1:

$$\text{OASPL} = 10 \text{ Log}_{10}\left[\frac{V^6}{h^2}\frac{S}{AR}\right] - 29.95 + \text{SPL}_{(\text{FLAP + GEAR})} \qquad (1)$$

This equation 1 was obtained from the Reference VI-5-4 equation shown below:

$$\text{OASPL} = 10 \text{ Log}_{10}\left[\frac{V^4}{h^2}\ \frac{W}{C_L}\ \frac{1}{AR}\right] - 0.7$$

To obtain Equation 1, the ratio of W/C_L was replaced by $1/2\ \rho\ V^2 S$ where ρ is the sea level air density.

Equation 1 was used to determine the airframe OASPL along the runway centerline directly under the airplane. Figure VI-5-3 shows the variation of airframe noise with axial distance along the runway centerline. At the FAR 36 measurement positions on the runway centerline (3.5 nautical miles from start of roll for takeoff and 1.0 nautical mile from 50 ft. threshold point for landing), the input values for the parameters of Equation 1 and the corresponding OASPL values are:

Parameter	Takeoff 3.5 n.mile pt.	Landing 1.0 n.mile pt.
AR	1.62	1.62
S - sq. ft.	9969	9969
$SPL_{(FLAPS + GEAR)}$ - DB	2.0	5.0
V - ft/sec	385 (228 knots)	269 (159 knots)
h - ft	933	369.0
OASPL - DB	105.6	107.7

From the above it can be seen that during takeoff the airframe noise level of 105.6 DB is 2.3 DB less than the FAR 36 limitation of 108 DB, whereas during landing the airframe noise of 107.4 DB is only 0.6 DB less than the FAR 36 limitation of 108 DB. During takeoff, the gear is retracted, and noise associated with 5° flaps is 2.0 DB. Comparison of the airframe noise with the engine noise is presented in Table VI-5-1.

The data employed by Lockheed (Reference VI-5-4) to correlate the airframe noise is based on high aspect ratio (AR > 6), light weight (W < 50000 lbs.) airframes. The most significant contributor to airframe noise is the wing lift. The strength of the wing vortices are dependent on the span loading. The span loading of the Reference Configuration is 5530 lb./ft. whereas the span loading from the Lockheed aircraft data were less than 500 lb./ft. Subsequent investigations were made by Lockheed to incorporate noise data from the C-5A which has an aspect ratio of 8.0, a weight of 750000 lbs, and a span loading of 3370 lb./ft. From the C-5A noise data the effect of aspect ratio on airframe noise is greater than shown in Equation 1. Using this new Lockheed correlation, the OASPL of the AST was found to be 125 DB during takeoff rather than 105 DB as calculated with equation 1. It appears that the airframe noise levels obtained from equation 1 may be low. The actual airframe noise of the low aspect ratio (AR = 1.62) AST needs to be ascertained.

VI-5

LIST OF REFERENCES

Reference No.	Title
VI-5-1	Federal Aviation Administration Department of Transportation Part 36, Noise Standards; Aircraft Type Certification.
VI-5-2	SAE AIR 876, Jet Noise Prediction, Society of Automotive Engineers Aerospace Information Report, 10 July, 1965.
VI-5-3	Noise Prediction Methods for Gas Turbine Engines, Volume I, by Noise Evaluation Staff of Flight Propulsion Division, General Electric Company, November 1964.
VI-5-4	LR 23640, Far Field Aerodynamic Noise Measurement Program, Lockheed California Company, 22 June 1970.

LIST OF SYMBOLS

AR	Aspect Ratio
C_L	Lift Coefficient
DB	Decibels
EPNL	Effective Perceived Noise Level - Decibels
OASPL	Overall Sound Pressure Level - Decibels
PNL	Perceived Noise Level - Decibels
R	Distance
SPL	Sound Pressure Level - Decibels
$SPL_{(flaps+gear)}$	Sound Pressure Level of Flaps and Landing Gear - Decibels
V	Airframe Velocity - Ft/Sec
V_{Jet}	Jet Exit Velocity at Sea Level Static - Ft/Sec

LIST OF TABLES

LIST OF FIGURES

TABLE VI-5-1

Takeoff and Approach Noise Summary

	FAR 36 Measurement Point 1 (Runway Centerline)	FAR 36 Measurement Point 2 (Sideline)	Maximum Engine (SPL)	Required Suppression Level	Airframe Noise (OASPL)
Takeoff	119.7	111.6	119.7	11.7	105.6
3° Approach	96.6	83.7	96.6	None	107.7

* All noise levels are in Decibels.

TABLE VI-5-II

Variation of Sound Pressure Level Corrections with Frequency and Directivity Angle

FREQUENCY (HZ)	Directivity Angle - Degrees 10	20	30	40	50	60	70	80	90
50	19.1	18.9	18.8	18.9	18.1	17.9	16.9	15.9	15.0
63	19.2	19.5	19.7	19.6	18.5	18.8	17.7	16.7	15.6
80	21.1	21.3	21.4	21.2	20.0	20.2	19.5	18.5	16.9
100	22.7	22.5	22.5	22.3	21.3	21.2	20.9	19.9	17.6
125	22.9	22.5	22.3	22.4	21.7	21.3	21.3	20.3	17.5
160	22.0	21.4	21.0	21.4	20.9	20.3	20.4	19.4	16.6
200	20.1	19.6	19.0	19.4	19.1	18.5	18.6	17.6	14.9
250	18.0	17.5	16.8	16.9	16.6	16.0	16.2	15.2	13.0
315	16.0	15.6	14.8	14.1	13.7	13.2	13.5	12.7	11.0
400	14.6	14.1	13.1	11.4	10.7	10.5	10.9	10.5	9.2
500	13.6	13.2	12.0	9.1	8.0	8.0	8.7	8.7	7.9
630	13.2	12.7	11.2	7.2	5.9	6.1	7.0	7.4	7.0
800	13.1	12.4	10.7	5.8	4.3	4.7	5.9	6.7	6.5
1000	12.9	12.1	10.1	4.9	3.4	3.9	5.3	6.3	6.2
1250	12.5	11.6	9.2	4.4	3.1	3.7	5.0	6.1	6.0
1600	11.6	10.7	8.1	4.1	3.1	3.6	4.8	5.9	5.8
2000	10.4	9.4	6.7	4.0	3.3	4.0	4.6	5.5	5.4
2500	8.9	8.0	5.2	3.9	3.5	4.2	4.3	4.9	4.8
3150	7.7	6.7	4.1	3.8	3.5	4.1	3.7	4.0	4.0
4000	7.0	5.9	3.7	3.8	3.3	3.7	3.0	3.0	3.2
5000	7.3	6.0	4.3	3.9	2.8	3.0	2.2	2.2	2.6
6300	8.5	6.8	5.7	4.3	2.4	2.2	1.8	1.7	2.4
8000	9.8	7.9	7.0	5.0	2.5	1.8	1.8	1.9	2.8
10000	9.3	7.3	6.2	5.7	3.9	2.7	2.7	2.7	3.8

Above SPL Values to be Subtracted from
Maximum Passby Sound Pressure Levels.

TABLE VI-5-II Cont'd.

Variation of Sound Pressure Level Corrections with Frequency and Directivity Angle

FREQUENCY (HZ)	Directivity Angle - Degrees								
	100	110	120	130	140	150	160	170	180
50	13.0	11.0	6.9	.9	0.0	0.0	-0.0	1.6	3.4
63	13.6	11.6	7.9	1.9	0.0	0.0	-.2	3.2	5.5
80	14.9	12.5	8.4	2.2	0.0	0.0	.7	5.1	7.5
100	15.7	13.0	8.2	2.1	0.0	0.0	1.7	6.7	9.2
125	15.5	12.7	7.4	1.7	0.0	0.0	2.4	7.9	10.4
160	14.5	11.5	6.2	1.2	0.0	0.0	2.6	8.4	11.2
200	12.8	9.8	4.7	.8	0.0	0.0	2.5	8.4	11.6
250	10.8	7.8	3.2	.4	0.0	0.0	2.2	8.0	11.7
315	9.0	5.9	1.9	.1	0.0	0.0	1.9	7.5	11.5
400	7.4	4.3	.9	-.1	0.0	0.0	1.7	7.0	11.2
500	6.3	3.1	.3	-.1	0.0	0.0	1.7	6.6	11.0
630	5.7	2.4	-.1	-.1	0.0	0.0	2.0	6.5	10.9
800	5.5	2.1	-.2	-.1	0.0	0.0	2.4	6.7	11.0
1000	5.5	2.1	-.1	0.0	0.0	0.0	3.0	7.1	11.4
1250	5.5	2.3	-0.0	.1	0.0	0.0	3.4	7.8	11.9
1600	5.4	2.5	.1	.1	0.0	0.0	3.7	8.5	12.5
2000	5.1	2.5	.1	0.0	0.0	0.0	3.8	9.0	13.0
2500	4.4	2.3	.1	0.0	0.0	0.0	3.6	9.2	13.2
3150	3.6	1.8	-0.0	-0.0	0.0	0.0	3.3	8.9	12.9
4000	2.7	1.2	-.1	-.1	0.0	0.0	2.9	8.2	12.1
5000	2.1	.7	-.1	-0.0	0.0	0.0	2.6	7.1	10.8
6300	1.8	.5	0.0	0.0	0.0	0.0	2.6	6.0	9.4
8000	2.1	.8	.1	.1	0.0	0.0	3.0	5.6	8.6
10000	2.0	1.8	-.1	-0.0	0.0	0.0	3.7	6.8	9.7

Above SPL Values to be Subtracted from Maximum Passby Sound Pressure Levels.

TABLE VI-5-III

Typical Noise Time History During Take-off

Aircraft Axial Distance from Brake Release (ft.)	Directivity angle (Degrees)	Time (Seconds)	Perceived Noise Level (DB)	Tone Corrected Perceived Noise Level (DB)
5358.0	10.8	-30.06	84.94	87.53
14967.2	15.0	-11.32	97.87	98.39
17601.7	19.5	-6.44	103.95	103.91
18373.2	24.4	-5.01	95.00	93.92
19145.1	29.2	-3.53	98.37	97.29
19724.1	35.0	-2.38	99.99	98.91
20110.0	40.7	-1.57	103.42	102.34
20496.0	49.0	-.74	105.38	104.30
20689.0	54.6	-.30	105.76	104.68
20882.0	61.4	.14	105.92	104.84
21075.0	69.7	.60	105.58	104.50
21268.0	79.5	1.07	105.66	104.58
21460.9	90.6	1.55	106.69	105.61
21653.9	94.9	2.05	106.71	105.62
21846.9	99.6	2.56	108.13	107.05
22039.9	104.2	3.09	107.98	106.90
22232.9	108.7	3.63	110.73	109.64
22425.9	113.0	4.18	110.44	109.36
22618.9	117.0	4.74	113.46	112.38
23004.8	124.4	5.90	112.66	111.58
23390.8	130.7	7.09	113.52	112.43
23776.8	136.1	8.32	113.48	112.40
24162.8	140.7	9.56	112.53	111.95
24741.7	146.2	11.45	111.12	110.62
25320.7	150.6	13.38	109.78	109.34
26092.6	155.0	15.97	108.10	108.10
27057.5	159.0	19.24	104.12	104.35
28601.4	163.3	24.51	101.47	102.02
31303.3	167.5	33.81	92.38	93.47
39022.7	171.5	60.50	84.90	87.66

EPNL = 111.56 DB
Excess Ground Attenuation = 1.38 DB
Multiengine Shield Factor = 1.08 DB

Observer Station at 21654 ft. from Brake Release and
Sideline position at 2128 ft. from Runway Centerline

*NOTE: Sideline noise is measured where noise level after liftoff is greatest.
**NOTE: Sideline noise is measured where noise level is greatest.

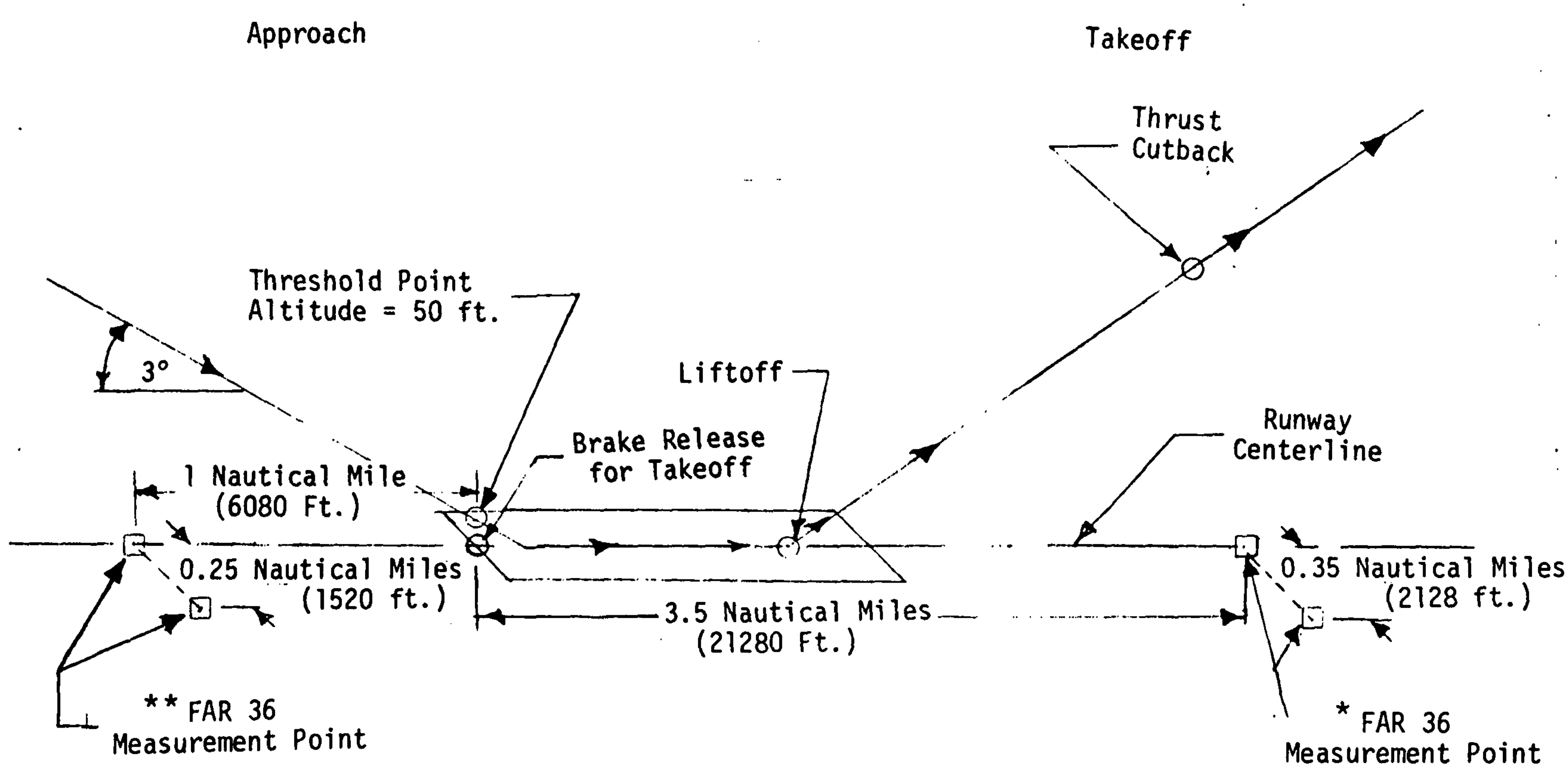

Figure VI-5-1 FAR 36 Noise Measurement Locations for Typical Approach and Takeoff

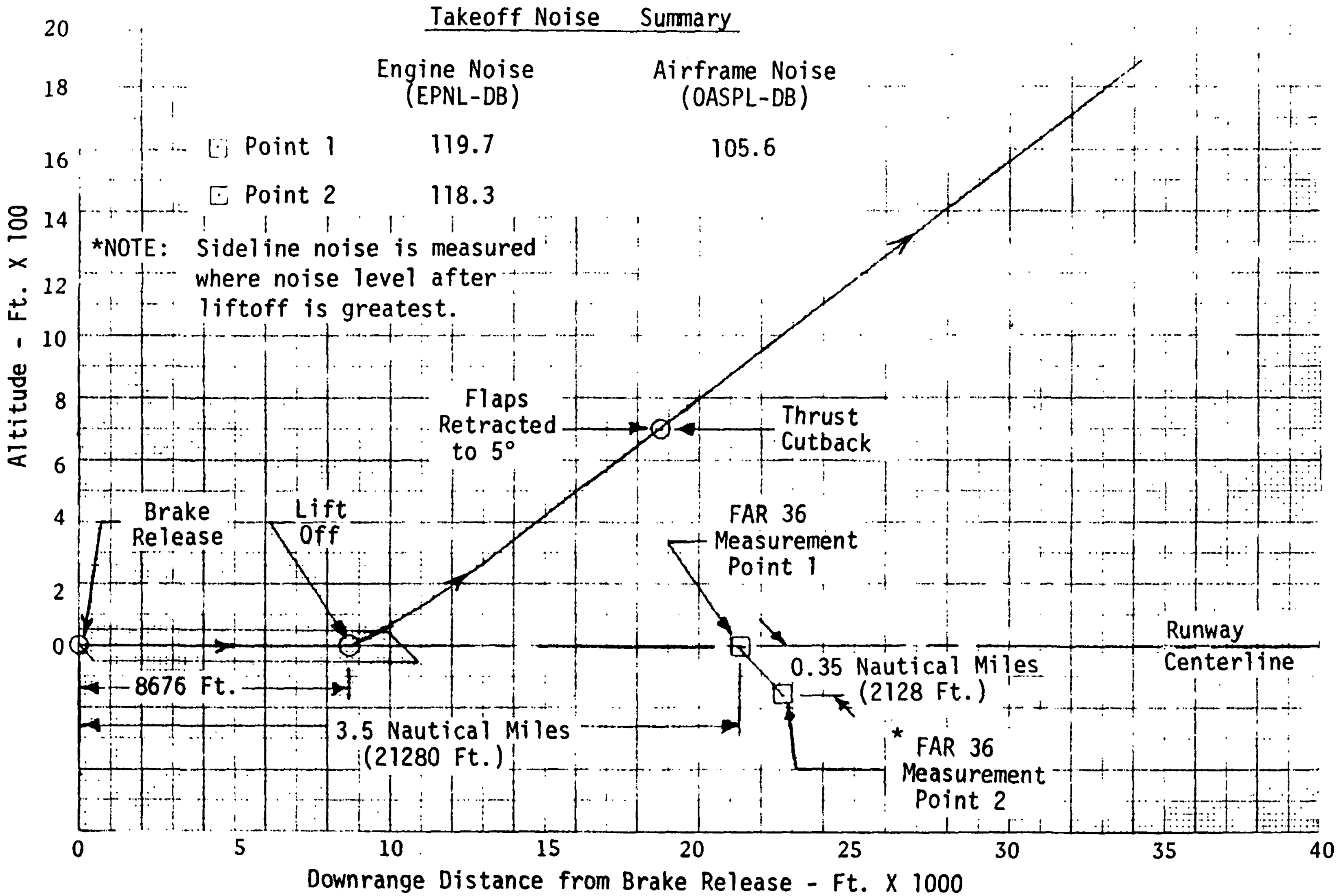

Figure VI-5-2 Reference Configuration Takeoff Profile and Noise Summary

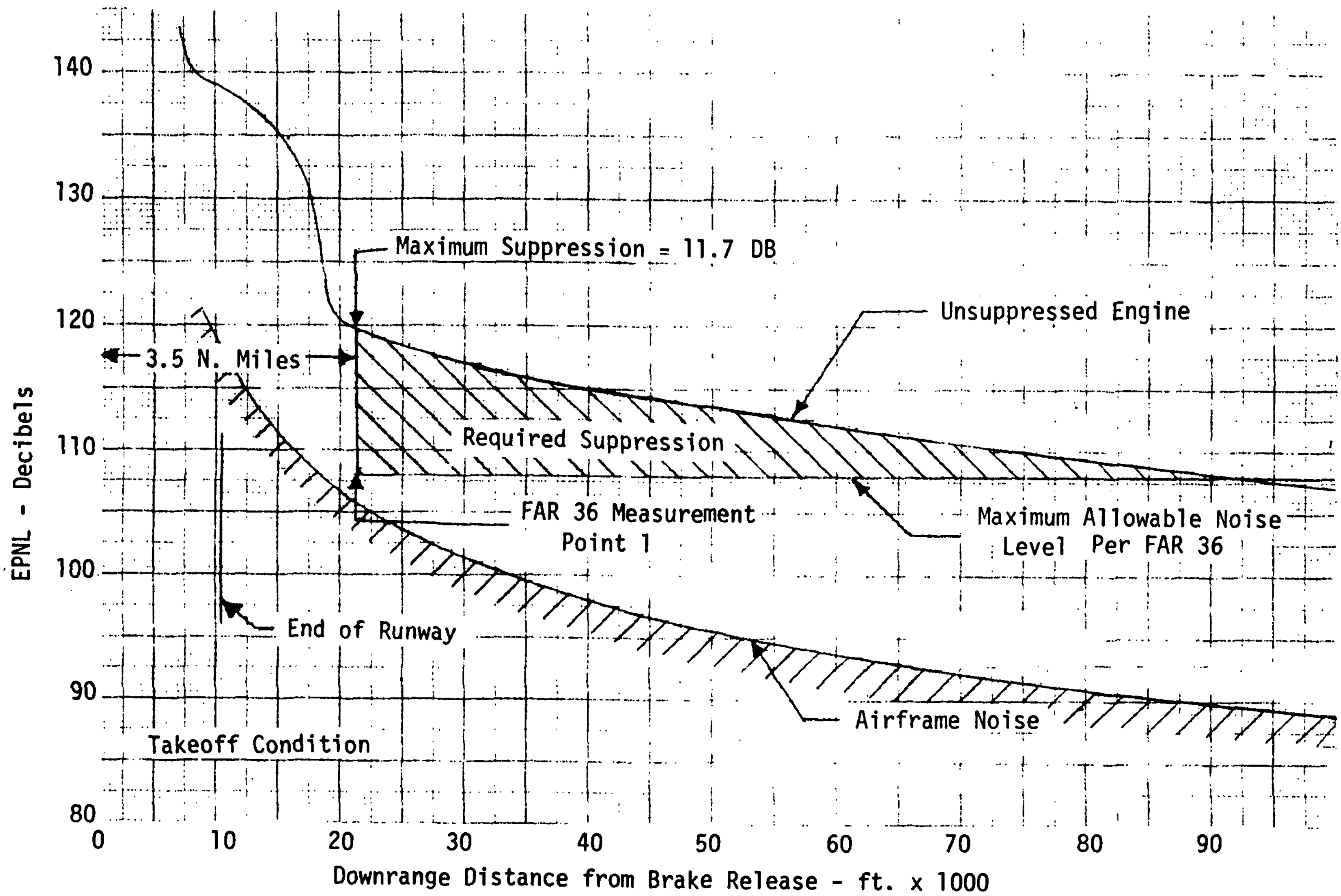

Figure VI-5-3 Variation of EPNL Along Runway Centerline with Downrange Distance

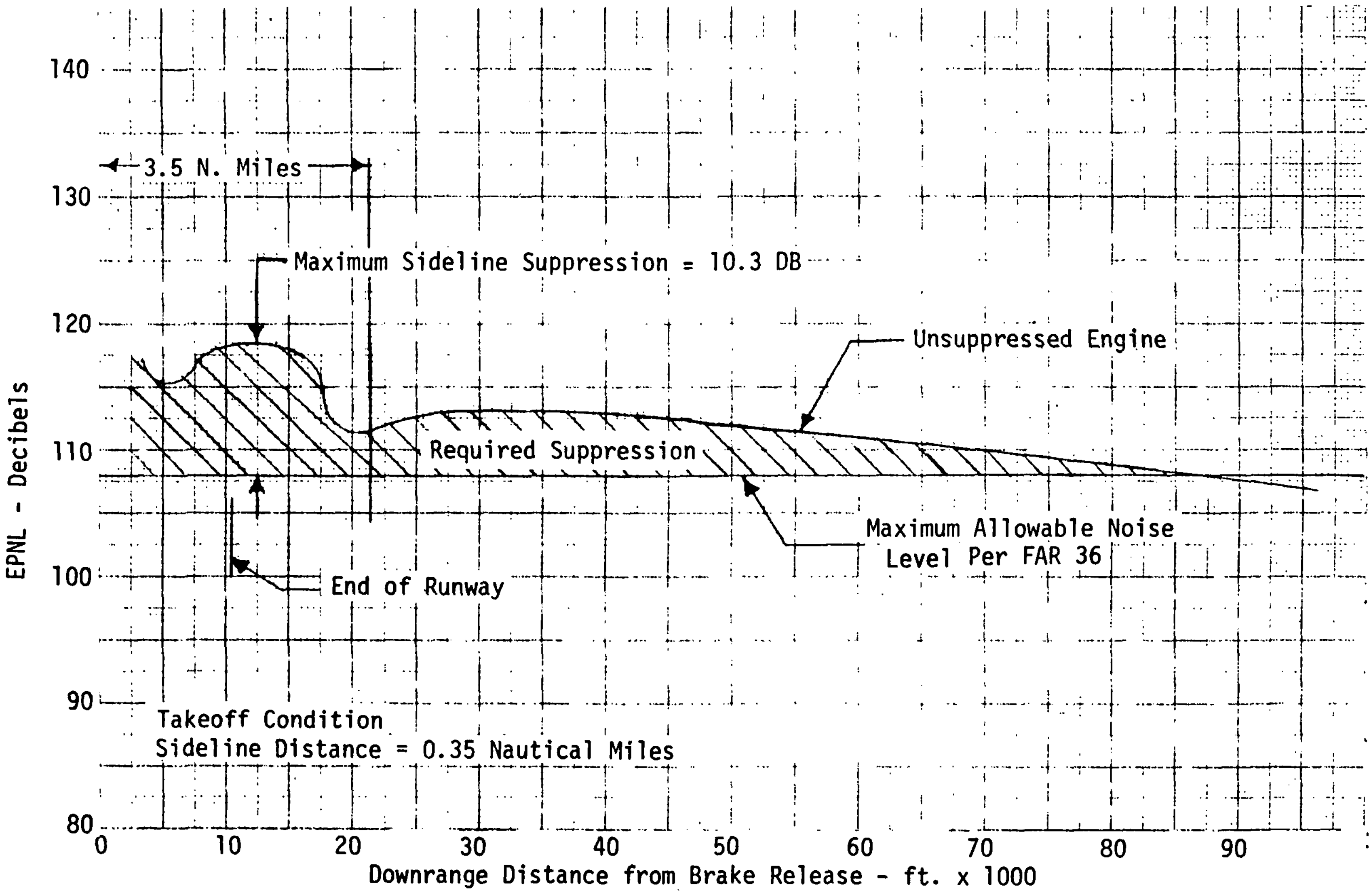

Figure VI-5-4 Variation of EPNL Along Sideline with Downrange Distance

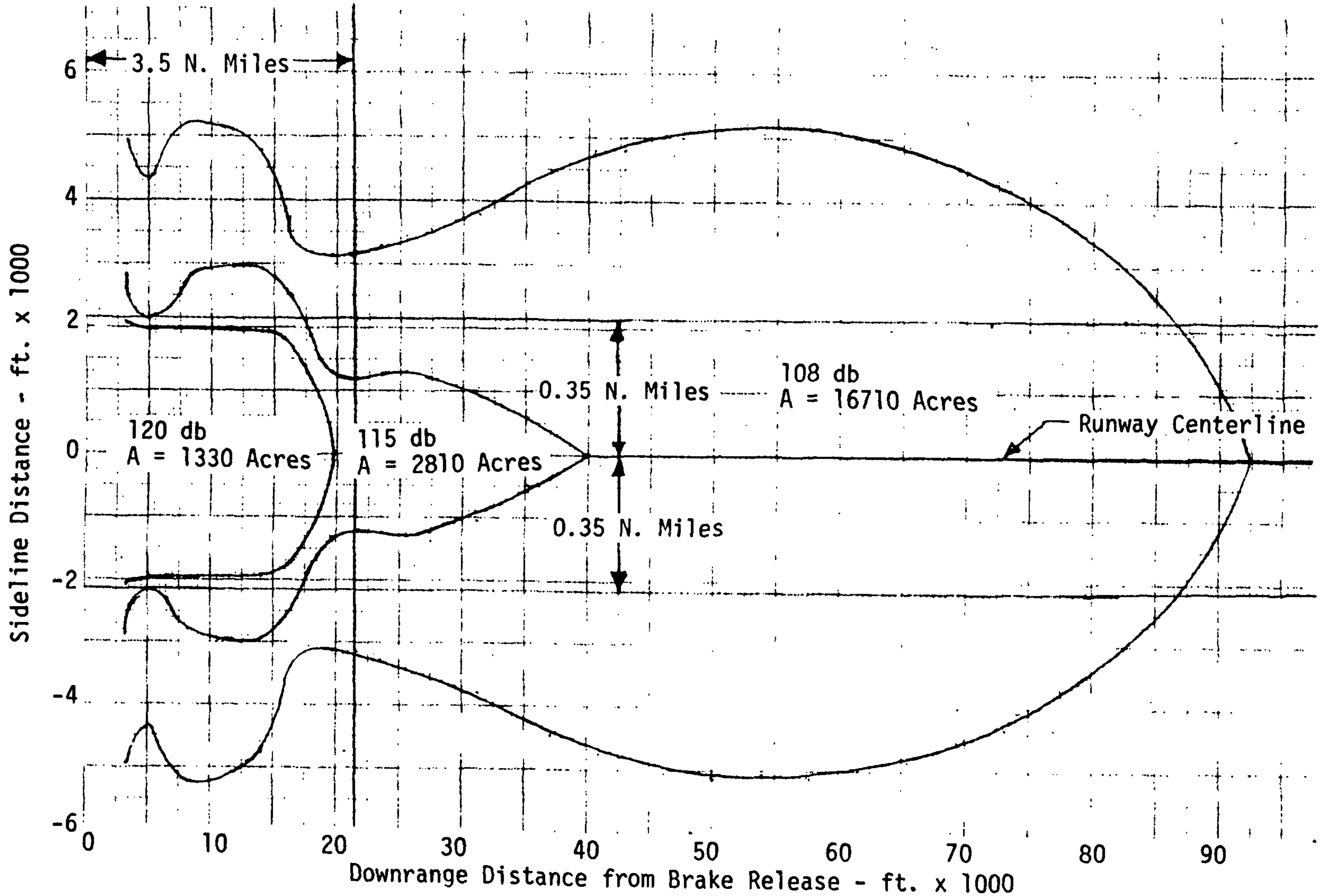

Figure VI-5-5 Contour Plots of Constant EPNL Values for Takeoff with Unsuppressed Engine

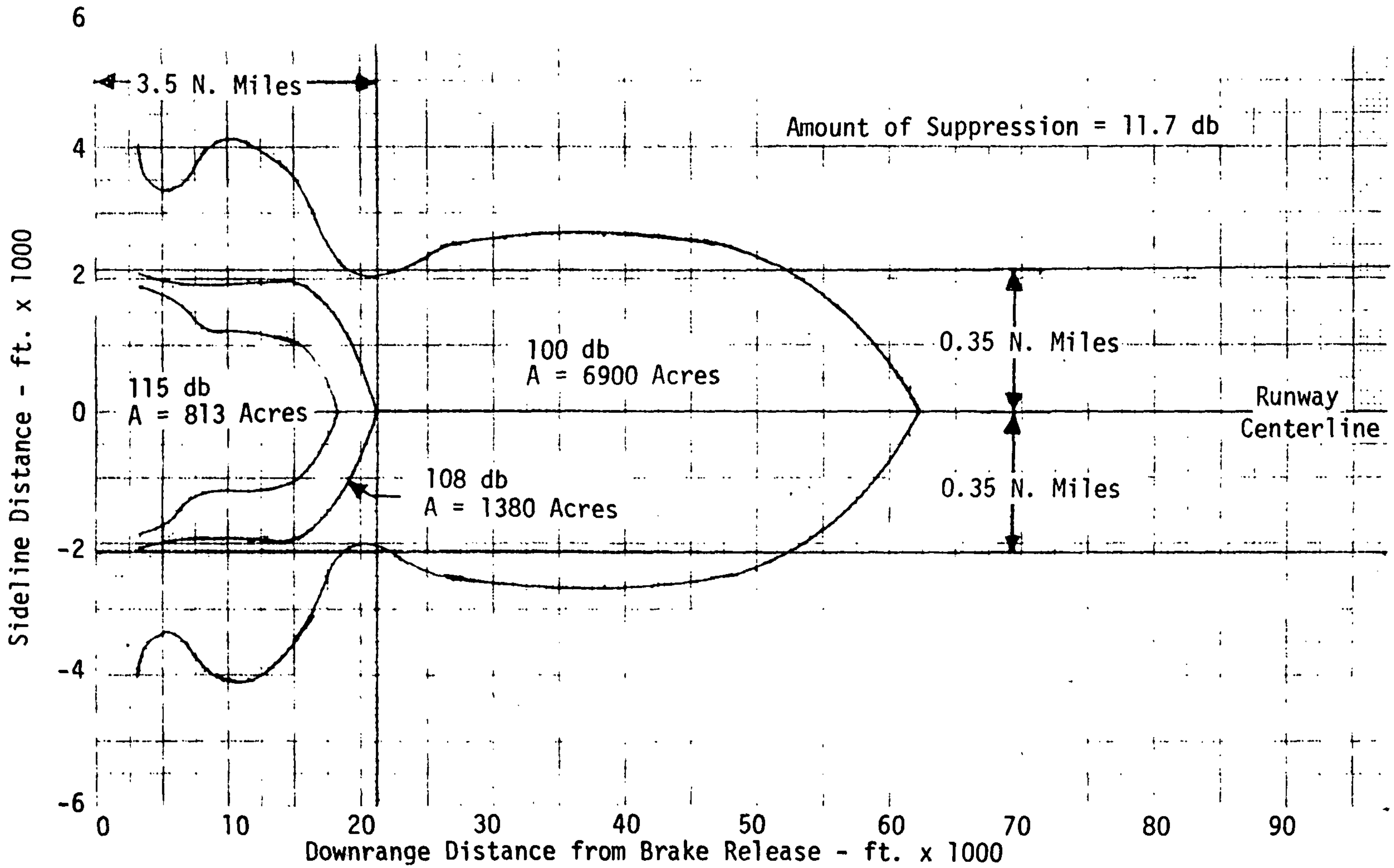

Figure VI-5-6 Contour Plots of Constant EPNL Values for Takeoff with Suppressed Engine

Approach Noise Summary

	Engine Noise (EPNL-DB)	Airframe Noise (OASPL-DB)
Point 1	96.6	107.7
Point 2	83.7	

*NOTE: Sideline noise is measured where noise level is greatest.

Flaps set at 20°

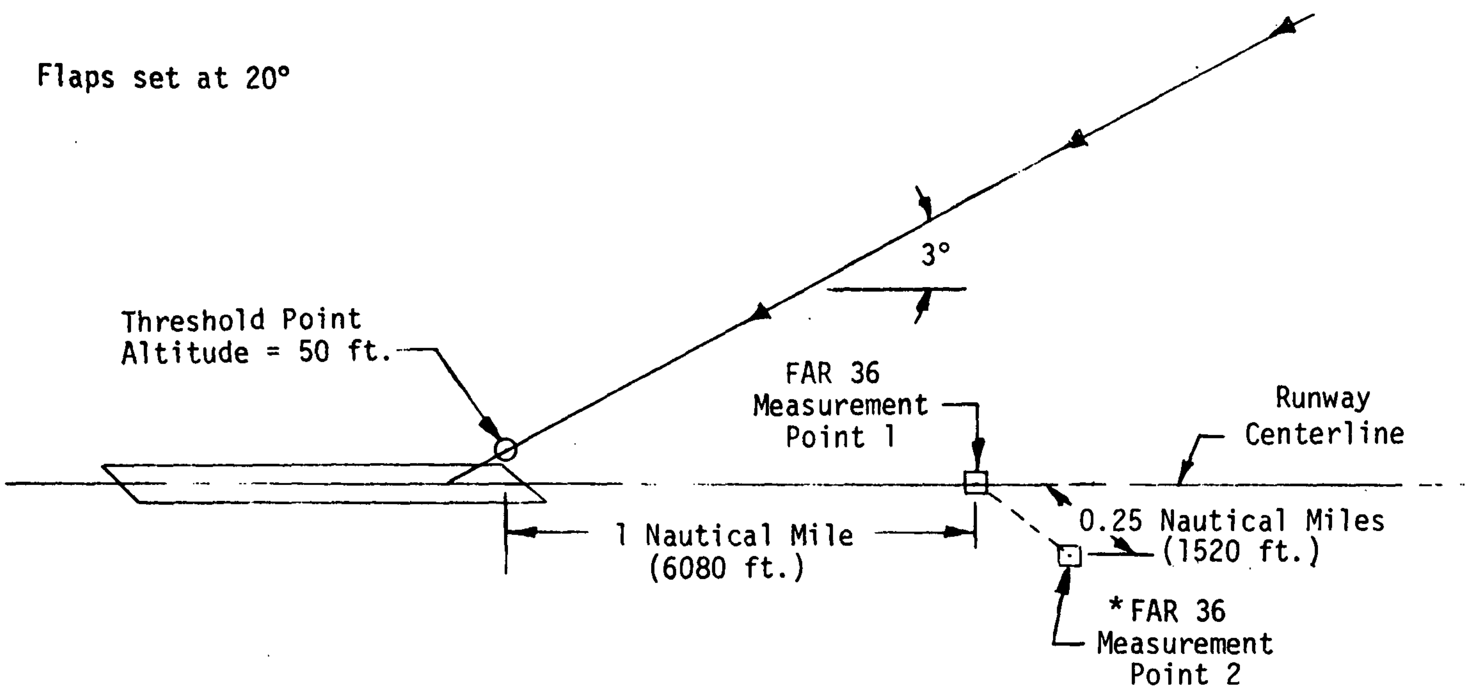

Figure VI-5-7 — Reference Configuration 3° Landing Profile and Approach Noise Summary

VI-6 MISSION ANALYSIS

INTRODUCTION

This section is addressed to the payload/range and take-off performance characteristics of the Reference Configuration.

The Reference Configuration is analyzed for the design supersonic cruise mission and take-off performance. Following this is an analysis of alternate missions (New York to Los Angeles - New York to Paris), special missions (ranges of 1500 to 3500 n.mi. in 500 n.mi. increments) and an overload mission (limited by flotation requirements).

The airplane design performance objectives were a range of approximately 4000 nautical miles at 2.7 cruise Mach number with 61,030 pounds (292 passengers with baggage) payload and a take-off field length not to exceed 10,500 feet with an acceptable noise level during normal all engine take-off (FAR 36). The range performance of the Reference Configuration is based upon the fuel reserves established by FAR 121,648 modified for holding altitude. The mission profile for this study is shown on Figure VI-6-1.

The aerodynamic, power plant, and weight data that were used in the performance analysis are presented in Sections VI-1, VI-3, and VI-4.

SUMMARY

The analysis shows that noise considerations determine the engine size and subsequently the aircraft gross weight. The requirement for acceptable noise

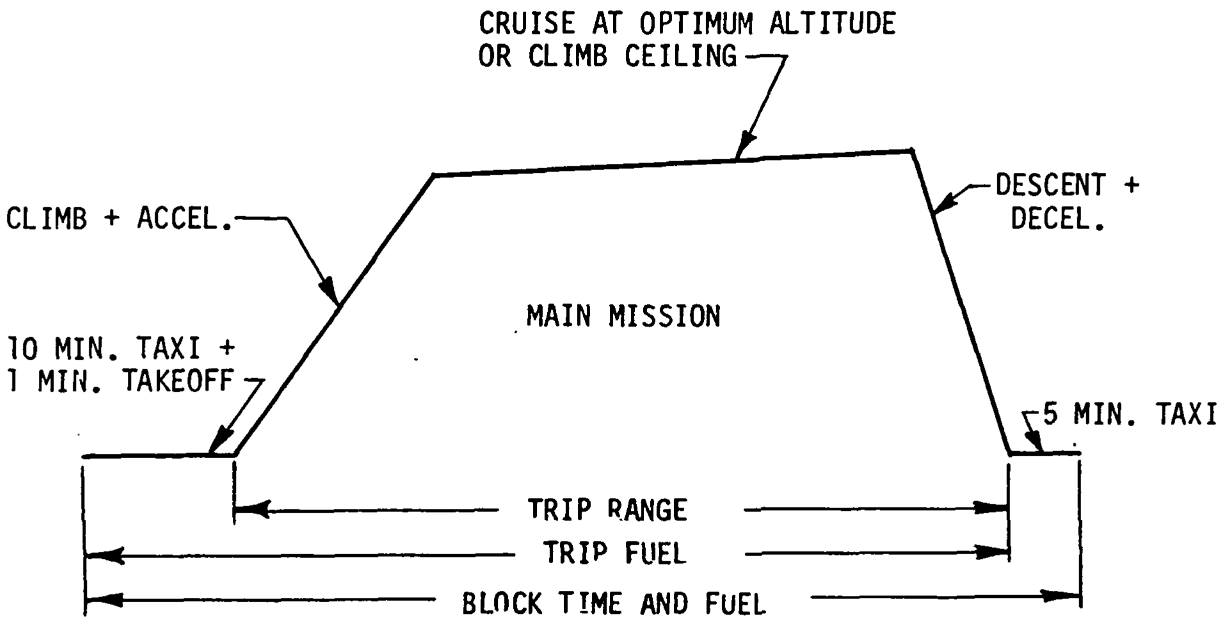

NOTE: C.A.B. RANGE = TRIP RANGE MINUS TRAFFIC ALLOWANCE AS SPECIFIED FOR SUPERSONIC AIRCRAFT

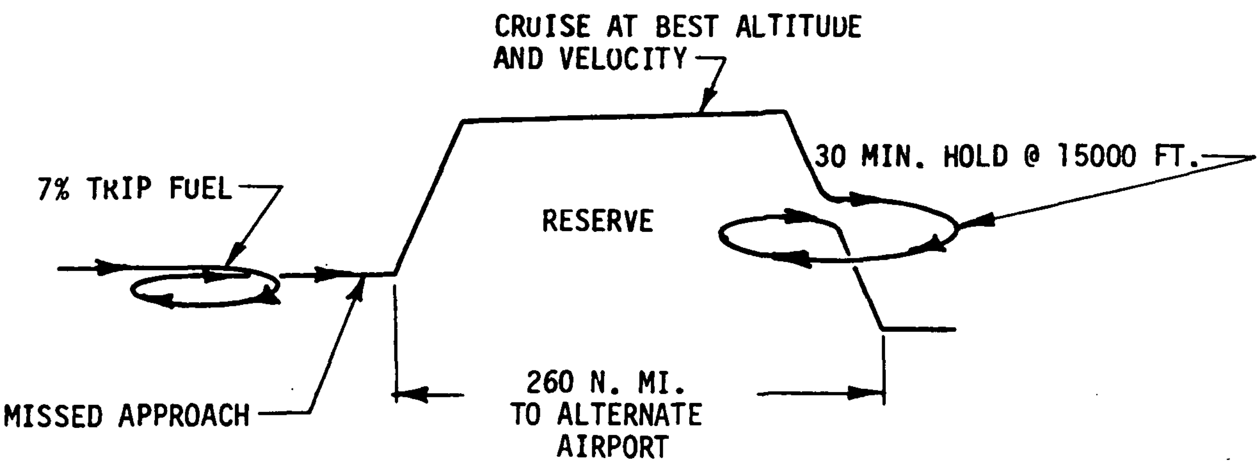

Figure VI-6-1 - Mission Profile and Reserves levels during take-off resulted in larger propulsion units than necessary for take-off within the prescribed field length or to fly the design mission. The design gross weight take-off mission performance analysis results are shown in Table VI-6-I and Figure VI-6-2 including an all-subsonic mission and a mixed mission, for the Reference Configuration with initial characteristics as follows:

Take-off gross weight	762,000 lbs.
Operating weight empty	351,140 lbs.
Payload (292 passengers)	61,030 lbs.
Engine-airflow	800 lbs/sec/eng.
S.L. static installed thrust on standard day	77,610 lbs/eng

Take-off Field Length Performance

FAR 25 Safety Requirements

Balanced field length on standard +8°C day with 3 engines at full thrust	7500 ft.
Take-off distance on standard +8°C day with all engines at full thrust	6600 ft.

FAR 36 Noise Requirements

Balanced field length part power (2400 ft/sec exhaust velocity)	10500 ft.

The alternate mission performance results, obtained by off loading fuel, for a New York to Los Angeles and a New York to Paris mission are summarized in Table VI-6-II.

Procedures and Ground Rules

An "en route" performance computer program developed by NASA Langley Research Center was used to determine the aircraft weight and fuel required for the design range. This program computes range based on the following major inputs:

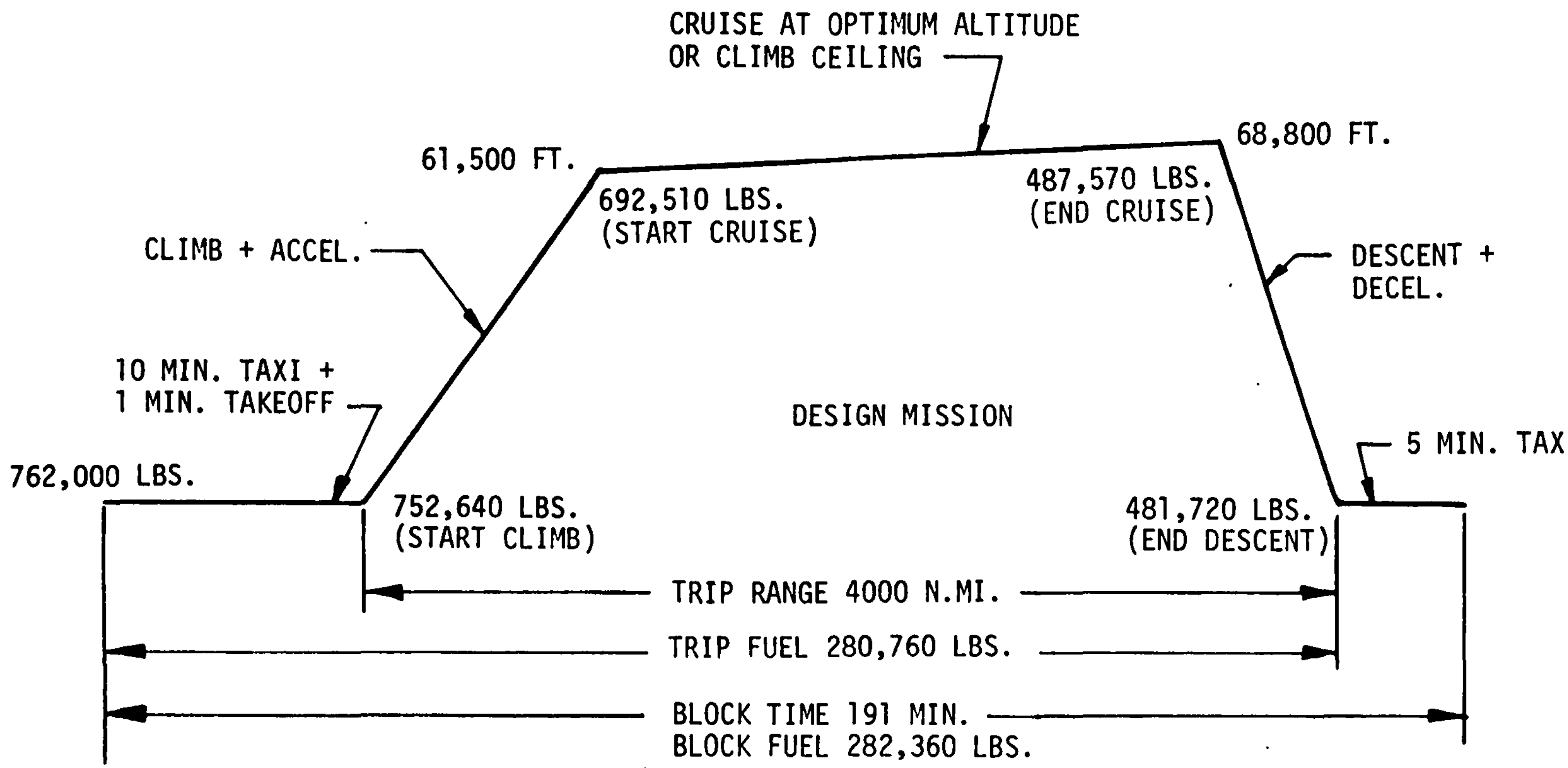

NOTE: C.A.B. RANGE = TRIP RANGE MINUS TRAFFIC ALLOWANCE AS SPECIFIED FOR SUPERSONIC AIRCRAFT

FIGURE VI-6-2 - DESIGN MISSION PERFORMANCE PROFILE

TABLE VI-6-I

PERFORMANCE SUMMARY

DESIGN GROSS WEIGHT MISSION (762,000 LBS.)

Characteristic	Supersonic Cruise Standard Day	Supersonic Cruise Hot Day (Std.Day+8°C)	Subsonic Cruise Standard Day	Subsonic Cruise Hot Day (Std.Day+8°C)	*Mixed Mission[1] Standard Day
1. Mach No.	2.70	2.62	.95	.95	2.70/.95
2. Range - N. Mi.	4000	3930	3360	3350	2000/2820
3. Initial Values					
a.[2] L/D	8.57	8.65	12.50	12.50	8.56/12.50
b. TSFC - lbs/hr/lb	1.312	1.330	.891	.909	1.310/.865
c. Altitude - ft.	61,500	60,500	28,500	28,500	61,000/33,500

*NOTE: 1. The mixed mission of supersonic and subsonic is identified as a supersonic cruise to mid-point of an all supersonic cruise mission then a subsonic mission completion utilizing all reserve fuel.

2. The L/D shown includes the propulsion drag shown in Section VI-1B, Figure VI-1B-15. (See also Section VI-3)

TABLE VI-6-II

PERFORMANCE SUMMARY

ALTERNATE MISSIONS (FUEL OFF-LOADED)

Characteristic	New York-Los Angeles Subsonic Cruise Standard Day	New York-Paris Supersonic Cruise Standard Day
1. Mach No.	.95	2.7
2. Range - N. Mi.	2150	3158
3. Take-Off Gross Weight	643500	696500
4. Initial Values		
a.[1] L/D	12.51	8.53
b. TSFC - lbs/hr/lb	.870	1.314
c. Altitude - ft.	32,500	63,500

NOTE: 1. The L/D shown includes the propulsion drag shown in Section VI-1B, Figure VI-1B-15. (See also Section VI-3)

°Desired mission profile and fuel reserve schedule

°Aircraft gross weight and operating weight empty

°Payload

°Aerodynamic polar

°Engine performance

The program also provides details of each of the mission segments such as required fuel, thrust, altitude, speed and time. The mission profile selected for this study is presented in Figure VI-6-1 and consists of the following segments:

1. A take-off fuel allowance of ten minutes taxi plus one minute at full take-off thrust, no credit for distance.
2. Climb and accelerate according to the speed schedule shown in Figure VI-6-3. The program automatically determines optimum initial cruise altitude for maximum range except when available thrust prevents the aircraft from reaching that height (climb ceiling).
3. The cruise is started at either optimum altitude or climb ceiling. The program then assumes that the range factor remains constant over the entire cruise range.
4. The program does not calculate descent but accepts estimated inputs of descent distance, time and fuel. In this study 200 n.mi. and 20 minutes were selected for the first two inputs. A fuel estimate was made based on 20 minutes idle flow at average descent altitude and speed.

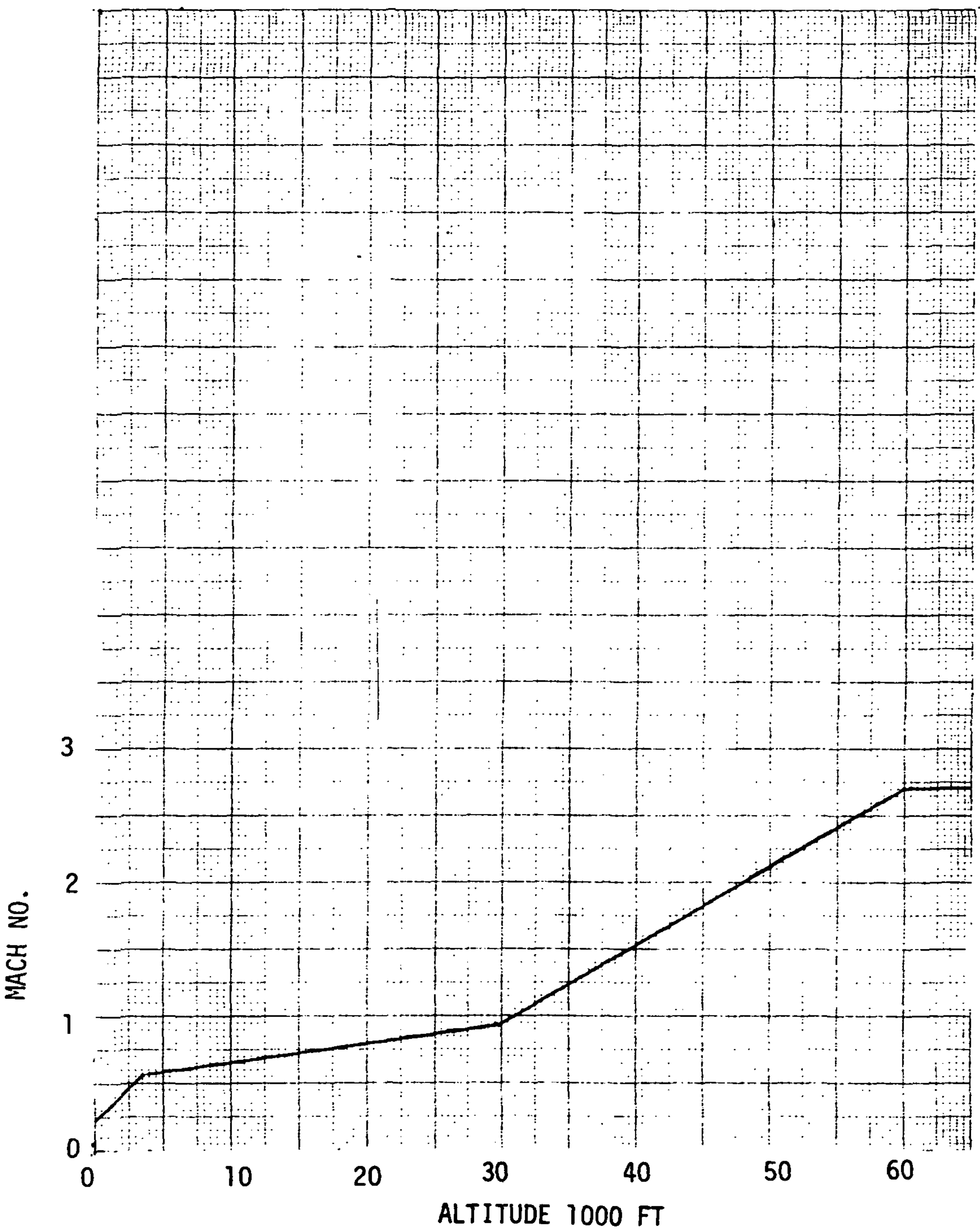

Figure VI-6-3- Climb Speed Schedule

Reserve Fuel Definition

The total reserve fuel consists of the following items:

1. 7% of trip fuel
2. Fuel for a missed approach, equivalent to two minutes take-off fuel flow.
3. Fuel for a 260 n.mi. (300 s.mi.) flight to an alternate airport at optimum (subsonic) speed and altitude.
4. 30 minutes holding fuel at 15,000 ft. and optimum velocity.

Payload/Range Performance

A breakdown of the design mission details are shown in Table VI-6-III. The effects of the following parameters on the design mission and the aircraft and powerplant size were investigated:

Thrust to Weight Ratio (engine sizing)

If noise is not taken into consideration as a criterion, the minimum powerplant size on an aircraft is determined by any of the following items:

a. Take-off within a specified field length
b. Safety rules during take-off such as balanced field length and climb capability with an inoperative engine
c. Climb ceiling which could prevent the aircraft from reaching the optimum cruise altitude
d. Acceleration to desired speed, in particular through the transonic region
e. Cruise efficiency (lowest fuel consumption)

f. Deterioration of engine performance due to above normal ambient temperatures, high power extraction or airbleed from the engine (e.g. surface blowing) etc.

g. Safety regulations during landing (climb capability with an inoperative engine)

Without noise restrictions a maximum range (or minimum gross weight for a given range) was obtained for this Reference Configuration, at an installed thrust to weight ratio of approximately .32 (engine airflow = 630 lbs/sec). This T/W value is defined as maximum standard day installed static take-off thrust over take-off gross weight.

However, inclusion of the noise as a parameter in the engine sizing increased the installed thrust to weight ratio to .41, which required a powerplant with an airflow of 800 lbs/sec/eng.

Hot Day

Standard atmospheric conditions were specified for the design mission. The effect on the range of an ambient temperature increase to 8°C above standard was investigated. For a cruise Mach no. of 2.7 the higher temperature resulted in a 75 n.mi. or approximately 1.9% range penalty. If limitations due to aerodynamic heating require decrease in cruise Mach number to 2.62, the analysis showed approximately the same range reduction as at M=2.7.

Holding Altitude

Current (FAR) reserve fuel regulations for international flight include a requirement for 30 minutes holding at 1500 ft altitude. The effect of an increase in this altitude to 15,000 ft was investigated. The result showed a 46 n.mi. range increase or about a 1% gain. During the holding the airplane flies at minimum drag. The minimum drag value did not change with altitude although it occurred at a higher velocity. The 1% range extension is therefore due to a 15% reduction in fuel flow at 15,000 ft.

Type of Powerplant

The design mission performance of the Reference Configuration is based on engines with variable turbine geometry. This type of powerplant showed approximately one percent improvement in the range of the design mission compared to conventional engines.

Since the variable geometry powerplants operate more efficiently in terms of fuel consumption when power is reduced, the range gain increased to 9 1/2% for an all subsonic mission at M=.80. However, possible weight differences were not considered in the comparison between the two types and could negate a portion of the range difference. The major advantage of the variable geometry engine is discussed in the noise section.

All Subsonic Mission

Completely subsonic missions were performed with the Reference Configuration at cruise speeds of M=.80 and M=.95. The same reserve fuel allowance was maintained as in the design (supersonic) mission. The range results were 3220 n.mi. at M=.8 and 3360 n.mi. at M=.95. Details of these subsonic flights are shown in Tables VI-6-IV and VI-6-V.

Supersonic/Subsonic Mission

The range capability of the Reference Configuration was investigated for an initially supersonic (M=2.7) flight that had to be continued subsonically. The selected mission profile included a supersonic distance equal one-half the design range (2000 n.mi.) and no reserves, except for 2000 lbs landing fuel. Thus it was assumed that the remaining cruise fuel plus the reserves were used for the subsonic continuation of the flight. The overall range was 4660 n.mi. for a subsonic speed of M=.80 and 4820 n.mi. at M=.95. Details of this mission are shown in Table VI-6-VI.

Take-Off

A computer program developed by LTV Hampton Technical Center was used in the study of the Reference Configuration take-off performance. This program determines the balanced field length with an inoperative engine and the normal all engine take-off distance. In addition, a time history is printed of the parameters that determine noise.

The Tentative Airworthiness Standards for supersonic Transports were followed as closely as practical in the evaluation of the study configuration take-off performance to satisfy the safety requirements. Certain regulations were not considered at this time due to the unavailability of related data at this preliminary stage of aircraft development. One of the major differences between the SST standards and the conventional aircraft safety regulations, FAR 25, is related to the lack of a definable wing stall on most supersonic configurations. The angle of attack at which stall occurs is so large that the drag would arrest the aircraft speed and consequently cause a loss in lift making 1 g flight unattainable before the stall attitude is reached. The flight regions that become critical instead are those where stability and/or control deteriorates and where drag starts to exceed available thrust resulting in the inability to maintain level flight.

To cover these two conditions, the tentative standards in paragraphs FAR 25.103 (B) and (C) define a "minimum demonstrated flight speed" (V_{min}) or a "maximum demonstrated angle of attack" and a "zero rate of climb speed" (V_{zrc}). In this study the V_{zrc} was found to be more critical than V_{min}.

The take-off performance of the study aircraft had to meet both safety and noise standards. The maximum acceptable take-off field length was set at 10,500 ft. The Reference Configuration with powerplants sized by noise considerations but with these engines at full throttle, needed approximately 7500 ft. for a balanced field length (with one engine inoperative) and 6600 ft. for an all engine take-off distance on a standard +8°C day. However, for noise abatement the normal all engine take-off had to be performed at a part throttle setting corresponding to a 2400 ft/sec jet velocity and at a standard day plus 10°C temperature.

Various take-off and climbout profiles were flown with flap changes and power cutbacks at different altitudes. (It should be noted that present day noise regulations FAR 36 do not permit any alterations of the aircraft configuration.) Noise requirements made it necessary to utilize the available 10,500 ft. field length. This allows the aircraft to accelerate more and consequently achieve a higher L/D in the climb.

The equation for available climb gradient in unaccelerated flight is as follows: $\text{Tangent}\,\gamma = \frac{\text{THRUST - DRAG}}{\text{GROSS WEIGHT}}$

If the excess thrust over drag is not entirely used for climbing, the airplane will also accelerate.

Since aerodynamic lift during the climb is nearly equal gross weight, it is possible to re-arrange the above: $\text{Tangent}\,\gamma = \frac{T}{W} - \frac{1}{L/D}$

It can be seen that for a higher value of L/D a steeper climb is obtained for a given thrust or that a lower thrust is required to maintain the same climb gradient. Both effects are beneficial for noise abatement.

The Reference Configuration at 762,000 lbs. take-off gross weight and a maximum ground rotation lift coefficient of .648 (20° flaps) could lift-off at 190 kts. However, Figure VI-6-4 shows that lower C_L values (and corresponding higher speeds) are required to achieve maximum L/D.

Alternate Missions

Two alternate missions were analyzed to determine the effect of off-loading fuel on the performance characteristics of the Reference Configuration. The alternate missions selected were New York to Los Angeles and New York to Paris. The mission range for these are 2150 and 3158 nautical miles respectively. The New York-Los Angeles mission performance is based on a subsonic cruise .95 Mach number while the New York to Paris is based on a supersonic cruise 2.7 Mach number. The Reference Configuration performance characteristics are shown in Tables VI-6-VII and VI-6-VIII.

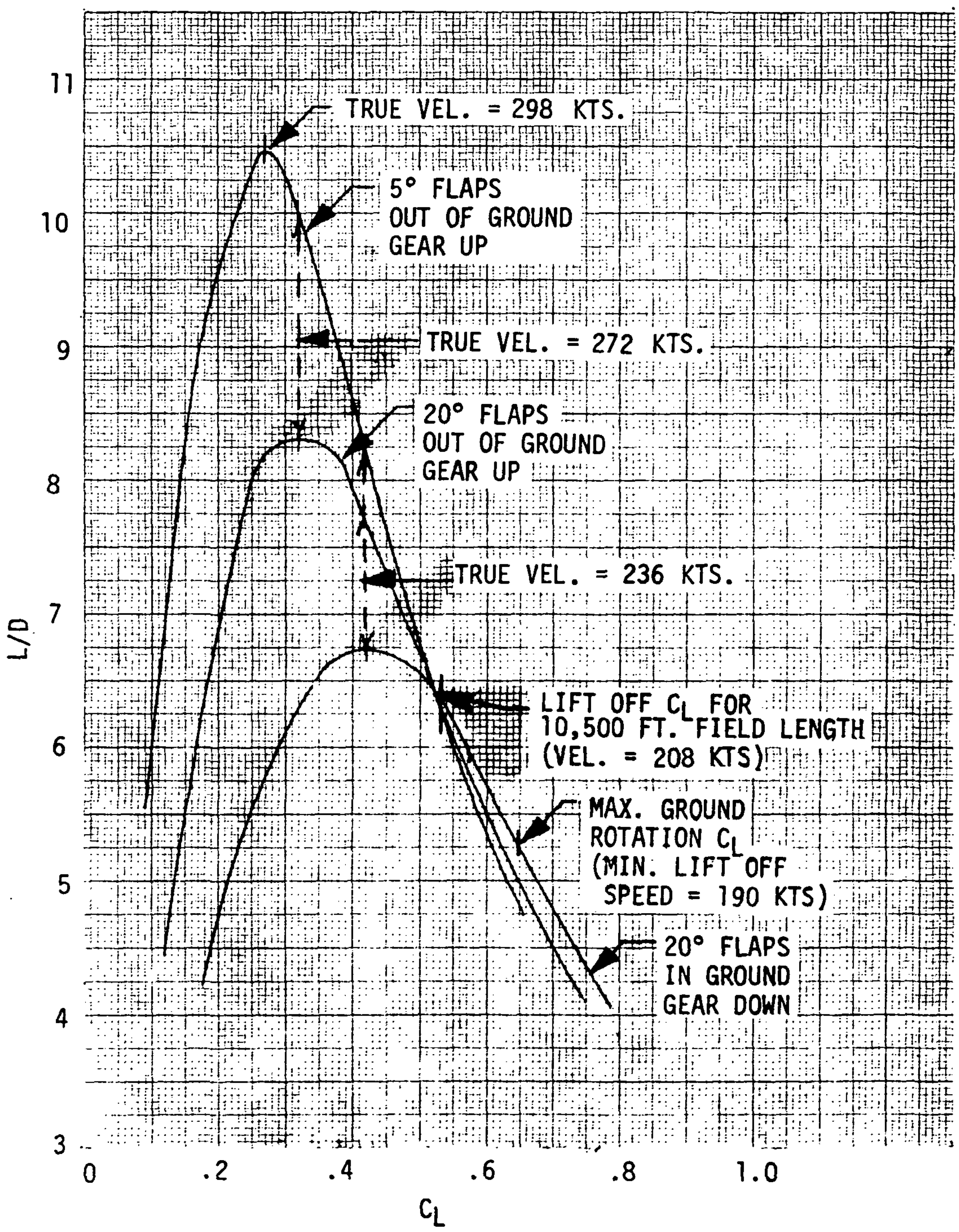

Figure VI-6-4 - Take off Lift to Drag Ratio vs. Lift Coeff.

Special Missions

A spectrum of mission ranges at supersonic cruise 2.7 Mach number were analyzed for performance characteristics to provide a basis on which to establish relative DOC values. The range of these missions are from 1500 nautical miles to 3500 nautical miles at 500 nautical mile increments. The mission profile used is that shown in Figure VI-6-1 and maintaining the same fuel reserves. Fuel is then off-loaded to that necessary to attain the selected range. The performance characteristics associated with the resultant gross weights are shown in Tables VI-6-IX thru VI-6-XIII.

Overload Mission

The overload mission was analyzed based on a gross weight limited by the flotation capability of the Boeing 969-336C/750,000 pound gross weight version. The flotation of the Reference Configuration with the landing gear and wheel arrangement shown in Figure V-5 was established to be within the range of the 969-336C when at a gross weight of 870,000 pounds. No structural increases are included and it was assumed that the airplane would operate under reduced flight load conditions. The increase to 870,000 pounds was provided by adding 108,000 pounds of fuel. This would provide a range of 5220 nautical miles for the Reference Configuration. The performance characteristics associated with this mission are shown in Table VI-6-XIV.

LIST OF FIGURES

LIST OF TABLES

LIST OF TABLES (Continued)

TABLE VI-6-III

MISSION PERFORMANCE

MISSION: DESIGN SUPERSONIC CRUISE MACH 2.7

Model No. REFERENCE CONFIGURATION

Aircraft Characteristics

Take off gross weight - lbs.	762,000
Operating weight empty - lbs.	351,140
Payload - No. passengers	292
Lbs. - cargo	0
Total weight - lbs.	61,030
Wing area - ft^2 - reference	9,969
- actual	10,996
S.L. static thrust per engine - lbs.	77,610
Initial thrust to weight ratio	.41
Initial wing loading - lbs/ft^2 - reference	76.4
- actual	69.3

Design Mission

	Operating Weight(lbs.)	ΔFuel lbs.	ΔRange N.Mi.	ΔTime min.
Take off	762,000			
		9,360	0	11
Start climb	752,640			
		60,130	254	17
Start cruise	692,510			
		204,940	3,549	138
End Cruise	487,570			
		5,850	200	20
End descent	481,720			
Taxi-in		2,080	0	5
Block fuel and time		282,360		191
Trip range			4,003	

NOTES: 1. Taxi-in fuel taken out of reserves on landing at destination.

2. C.A.B. range corresponding to block time and fuel equals trip range minus traffic allowances as will be specified for supersonic aircraft.

TABLE VI-6-III

MISSION PERFORMANCE (Continued)

Model No. REFERENCE CONFIGURATION

Reserve Fuel Breakdown:

1.	7% Trip fuel	19,620
2.	Missed approach	10,420
3.	260 N. Mi. to alternate airport	24,550
4.	30 min. holding at 15,000 feet	14,960
	Total Reserve	69,550

Initial Cruise Conditions:

Lift Coefficient	.09683
Drag Coefficient	.01129
Lift/Drag	8.57
TSFC - lbs/hr/lb	1.312
Altitude - ft.	61,500

TABLE VI-6-IV

MISSION PERFORMANCE

MISSION: ALL SUBSONIC DESIGN MISSION MACH .80

Model No. REFERENCE CONFIGURATION

Aircraft Characteristics

Take off gross weight - lbs.	762,000
Operating weight empty - lbs.	351,140
Payload - No. passengers	292
Lbs. - cargo	0
Total weight - lbs.	61,030
Wing area - ft^2 - reference	9,969
- actual	10,996
S.L. static thrust per engine - lbs.	77,610
Initial thrust to weight ratio	.41
Initial wing loading - lbs/ft^2 - reference	76.4
- actual	69.3

Design Mission

	Operating Weight(lbs.)	ΔFuel lbs.	ΔRange N.Mi.	ΔTime min.
Take off	762,000			
		9,360	0	11
Start climb	752,640			
		18,520	23	4
Start cruise	734,120			
		249,900	3,117	383
End cruise	484,220			
		2,510	75	8
End descent	481,710			
Taxi-in		2,080	0	5
Block fuel and time		282,370		411
Trip range			3,215	

NOTES: 1. Taxi-in fuel taken out of reserves on landing at destination.

2. C.A.B. range corresponding to block time and fuel equals trip range minus traffic allowances as will be specified for supersonic aircraft.

TABLE VI-6-IV

MISSION PERFORMANCE (Continued)

Model No. REFERENCE CONFIGURATION

Reserve fuel Breakdown:

1.	7% trip fuel	19,620
2.	Missed approach	10,420
3.	260 N. Mi. to alternate airport	24,540
4.	30 min. holding at 15,000 feet	14,960
	Total Reserve	69,540

Initial Cruise Conditions:

Lift Coefficient	.17989
Drag Coefficient	.01343
Lift/Drag	13.39
TSFC - lbs/hr/lb	.872
Altitude - ft.	21,500

TABLE VI-6-V

MISSION PERFORMANCE

MISSION: ALL SUBSONIC DESIGN MISSION MACH .95

Model No. REFERENCE CONFIGURATION

Aircraft Characteristics

Take off gross weight - lbs.	762,000
Operating weight empty - lbs.	351,140
Payload - No. passengers	292
Lbs. - cargo	0
Total weight - lbs.	61,030
Wing area - ft^2 - reference	9,969
- actual	10,996
S.L. static thrust per engine - lbs.	77,610
Initial thrust to weight ratio	.41
Initial wing loading - lbs/ft^2 - reference	76.4
- actual	69.3

Design Mission

	Operating Weight(lbs.)	ΔFuel lbs.	ΔRange N.Mi.	ΔTime min.
Take off	762,000			
		9,360	0	11
Start climb	752,640			
		22,810	33	5
Start cruise	729,830			
		244,980	3,231	344
End cruise	484,850			
		3,140	95	10
End descent	481,710			
Taxi-in		2,080	0	5
Block fuel and time		282,370		375
Trip Range			3,359	

NOTES: 1. Taxi-in fuel taken out of reserves on landing at destination.

2. C.A.B. range corresponding to block time and fuel equals trip range minus traffic allowances as will be specified for supersonic aircraft.

TABLE VI-6-V

MISSION PERFORMANCE (Continued)

Model No. REFERENCE CONFIGURATION

Reserve Fuel Breakdown:

1.	7% trip fuel	19,620
2.	Missed approach	10,420
3.	260 N. Mi. to alternate airport	24,540
4.	30 min. holding at 15,000 feet	14,960
	Total Reserve	69,540

Initial Cruise Conditions:

Lift Coefficient	.17200
Drag Coefficient	.01376
Lift/Drag	12.50
TSFC - lbs/hr/lb	.891
Altitude - ft.	28,500

TABLE VI-6-VI

MISSION PERFORMANCE

MISSION: MIXED SUPERSONIC/SUBSONIC MISSION

Model No. REFERENCE CONFIGURATION

Aircraft Characteristics

Take off gross weight - lbs.	762,000
Operating weight empty - lbs.	351,140
Payload - No. passengers	292
Lbs. - cargo	0
Total weight - lbs.	61,030
Wing area - ft^2 - reference	9,969
- actual	10,996
S.L. static thrust per engine - lbs.	77,610
Initial thrust to weight ratio	.41
Initial wing loading - lbs/ft^2 - reference	76.4
- actual	69.3

Design Mission

	Operating Weight(lbs.)	ΔFuel lbs.	ΔRange N.Mi.	ΔTime min.
Take off	762,000			
		9,360	0	11
Start climb (61,000 ft.)	752,640			
		59,970	253	17
Start supersonic cruise (M=2.7)	692,670			
		109,950	1,747	68
End Supersonic cruise	582,720			
		2,950	100	10
End descent to subsonic cruise alt. 33,500 ft. (= start subsonic cruise at M=.95)	579,770			
		162,700	2,622	285
End subsonic cruise	417,070			
		2,900	100	10
End des ent to sea level	414,170			
		2,000	0	5
End mission	412,170			
Block fuel and time		349,830		406
Trip range			4,822	

NOTE: All reserve fuel expended.

TABLE VI-6-VII

MISSION PERFORMANCE

MISSION: ALL SUBSONIC CRUISE (M=.95) NEW YORK TO LOS ANGELES

Model No. REFERENCE CONFIGURATION

Aircraft Characteristics

Take off gross weight - lbs.	643,500 (fuel off loaded)
Operating weight empty - lbs.	351,140
Payload - No. passengers	292
Lbs. - cargo	0
Total weight - lbs.	61,030
Wing area - ft^2 - reference	9,969
- actual	10,996
S.L. static thrust per engine - lbs.	77,610
Initial thrust to weight ratio	.48
Initial wing loading - lbs/ft^2 - reference	64.6
- actual	58.5

Design Mission

	Operating Weight(lbs.)	ΔFuel lbs.	ΔRange N. Mi.	ΔTime min.
Take off	643,500			
		9,360	0	11
Start climb	634,140			
		18,540	29	4
Start cruise	615,600			
		138,500	2,026	220
End cruise	477,100			
		3,140	95	10
End descent	473,960			
Taxi-in		2,080	0	5
Block fuel and time		171,620		250
Trip range			2,150	

NOTES: 1. Taxi-in fuel taken out of reserves on landing at destination.

2. C.A.B. range corresponding to block time and fuel equals trip range minus traffic allowances as will be specified for supersonic aircraft.

TABLE VI-6-VII

MISSION PERFORMANCE (Continued)

Model No. REFERENCE CONFIGURATION

Reserve Fuel Breakdown:

1.	7% trip fuel	11,870
2.	Missed approach	10,420
3.	260 N. Mi. to alternate airport	24,540
4.	30 min. holding at 15000 feet	14,960
	Total Reserve	61,790

Initial Cruise Conditions:

Lift Coefficient	.17410
Drag Coefficient	.01392
Lift/Drag	12.51
TSFC - lbs/hr/lb	.870
Altitude - ft.	32,500

TABLE VI-6-VIII

MISSION PERFORMANCE

MISSION: ALL SUPERSONIC CRUISE (M=2.7) NEW YORK TO PARIS

Model No. REFERENCE CONFIGURATION

Aircraft Characteristics

Take off gross weight - lbs.	696,500 (fuel off loaded)
Operating weight empty - lbs.	351,140
Payload - No. passengers	292
Lbs. - cargo	0
Total weight - lbs.	61,030
Wing area - ft^2 - reference	9,969
- actual	10,996
S.L. static thrust per engine - lbs.	77,610
Initial thrust to weight ratio	.45
Initial wing loading - lbs/ft^2 - reference	69.9
- actual	63.3

Design Mission

	Operating Weight(lbs.)	ΔFuel lbs.	ΔRange N. Mi.	ΔTime min.
Take off	696,500			
		9,360	0	11
Start climb	687,140			
		43,800	226	15
Start cruise	643,340			
		160,070	2,732	106
End cruise	483,270			
		5,850	200	20
End descent	477,420			
Taxi-in		2,080	0	5
Block fuel and time		221,160		157
Trip range			3,158	

NOTES: 1. Taxi-in fuel taken out of reserves on landing at destination.

2. C.A.B. range corresponding to block time and fuel equals trip range minus traffic allowances as will be specified for supersonic aircraft.

TABLE VI-6-VIII

MISSION PERFORMANCE (Continued)

Model No. REFERENCE CONFIGURATION

Reserve Fuel Breakdown:	
1. 7% trip fuel	15,330
2. Missed approach	10,420
3. 260 N. Mi. to alternate airport	24,540
4. 30 min. holding at 15000 feet	14,960
Total Reserve	65,250
Initial Cruise Conditions:	
Lift Coefficient	.09759
Drag Coefficient	.01144
Lift/Drag	8.53
TSFC - lbs/hr/lb	1.314
Altitude - ft.	63,500

TABLE VI-6-IX

MISSION PERFORMANCE

MISSION: 1500 N.MI. RANGE/A/C OFF LOADED/ALL SUPERSONIC CRUISE M=2.7

Model No. REFERENCE CONFIGURATION

Aircraft Characteristics

Take off gross weight - lbs.	584,300
Operating weight empty - lbs.	351,140
Payload - No. passengers	292
Lbs. - cargo	0
Total weight - lbs.	61,030
Wing area - ft^2 - reference	9,969
- actual	10,996
S.L.static thrust per engine - lbs.	77,610
Initial thrust to weight ratio	.53
Initial wing loading - lbs/ft^2 - reference	58.6
- actual	53.1

Design Mission

	Operating Weight(lbs.)	ΔFuel lbs.	ΔRange N.Mi.	ΔTime min.
Take off	584,300			
		9,360	0	11
Start climb	574,940			
		42,190	184	12
Start cruise	532,750			
		56,820	1,115	43
End cruise	475,930			
		5,850	200	20
End descent	470,080			
Taxi-in		2,080	0	5
Block fuel and time		116,300		91
Trip range			1,499	

NOTES: 1. Taxi-in fuel taken out of reserves on landing at destination.

2. C.A.B. range corresponding to block time and fuel equals trip range minus traffic allowances as will be specified for supersonic aircraft.

TABLE VI-6-IX

MISSION PERFORMANCE (Continued)

Model No. REFERENCE CONFIGURATION

ReservesFuel Breakdown:

1.	7% trip fuel	7,990
2.	Missed approach	10,420
3.	260 N. Mi. to alternate airport	24,540
4.	30 min. holding at 15000 feet	14,960
	Total Reserve	57,910

Initial Cruise Conditions:

Lift Coefficient	.09459
Drag Coefficient	.01126
Lift/Drag	8.40
TSFC - lbs/hr/lb	1.315
Altitude - ft.	66,500

TABLE VI-6-X

MISSION PERFORMANCE

MISSION: 2000 N.MI. RANGE/A/C OFF LOADED/ALL SUPERSONIC CRUISE M=2.7

Model No. REFERENCE CONFIGURATION

Aircraft Characteristics

Take off gross weight - lbs.	616,000
Operating weight empty - lbs.	351,140
Payload - No. passengers	292
Lbs. - cargo	0
Total weight - lbs.	61,030
Wing area - ft^2 - reference	9,969
- actual	10,996
S.L. static thrust per engine - lbs.	77,610
Initial thrust to weight ratio	.50
Initial wing loading - lbs/ft^2 - reference	61.8
- actual	56.0

Design Mission

	Operating Weight(lbs.)	ΔFuel lbs.	ΔRange N. Mi.	ΔTime min.
Take off	616,000			
		9,360	0	11
Start climb	606,640			
		44,930	194	13
Start cruise	561,710			
		83,700	1,605	62
End cruise	478,010			
		5,850	200	20
End descent	472,160			
Taxi-in		2,080	0	5
Block fuel and time		145,920		111
Trip range			1,999	

NOTES: 1. Taxi-in fuel taken out of reserves on landing at destination.

2. C.A.B. range corresponding to block time and fuel equals trip range minus traffic allowances as will be specified for supersonic aircraft.

TABLE VI-6-X

MISSION PERFORMANCE (Continued)

Model No. REFERENCE CONFIGURATION

Reserve Fuel Breakdown:

1.	7% trip fuel	10,070
2.	Missed approach	10,420
3.	260 N. Mi. to alternate airport	24,540
4.	30 min. holding at 15000 feet	14,960
	Total Reserve	59,990

Initial Cruise Conditions:

Lift Coefficient	.09508
Drag Coefficient	.01127
Lift/Drag	8.44
TSFC - lbs/hr/lb	1.313
Altitude - ft.	65,500

TABLE VI-6-XI

MISSION PERFORMANCE

MISSION: 2500 N.MI. RANGE/A/C OFF LOADED/ALL SUPERSONIC CRUISE M=2.7

Model No. REFERENCE CONFIGURATION

Aircraft Characteristics

Take off gross weight - lbs.	649,500
Operating weight empty - lbs.	351,140
Payload - No. passengers	292
Lbs. - cargo	0
Total weight - lbs.	61,030
Wing area - ft^2 - reference	9,969
- actual	10,996
S.L. static thrust per engine - lbs.	77,610
Initial thrust to weight ratio	.48
Initial wing loading - lbs/ft^2 - reference	65.2
- actual	59.1

Design Mission

	Operating Weight(lbs.)	ΔFuel lbs.	ΔRange N.Mi.	ΔTime min.
Take off	649,500			
		9,360	0	11
Start climb	640,140			
		48,010	206	14
Start cruise	592,130			
		111,930	2,094	81
End cruise	480,200			
		5,850	200	20
End descent	474,350			
Taxi-in		2,080	0	5
Block fuel and time		177,230		131
Trip range			2,500	

NOTES: 1. Taxi-in fuel taken out of reserves on landing at destination.

2. C.A.B. range corresponding to block time and fuel equals trip range minus traffic allowances as will be specified for supersonic aircraft.

TABLE VI-6-XI

MISSION PERFORMANCE (Continued)

Model No. REFERENCE CONFIGURATION

Reserve Fuel Breakdown:

1.	7% trip fuel	12,260
2.	Missed approach	10,420
3.	260 N. Mi. to alternate airport	24,540
4.	30 min. holding at 15000 feet	14,960
	Total Reserve	62,180

Initial Cruise Conditions:

Lift Coefficient	.09556
Drag Coefficient	.01128
Lift/Drag	8.47
TSFC - lbs/hr/lb	1.312
Altitude - ft.	64,500

TABLE VI-6-XII

MISSION PERFORMANCE

MISSION: 3000 N.MI. RANGE/A/C OFF LOADED/ALL SUPERSONIC CRUISE AT M=2.7

Model No. REFERENCE CONFIGURATION

Aircraft Characteristics

Take off gross weight - lbs.		684,700
Operating weight empty - lbs.		351,140
Payload - No. passengers		292
Lbs. - cargo		0
Total weight - lbs.		61,030
Wing area - ft^2 - reference		9,969
- actual		10,996
S.L. static thrust per engine - lbs.		77,610
Initial thrust to weight ratio		.45
Initial wing lo ding - lbs/ft^2	- reference	68.7
	- actual	62.3

Design Mission

	Operating Weight(lbs.)	ΔFuel lbs.	ΔRange N. Mi.	ΔTime min.
Take off	684,700			
		9,360	0	11
Start climb	675,340			
		51,480	220	15
Start cruise	623,860			
		141,360	2,578	100
End cruise	482,500			
		5,850	200	20
End descent	476,650			
Taxi-in		2,080	0	5
Block fuel and time		210,130		151
Trip range			2,998	

NOTES: 1. Taxi-in fuel taken out of reserves on landing at destination.

2. C.A.B. range corresponding to block time and fuel equals trip range minus traffic allowances as will be specified for supersonic aircraft.

TABLE VI-6-XII

MISSION PERFORMANCE (Continued)

Model No. REFERENCE CONFIGURATION

Reserve Fuel Breakdown:

1.	7% trip fuel	14,560
2.	Missed approach	10,420
3.	260 N. Mi. to alternate airport	24,540
4.	30 min. holding at 15000 feet	14,960
	Total Reserve	64,480

Initial Cruise Conditions:

Lift Coefficient	.09598
Drag Coefficient	.01128
Lift/Drag	8.51
TSFC - lbs/hr/lb	1.312
Altitude - ft.	63,500

TABLE VI-6-XIII

MISSION PERFORMANCE

MISSION: 3500 N.MI. RANGE/A/C OFF LOADED/ALL SUPERSONIC CRUISE AT M=2.7

Model No. REFERENCE CONFIGURATION

Aircraft Characteristics

Take off gross weight - lbs.	722,400
Operating weight empty - lbs.	351,140
Payload - No. passengers	292
Lbs. - cargo	0
Total weight - lbs.	61,030
Wing area - ft^2 - reference	9,969
- actual	10,996
S.L. static thrust per engine - lbs.	77,610
Initial thrust to weight ratio	.43
Initial wing loading - lbs/ft^2 - reference	72.5
- actual	65.7

Design Mission

	Operating Weight(lbs.)	ΔFuel lbs.	ΔRange N. Mi.	ΔTime min.
Take off	722,400			
		9,360	0	11
Start climb	713,040			
		55,500	236	16
Start cruise	657,540			
		172,570	3,066	119
End cruise	484,970			
		5,850	200	20
End descent	479,120			
Taxi-in		2,080	0	5
Block fuel and time		245,360		171
Trip range			3,502	

NOTES: 1. Taxi-in fuel taken out of reserves on landing at destination.

2. C.A.B. range corresponding to block time and fuel equals trip range minus traffic allowances as will be specified for supersonic aircraft.

TABLE VI-6-XIII

MISSION PERFORMANCE (Continued)

Model No. REFERENCE CONFIGURATION

Reserve Fuel Breakdown:

1.	7% trip fuel	17,030
2.	Missed approach	10,420
3.	260 N. Mi. to alternate airport	24,540
4.	30 min. holding at 15000 feet	14,960
	Total Reserve	66,950

Initial Cruise Conditions:

Lift Coefficinnt	.09644
Drag Coefficient	.01129
Lift/Drag	8.54
TSFC - lbs/hr/lb	1.312
Altitude - ft.	62,500

TABLE VI-6-XIV

MISSION PERFORMANCE

MISSION: ALL SUPERSONIC CRUISE (MACH = 2.7) WITH MAX FUEL (OVERLOADED GROSS WEIGHT)

Model No. REFERENCE CONFIGURATION

Aircraft Characteristics

Take off gross weight - lbs.	870,000
Operating weight empty - lbs.	351,140
Payload - No. passengers	292
Lbs. - cargo	0
Total weight - lbs.	61,030
Wing area - ft^2 - reference	9,969
- actual	10,996
S.L. static thrust per engine - lbs.	77,610
Initial thrust to weight ratio	.36
Initial wing loading - lbs/ft^2 - reference	87.3
- actual	79.1

Design Mission

	Operating Weight(lbs.)	ΔFuel lbs.	ΔRange N. Mi.	ΔTime min.
Take off	870,000			
		9,360	0	11
Start climb	860,640			
		75,940	321	22
Start cruise	784,700			
		290,070	4,699	182
End cruise	494,630			
		5,850	200	20
End descent	488,780			
Taxi-in		2,080	0	5
Block fuel and time		383,300		240
Trip range			5,220	

NOTES: 1. Taxi-in fuel taken out of reserves on landing at destination.

2. C.A.B. range corresponding to block time and fuel equals trip range minus traffic allowances as will be specified for supersonic aircraft.

TABLE VI-6-XIV

MISSION PERFORMANCE (Continued)

Model No. REFERENCE CONFIGURATION

Reserve Fuel Breakdown:

1.	7% trip fuel	26,690
2.	Missed approach	10,420
3.	260 N. Mi. to alternate airport	24,540
4.	30 min. holding at 15000 feet	14,960
	Total Reserve	76,610

Initial Cruise Conditions:

Lift Coefficient	.10213
Drag Coefficient	.01179
Lift/Drag	8.66
TSFC - lbs/hr/lb	1.317
Altitude - ft.	60,000